ALMA MATER STUDIORUM - UNIVERSITÀ DEGLI STUDI DI BOLOGNA

FACOLTÀ DI INGEGNERIA

DICAM
Dipartimento di Ingegneria Civile, Ambientale e dei Materiali

Svolta presso

THE CITY COLLEGE OF NEW YORK

CITY UNIVERSITY OF NEW YORK

CIVIL ENGINEERING DEPARTMENT

EXPERIMENTAL ANALYSIS OF FIBER REINFORCED CEMENTITIOUS MATRIX (FRCM) CONFINED MASONRY COLUMNS

TESI DI LAUREA DI:
Lorenzo Zucchini

RELATORE:
Chiar.mo Prof. Ing. Marco Savoia

CORRELATORI:
Prof. Ing. Kolluru V. Subramaniam
Prof. Ing. Christian Carloni

Anno Accademico 2010–2011

A B S T R A C T

The increasing use of Fiber Reinforced methods for strengthening existing brick masonry walls and columns, especially for the rehabilitation of historical buildings, has generated considerable research interest in understanding the failure mechanism in such systems.

This dissertation is aimed to provide a basic understanding of the behavior of solid brick masonry walls unwrapped and wrapped with Fiber Reinforced Cementitious Matrix Composites. This is a new type of composite material, commonly known as FRCM, featuring a cementitious inorganic matrix (binder) instead of the more common epoxy one.

The influence of the FRCM-reinforcement on the load-carrying capacity and strain distribution during compression test will be investigated using a full-field optical technique known as Digital Image Correlation.

Compression test were carried on 6 clay bricks columns and on 7 clay brick walls in three different configuration, casted using bricks scaled respect the first one with a ratio 1:2, in order to determinate the effects of FRCM reinforcement.

The goal of the experimental program is to understand how the behavior of brick masonry will be improved by the FRCM-wrapping.

The results indicate that there is an arching action zone represented in the form of a parabola with a varying shape according to the used configuration. The area under the parabolas is considered as ineffectively confined.

The effectively confined area is assumed to occur within the region where the arching action had been fully developed.

KEY WORDS

BRICK MASONRY;

FIBER REINFORCED CEMENTITIOUS MATRIX;

DIGITAL IMAGE CORRELATION;

FRCM-REINFORCED MASONRY;

AXIAL COMPRESSION TEST.

SUMMARY

S U M M A R Y

INTRODUCTION

OPTICAL METHODS AND FRP.....pag. 1

0.1. Digital Image.....pag. 2

0.2. Digital Image Correlation.....pag. 4

0.3. Differential Digital Image Tracking.....pag. 10

0.4. Application of Digital Image Correlation.....pag. 13

0.5. Resolution of Digital Image Correlation.....pag.14

0.6. Fiber Reinforced Polymer.....pag. 17

1. CHAPTER 1

BACKGROUND.....pag.23

1.1. Brick Masonry Buildings.....pag.24

1.2. Previous Researches on FRP-Reinforced Masonry.....pag.33

1.3. Experimental Program.....pag.37

1.3.1. Material characterization.....pag.38

1.3.2. Experimental test setup.....pag.51

2. CHAPTER 2

BRICK MASONRY COLUMNS.....pag.54

2.1. Axial Compression Test.....pag.55

2.1.1. Experimental result and failure mode.....pag.58

2.1.1.1. Column unwrapped 1.....pag.61

2.1.1.2. Column unwrapped 2.....pag.69

2.1.1.3. Column unwrapped 3.....pag.77

2.1.2. Discussion of result.....pag.81

3. CHAPTER 3

FRCM-REINFORCED BRICK MASONRY COLUMNS.....pag.84

3.1. Axial Compression Test.....pag.85

3.1.1. Experimental result and failure mode.....pag.89

3.1.1.1. Column wrapped 1.....pag.93

3.1.1.2. Column wrapped 2.....pag.100

3.1.1.3. Column wrapped 3.....pag.106

3.1.2. Discussion of result.....pag.113

4. CHAPTER 4

BRICK MASONRY WALLS.....pag.116

4.1. Experimental Test Description.....pag.117

4.1.1. Material characterization.....pag.121

4.2. Axial Compression Test First Configuration.....pag.127

4.2.1. Experimental result and failure mode.....pag.129

4.2.1.1. Square wall unwrapped 1.....pag.132

4.2.1.2. Square wall unwrapped 2.....pag.136

4.2.1.3. Square wall unwrapped 3.....pag.143

4.2.2. Discussion of result.....pag.148

4.3. Axial Compression Test Second Configuration.....pag.149

4.3.1. Experimental result and failure mode.....pag.151

4.3.1.1. Rectangular1 wall unwrapped 1.....pag.153

4.3.1.2. Rectangular1 wall unwrapped 2.....pag.159

4.3.1.3. Rectangular1 wall unwrapped 3.....pag.163

4.3.2. Discussion of result.....pag.169

4.4. Axial Compression Test Third Configuration.....pag.170

4.4.1. Experimental result and failure mode.....pag.172

4.4.1.1. Rectangular2 wall unwrapped 1.....pag.174
4.4.1.2. Rectangular2 wall unwrapped 2.....pag.177
4.4.1.3. Rectangular2 wall unwrapped 3.....pag.182
4.4.2. Discussion of result.....pag.188

5. CHAPTER 5
FRCM-REINFORCED BRICK MASONRY WALLS.....pag.189
5.1. Axial Compression Test First Configuration.....pag.190
5.1.1. Experimental result and failure mode.....pag.194
5.1.1.1. Square wall wrapped 1.....pag.196
5.1.1.2. Square wall wrapped 2.....pag.204
5.1.1.3. Square wall wrapped 3…..pag.213
5.1.2. Discussion of result.....pag.222
5.2. Axial Compression Test Second Configuration.....pag.226
5.2.1. Experimental result and failure mode.....pag.230
5.2.1.1. Rectangular1 wall wrapped 1.....pag.232
5.2.1.2. Rectangular1 wall wrapped 2.....pag.241
5.2.1.3. Rectangular1 wall wrapped 3.....pag.250
5.2.2. Discussion of result.....pag.259
5.3. Axial Compression Test Third Configuration.....pag.262
5.3.1. Experimental result and failure mode.....pag.265
5.3.1.1. Rectangular2 wall wrapped 1.....pag.267
5.3.1.2. Rectangular2 wall wrapped 2.....pag.276
5.3.2. Discussion of result.....pag.285

6. **CONCLUSIONS**.....pag.289

REFERENCES.....pag.301

ACKNOWLEDGMENTS.....pag.304

INTRODUCTION

OPTICAL METHODS AND FRP

I N T R O D U C T I O N

OPTICAL METHODS AND FRP

0.1. Digital Image

A digital image is a representation of a two-dimensional image using ones and zeros, binary code. Depending on whether or not the image resolution is fixed, it may be of vector or raster type. Without qualifications, the term digital image usually refers to raster images also called bitmap images, figure 0.1.

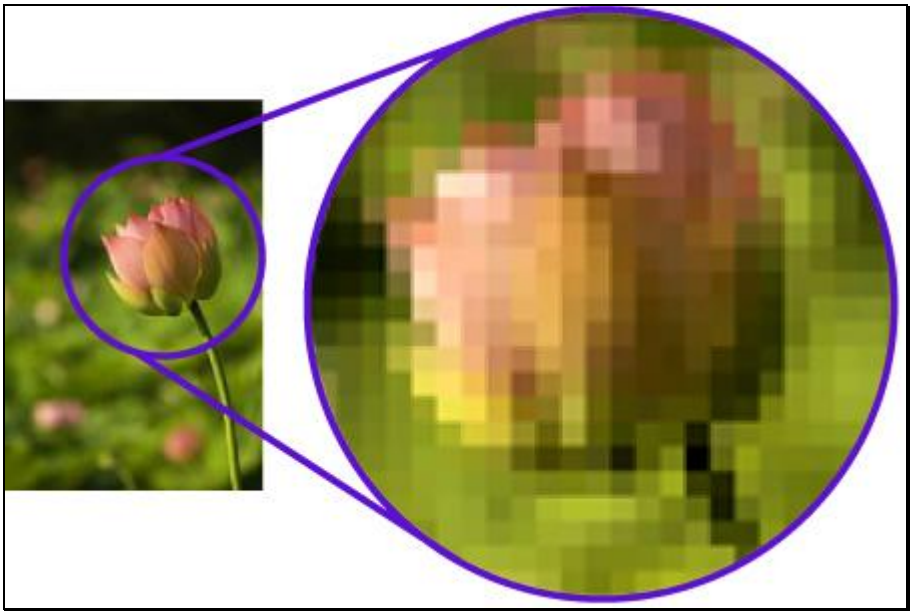

Fig. 0.1 – Basic concept of digital image correlation

Raster images have a finite set of digital values, called picture elements or pixels. The digital image contains a fixed number of rows and columns of pixels.

Pixels are the smallest individual element in an image, holding quantized values that represent the brightness of a given color at any specific point.

Typically, the pixels are stored in computer memory as a raster image or raster map, a two-dimensional array of small integers. These values are often transmitted or stored in a compressed form.

Raster images can be created by a variety of input devices and techniques, such as digital cameras, scanners, coordinate-measuring machines, seismographic profiling, airborne radar, and more.

They can also be synthesized from arbitrary non-image data, such as mathematical functions or three-dimensional geometric models; the latter being a major sub-area of computer graphics. The field of digital image processing is the study of algorithms for their transformation.

Each pixel of a raster image is typically associated to a specific position in some 2D region, and has a value consisting of one or more quantities related to that position.

Digital images can be classified according to the number and nature of those samples:

- binary;
- grayscale;
- color;
- false-color;
- multi-spectral;
- thematic;
- picture function.

The term digital image is also applied to data associated to points scattered over a three-dimensional region.

0.2. Digital Image Correlation

This dissertation concern the use of optical methods, in particular digital image correlation, for displacement measurements during static or fatigue tests on specimens.

The accurate measurement of displacement and strains during deformation of advanced materials and devices continues to be a primary challenge to designers and experimental mechanicians. The increasing complexity of technological devices with stringent space requirements leads to imperfect boundary conditions that have to be properly accounted for. The push toward miniaturizing devices down to nanometer length scales imparts additional difficulties in measuring strains as the application of conventional extensometers and resistance foil gages are cumbersome, damaging, or even impossible. Compounding this problem is also the fact that compliance of small-scale testing machines precludes the use of the displacement of external actuators for estimating specimen strain. As a consequence, a technique with the following features is extremely desirable:

- no contact with the specimen required;
- sufficient spatial resolution to measure locally at the region of interest;
- the ability to capture non-uniform full-field deformations;
- a direct measurement that does not require recourse to a numerical or analytical model.

Optical methods are a logical solution to this litany of challenges.

One approach is the interferometric strain-displacement gage developed by Sharpe. A laser-based technique that affords significant advantages over conventional strain measurement methods.

It utilizes two markers on the surface of the specimen that provide interference fringes. This technique offers a very good resolution and local

strain determination, but is limited to 1D measurements and requires some degree of experimental complexity. It also demands the use of markers.

In the case of thin film mechanical testing where thicknesses are in the submicrometre range, hardness indents are out of the question and deposited lines can be up to an order of magnitude thicker than the specimen itself, which could significantly alter the apparent intrinsic properties of the material being tested.

Digital image correlation techniques have been increasing in popularity, especially in micro- and nano-scale mechanical testing applications due to its relative ease of implementation and use.

Advances in digital imaging have been the enabling technology for this method and while white-light optics has been the predominate approach, DIC has recently been extended to SEM and AFM. Above and beyond the ability of image-based methods to provide a “box-seat” to the events that are occurring during deformation, these techniques have been applied to the testing of many materials systems because it offers a full-field description and is relatively robust at tracking a wide range of “markers” and varying surface contrast.

The appeal of these image-based techniques, coupled with the lack of flexibility and prohibitive cost of commercial DIC software packages, provided the impetus for the development of a custom in-house software suite using the mathematical package MATLAB as the engine for calculations.

This resulted in an open-source package that was uploaded to the public domain in an effort to provide free tools to users, but also to generate feedback for potential improvements and addition to the code.

DIC for strain measurement constitutes a major field of research and is followed by a healthy, vigorous, and dynamic discussion and discourse.

DIC was first conceived and developed at the University of South Carolina in the early 1980s and has been optimized and improved in recent years.

DIC is predicated on the maximization of a correlation coefficient that is determined by examining pixel intensity array subsets on two or more corresponding images and extracting the deformation mapping function that relates the images, Figure 0.2.

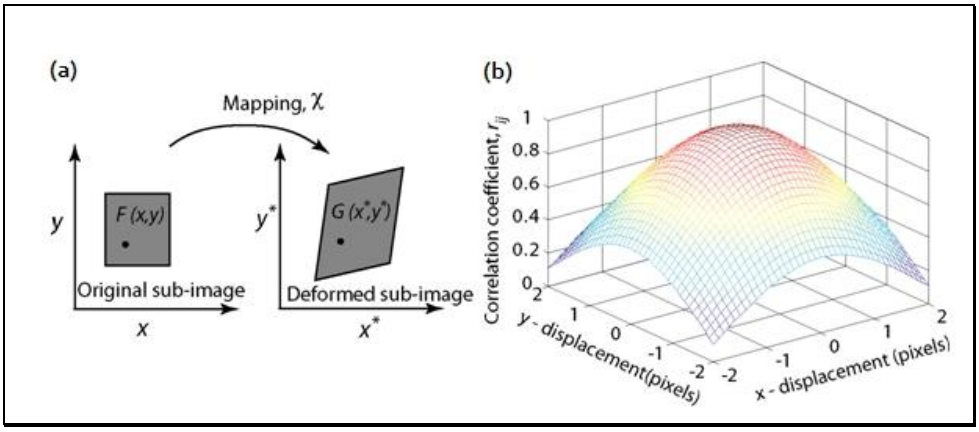

Fig. 0.2 – Basic concept of digital image correlation

The cross correlation coefficient r_{ij} is defined as:

$$r_{ij}(u,v,\frac{\partial u}{\partial x},\frac{\partial u}{\partial y},\frac{\partial v}{\partial x},\frac{\partial v}{\partial y}) = 1 - \frac{\sum_i \sum_j \left[F(x_i,y_j)-\overline{F}\right]\left[G(x_{i_x}^*,y_j^*)-\overline{G}\right]}{\sqrt{\sum_i \sum_j \left[F(x_i,y_j)-\overline{F}\right]^2 \left[G(x_{i_x}^*,y_j^*)-\overline{G}\right]^2}}$$

Here $F(x_i,y_j)$ is the pixel intensity or the gray scale value at a point (x_i,y_j) in the undeformed image. $G(x_{i_x}^*,y_j^*)$ is the gray scale value at a point $(x_{i_x}^*,y_j^*)$ in the deformed image. $\overline{F}$ and $\overline{G}$ are mean values of the intensity matrices F and G, respectively. The coordinates or grid points (x_i,y_j) and $(x_{i_x}^*,y_j^*)$ are related by the deformation that occurs between the two images. If the motion is perpendicular to the optical axis of the camera, then the relation between (x_i,y_j) and $(x_{i_x}^*,y_j^*)$ can be approximated by a 2D affine transformation such as:

$$x^* = x + u + \frac{\partial u}{\partial x}\Delta x + \frac{\partial u}{\partial y}\Delta y;$$

$$y^* = y + v + \frac{\partial v}{\partial x}\Delta x + \frac{\partial v}{\partial y}\Delta y.$$

Here u and v are translations of the center of the sub-image in the x and y directions, respectively. The distances from the center of the sub-image to the point (x, y) are denoted by Δx and Δy. Thus, the correlation coefficient r_{ij} is a function of displacement components (u, v) and displacement gradients:

$$\frac{\partial u}{\partial x}; \frac{\partial u}{\partial y}; \frac{\partial v}{\partial x}; \frac{\partial v}{\partial y}.$$

DIC has proven to be very effective at mapping deformation in macroscopic mechanical testing, where the application of specular markers or surface finishes from machining and polishing provide the needed contrast to correlate images well.

However, these methods for applying surface contrast do not extend to the application of freestanding thin films for several reasons. First, vapor deposition at normal temperatures on semiconductor grade substrates results in mirror-finish quality films with roughnesses that are typically on the order of several nanometers.

No subsequent polishing or finishing steps are required, and unless electron imaging techniques are employed that can resolve microstructural features, the films do not possess enough useful surface contrast to adequately correlate images.

Typically this challenge can be circumvented by applying paint that results in a random speckle pattern on the surface, although the large and turbulent forces resulting from either spraying or applying paint to the surface of a freestanding thin film are too high and would break the specimens. In addition, the sizes of individual paint particles are on the order of μms,

while the film thickness is only several hundred nms, which would be analogous to supporting a large boulder on a thin sheet of paper.

Very recently, advances in pattern application and deposition at reduced length scales have exploited small-scale synthesis methods including nano-scale chemical surface restructuring and photolithography of computer-generated random specular patterns to produce suitable surface contrast for DIC.

The application of very fine powder particles that electrostatically adhere to the surface of the specimen and can be digitally tracked is one approach. For thin films, fine alumina abrasive polishing powder was initially used since the particle sizes are relatively well controlled, although the adhesion to films was not very good and the particles tended to agglomerate excessively.

A light blanket of powder would coat the gage section of the tensile sample and the larger particles could be blown away gently. The remaining particles would be those with the best adhesion to the surface, and under low-angle grazing illumination conditions, the specimen gage section would appear as shown in Figure 0.3.

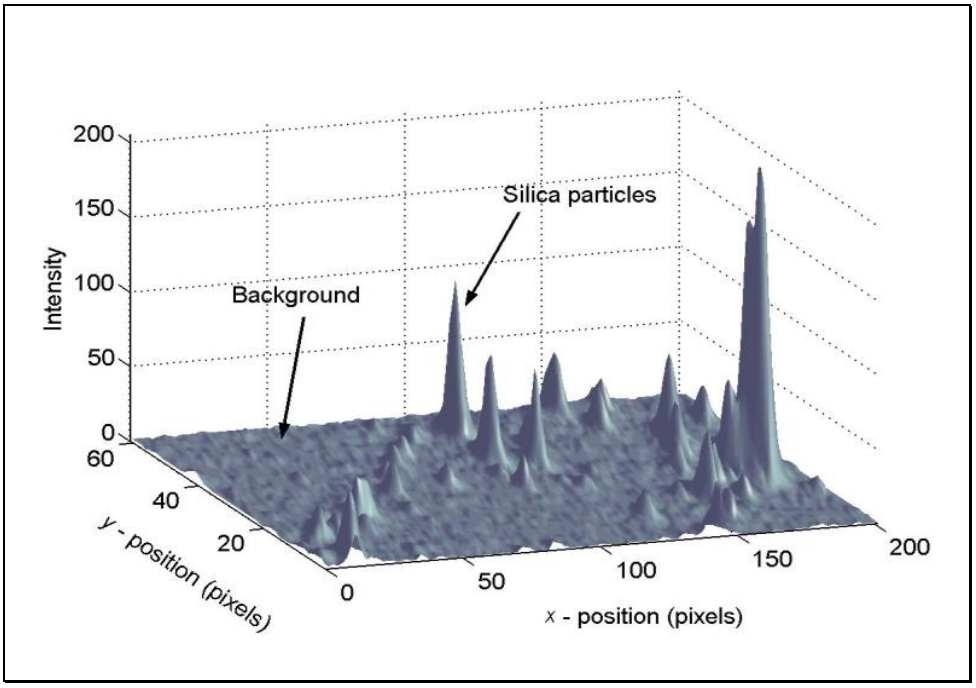

Fig. 0.3 – Basic concept of digital image correlation

While the surface contrast present is not ideal for DIC, the high intensity ratio between the particles and the background provide a unique opportunity to track the particles between consecutive digital images taken during deformation. This can be achieved quite straight forwardly using digital image processing techniques, although the resolution is always limited to a single pixel. To attain tracking with subpixel resolution, a novel image-based tracking algorithm using MATLAB was developed, dubbed Digital Differential Image Tracking.

0.3. Differential Digital Image Tracking

The differential digital image tracking method exploits the shape of these powder particles when digitally imaged in the intensity domain as shown in Figure 0.2. The resemblance of the particles to mathematical functions that are adept at describing peak shapes with precise center locations and broadening allow them to be fit to a given function and thus tracked.

It is perhaps coincidental that the symmetric normal distribution function proficiently fits the intensity profiles of the particles. This function can also be described in two dimensions.

The quality of the Gaussian fit to a peak profile is shown in Figure 0.4.

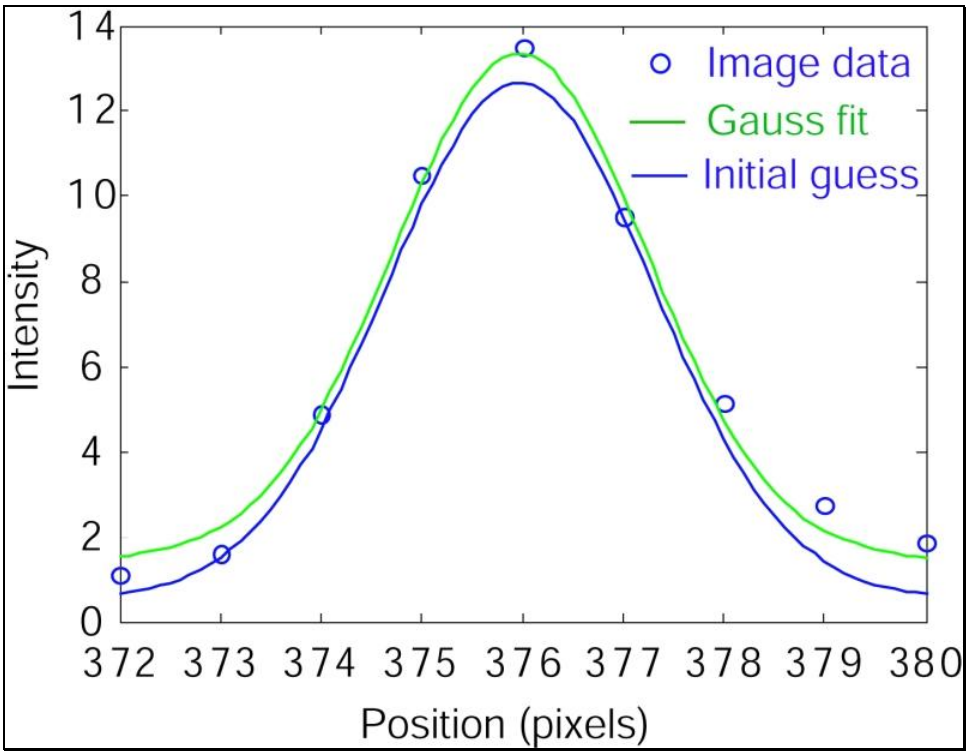

Fig. 0.4 – Peak profile of marker with corresponding Gaussian fit

First, images are captured during the course of a mechanical test. Second, a list of image filenames is generated and the image capture times are

extracted from the original images in order to synchronize the DDIT data to that of the data acquisition system.

The markers are then automatically detected in the first image by an image processing algorithm that labels connected components in a binary image and subsequently, information regarding the size and shape of these components are extracted.

Particles with properties that do not conform to specifications for ideal shapes are thrown out, and the remaining markers in the first image are fit to a Gaussian function using a nonlinear least-squares algorithm in both the longitudinal and transverse directions.

The normalized residuals of the fit of the peak to the function are calculated for every peak and again, fits deemed poor as given by the value of the residual are removed from the analysis.

This process now continues for every image in the sequence, and the result includes the position of the peak center, which is then post-processed using a visualization and data analysis script that allows visualization and output of the quantities of interest. [1]

A digital image correlation process in shown in figure 0.5.

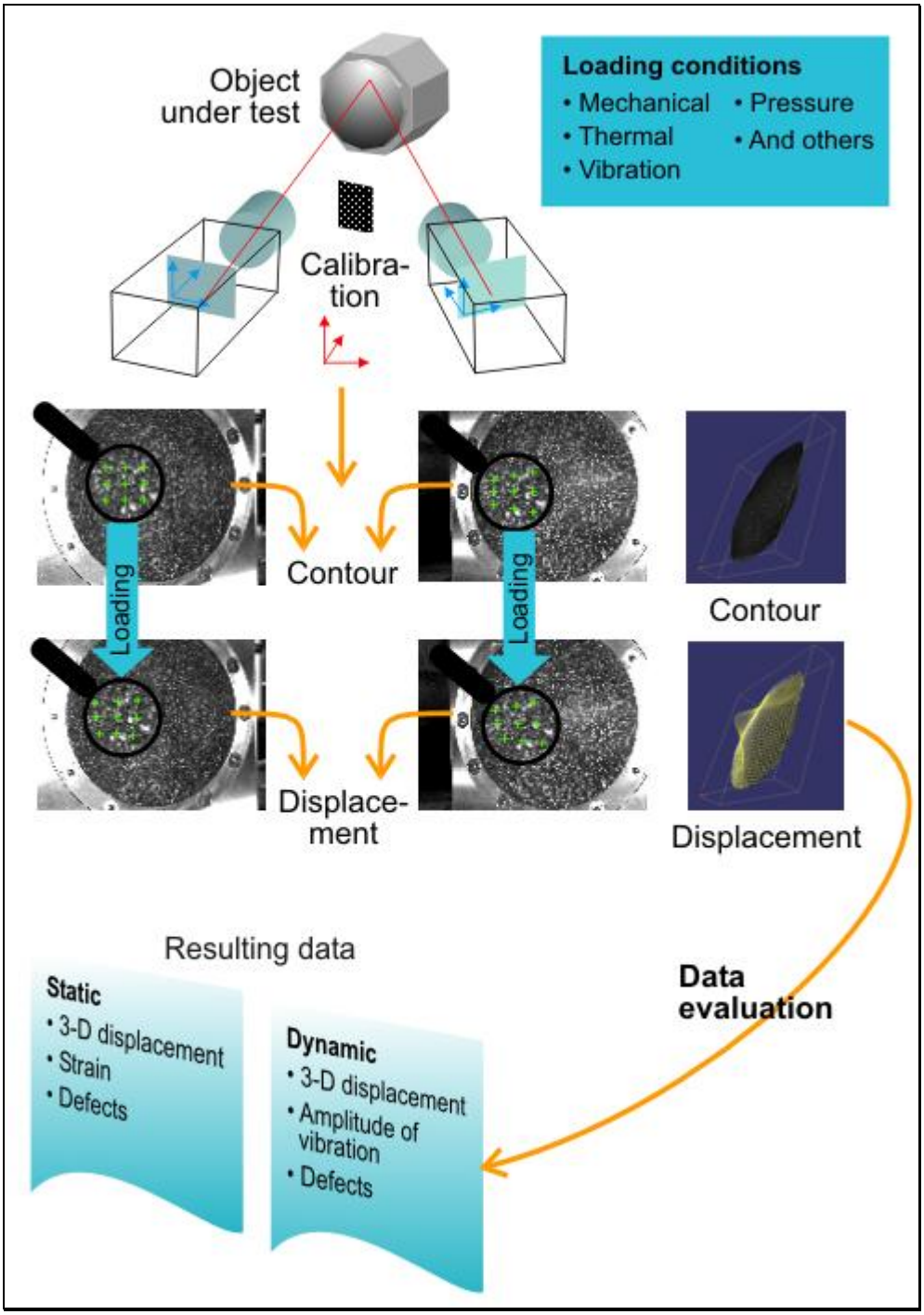

Fig. 0.5 – Digital image correlation process [2]

0.4. Application of Digital Image Correlation

Digital Image Correlation offers characterization of material parameters far into the range of plastic deformation.

Its powerful data analysis tools allow the determination of the location and amplitude of maximum strain, which are important functions in material testing.

DIC is also ideal for fracture mechanics investigation. The full-field measurement delivers exact information about local and global strain distribution, crack growth, and can be used for the determination of important fracture mechanics parameters.

The next figure shown typical application for DIC:

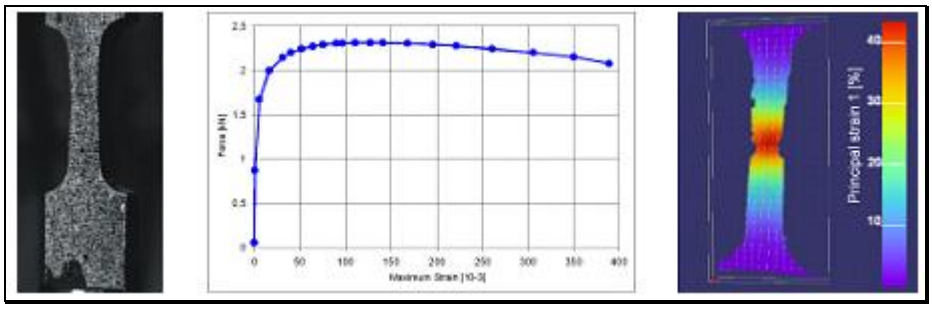

Fig. 0.6 – Material properties

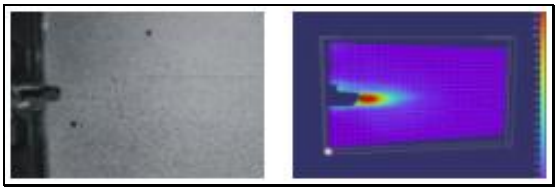

Fig. 0.7 – Fracture mechanics

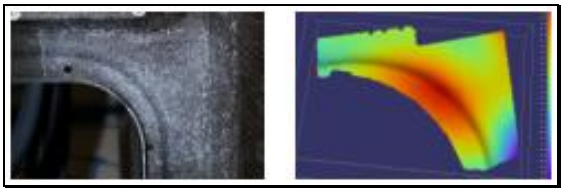

Fig. 0.8 – Component test

0.5. Resolution of Digital Image Correlation

The resolution that one can achieve in practice using these image-based techniques depends on a number of factors, including but not limited to camera resolution, lens optical quality, and marker size and quality.

For a digital image the resolution can be described in many different ways:

- pixel resolution: the term resolution is often used as a pixel count in digital imaging, even though international standards specify that it should not be so used, at least in the digital camera field. An image of N pixels high by M pixels wide can have any resolution less than N lines per picture height, or N TV lines. But when the pixel counts are referred to as resolution, the convention is to describe the pixel resolution with the set of two positive integer numbers, where the first number is the number of pixel columns and the second is the number of pixel rows. Another popular convention is to cite resolution as the total number of pixels in the image, typically given as number of megapixels, which can be calculated by multiplying pixel columns by pixel rows and dividing by one million. Other conventions include describing pixels per unit length or pixels per unit area, such as pixels per inch or per square inch. None of these pixel resolutions are true resolutions, but they are widely referred to as such; they serve as upper bounds on image resolution, figure 0.9.

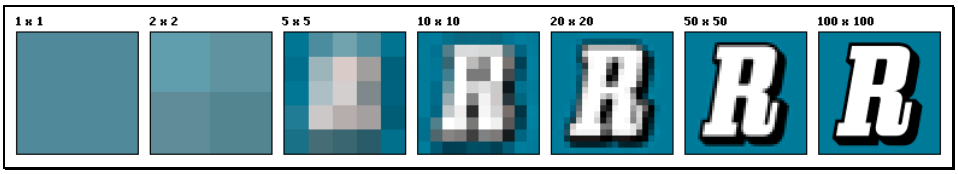

Fig. 0.9 – different pixel resolution

- spatial resolution: the measure of how closely lines can be resolved in an image is called spatial resolution, and it depends on properties

of the system creating the image, not just the pixel resolution in pixels per inch. For practical purposes the clarity of the image is decided by its spatial resolution, not the number of pixels in an image. In effect, spatial resolution refers to the number of independent pixel values per unit length.

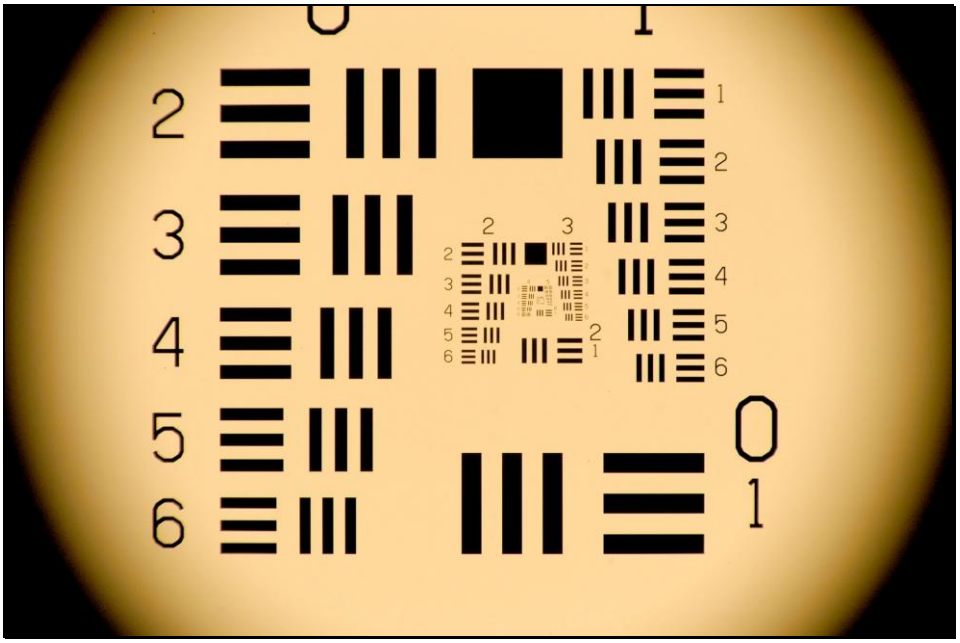

Fig. 0.10 – resolution test target

- Spectral resolution: color images distinguish light of different spectra. Multi-spectral images resolve even finer differences of spectrum or wavelength than is needed to reproduce color. That is, they can have higher spectral resolution. that is the strength of each band that is created.
- Temporal resolution: movie cameras and high-speed cameras can resolve events at different points in time. The time resolution used for movies is usually 15 to 30 frames per second, while high-speed cameras may resolve 100 to 1000 frame per second. Many cameras

and displays offset the color components relative to each other or mix up temporal with spatial resolution, figure 0.11.

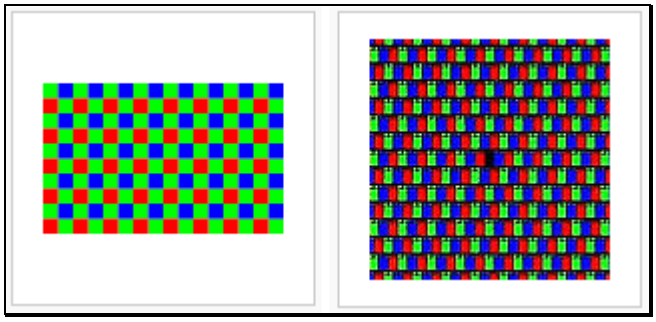

Fig. 0.11 – digital camera and LCD

- Radiometric resolution: radiometric resolution determines how finally a system can represent or distinguish differences of intensity, is usually expressed as a number of levels or a number of bits, 8 bits or 256 levels is typical of computer image files. The effective radiometric resolution is typically limited by the noise level, rather than by the number of bits of representation.

0.6. Fiber Reinforced Polymer

Continuous fiber-reinforced materials with polymeric matrix (FRP) can be considered as composite, heterogeneous, and anisotropic materials with a prevalent linear elastic behavior up to failure. They are widely used for strengthening and repairing civil structures.

There are many advantages of using FRPs: lightweight, good mechanical properties, corrosion-resistant, etc.

Composites for structural strengthening are available in several geometries from laminates used for strengthening of members with regular surface to bi-directional fabrics easily adaptable to the shape of the member to be strengthened.

Composites are also suitable for applications where the aesthetic of the original structures needs to be preserved, historic or artistic interest buildings, or where strengthening with traditional techniques cannot be effectively employed.

There are also examples of applications of composite strengthening with discontinuous fibers and polymeric matrix as well as continuous fibers and inorganic matrix; the latter has been proven to be of particular interest.

The fibers are usually fiberglass, carbon, or aramid, while the polymer is in case of organic matrix an epoxy, vinylester or polyester thermosetting plastic and in case of inorganic matrix, FRCM, a cementitious mortar matrix designed to connect the mesh with the substrate.

The FRPs are commonly used in the aerospace, automotive, marine, and construction.

FRP involves two distinct processes, the first is the process whereby the fibrous material is manufactured and formed, the second is the process whereby fibrous materials are bonded with the matrix during the molding process.

The matrix may be considered as an isotropic material, while the reinforcing phase is an anisotropic material. The defining characteristics of FRP materials are as follows:

- Geometry: shape and dimensions.
- Fiber orientation: the orientation with respect to the symmetry axes of the material; when random, the composite characteristics are similar to an isotropic material. In all other cases the composite can be considered as an anisotropic material.
- Fiber concentration: volume fraction, distribution, dispersion.
- Type of matrix: organic or inorganic matrix.

Composite materials can be stronger and stiffer than traditional construction materials.

As a result, composites may become very attractive when the weight of the structure becomes an issue. FRP tensile strength and Young's modulus of elasticity can be up to four and two times that of traditional materials, respectively.

This means that there is a notable reduction of the section.

The nature of the phases of the composite determines the final properties of FRP materials.

To obtain a composite with high mechanical strength, using fibers is not enough. A good adhesion between matrix and fibers used as loading carrying component is also necessary.

The adhesion is usually obtained through a third component applied in a very thin layer on the fiber surface that makes them compatible with the organic matrix.

Such surface treatment requires the presence of an intermediate phase between the matrix and the fibers, named interface, or interphase, figure 0.12.

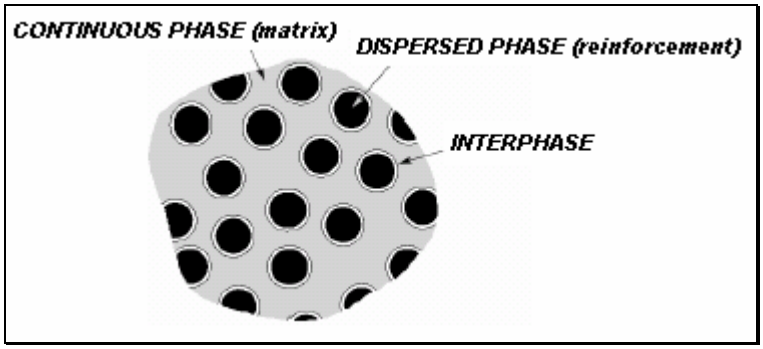

Fig. 0.12 – Representation of phases in a FRP composite

The interphase is typically made of a very thin layer placed directly on the fiber that is essential for determining the final properties of the material. Fibers are made of very thin continuous filaments, and therefore, are quite difficult to be individually manipulated. For this reason, they are commercially available in different shapes, figure 0.13.

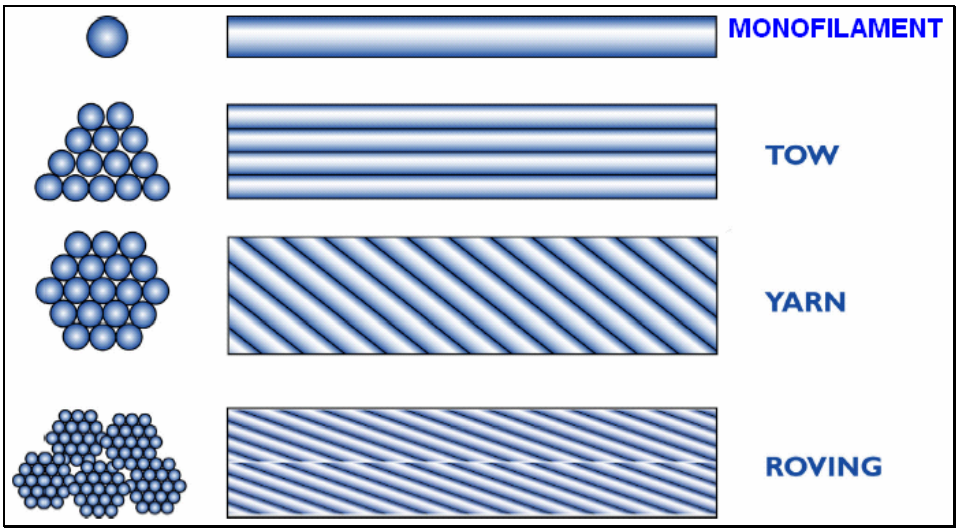

Fig. 0.13 – Types of fibers

A brief description of the most used is summarized as follows:

- Monofilament: basic filament with a diameter of about 10 μm.

- Tow: untwisted bundle of continuous filaments.
- Yarn: assemblage of twisted filaments and fibers formed into a continuous length that is suitable for use in weaving textile materials.
- Roving: a number of yarn or tows collected into a parallel bundle with little or no twist. [3]

Reinforcing Fiber is manufactured in both two dimensional and three dimensional orientations:

- Two Dimensional Fiber Reinforced Polymer are characterized by a laminated structure in which the fibers are only aligned along the plane in x-direction and y-direction of the material. This means that no fibers are aligned in the through thickness or the z-direction, this lack of alignment in the through thickness can create a disadvantage in cost and processing.
- Three-dimensional Fiber Reinforced Polymer composites are materials with three dimensional fiber structures that incorporate fibers in the x-direction, y-direction and z-direction.

Fiber preforms are how the fibers are manufactured before being bonded to the matrix, they are often in sheets, continuous mats, or as continuous filaments for spray applications.

Reinforcing Material	Most Common Matrix Materials	Properties Improved
Glass Fibers	UP, EP, PA, PC, POM, PP, PBT, VE	Strength, Elastic, heat resistance
Carbon and Aramid Fibers	EP, UP, VE, PA	Elasticity, Tensile Strength
Inorganic Particulates	Semicrystalline Thermoplastics, UP	Isotropic shrinkage, abrasion, compression strength

Tab. 0.1 – Example of polymer best suited for the process

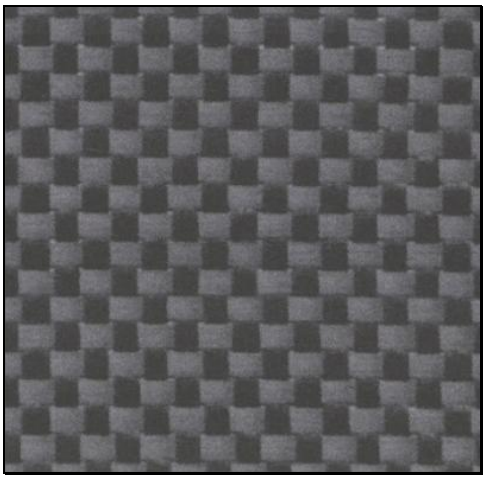

Fig. 0.14 – Carbon fiber

Fig. 0.15 – Glass fiber

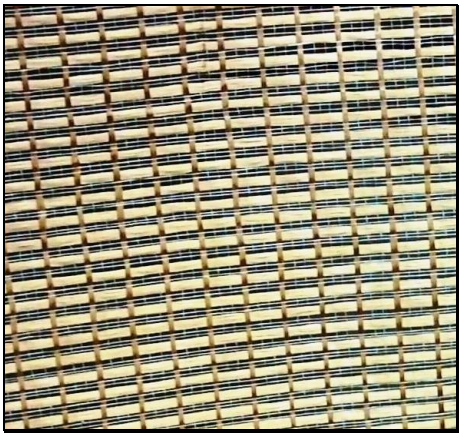

Fig. 0.16 – Aramid fiber

FRP can be applied to strengthen the beams, columns and slabs in buildings. It is possible to increase strength of these structural members even after these have been severely damaged due to loading conditions.

For strengthening beams, two techniques are adopted.

First one is to apply FRP plates to the bottom of a beam. This increases the flexural strength of beam, deflection capacity of beam and stiffness.

Alternately, FRP strips can be apply in 'U' shape around the sides and bottom of a beam, resulting in higher shear resistance.

Columns in building can be wrapped with FRP for achieving higher strength. This is called wrapping of columns and the technique works by restraining the lateral expansion of the column.

Carbon fiber reinforced polymer composite have been extensively used for increasing the stiffness and load-carrying capacity of existing brick masonry columns.

The FRP is used as supplementary reinforcement which determines an increase of the cross-sectional ultimate capacity.

The increase in the stiffness of the structural element for a given amount of FRP depends upon the stresses generated in the FRP. [4]

CHAPTER 1

BACKGROUND

C H A P T E R 1

BACKGROUND

1.1. Brick Masonry Buildings

Masonry structures in need of intervention through strengthening constitute a significant portion of the building stock throughout the world, as either they have suffered from the accumulated effects of inadequate construction techniques and materials, seismic and wind loads, foundation settlements, and environmental deterioration, or they need to be upgraded to meet more stringent seismic design requirements, often combined with change in use.

Bricks were first fired around 3500 BC, in Mesopotamia, present-day Iraq, one of the high-risk seismic areas of the world.

From Roman aqueducts and public buildings to the Great Wall of China, from the domes of Islamic architecture to the early railway arch bridges, from the first 19th century American tall buildings to the 20th century nuclear power plants, bricks have been used as structural material in all applications of building and civil engineering.

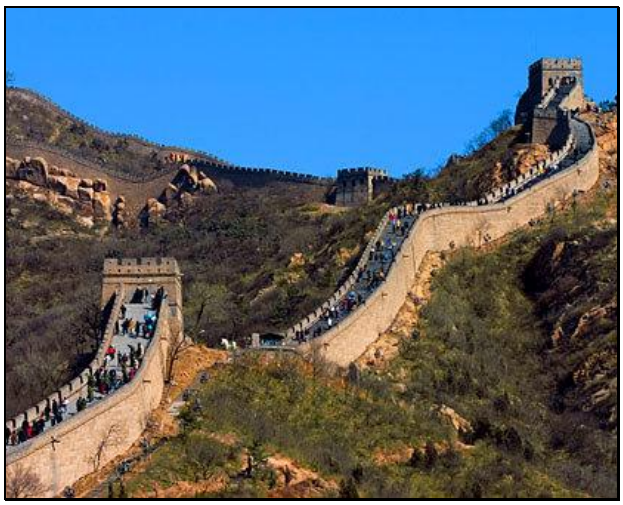

Fig. 1.1 – Great wall of China

The most commonplace use of bricks worldwide throughout time is in residential dwellings.

The shape and size of bricks can vary considerably, and similarly the mortars used depend on local material availability, but the basic form of construction for houses has minor geographical variations and has changed relatively little over time.

Actually the brick or stone buildings hide a steel support that does the structure work. Before steel was used to create rigid frames, buildings relied on the load-bearing capacity of that incredibly thick solid materials. This amazing structure has walls at its base up to 7 meters thick to hold the weight. Due to the cost of doing so, no designer has even tried to exceed the height of this towering structure in stone or brick in over a century.

Fig. 1.2 – Philadelphia city hall

At 167 meters high, the Philadelphia City Hall was the tallest skyscraper in the world when it was constructed and today it still holds the title of tallest load-bearing structure on the planet.

The building took 30 years and 24 million dollars to complete. It was also the first non-religious structure to hold the record for the world's tallest building.

Fig. 1.3 – Historical picture of Philadelphia city hall

Before elevators the pricing and desirability of living on upper versus lower floors was actually reversed. People were loathe to travel up many flights of stairs multiple times a day so it was often the top rooms with the best views overlooking a city that were left to starving artists and others of lesser means.

With frame and cladding building techniques the paradigm reversed itself and forever gone were the days of tall masonry building and cheap living with a view out over the top of the built environment.

The advantages of masonry construction can be summaries in:

- The use of materials such as brick and stone can increase the thermal mass of a building, giving increased comfort in the heat of summer and the cold of winter, and can be ideal for passive solar applications.
- Masonry units are available in a rainbow of colors, textures, shapes, and sizes, offering building designers the chance to create structural

walls that are also beautiful. Architectural masonry units offer a natural appearance that is striking in urban applications, and blends in with the natural beauty of rural areas always complementing the building's surrounding environment.

- Brick typically will not require painting and so can provide a structure with reduced life-cycle costs, although sealing appropriately will reduce potential spalling due to frost damage.
- The appearance, especially when well crafted, can impart an impression of solidity and permanence.

Fig. 1.4 – appearance of a brick masonry building

- Masonry is very heat resistant and thus provides good fire protection.
- Masonry walls are more resistant to projectiles, such as debris from hurricanes or tornadoes than walls of wood or other softer, less dense materials.

When it comes to fire resistance, masonry is a true performer, offering excellent protection from fire damage. In fact, post-9/11 research performed on a building in close proximity to the World Trade Center

showed that masonry absorbed much of the debris impact and helped save the structure from collapsing.

The disadvantages of masonry construction can be summaries in:

- Extreme weather causes degradation of masonry wall surfaces due to frost damage. This type of damage is common with certain types of brick, though rare with concrete block. If clay brick is to be used, care should be taken to select bricks suitable for the climate in question.
- Masonry tends to be heavy and must be built upon a strong foundation, usually reinforced concrete, to avoid settling and cracking. If expansive soils, such as adobe clay, are present this foundation needs to be quite elaborate and the services of a qualified structural engineer may be required, particularly in earthquake prone regions.

The worst death toll from an earthquake in the past century occurred in 1976 in China, it is estimated that 240,000 people were killed. Most of the deaths were due to the collapse of brick masonry buildings.

In more recent times, seismic codes place substantial constraints on unreinforced brick masonry construction in earthquakes areas, limiting the allowed number of stories, the minimum thickness of walls, and the number and position of openings.

As a result, construction of load-bearing unreinforced brick masonry structures has dwindled in these countries, and alternative forms of construction such as confined masonry or reinforced masonry, considered less vulnerable, have been developed instead.

Examples of this construction typology range from Colombia to Kazakistan, from India to Italy.

Fig. 1.5 – Example of an old masonry building in Italy

Masonry is an assembly of brick units bonded together with mortar. While brick size can vary considerably depending on the quality of the clay and the manufacturing tradition, the basic firing technology is common worldwide.

Variations of typology are very limited. The major factors influencing the strength of the bricks are the purity of the clay and the firing temperature.

Mortars are subject to greater variation, but the basic materials used in mortar mixes are sand, water, and one or more of the bonding agents, mud, clay, or cement, depending on local availability.

The proportion of bonding agent/s to sand determines the compressive and bonding strength of the mortar.

In earthquakes areas, the development of an effective level of bonding between mortar and bricks is essential to resist shear-cracking.

Bricks might be frogged or specially shaped to create mechanical interlocking and improve bonding.

Brick construction is relatively simple and cheap. In certain cases bricklaying may require highly skilled labor; however, this type of construction is usually performed by small building contractors.

From an architectural point of view, brick construction is rather flexible, allowing substantial freedom in the layout of internal spaces and the distribution of openings, making it quite adaptable to different climatic conditions.

Fig. 1.6 – Example of modern masonry construction

From an environmental and structural point of view, masonry performance depends on the performance of mortar and brick units, and their composite behavior.

Modern building codes provide guidelines for the preferred combinations of mortar mixes and brick units in order to optimize both the strength and the environmental performance of the wall assemblages made of these components.

The structural performance of brick masonry buildings depends on the following types of connections within masonry elements:

- Integrity and shear resistance of brick masonry walls is influenced by the extent and quality of bond between mortar and bricks. It is essential for the brickwork to be properly constructed to allow for the best possible level of bonding to develop. It is also important to ensure repointing of bed and head joints at regular time intervals so as to ensure the maximum possible surface of contact.
- The second level of connection is among the wythes of brick walls. Modern masonry construction standards require regularly spaced ties between the wythes of a cavity wall to ensure monolithic behavior and redistribution between the wall wythes. In historic

masonry construction it is common for the walls to be either one or two-rick-wide solid brick, or to consist of two external withes with a cavity filled with rubble.

- The third level of connection is among the walls at the corners and junctions and depends on the specific fabric of corner returns. Such connections ensure 3-D behavior of the masonry box-like structure and the redistribution of lateral forces among walls.
- The forth level of connection is between the walls and the horizontal structures, this connection highly influences the seismic performance of the building.

In proportion to its widespread presence worldwide, there are many examples of brick masonry performance in past earthquakes. The extent of damage depends on the seismic hazard and the earthquake intensity at a particular site.

Evidence from recent earthquakes has confirmed that the overall performance of brick masonry buildings is dependent on the type of roof system: buildings with lightweight roofs suffered relatively less damage while buildings with reinforced concrete roofs suffered much greater damage.

This is in line with the evidence collected after the 1997 Umbria-Marche earthquake, where many buildings with heavy reinforced concrete roofs suffered substantial structural damage and partial collapse.

Fig. 1.7 – Collapsed masonry building in Italy

It can be observed that the seismic performance rating for brick masonry buildings is fairly homogenous worldwide.

1.2. Previous Researches on FRP-Reinforced Masonry

In the past decade or so, traditional strengthening techniques for masonry have been supplemented with the Fiber-Reinforced Polymer strengthening technique, which involves epoxy bonding of strips or sheets, mainly in the direction of principal tensile stresses.

Fig. 1.8 – Wrapped column

Studies on the use of FRP as a strengthening material for masonry have been numerous. Detailed concepts and analytical results on the applicability and effectiveness of FRP tendons used to apply circumferential prestressing to historic masonry structures were developed first by Triantafillou and Fardis (1993, 1997).

A study on the use of epoxy-bonded Carbon Fiber-Reinforced Polymer strips as seismic strengthening elements of masonry was performed by Schwegler (1994), who demonstrated the effectiveness of this technique through full-scale in-plane and out of-plane cyclic testing of one-story masonry walls and developed an analytical model for the in-plane behavior of CFRP strengthened walls within the framework of stress fields theory.

The work reported by Ehsani et al. (1995~1997) focused on in-plane shear testing of unreinforced masonry specimens strengthened with epoxy-bonded glass fabrics.

A similar concept involving epoxy-bonded carbon overlays was studied by Laursen et al. (1995) and Seible et al. (1995), who performed cyclic tests on approximately half-scale masonry wall panels and on a full-scale masonry building and proved that such overlays are highly effective in increasing the strength, reducing the shear deformations, and improving the overall structural ductility.

Detailed design equations and interaction diagrams for FRP-strengthened masonry under out-of-plane bending, in-plane shear, and in-plane bending, all combined with axial load, were developed by Triantafillou et al. (1998).

Experimental studies performed on masonry walls subjected to monotonic by Albert et al. (2001); Hamilton and Dolan (2001) and cyclic by Ehsani et al. (1999); Velazquez-Dimas and Ehsani (2000); Kuzik et al. (2003) out-of-plane loading, demonstrated the effectiveness of vertically placed glass fiber reinforced polymer strips.

The effectiveness of this system was also confirmed by Paquette et al. (2001) through shake table testing.

Similar studies were conducted by Hamoush et al. (2001) on walls strengthened with overlays covering the full tensile zone, as well as with vertical and horizontal stripes, and confirmed the effectiveness of the FRP systems as out-of-plane flexural strengthening elements. Tumialan et al. (2001) investigated the in-plane shear response of masonry walls strengthened with GFRP rods embedded into epoxy-based paste near the surface, at the locations of bed joints.

Recently the in-plane response of FRP-strengthened masonry has received a bit more attention than in past years: failure modes associated with in-plane response of masonry buildings and global response were analyzed by Moon et al. (2002) through pushover analysis; shake table testing of single

masonry walls strengthened on one side with GFRP fabrics or vertical CFRP strips was performed by Badoux et al. (2002); cyclic loading of walls strengthened with vertical and horizontal GFRP or CFRP strips were conducted by Fam et al. (2002) and Marcari et al. (2003), supporting the effectiveness of this system; damage mechanisms of walls strengthened with CFRP strips under cyclic loading were studied by Gu et al. (2003); coupon-size masonry panels were tested in diagonal compression to simulate in-plane shear by Valuzzi et al. (2002) and Russo et al. (2003); and a strut-and-tie modeling methodology for the determination of optimum location and dimensioning of the FRP strips was developed by Krevaikas and Triantafillou (2005).

In another field of application, epoxy-bonded CFRP strips have been bonded to the extrados of vaults and arches, thus providing increased capacity against lateral loads, Borri et al. (2000); Faccio and Foraboschi (2000).

The range of applicability of FRP has been extended to blast-loaded masonry by Muszynski and Purcell (2003), Patoary and Tan (2003), and Crawford and Morrill (2003), where it was proved that flexible, easy-to-apply glass, carbon, or hybrid glass/aramid fabrics offer interesting solutions.

The above survey of the literature reveals that the application of FRP as a means of increasing the axial capacity of masonry, for example, through confinement, has not been explored, except in Triantafillou and Fardis (1993, 1997), through the introduction of external prestressing, and Valuzzi et al. (2003), through the use of horizontally placed near-surface-mounted FRP strips. [5]

The great potential of FRP confinement and the need to develop effective methods of masonry confinement as a means of preventing catastrophic failures through FRP wrapping was studied by Krevaikas and Triantafillou (2005).

The gap that the writer intends to fill with this study, through experimental developments, is to understand how the behavior of brick masonry will be improved by the FRCM-wrapping.

This will be done using the axial compression test with the Digital Image Correlation.

1.3. Experimental Program

In this chapter all the experimental test procedures will be explained in detail. This dissertation presents an experimental investigation on the behavior of axially loaded masonry columns confined with FRCM-reinforcement.

In order to understand how the behavior of brick masonry will be improved by the FRCM-wrapping, compression test were carried on 6 bricks columns, at the beginning unwrapped and then with the FRCM-reinforcement.

A total of 6 brick masonry columns were prepared using clay bricks bonded together with a premixed mortar.

Every material was singly tested for the characterizations.

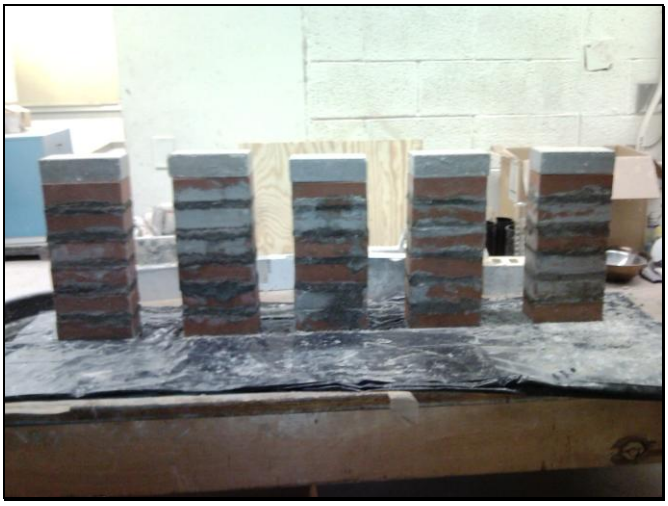

Fig. 1.9 – Brick masonry specimens

1.3.1. Material characterization

Materials characterization was carried out to investigate the mechanical properties of the materials involved in the experimental program.

Masonry columns were prepared using clay bricks with dimensions of 90 mm width, 200 mm length and 55 mm height, figure 1.10, bonded together.

Fig. 1.10 – Brick

The cross-sectional area of the specimens was 200 x 90 mm and 380 mm height.

Each model column is composed of 6 bricks with 5 mortar joints, as shown in figure 1.11.

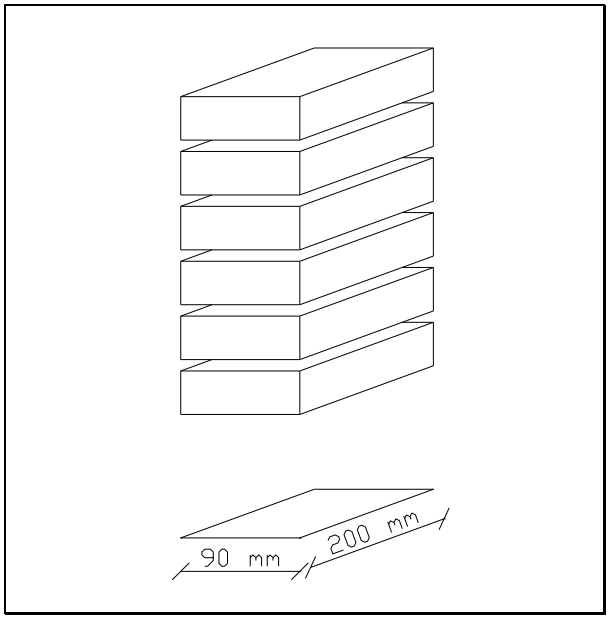

Fig. 1.11 – Model column

The thickness of mortar was, in general, 10 mm.

For the wrapped specimens the corners were rounded using a grinding machine with a radius of 10 mm, figure 1.12.

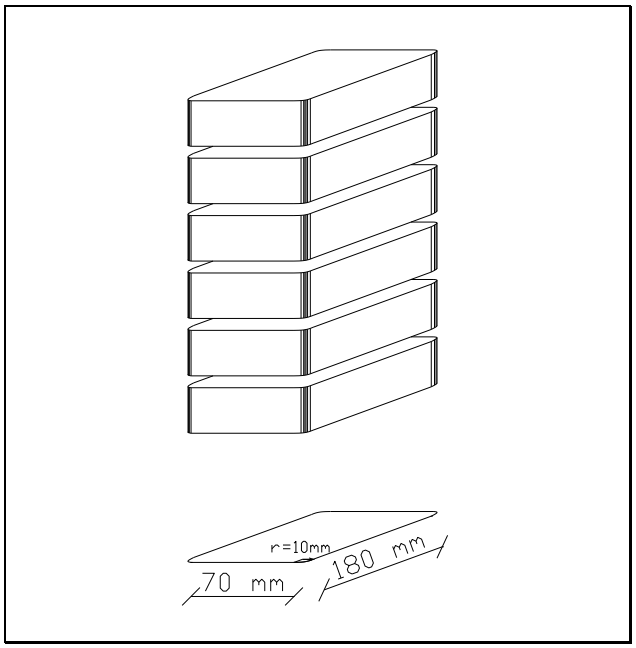

Fig. 1.12 – Model column with rounded corners

Specimens were wrapped with one layers of Fiber Reinforced Cementitious Matrix, an high performance fiber structural reinforcement systems.

The RUREDIL X MESH GOLD^{TM} system consists of a Polyparaphenylene benzobisoxazole mesh and a stabilized inorganic matrix designed to connect the mesh with the substrate, RUREDIL X MESH M750^{TM}.

Its mechanical performance allows this composite material to equal the performance of conventional carbon fiber FRP's with epoxy binders.

This system is suitable for reinforcement of masonry, reinforced concrete and precompressed reinforced concrete structures, including those subject to the simultaneous action of fire and high temperatures.

It's used as reinforcement for:

- Flexural reinforcement;
- Shear strength;
- Torsion reinforcement;
- Confinement and longitudinal reinforcement of beam columns with eccentricity.

It's suitable for work in seismic zones for:

- Increasing resistance to simple flex fatigue or combined pressing and bending action of pillars and beams;
- Increasing resistance to shear stress of pillars and beams;
- Increasing the flexibility of the terminal portions of beams and pillars by binding;
- Increasing the resistance to tensile stress of the panels of beam-pillar nodes with fibers aligned with tensile stress.

The product is a roll of PBO fiber mesh 100 cm wide and 15 m long, figure 1.13.

Fig. 1.13 – Roll of PBO fiber mesh

This inorganic matrix used, if compared to a system employing epoxy or polyester resins, offers the following benefits:

- Same resistance to high temperatures as substrate, when the outdoor temperature exceeds the glassy transition temperature, the epoxy resin is no longer capable of serving the function of transferring stress from the structure to the high modulus fiber buried in it, making it ineffective as structural reinforcement. This behavior is attributable to total loss of the adhesive bond between the resin and the fiber and/or between the resin and the support. This system is not influenced by outdoor temperature after it hardens, and is fire-resistant because it is inorganic, like the base.
- The adhesion to the surface is not affected by relative humidity, unlike FRP systems. Epoxy resin degrades with prolonged

exposure to moisture, losing its adhesive properties and therefore its ability to transfer stress to structural fiber.

- FRP classic systems can only be applied to dry substrates, as polyester and epoxy resins will not catalyze in the presence of water.
- It is not toxic like the resins used in FRPs. It's applied under ordinary working conditions applicable to cement mortars.

This product increase load according to temperature, figure 1.14. [20]

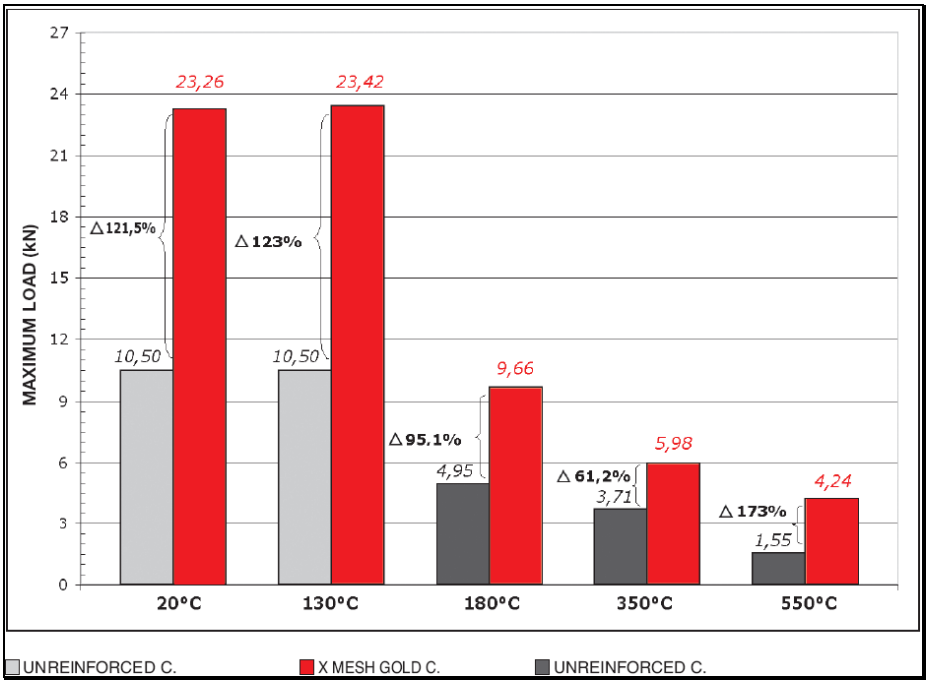

Fig. 1.14 – Load increase according to temperature [20]

In fact, traditional FRP systems completely lose their mechanical properties after one hour of exposure to +80°C because rigid resin becomes gummy. Resin becomes unable to transfer concrete stress to carbon fiber from +45°C.

The RUREDIL X MESH GOLD™ have an equivalent dry fabric thickness in the direction of the warp of 0,0455 mm, and an equivalent dry fabric thickness in the direction of the weft of 0,0115 mm.
The following properties for the PBO fibers, average values, were provided by the supplier: ultimate tensile stress of the warp per unit of width is 264 kN/m and ultimate tensile stress of the weft per unit of width is 66,5 kN/m, the elastic modulus is 270 GPa. [20]
The inorganic matrix, RUREDIL X MESH M750™, has a compressive strength equal or superior to 15 MPa after 28 days, figure 1.15.

Fig. 1.15 – Inorganic matrix

Materials characterization included tests of bricks and mortar specimens.
A commercially available mortar premixed, which was certified to provide a final product meeting the requirements of ASTM C270, was used, figure 1.16.

Fig. 1.16 – Mortar

Three mortar cylinders 150 mm × 75 mm diameter (L/D=2) were cast from the same batch used to cast the specimens used for the tests, figure 1.17.

Fig. 1.17 – Mortar cylinders

Mortar and masonry specimens were demolded 24 hours after casting and subjected to curing at 99% RH until tested.

Fig. 1.18 – Curing room

Cylinders were tested for ultimate strength and elastic modulus using the clip-gauge, is a type of electrical transformer used for measuring linear displacement., figure 1.19.

Fig. 1.19 – Cylinder under axial compression test

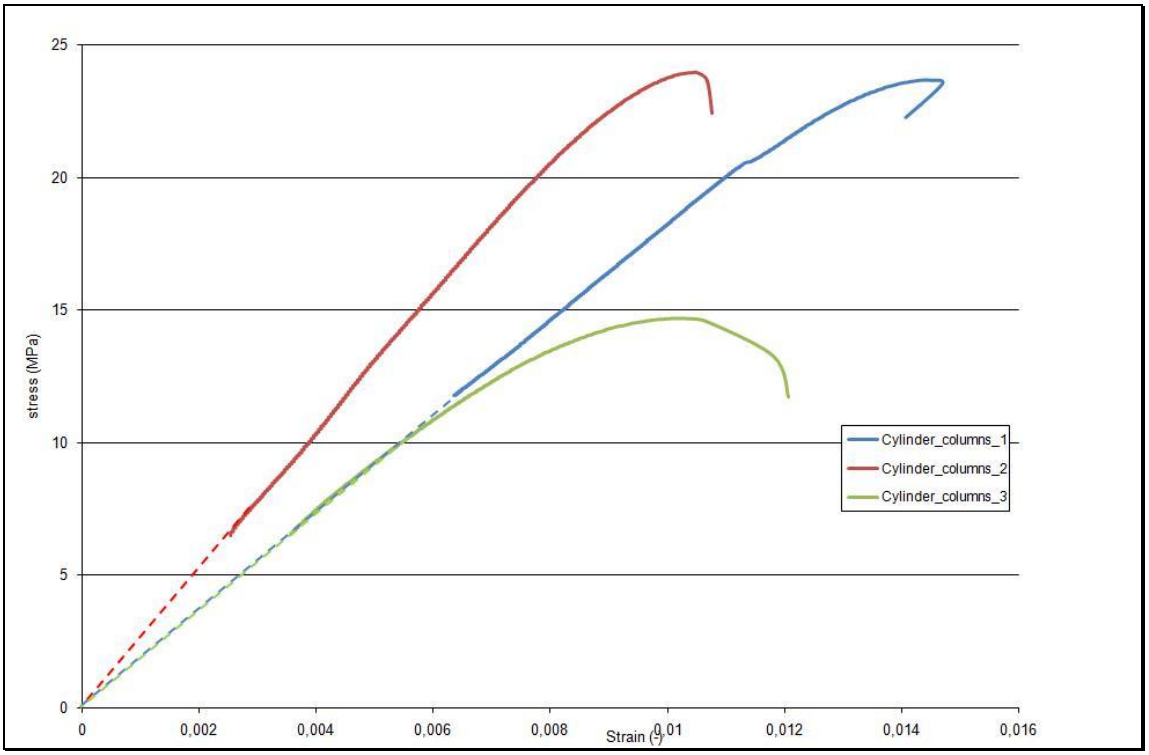

Fig. 1.20 – Stress–strain diagram of mortar cylinders

Specimens notation	**5 precycle (kN)**	**Area (cm^2)**	**Compressive strenght (MPa)**	**Elastic modulus (MPa)**
1	5-27	44,16	23,69	1780
2	5-27	44,16	23,96	2580
3	5-27	44,16	14,69	1785
Load control mode of 1.5 kips/min, about 7 kN/min				

Tab. 1.1 – Summary of test results for mortar cylinder

The average values of the elastic modulus and compression strength for mortar were determined to be 2050 MPa and 20,8 MPa, respectively.

Fig. 1.21 – Failure of cylinder specimens

Three brick were tested for ultimate strength and elastic modulus using the Digital Image Correlation, figure 1.22.

Fig. 1.22 – Brick specimens ready for the DIC

The load was applied parallel to the direction along which bricks are normally loaded on 3 half brick specimens.

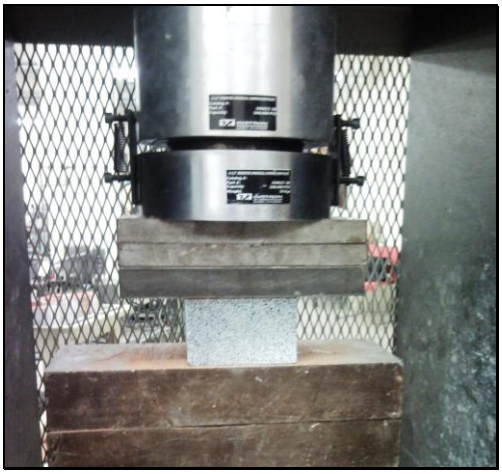

Fig. 1.23 – Brick specimen ready for the test

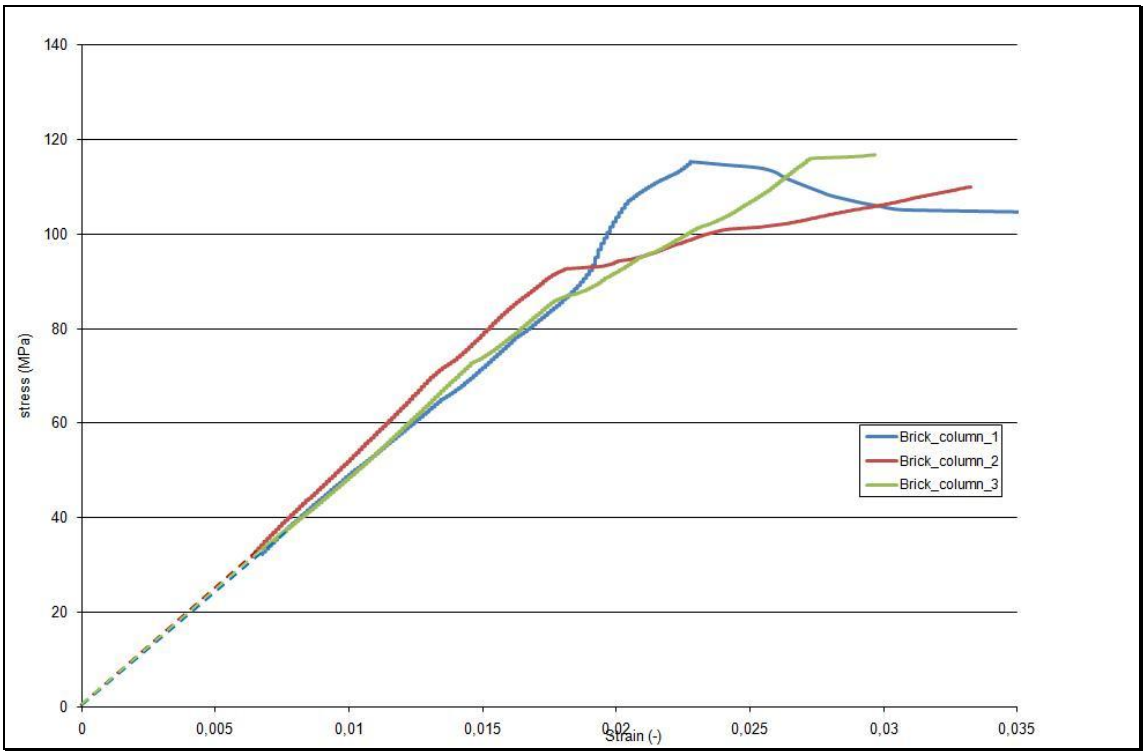

Fig. 1.24 – Stress–strain diagram of brick specimens

Specimens notation	3 precycle (kN)	Area (cm^2)	Compressive strenght (MPa)	Elastic modulus (MPa)
1	130-265	90	115,46	4730
2	130-265	90	92,00	5362
3	130-265	90	114,80	4886
Load control mode of 10 kips/min, about 45 kN/min				

Tab. 1.2 – Summary of test results for brick specimens

The average values of the elastic modulus and compression strength for brick were determined to be 4990 MPa and 107.42 MPa, respectively.
In the next table there is a summary of all the material characterization.

Fig. 1.25 – Failure of brick specimens

Material	Specimen	Properties
Brick	100 x 90 x 55mm	elastic modulus: 4990 MPa; compression strength: 107,42 MPa.
Mortar	Cylinders 150 × 75 mm	elastic modulus: 2050 MPa; compression strength: 20,78 MPa.
Fiber-Reinforced Cementitious Matrix	Supplier	elastic modulus: 270 GPa; tensile stress of the warp per unit of width: 264 kN/m; tensile stress of the weft per unit of width: 66,5 kN/m.

Tab. 1.3 – Material characterization

1.3.2. Experimental test setup

For each test, the surface strains in the FRCM composite and the masonry were obtained using the digital image correlation, DIC technique. DIC is a data analysis procedure that uses the mathematical correlation method to analyze digital images of a specimen undergoing deformation. This technique offers the advantage of obtaining spatially continuous measurements of displacements.

All the specimens need a smooth surface for the digital image correlation. The surface preparation for the specimen consisted of creating a random, sprayed-on speckle pattern, obtained by spraying the FRCM and the masonry surfaces with white paint followed by a mist of black paint, figure 1.26.

Fig. 1.26 – Masonry ready for test

The test setup for DIC measurements comprised a high-resolution digital camera, 1280x1024 pixels, which was interfaced with a computer using an image acquisition board, figure 1.27.

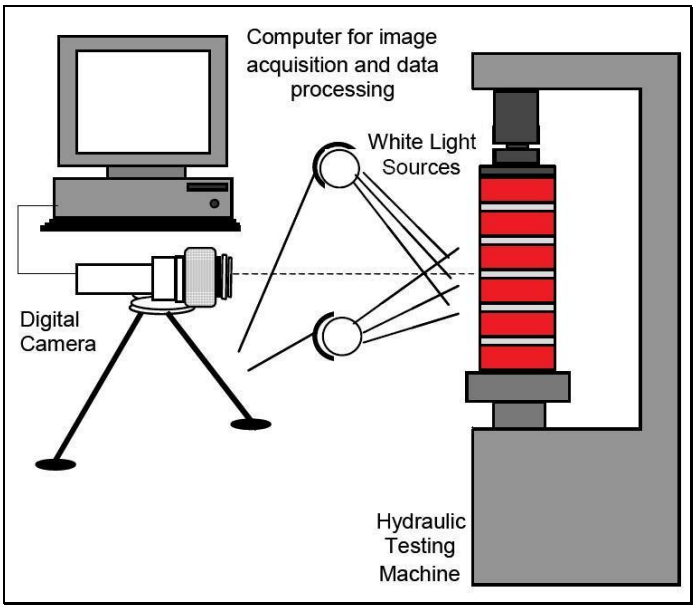

Fig. 1.27 – Digital image correlation setup

The specimen was illuminated using normal white light to provide uniform light intensity across the surface. The camera was placed perpendicular to the specimen surface. A reference image was recorded prior to the start of the loading procedure.

The field of view captured in the digital image was 250 x 200 mm. Digital images were recorded, at regular intervals during each test and stored in the computer for later analysis.

The correlation between the deformed images and the undeformed reference image was used to obtain a two-dimensional displacement field for all points on the specimen surface. The displacement fields were computed through a correlation of gray levels between the reference image and the images of the specimen undergoing deformation using the commercially available software, Vic 2D.

The image displacement accuracy was determined to be equal to 0.005 pixels.

The strain fields were calculated from the gradients of a set of displacements.

Prior to testing, 3 loading cycles were performed to stabilize the specimen.

Fig. 1.28 – Axial compression test ready

CHAPTER 2

BRICK MASONRY COLUMNS

C H A P T E R 2

BRICK MASONRY COLUMNS

2.1. Axial Compression Test

A compression test is typically used to determine the behavior of materials under axial loads. The specimen is compressed and deformation at various loads is recorded. Compressive stress and strain are calculated and plotted as a stress-strain diagram.

Graph of stress as a function of strain can be constructed from data obtained in any mechanical test where load is applied to a material, and continuous measurements of stress and strain are made simultaneously. It is constructed for compression, tension and torsion tests, figure 2.1.

In particular the test of this dissertation foresees the use of the digital image correlation to appraise the deformations.

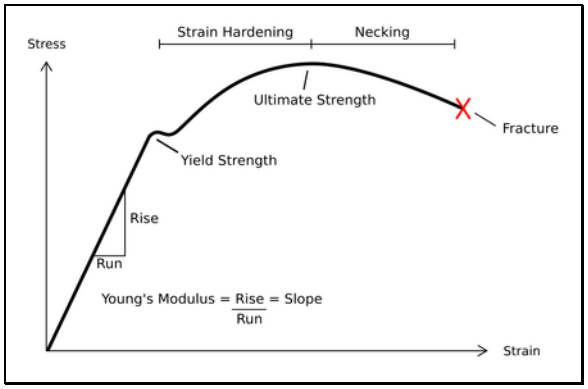

Fig. 2.1 – Stress–strain diagram

Axial compression testing is a useful procedure for measuring the plastic flow behavior and ductile fracture limits of a material. Measuring the plastic flow behavior requires frictionless, homogenous compression, test conditions, while measuring ductile fracture limits takes advantage of the

barrel formation and controlled stress and strain conditions at the equator of the barreled surface when compression is carried out with friction.

Axial compression testing is also useful for measurement of elastic and compressive fracture properties of brittle materials or low-ductility materials.

In any case, the use of specimens having large *L/D* ratios should be avoided to prevent buckling and shearing modes of deformation.

The main objective of testing is to record the axial stress-strain curve and the failure mode of all the masonry specimens, which are subjected to axial loading applied monotonically under a loading control mode in a compression testing machine of 500 kips capacity, about 2,200 kN.

Fig. 2.2 – Masonry ready for the test

Spatially continuous measurements of displacements are obtained using the Digital Image Correlation after the tests.

The specimens were manufactured using clay bricks and mortar.

All the tests exhibited a relatively high degree of consistency, and confirmed the material characterization initially made.

2.1.1. Experimental result and failure mode

The main results of the tests are presented in the table 2.1.

Specimens notation	3 precycle (kN)	Maximum load (kN)	Area (cm^2)	Compressive strenght (MPa)	Ultimate machine strain ε
1	20-90	800,11	180	44,09	0,0067
2	20-90	728,25	180	40,13	0,0062
3	20-90	432,38	180	24,65	0,0038
Load control mode of 5 Kips/min, about 22 kN/min					

Tab. 2.1 – Summary of test results for columns unwrapped

The stress-strain diagrams for the unwrapped specimens are presented in figure 2.3.

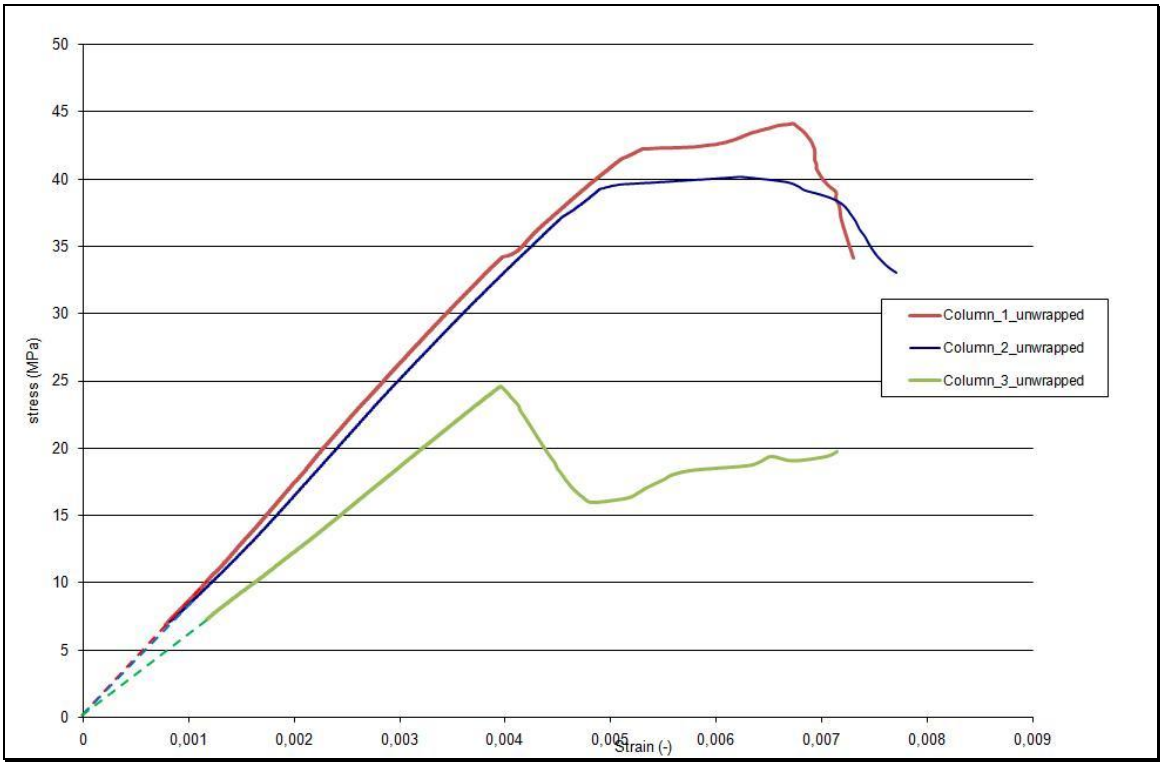

Fig. 2.3 – Stress–strain diagram of unwrapped columns

It can be observed that in all cases the diagrams are linear up to about 80% of the maximum load.

The control specimens failed in a brittle manner by the formation of vertical cracks through the joints and the bricks, it can be seen in the picture of the digital image correlation.

Fig. 2.4 – Specimen failure

After their formation through mortar joints and bricks, vertical cracks became increasingly wide and the masonry between the cracks was crushed.

The crash happens along the minor inertia direction, for rectangular cross sections we can see in the specimens an almost perfect cracking in the middle of the masonry thin side, figure 2.5.

Fig. 2.5 – Masonry crushed

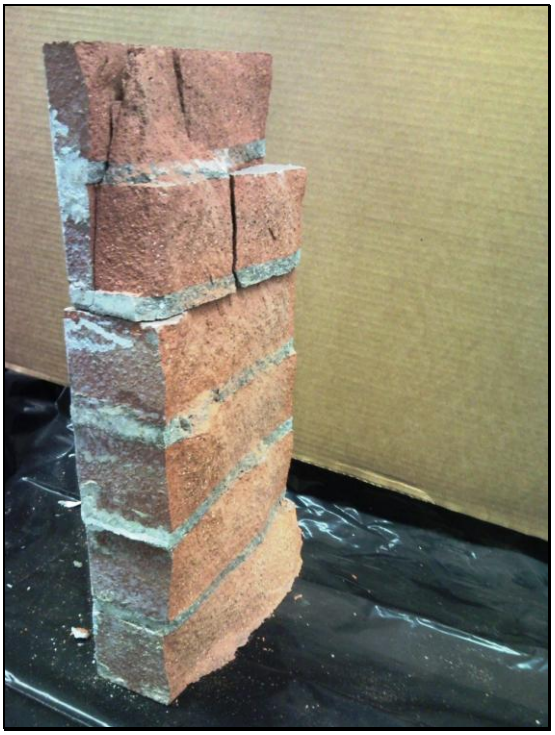

Fig. 2.6 – Masonry crushed

2.1.1.1. Column unwrapped 1

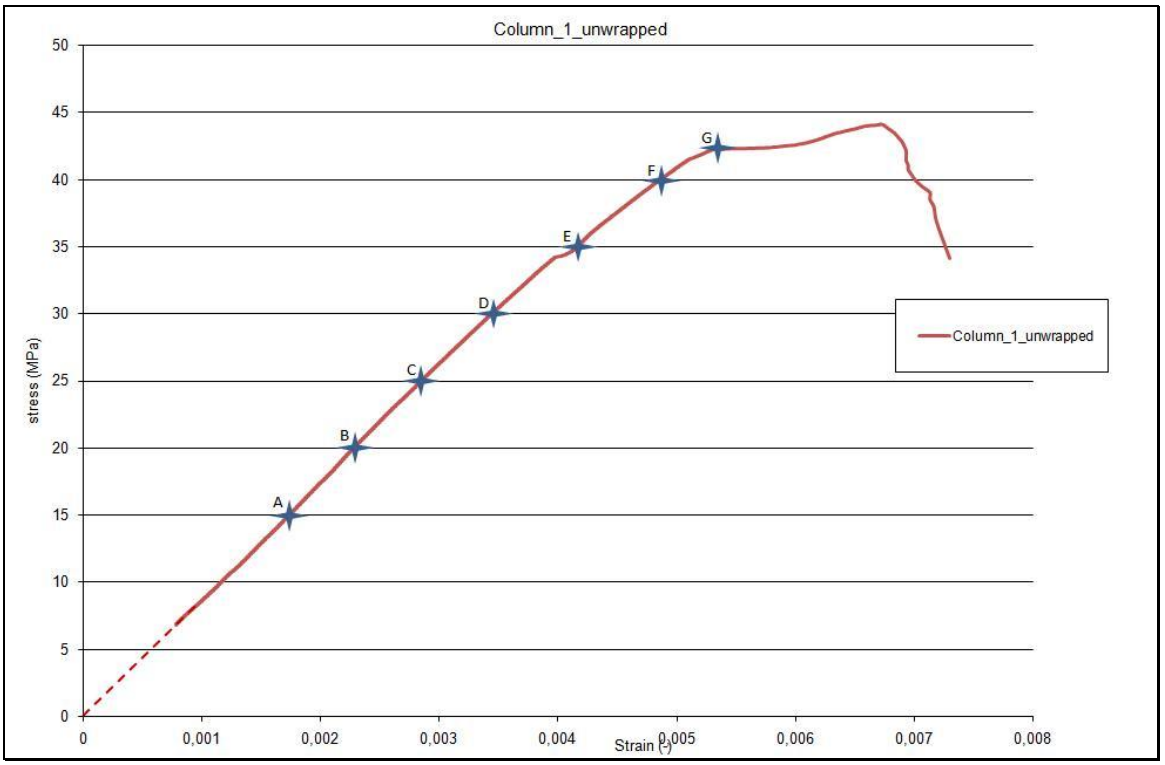

Fig. 2.7 – Stress–strain diagram of column unwrapped 1

The contour plots of ε_{xx} , ε_{yy} and the correlation factor for all the points in figure are reported below.

- A: 60.04 kips; 14,72 MPa

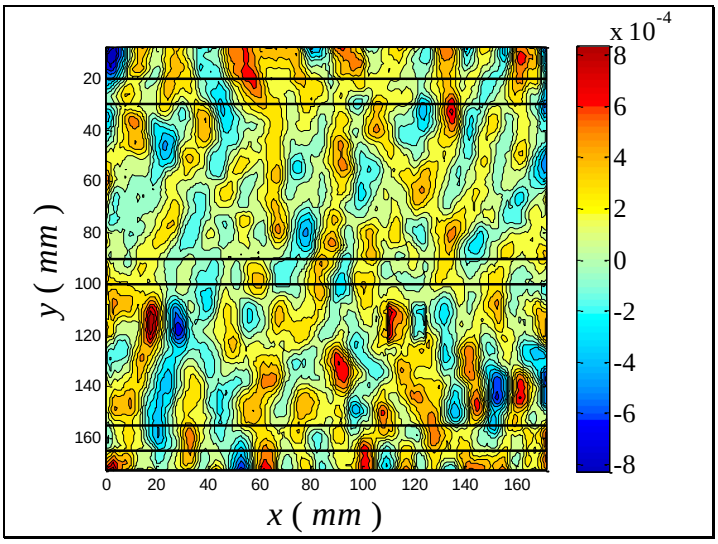

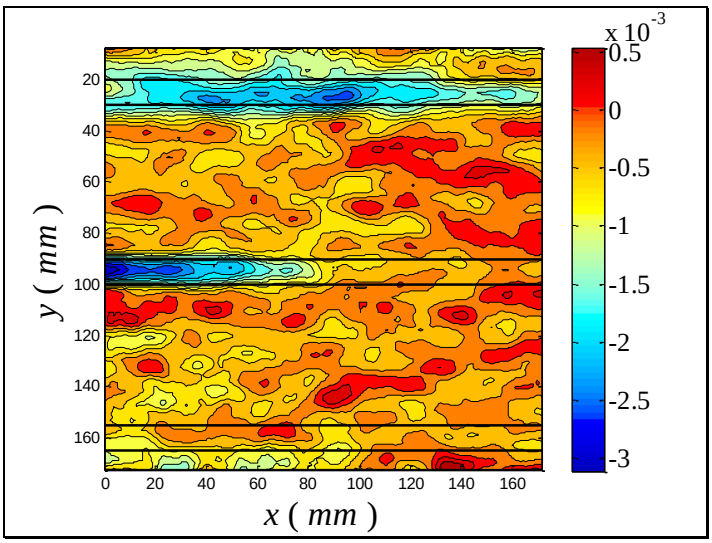

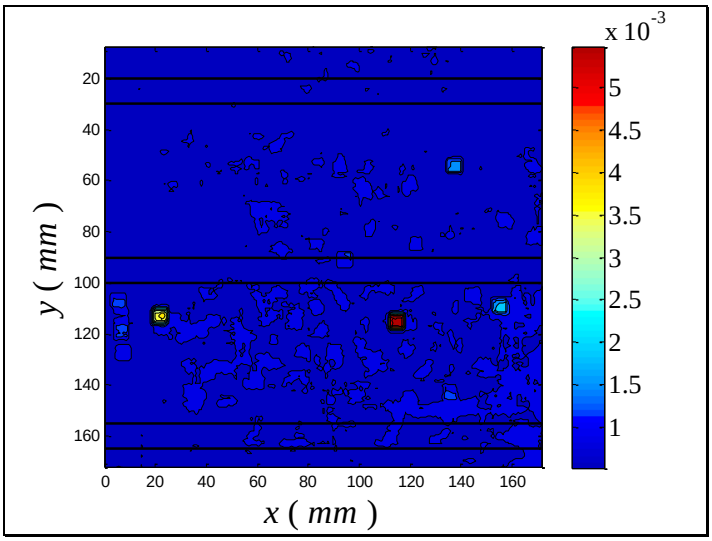

- B: 80.05 kips; 19,62 MPa

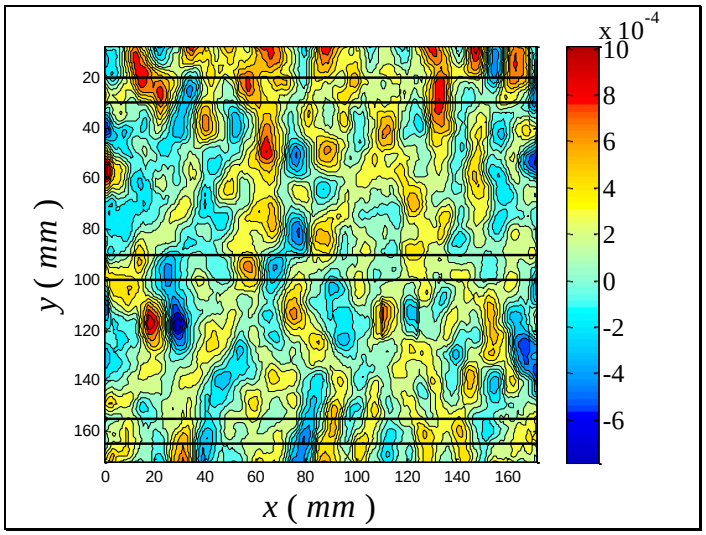

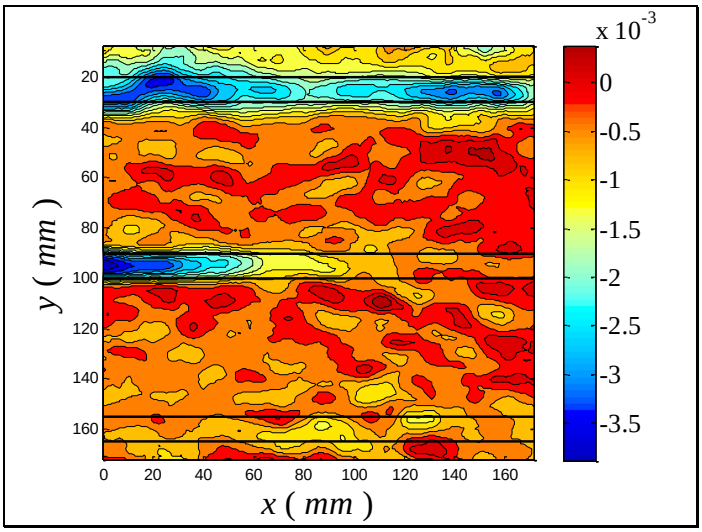

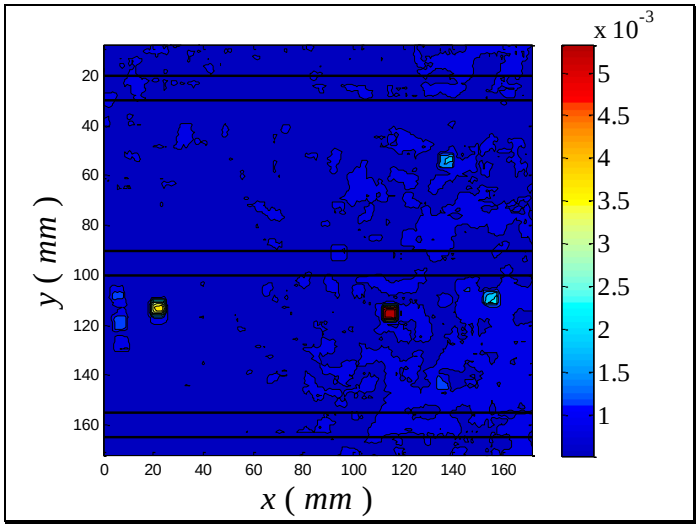

- C: 99.83 kips; 24,47 MPa

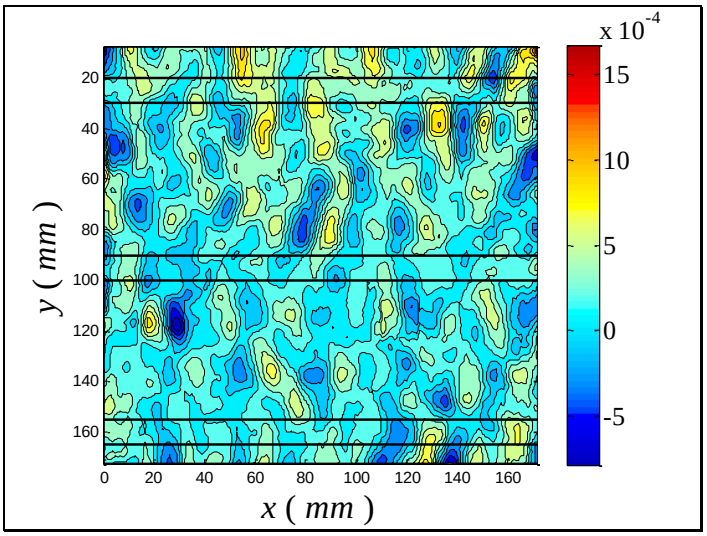

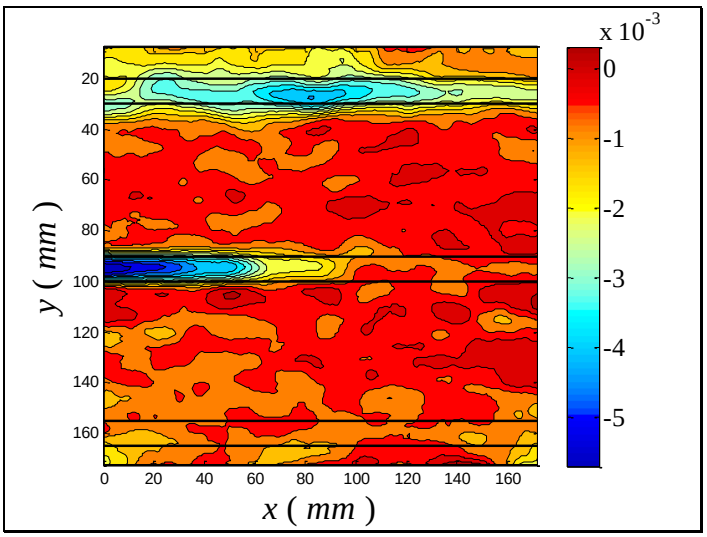

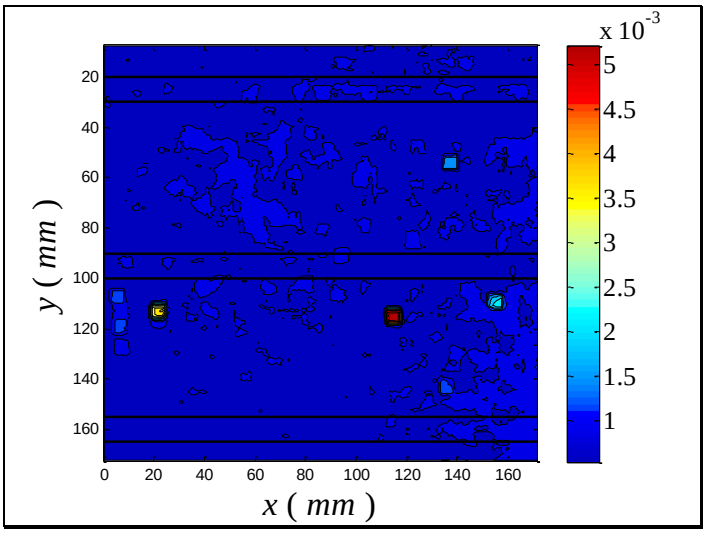

- D: 120.00 kips; 29,41 MPa

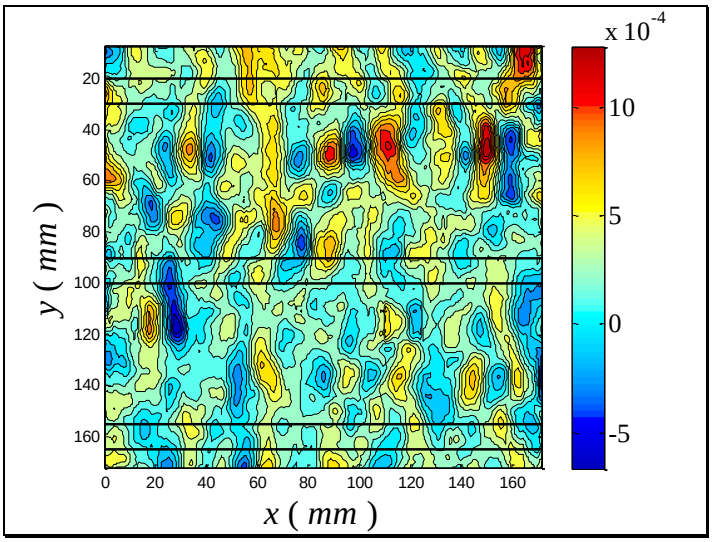

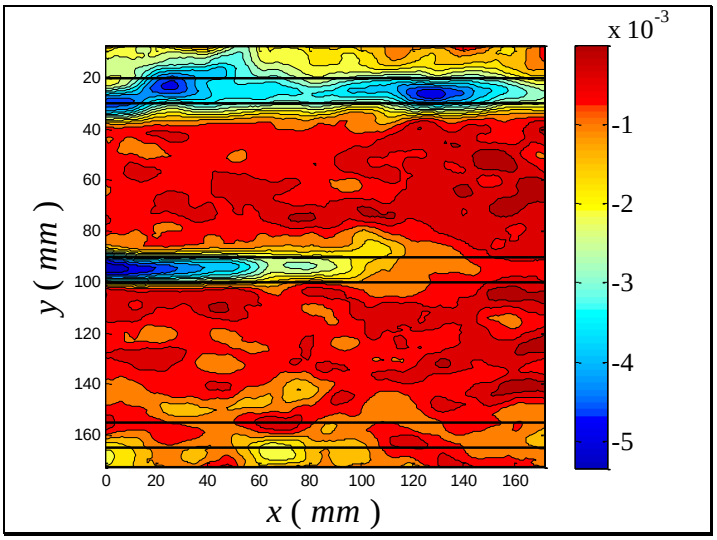

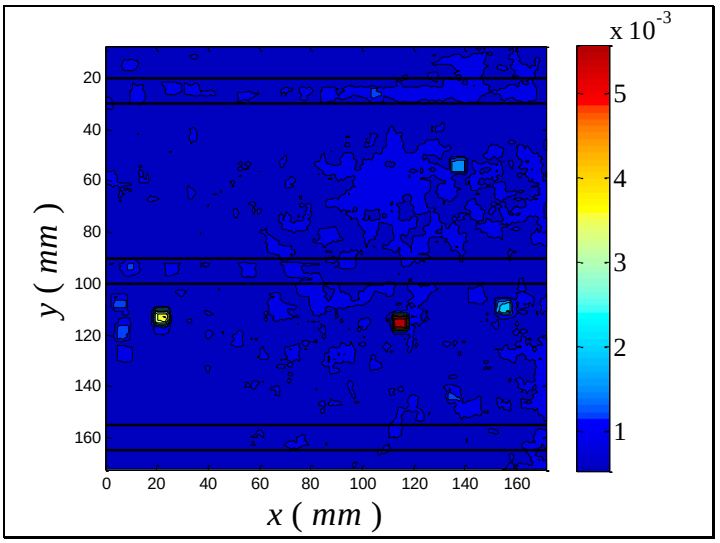

- E: 140.00 kips; 34,32 MPa

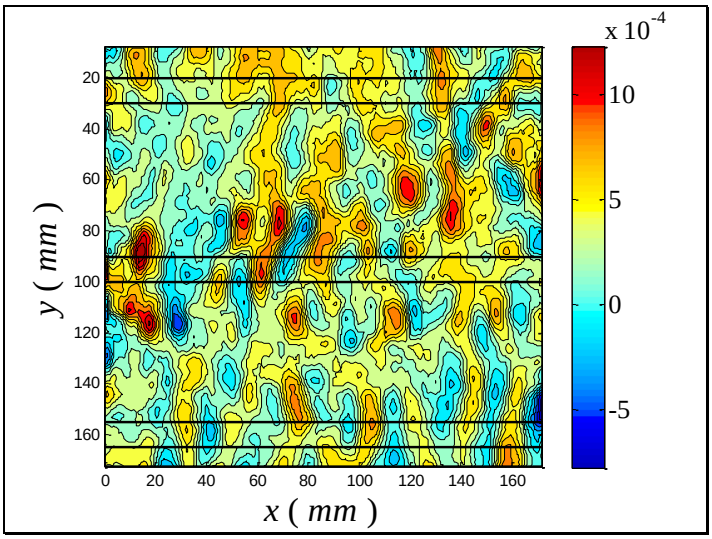

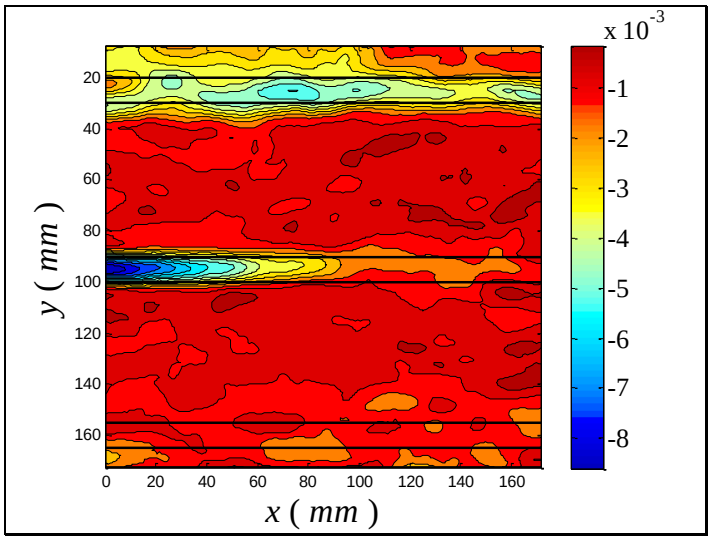

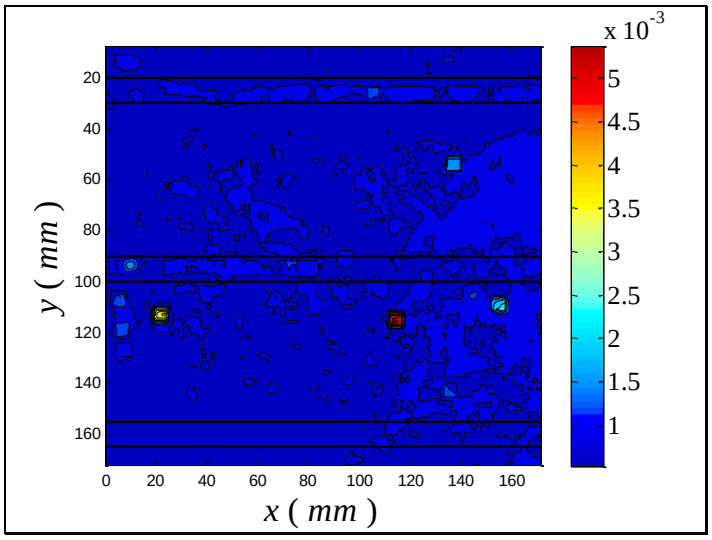

- F: 159.00 kips; 38,98 MPa

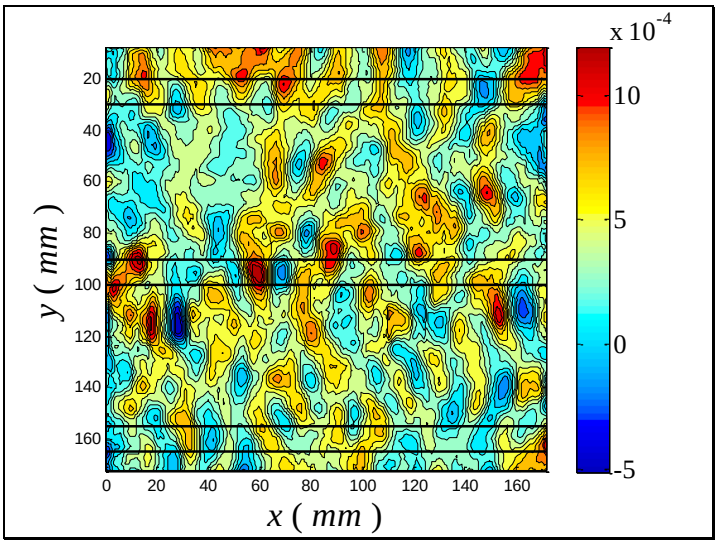

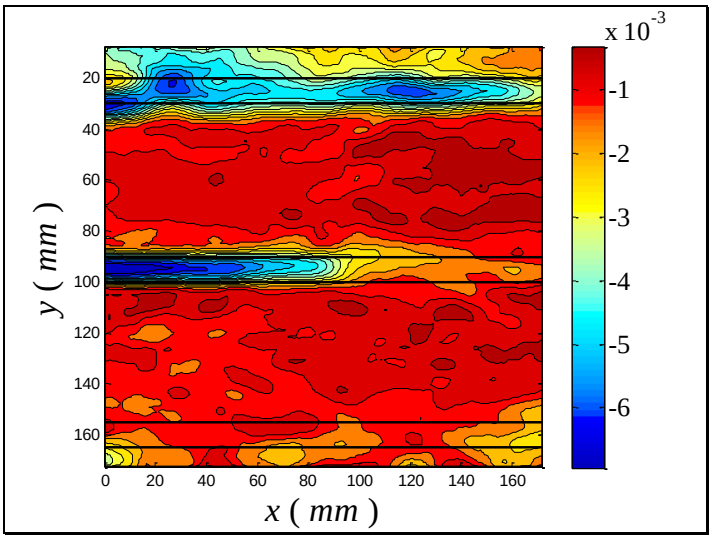

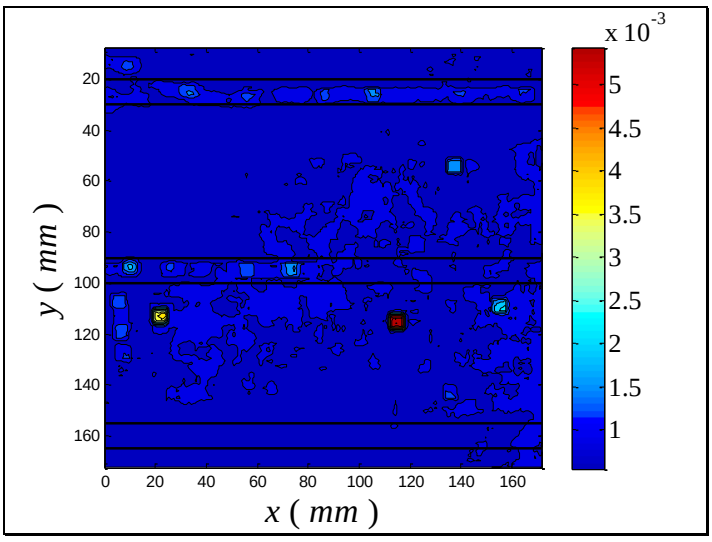

- G: 173.30 kips; 42,48 MPa

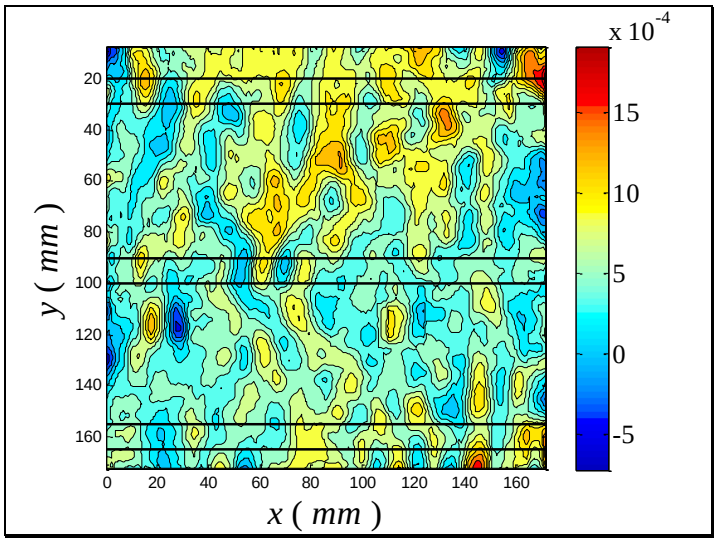

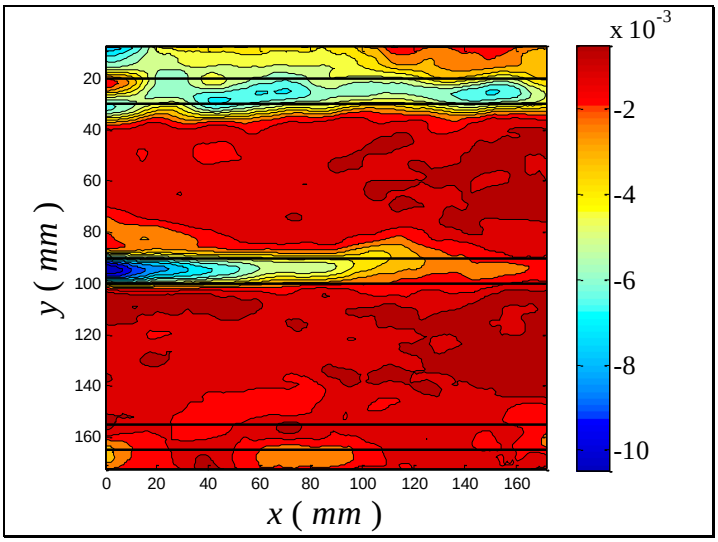

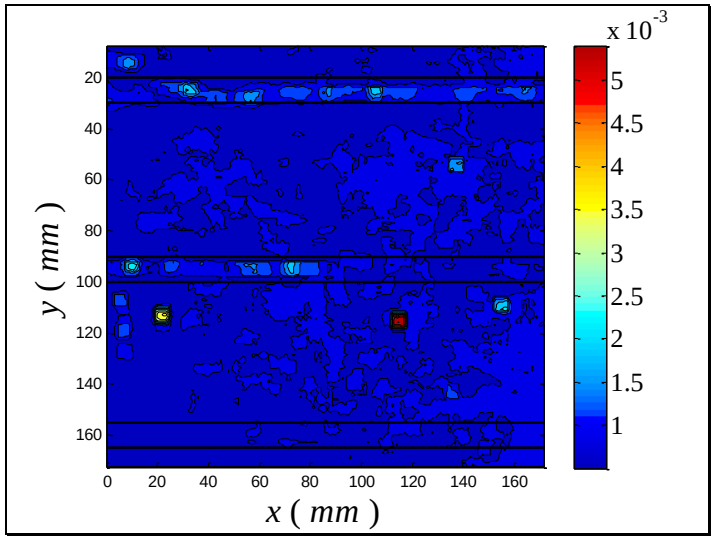

2.1.1.2. Column unwrapped 2

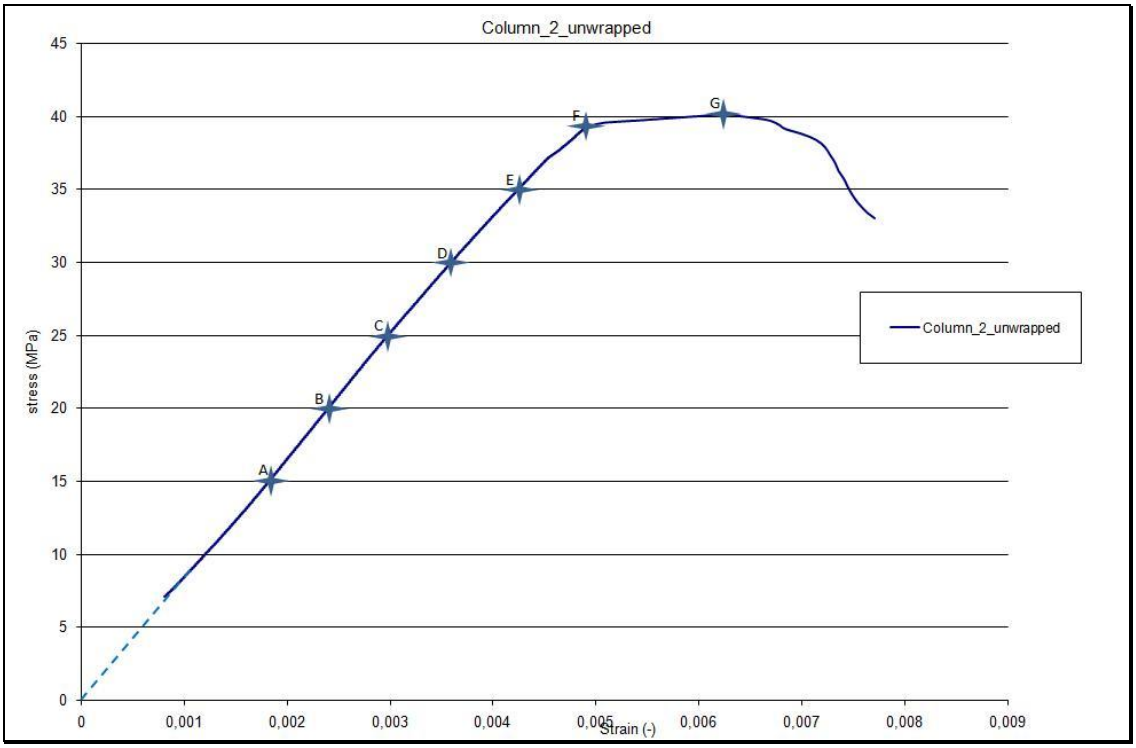

Fig. 2.8 – Stress–strain diagram of column unwrapped 2

The contour plots of ε_{xx} , ε_{yy} and the correlation factor for all the points in figure are reported below.

- A: 60.04 kips; 14,72 MPa

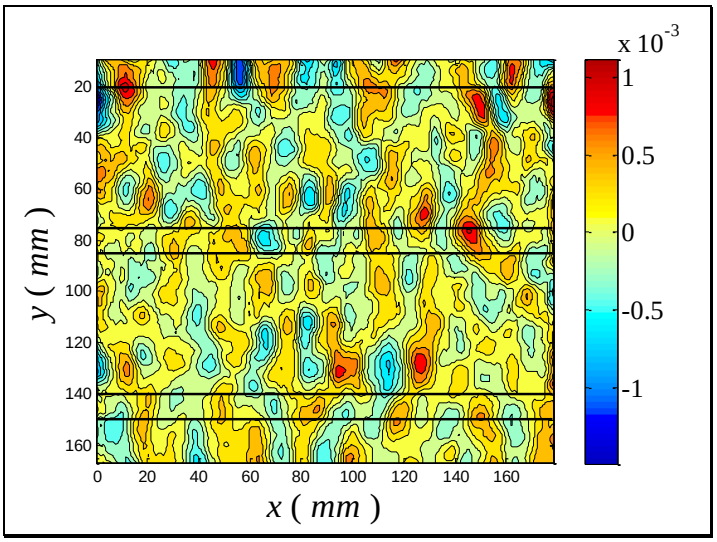

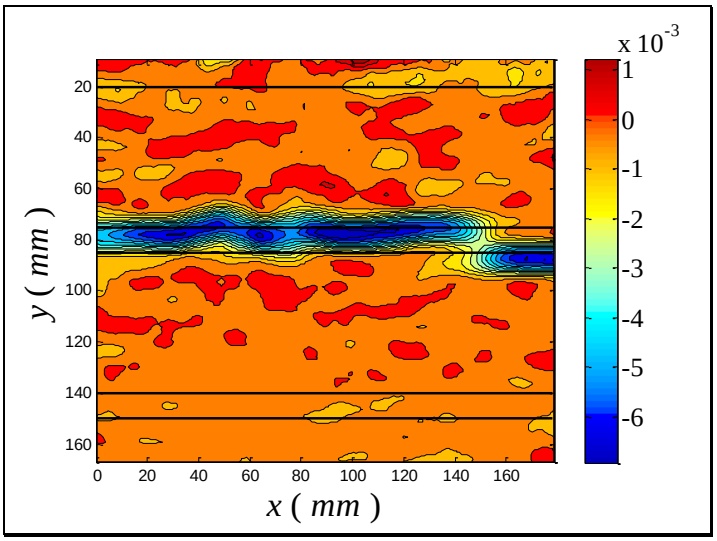

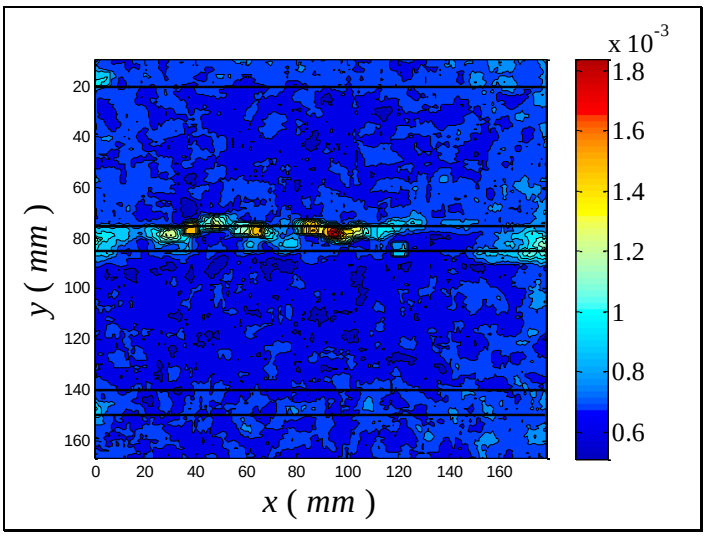

- B: 80.08 kips; 19,63 MPa

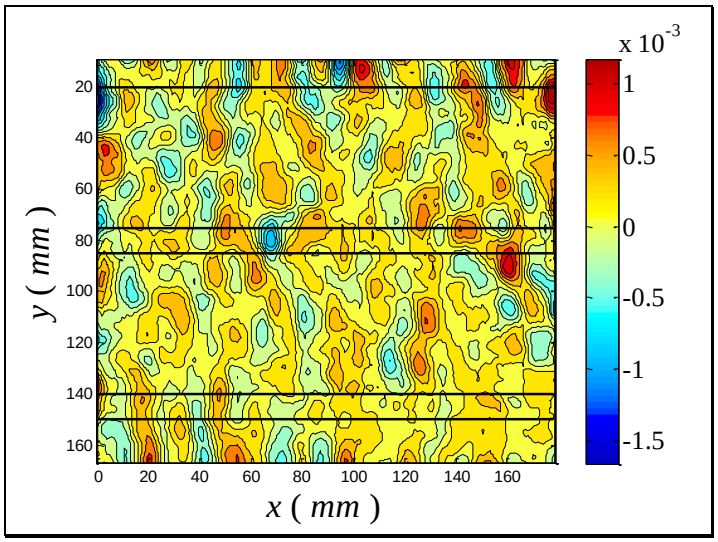

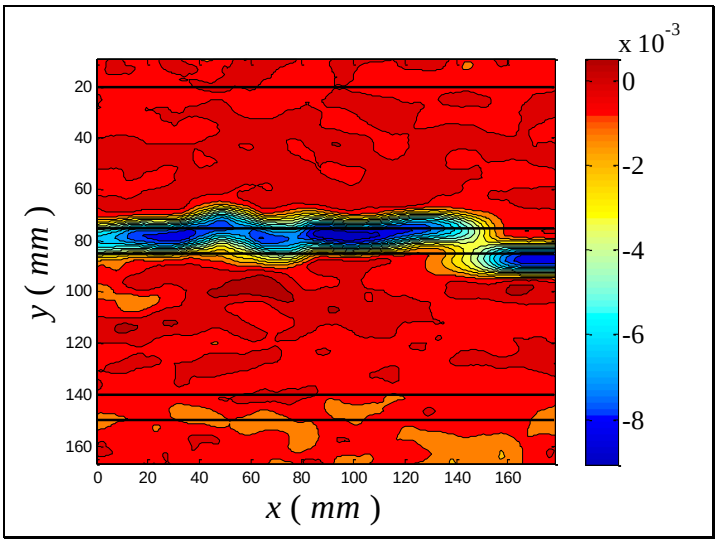

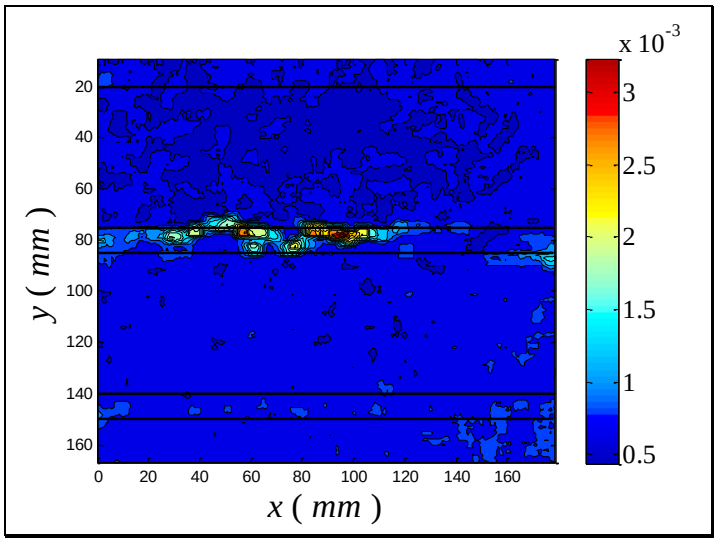

- C: 100.00 kips; 24,51 MPa

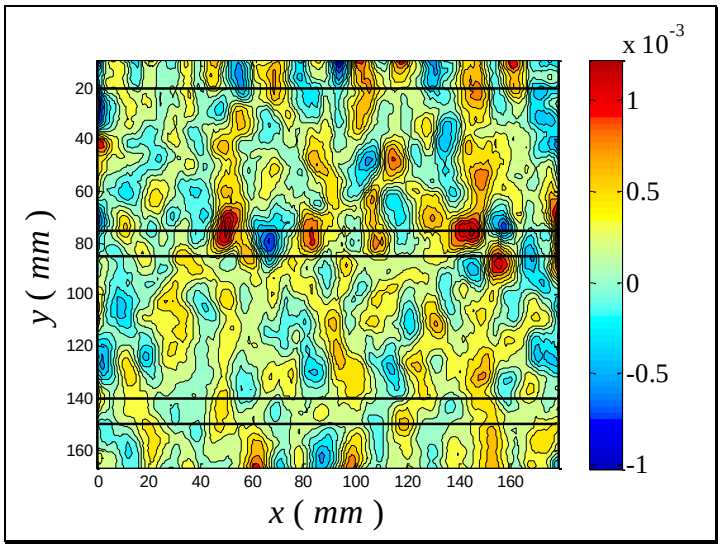

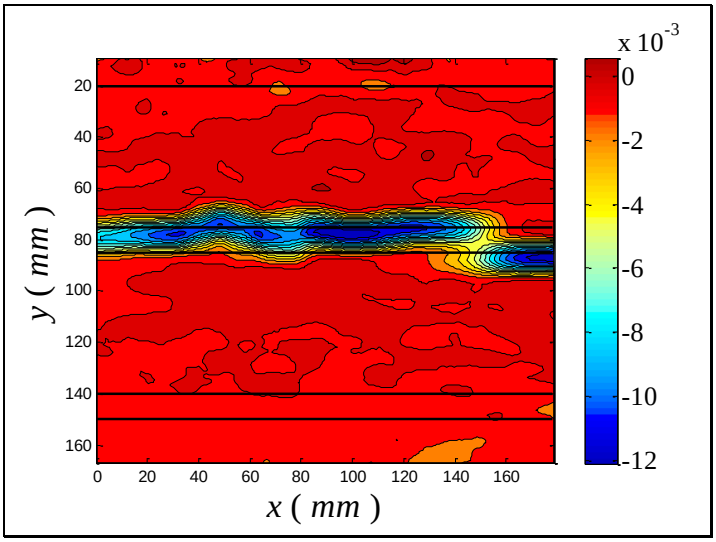

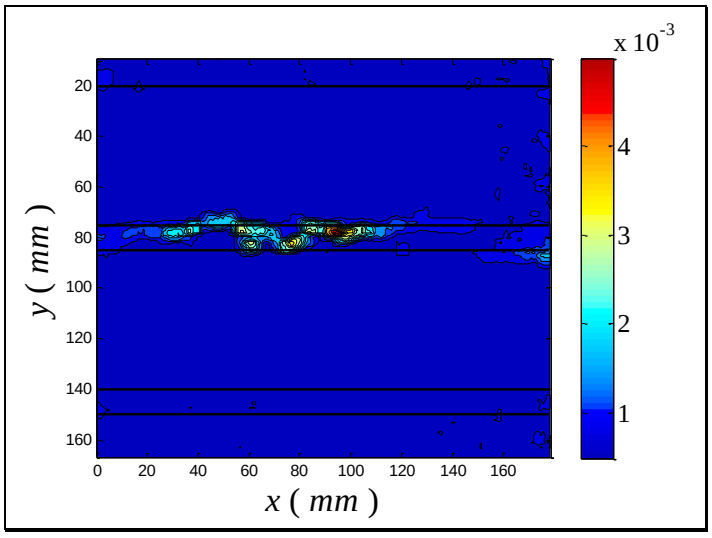

- D: 120.00 kips; 29,41 MPa

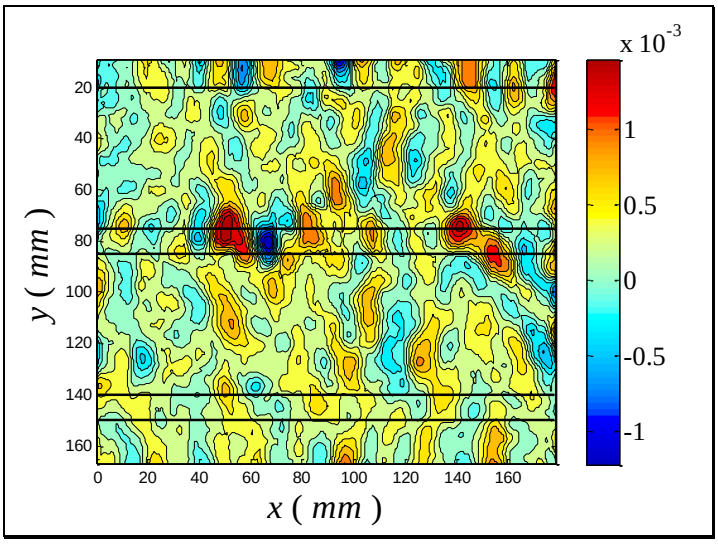

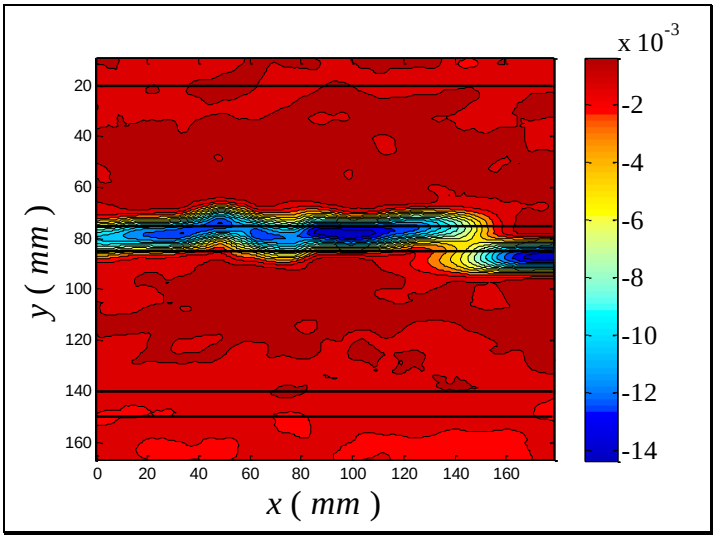

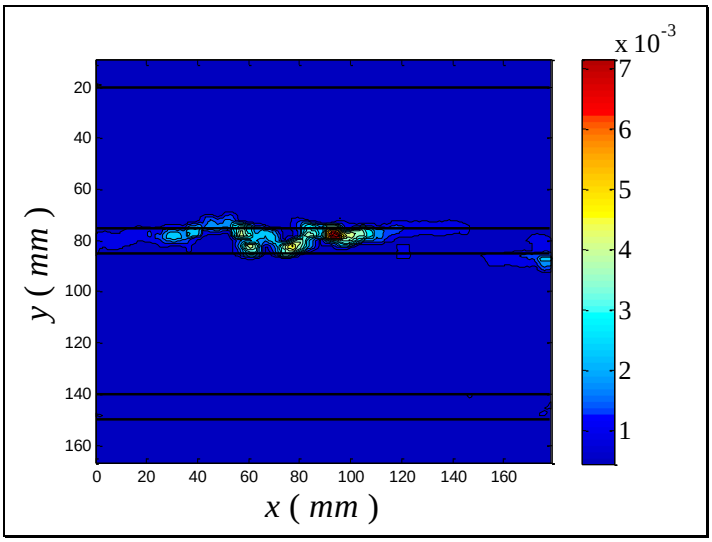

- E: 140.20 kips; 34,37 MPa

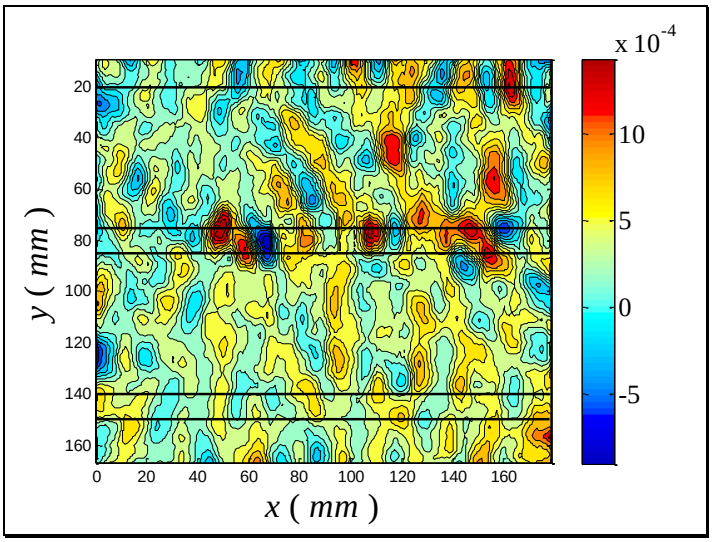

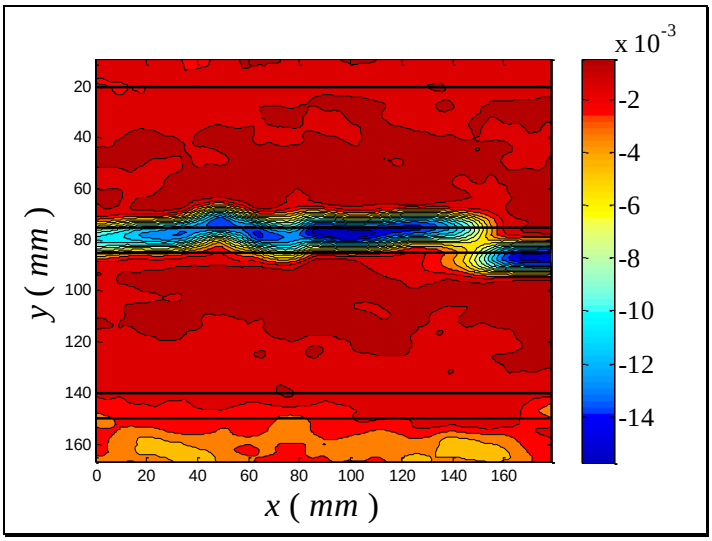

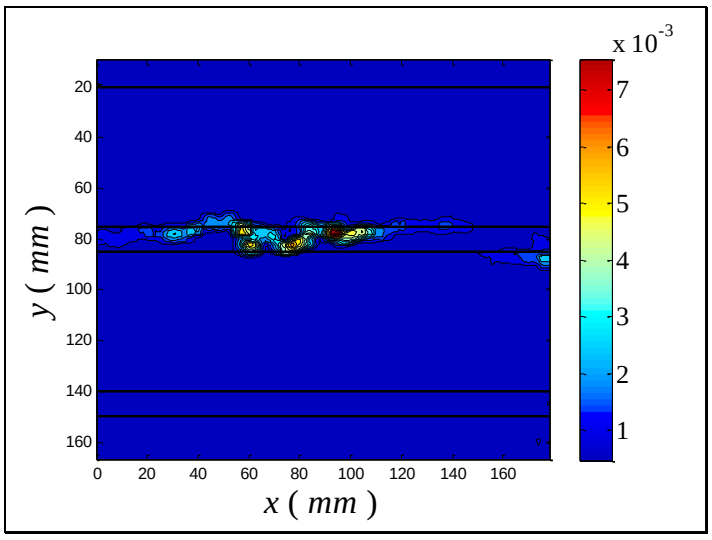

- F: 160.00 kips; 39,22 MPa

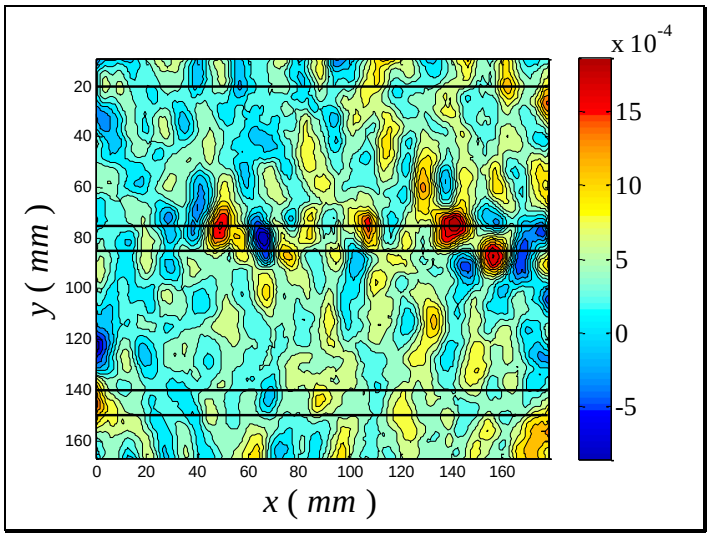

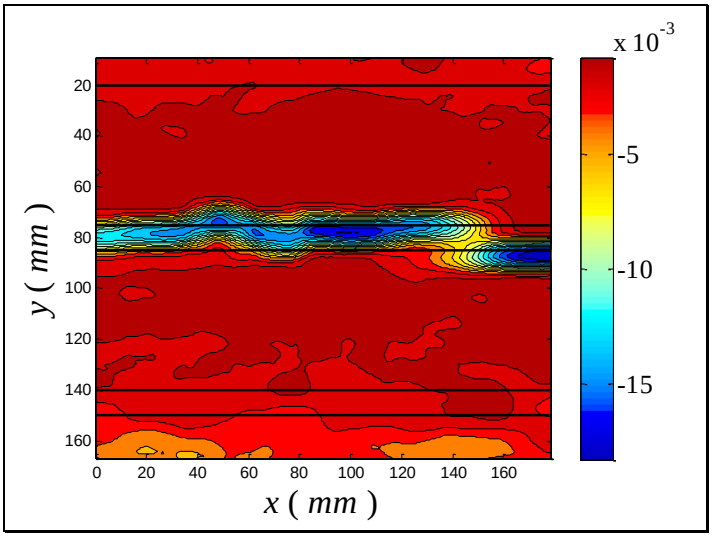

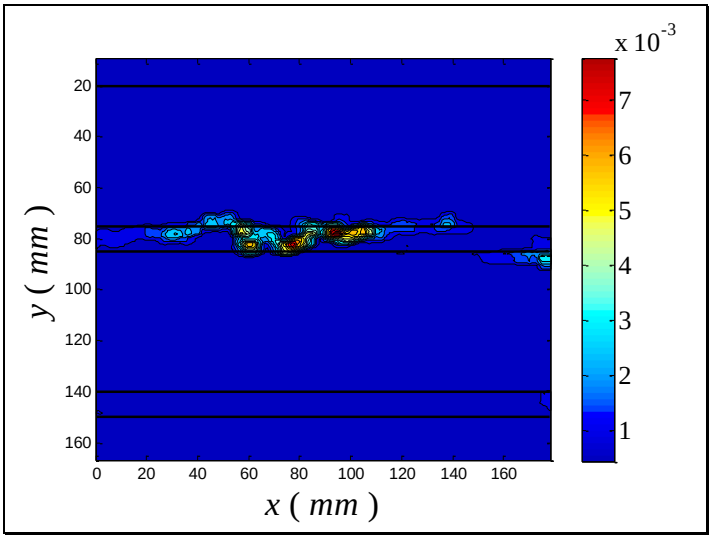

- G: 163.00 kips; 42,48 MPa

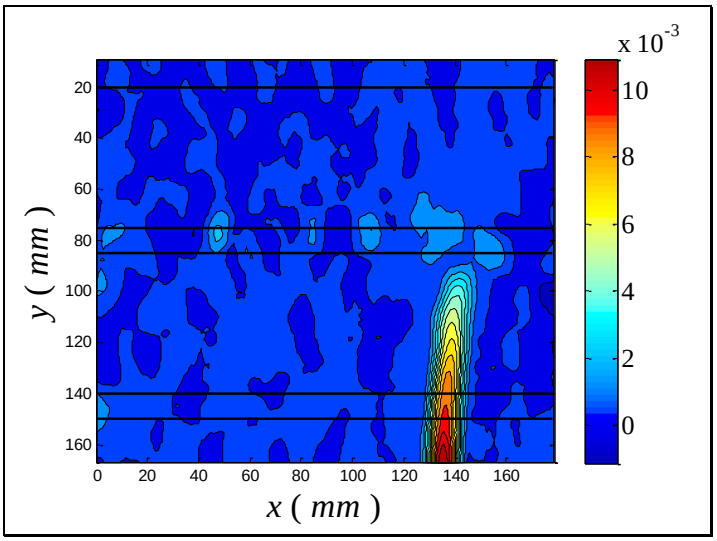

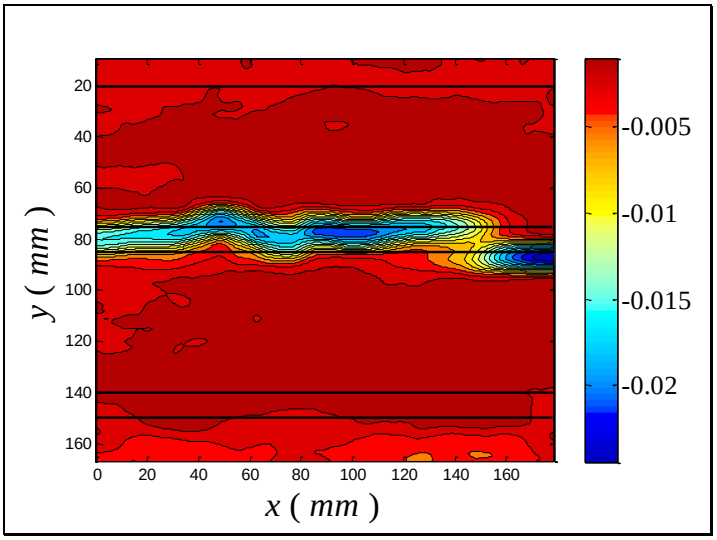

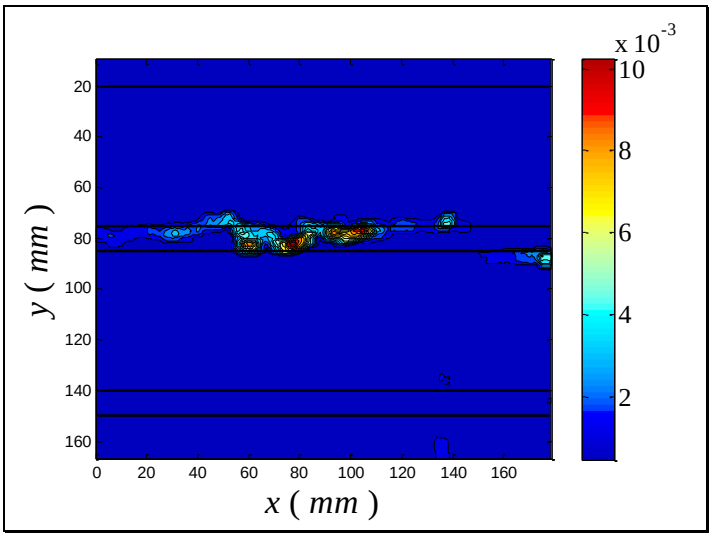

2.1.1.3. Column unwrapped 3

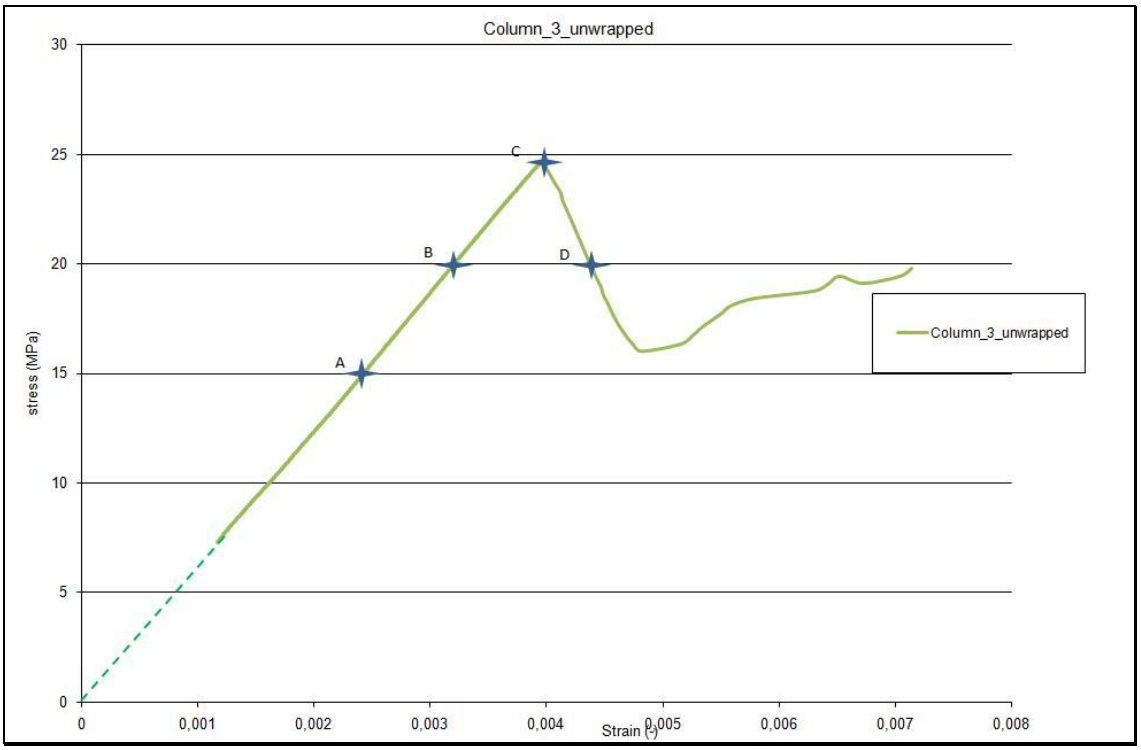

Fig. 2.9 – Stress–strain diagram of column unwrapped 3

The contour plots of ε_{xx} , ε_{yy} and the correlation factor for all the points in figure are reported below.

- A: 64.00 kips; 15,69 MPa

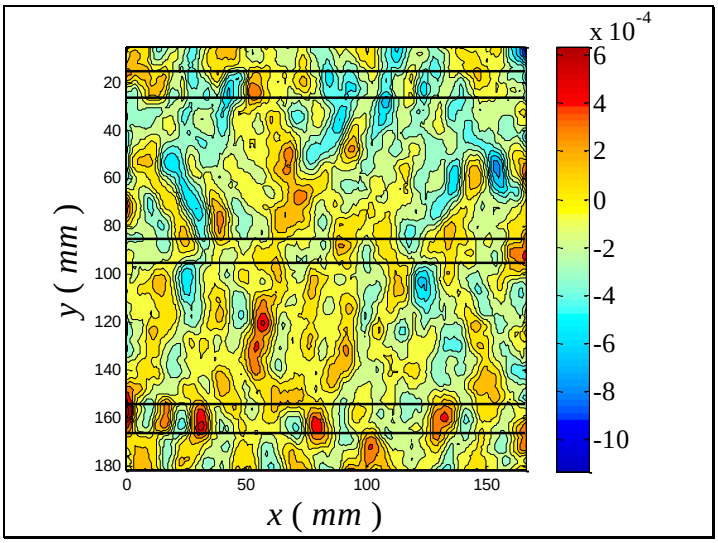

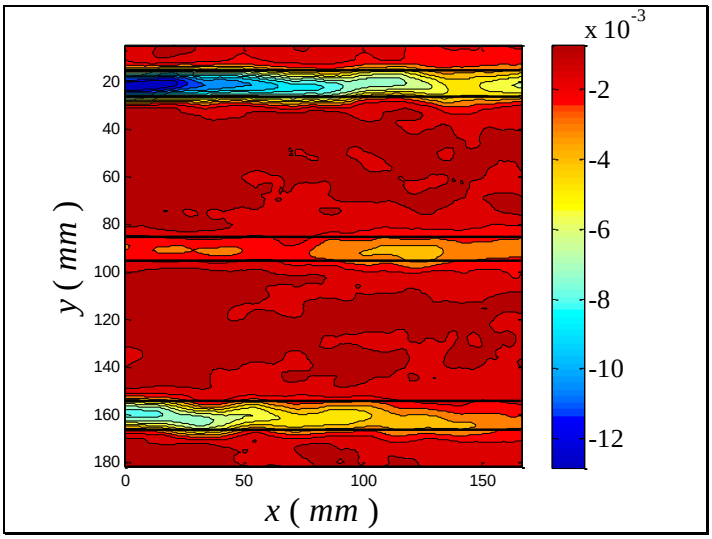

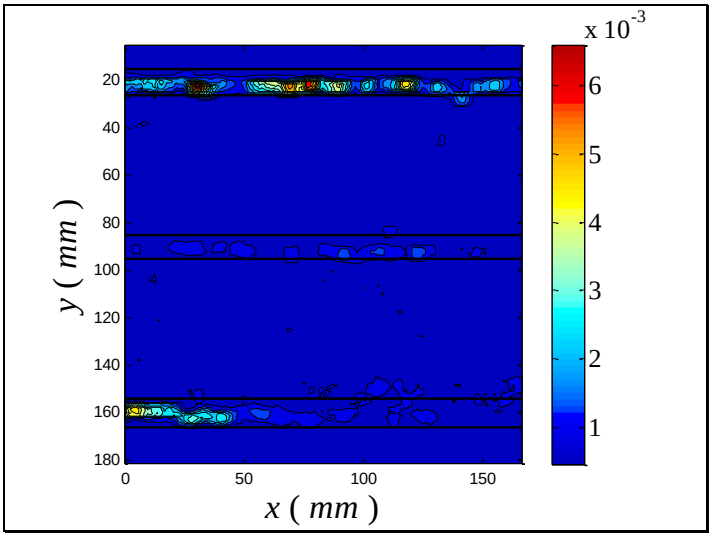

- B: 80.00 kips; 19,61 MPa

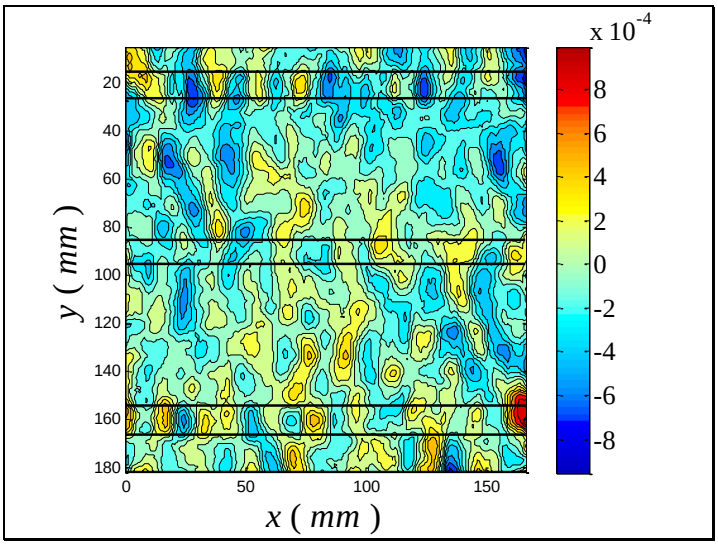

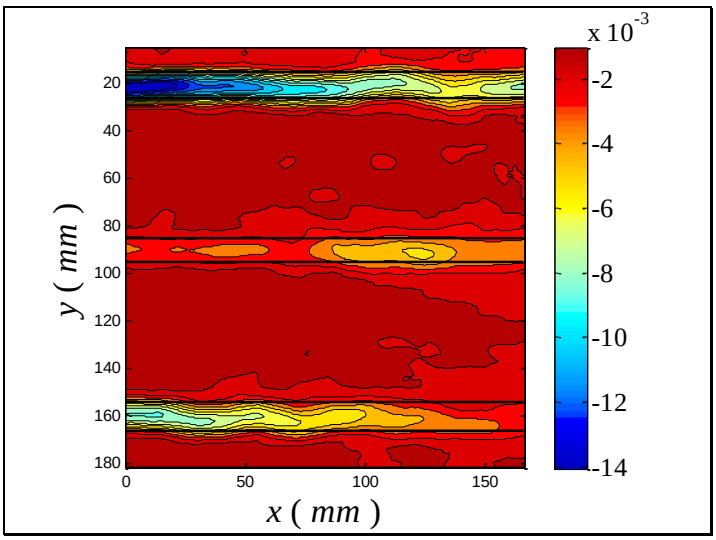

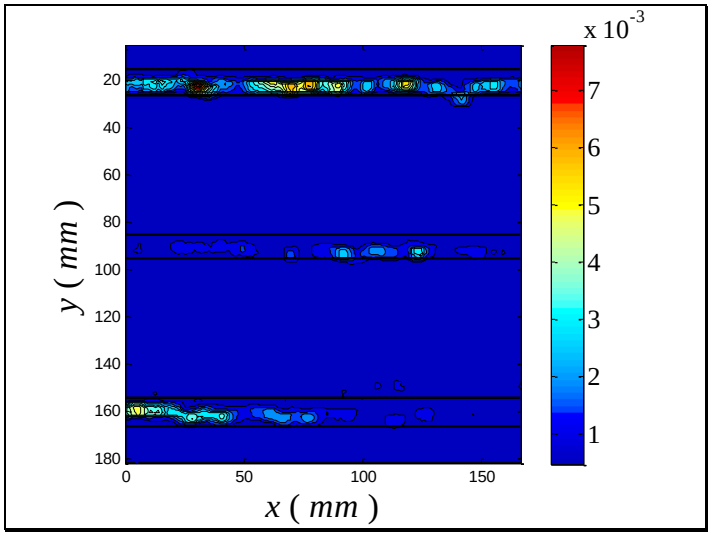

- C: 100.00 kips; 24,51 MPa

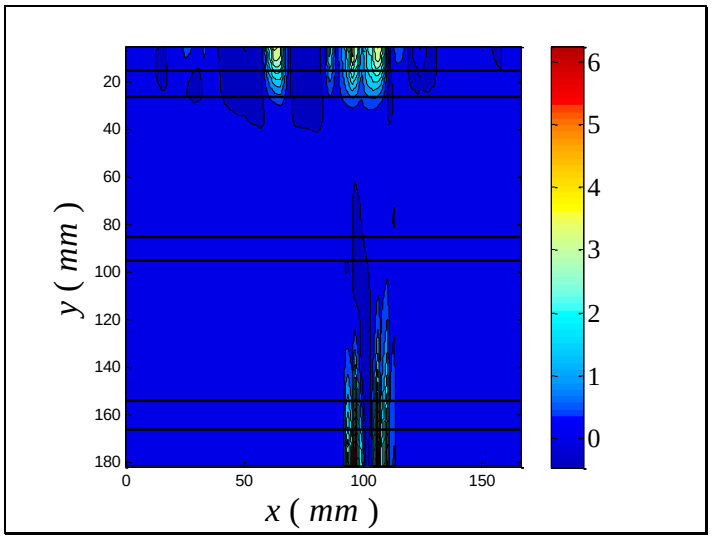

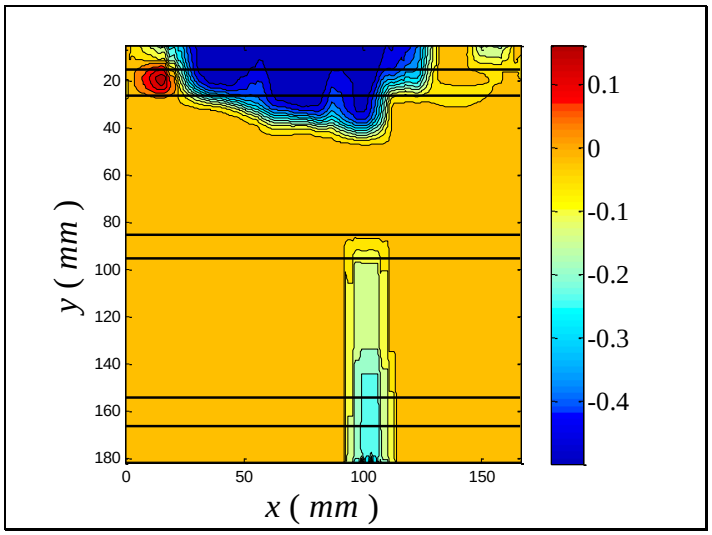

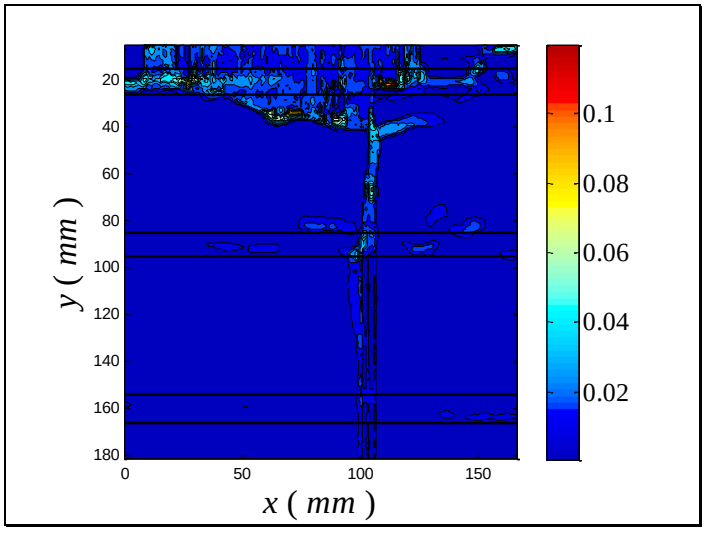

2.1.2. Discussion of result

In general, failure of the test specimens appeared to be initiated by crushing and squeezing of the mortar from the mortar joints followed by vertical splitting of the bricks, as shown in figure 2.10. It is worth noticing that the images were taken on the wider face, whereas the cracking occurred on the perpendicular one.

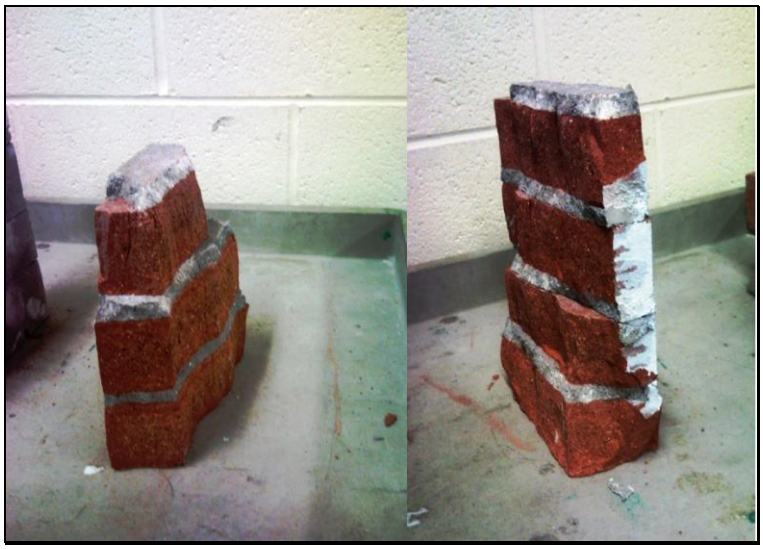

Fig. 2.10 – Vertical splitting of the bricks

The main conclusions that can be drawn from the tests on laboratory specimens are as follows.

In particular on the DIC pictures is clearly visible that the ε_{yy} of the joint has the bigger value instead of the brick surface.

The strengths of brick masonry depend upon several parameters including the strengths of the bricks and mortar, the nature of the applied loading and the configuration of the bricks and mortar. While the present tests provides an indication of trends for a limited range of parameters, more experimental data is required to extend the results to a wider range of parameters and combined loading conditions, for example compression and shear.

Is possible to compare the unwrapped results obtained with the results of another thesis named “Statistical analysis of compressive strength of clay brick masonry prisms” [19]

This thesis studied masonries with different kind of mortar and made a statistical analysis of the results obtained in some model named “A,B,C,D,F,G”.

The results for model “D” and “F” are the most comparable to the performed tests.

Model “D” evaluates the data points for 28-day moist-cured prisms only, and Model “F” analyzes Model “D” data set, modified such that the compressive strengths are based on net areas.

The Model “D” data was analyzed based on mortar type using liner regression that related prism compressive strength to the compressive strength of the clay masonry unit for each mortar type.

For the N-type mortar used in this study the linear regression is represented in figure 2.11.

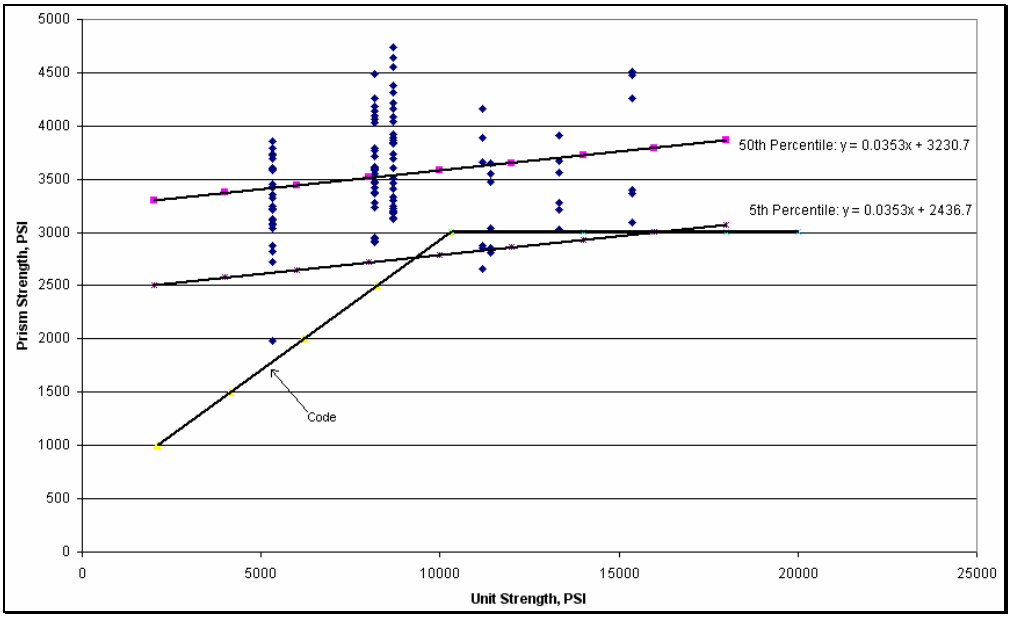

Fig. 2.11 – Linear regression for type N mortar

Type N Mortar, 50th Percentile:

$$f'_m = 0.035 \cdot f_u + 3231$$

Type N Mortar, 5th Percentile:

$$f'_m = 0.035 \cdot f_u + 2437$$

f'_m : specified compressive strength of masonry, psi,

f_u : average compressive strength of brick, psi.

The Model "F" for the N-type mortar used in this study the linear regression is represented in figure 2.12.

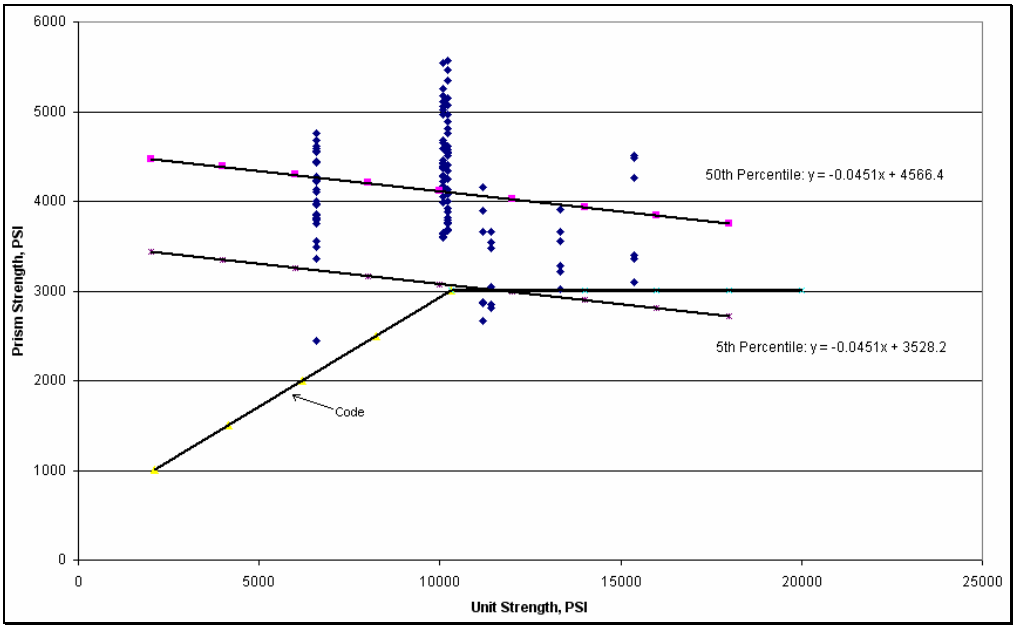

Fig. 2.12 – Linear regression for type N mortar

Type N Mortar, 50th Percentile:

$$f'_m = -0.045 \cdot f_u + 4566$$

Type N Mortar, 5th Percentile:

$$f'_m = -0.045 \cdot f_u + 3528$$

f'_m : specified compressive strength of masonry, psi,

f_u : average compressive strength of brick, psi.

CHAPTER 3

FRCM-REINFORCED BRICK MASONRY COLUMNS

C H A P T E R 3

FRCM-REINFORCED BRICK MASONRY COLUMNS

3.1. Axial Compression Test

In this chapter the masonry specimens will be wrapped to perform compression test.

After the test the result will be analyzed and compared with the unwrapped specimens.

Before wrapping all the corner of the specimens were rounded using a grinding machine at a radius of 10 mm, figure 3.1.

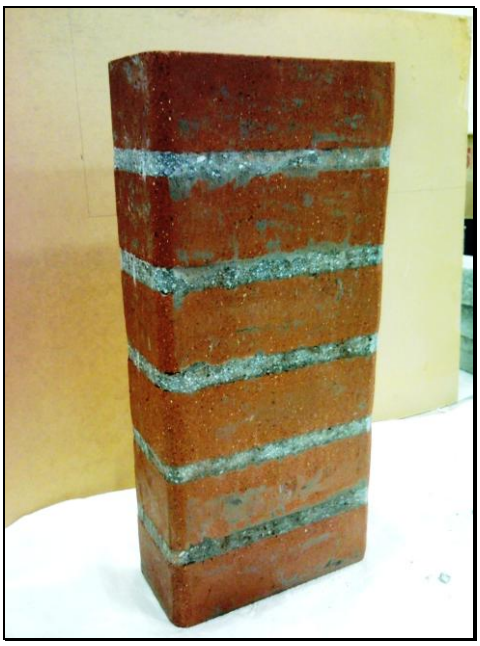

Fig. 3.1 – Masonry with rounded corners

The main objective of testing is to record the axial stress-strain curve, the failure mode of all the masonry specimens and compare them with the unwrapped specimens.

Displacements of the central section on each specimen were measured using also a Linear Variable Differential Transformer (LVDT) on the left side of the columns attached to the wrapping surface.

A layer of a stabilized inorganic matrix designed to connect the mesh with the substrate was applied on the surface of each specimen, figure 3.2, and then a PBO mesh was applied with the fibers in the hoop direction, figure 3.3.

Fig. 3.2 – Mortar application on the masonry column surface

The wrapping curing of the masonries took place after curing, at least 14 days, and testing started approximately one month after the casting of the columns.

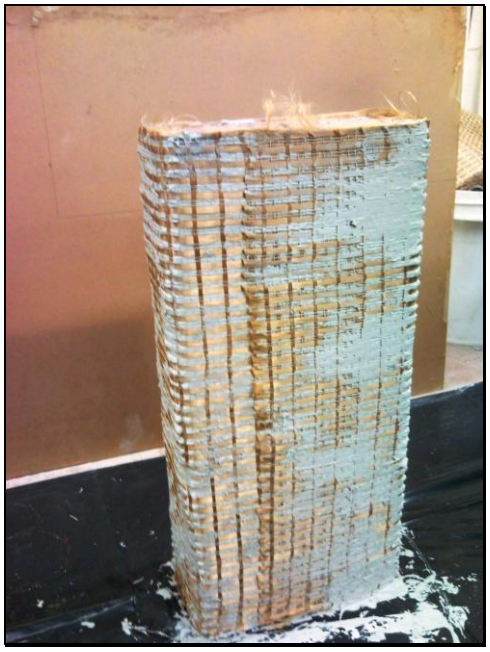

Fig. 3.3 – Wrapping of the masonry column

The finishing end of the mesh overlapped the starting end by approximately 100 mm.

After the wrapping all the fiber were covered with the same cementitious inorganic matrix used before, figure 3.4.

Fig. 3.4 – Masonry column after the complete wrapping

The specimens face need to be prepared for the DIC with a layer of white paint followed by a layer of a light drops of black paint, figure 3.5.

Fig. 3.5 – Masonry column ready for the DIC

Fig. 3.6 – FRCM-reinforced masonry column ready for test

Displacements are obtained using the Digital Image Correlation after the tests.

3.1.1. Experimental result and Failure mode

The main results of the tests are presented in the table 3.1.

Specimens notation	3 precycle (kN)	Maximum load (kN)	Area (cm^2)	Compressive strenght (MPa)	Ultimate machine strain ε
1	110-220	941,51	171,40	45,77	0,0061
2	155-310	625,43	171,40	30.41	0,0050
3	155-310	690.14	171,40	33.55	0,0050
Displacement control mode of 0.016 inch/min, about 0.4 mm/min					

Tab. 3.1 – Summary of test results for columns wrapped

The stress-strain diagrams for the wrapped specimens are presented in figure 3.7.

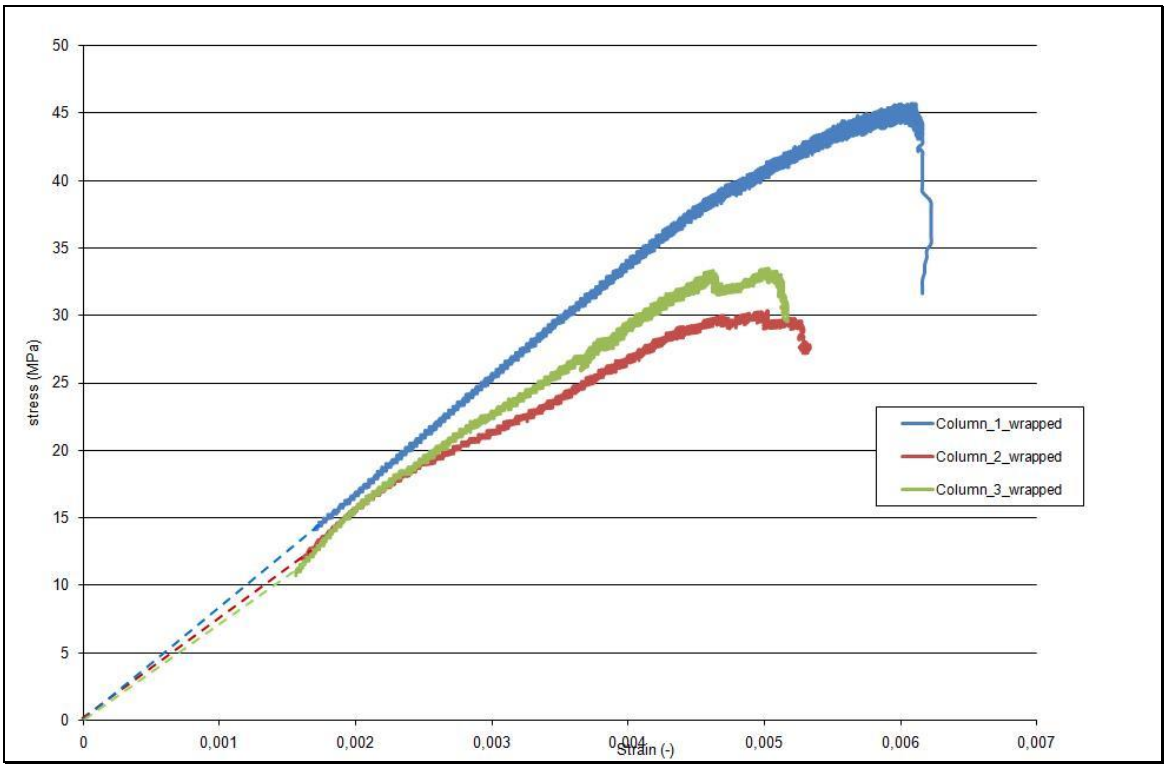

Fig. 3.7 – Stress–strain diagram of wrapped columns

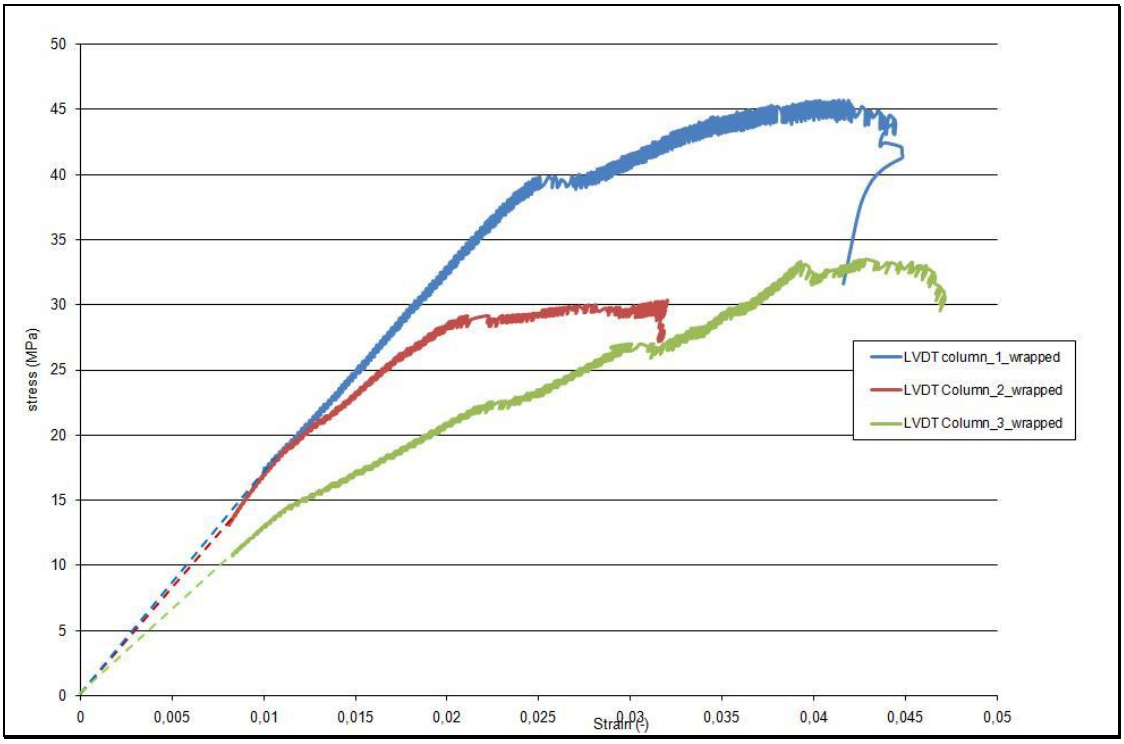

Fig. 3.8 – Stress–LVDTstrain diagram of wrapped columns

It can be observed that in all cases the diagrams are linear up to about 80% of the maximum load, with a curved transition curve between a second linear part; no descending branch was recorded.

The control failed by the formation of a vertical crack on the FRCM overlapping from the head of the specimen through all the surface, figure 3.9.

Fig. 3.9 – Vertical cracks

After the formation vertical crack became increasingly wide and the masonry between was crushed. This continued until the lateral expansion reached the capacity of FRCM. The formation of fracture at the corners, figure 3.10, denotes a concentration of the efforts in this area.

Fig. 3.10 – Fracture at the corner

3.1.1.1. Column wrapped 1

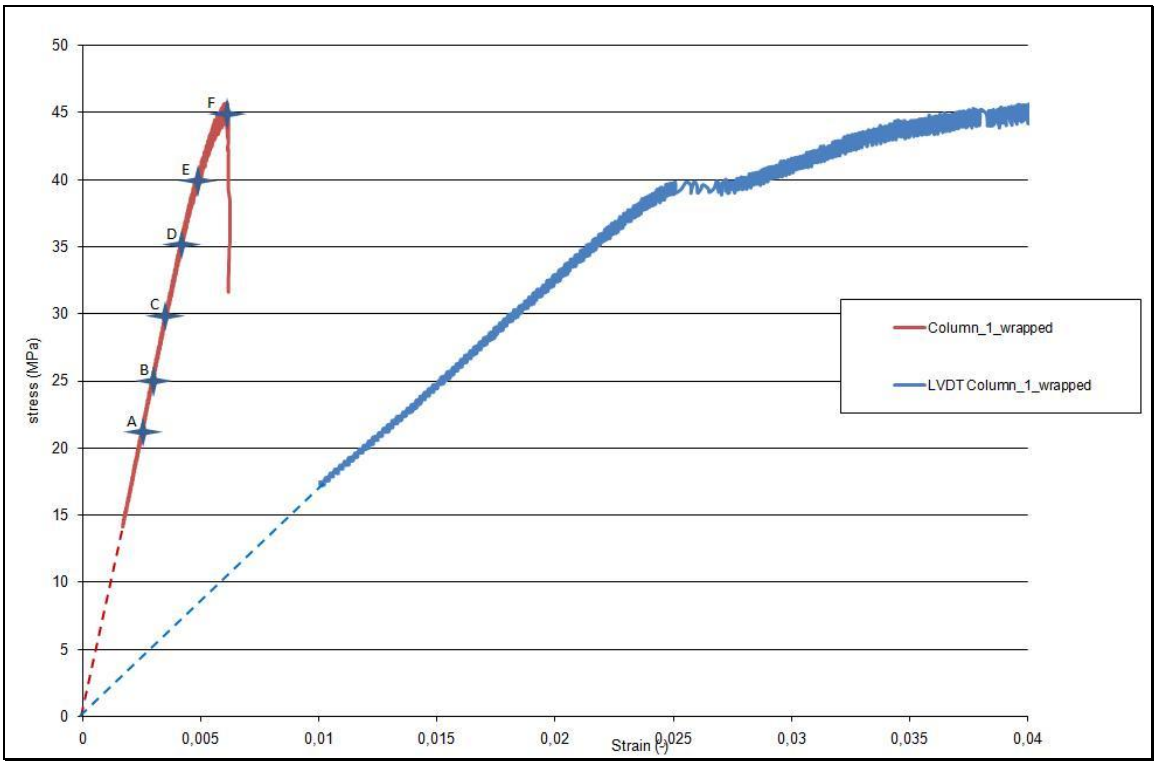

Fig.3.11 – Stress–strain diagram of column wrapped 1

The contour plots of ε_{xx}, ε_{yy} and the correlation factor for all the points in figure are reported below.

- A: 97.53 kips; 21,09 MPa

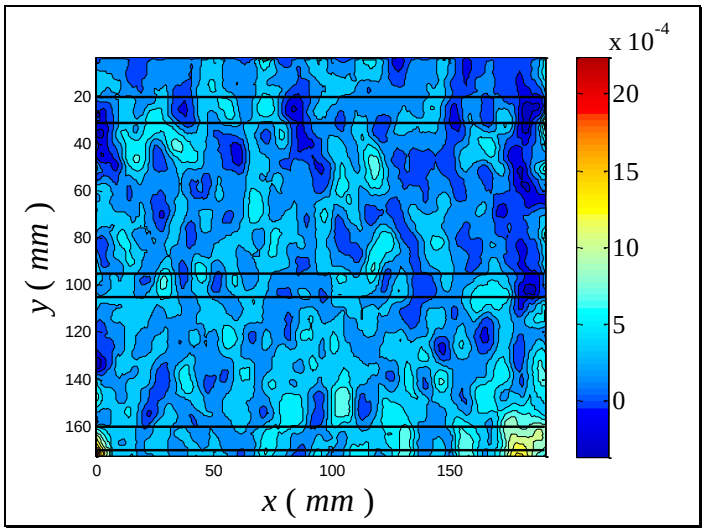

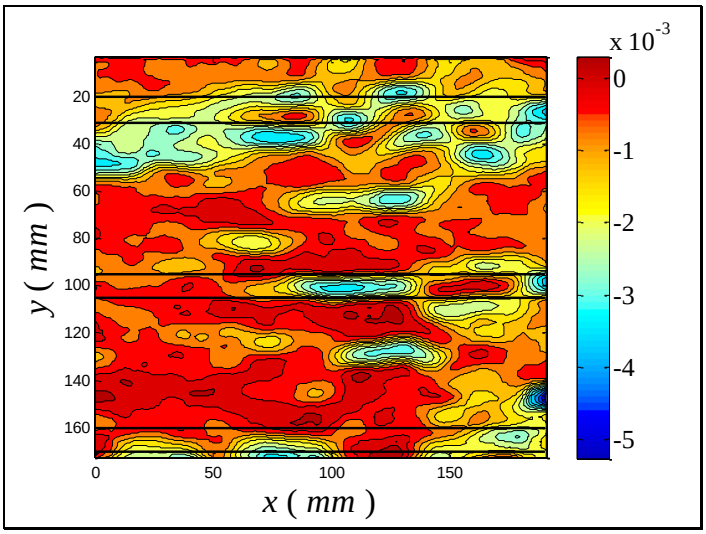

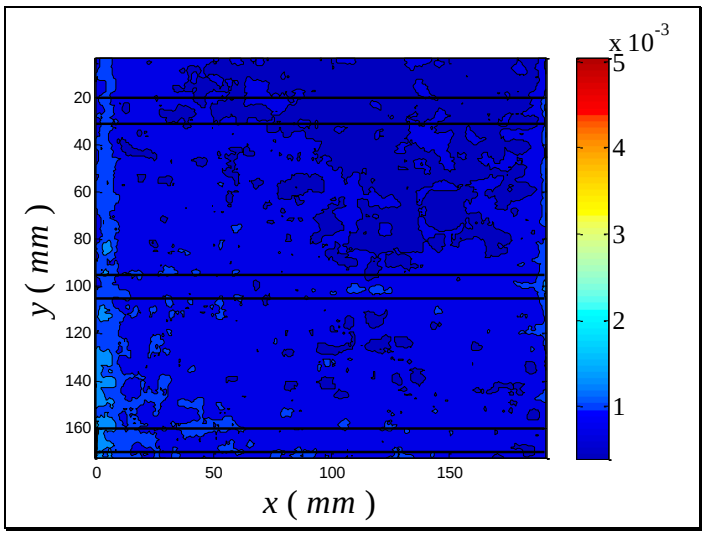

- B: 116.00 kips; 25,09 MPa

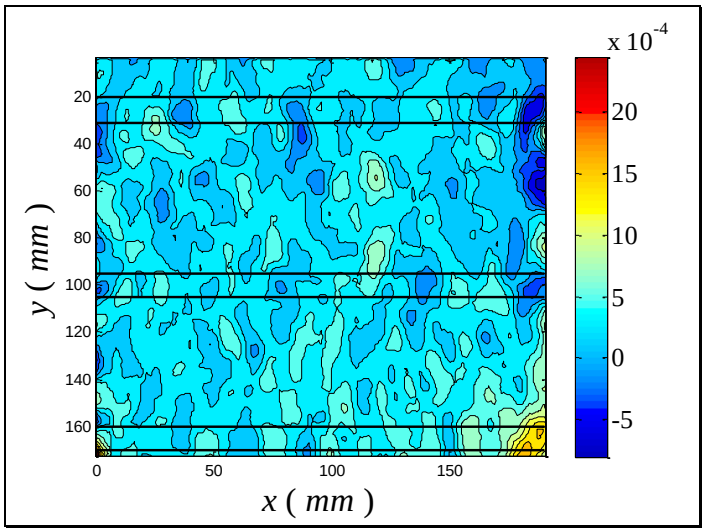

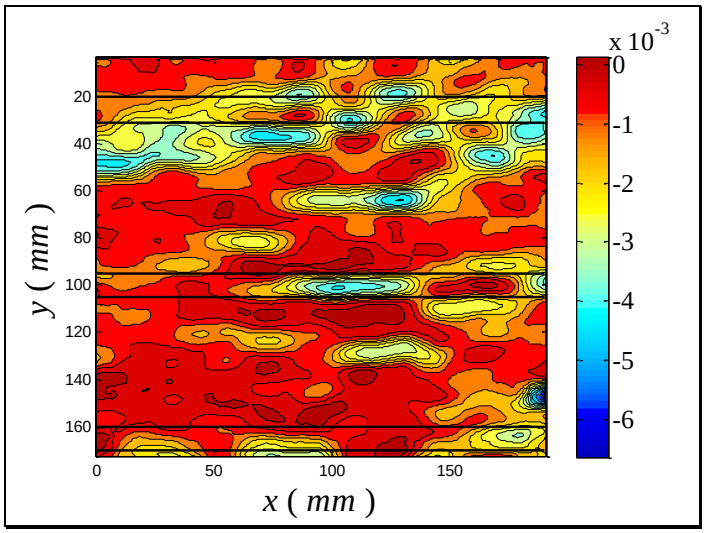

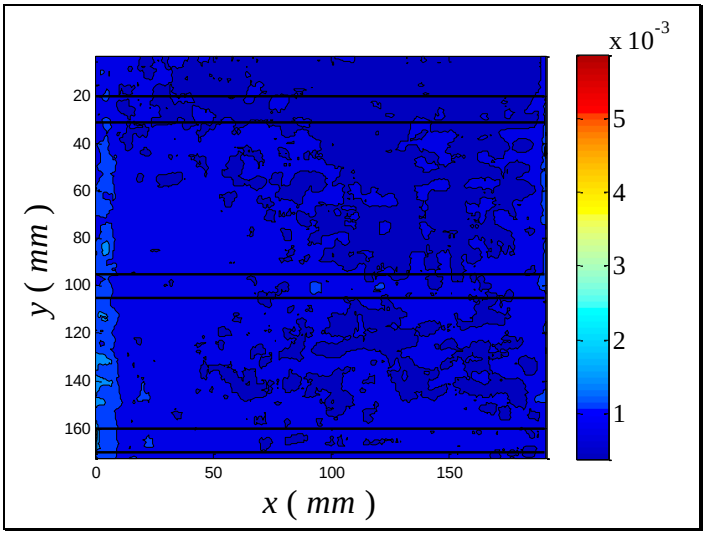

- C: 134.30 kips; 29,04 MPa

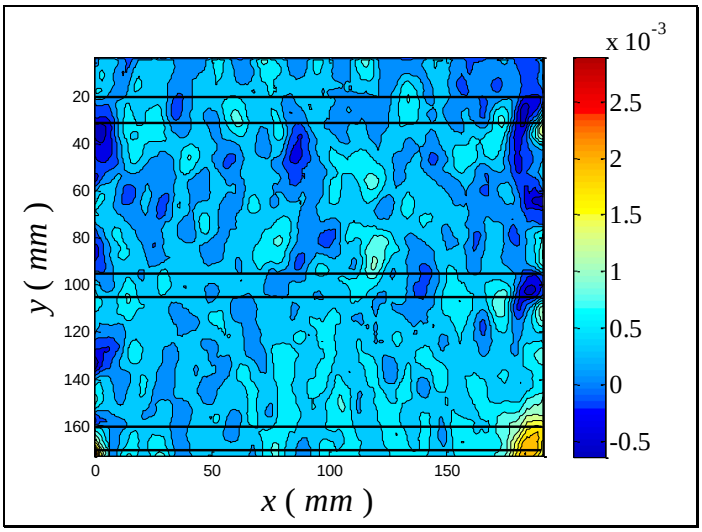

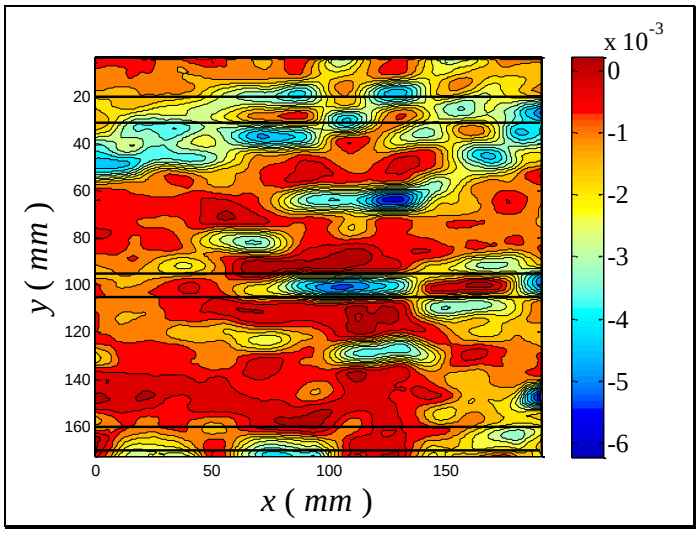

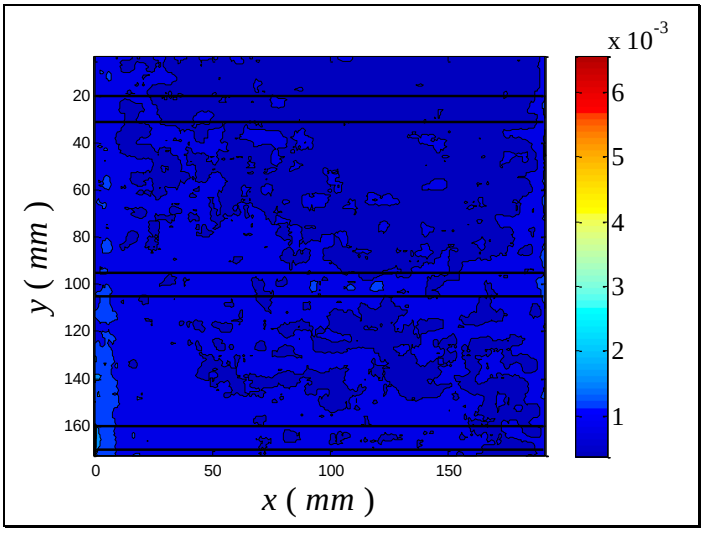

- D: 162.90 kips; 35,23 MPa

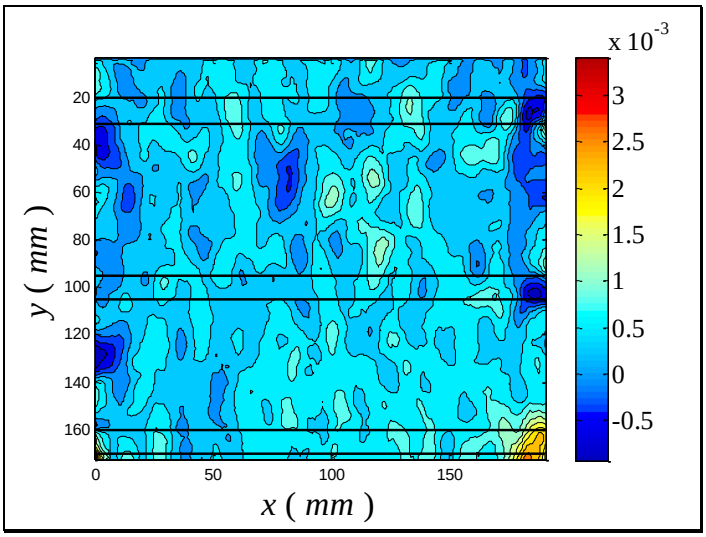

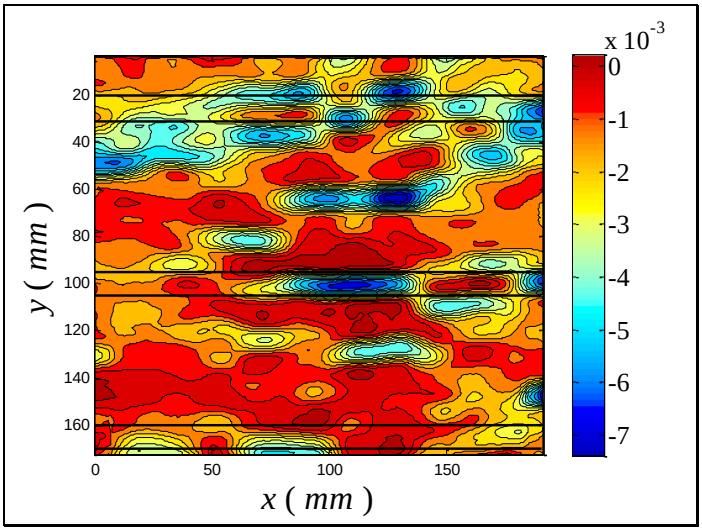

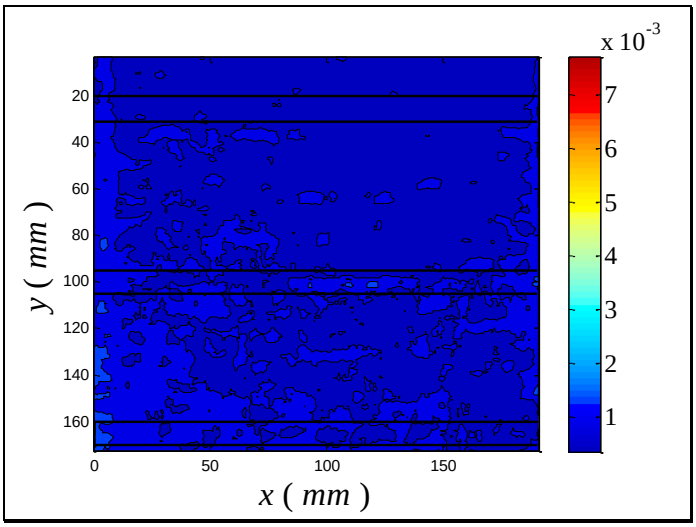

- E: 185.00 kips; 40,01 MPa

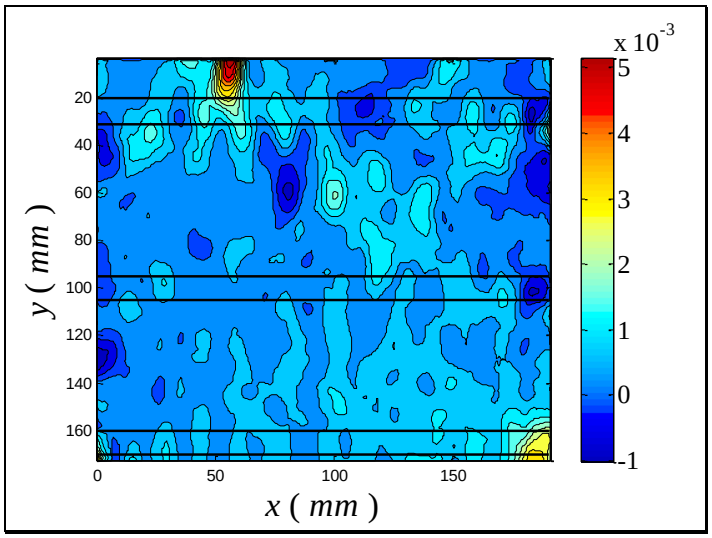

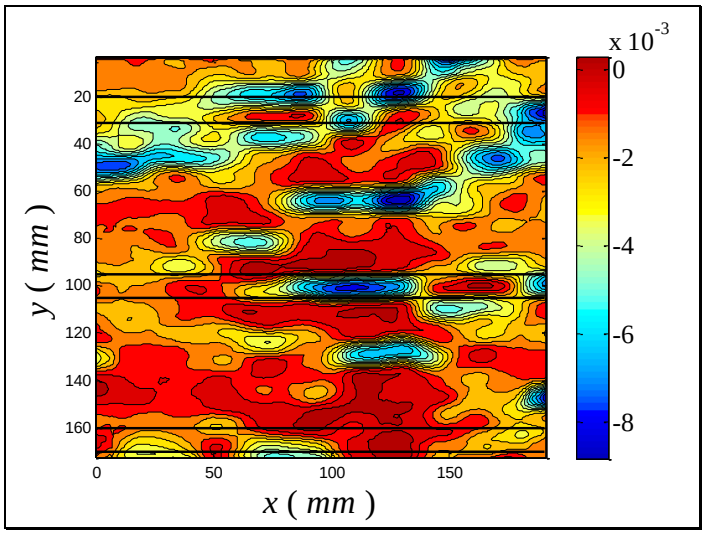

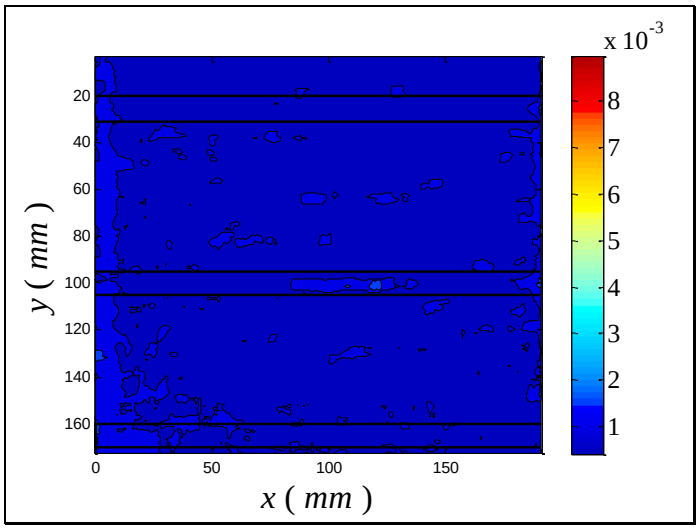

- F: 208.00 kips; 44,98 MPa

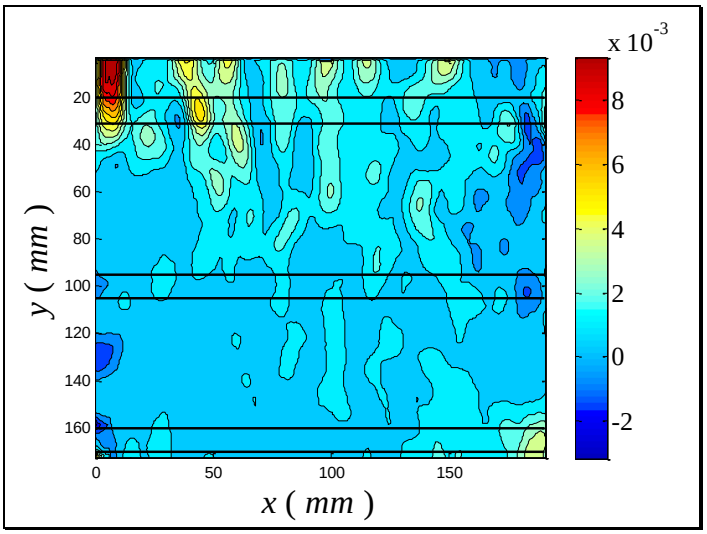

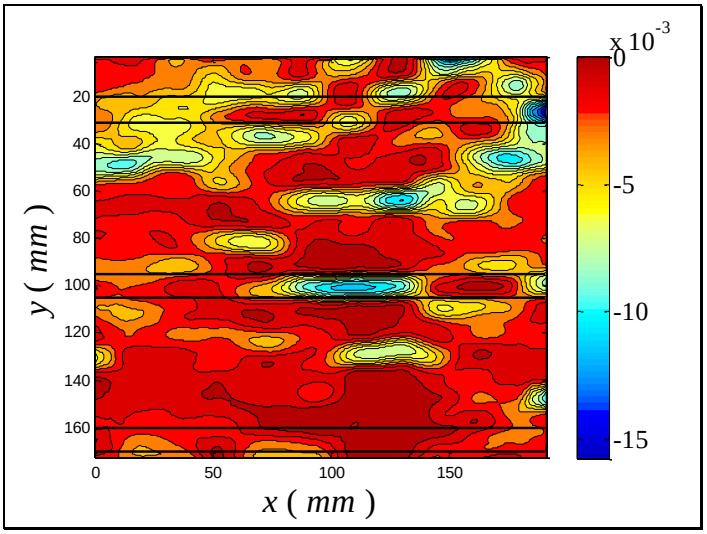

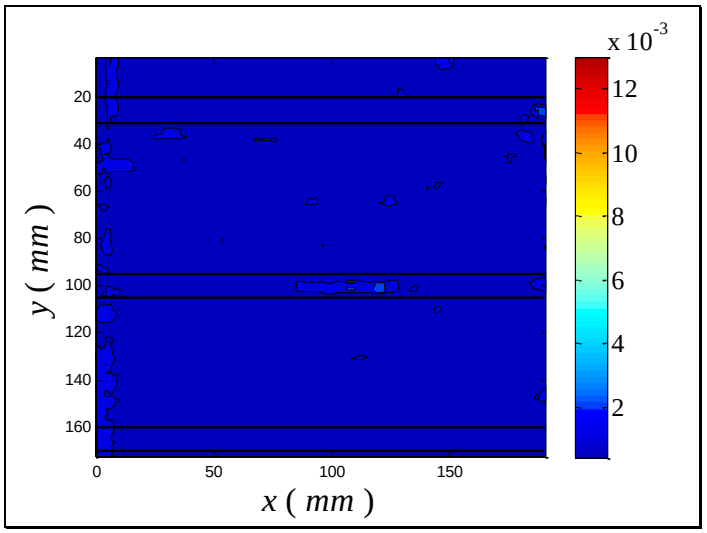

3.1.1.2. Column wrapped 2

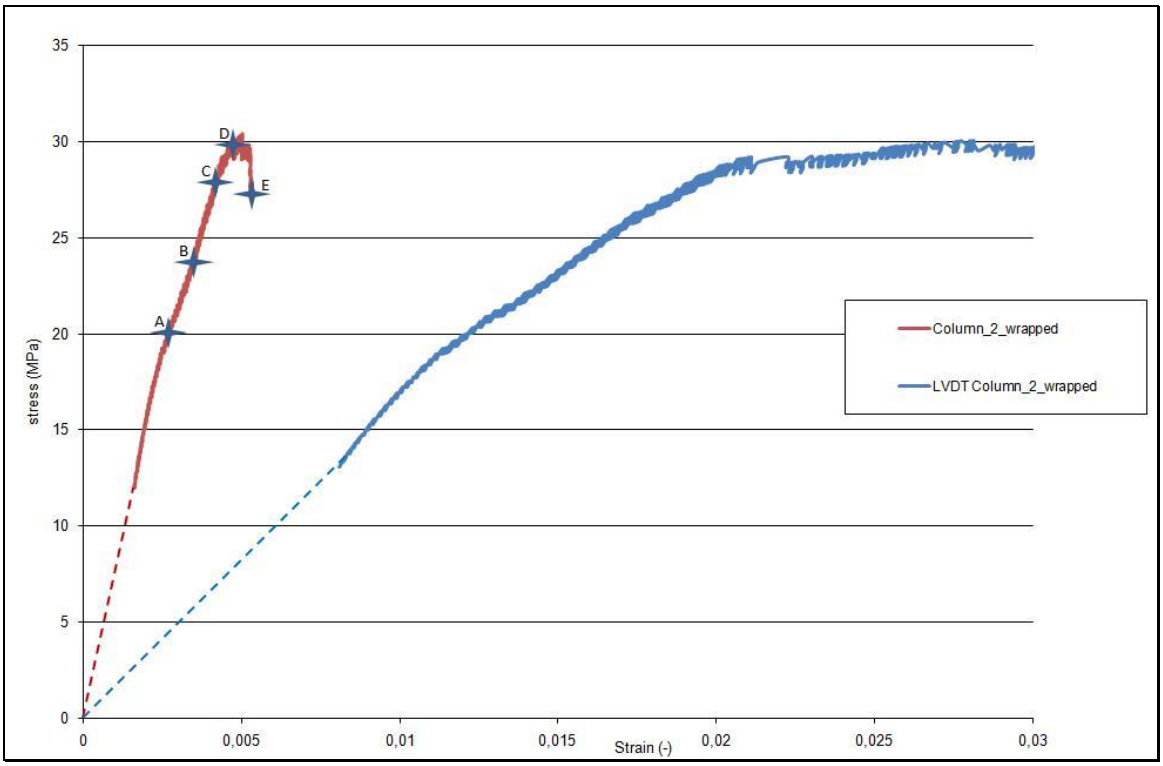

Fig.3.12 – Stress–strain diagram of column wrapped 2

The contour plots of ε_{xx}, ε_{yy} and the correlation factor for all the points in figure are reported below.

- A: 90.22 kips; 19,51 MPa

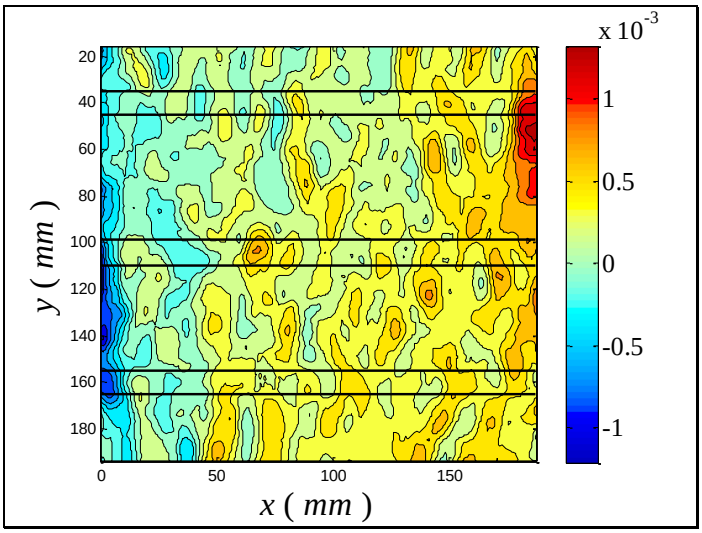

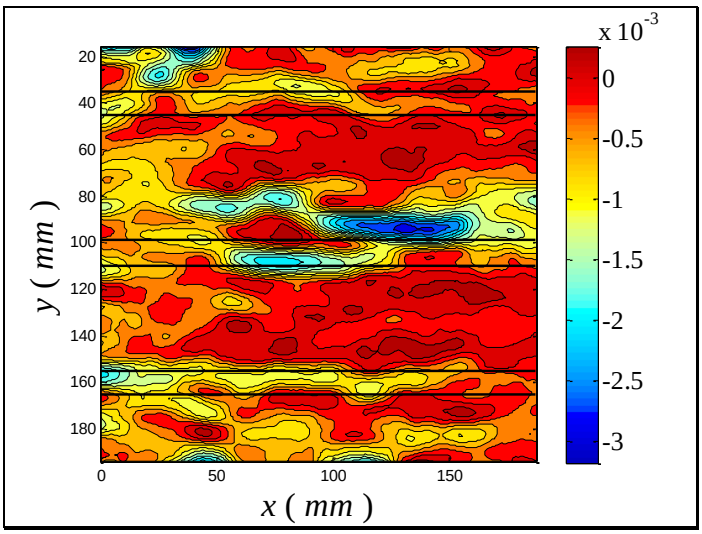

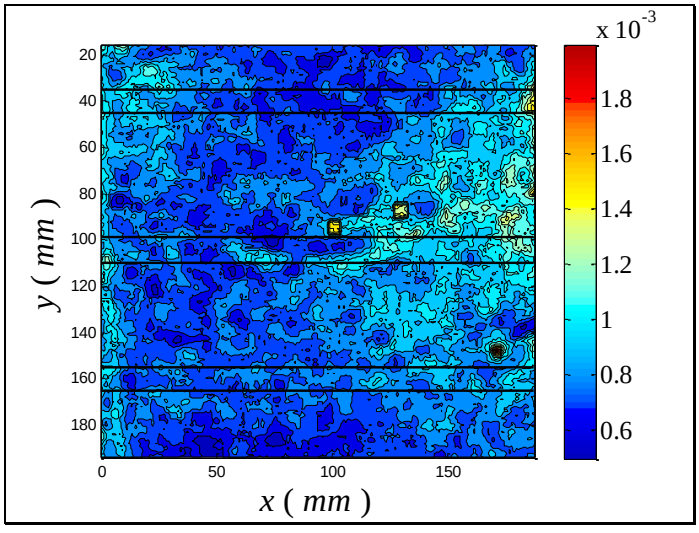

- B: 105.90 kips; 23,90 MPa

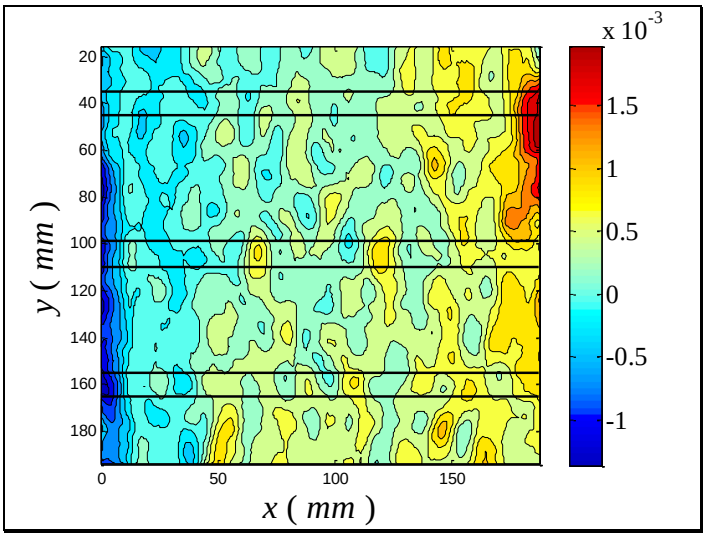

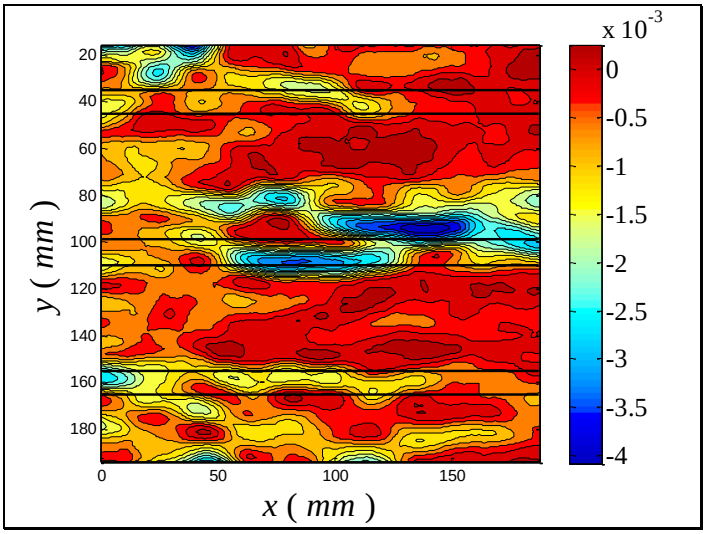

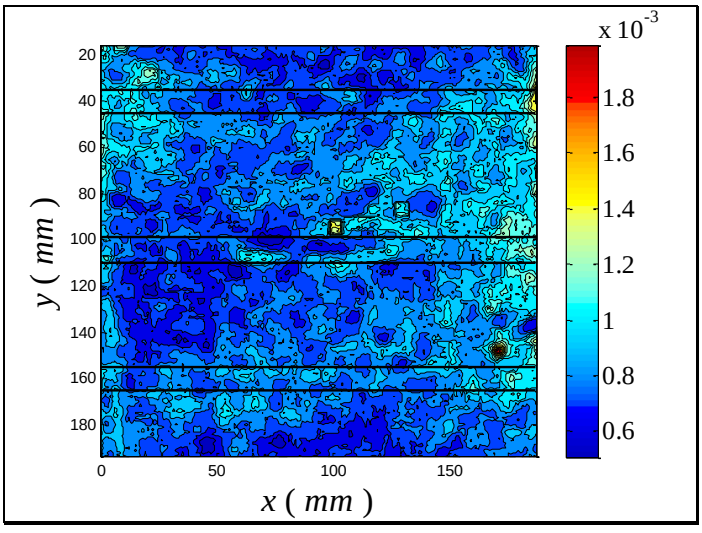

- C: 130.50 kips; 28,22 MPa

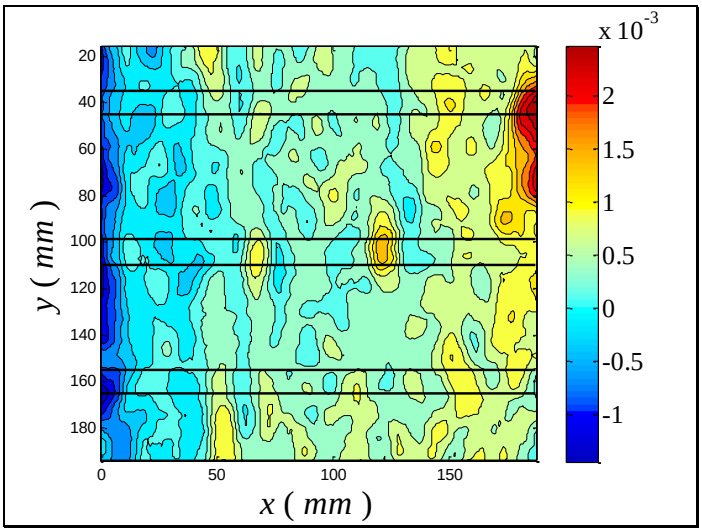

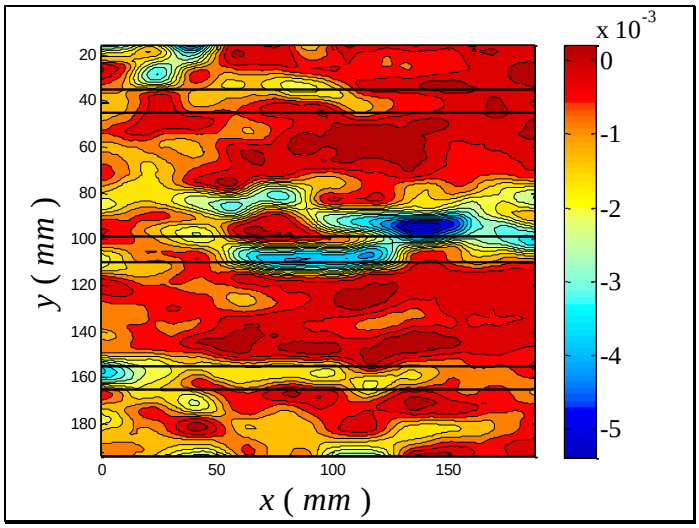

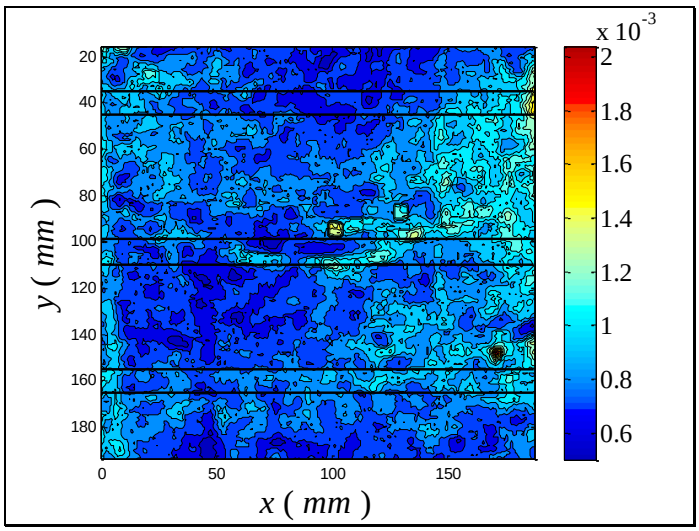

- D: 136.40 kips; 29,50 MPa

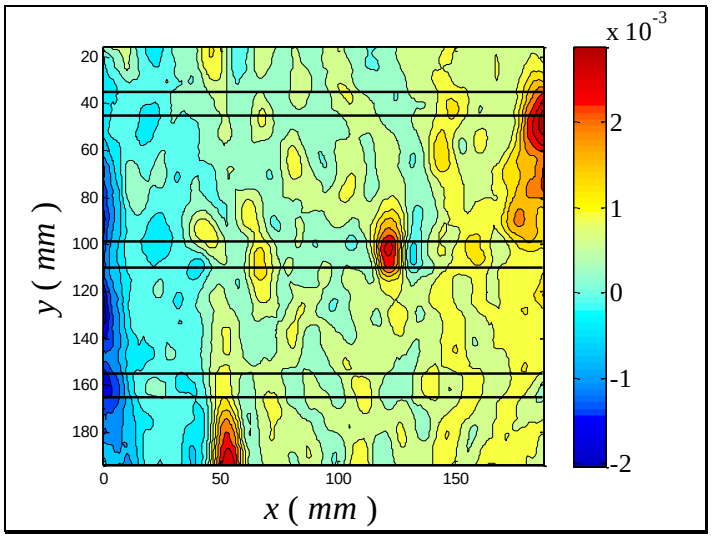

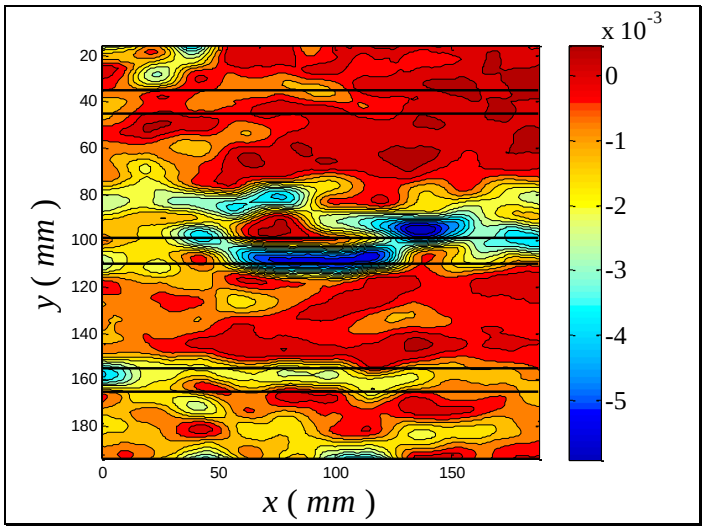

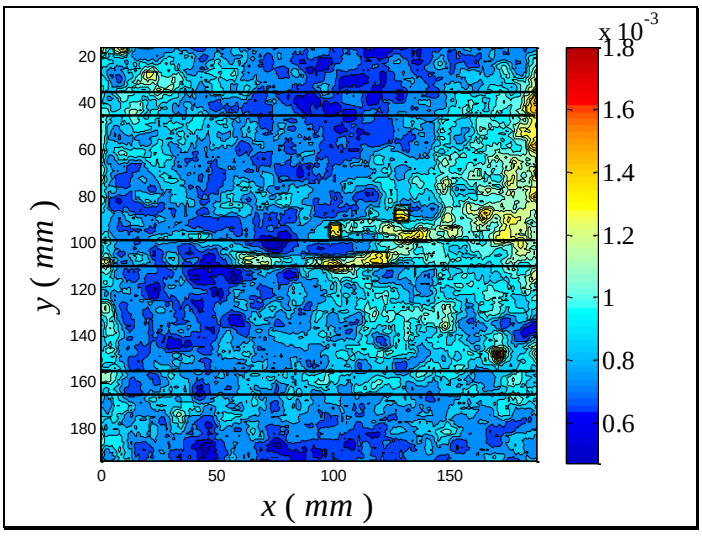

- E: 120.00 kips; 25,95 MPa

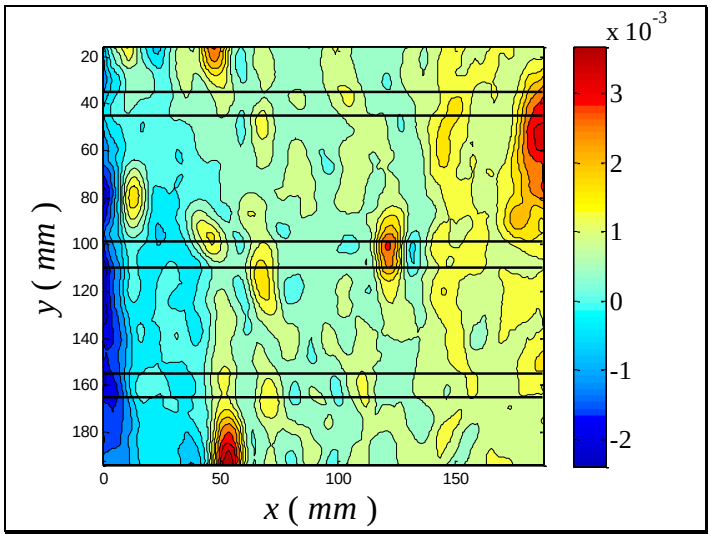

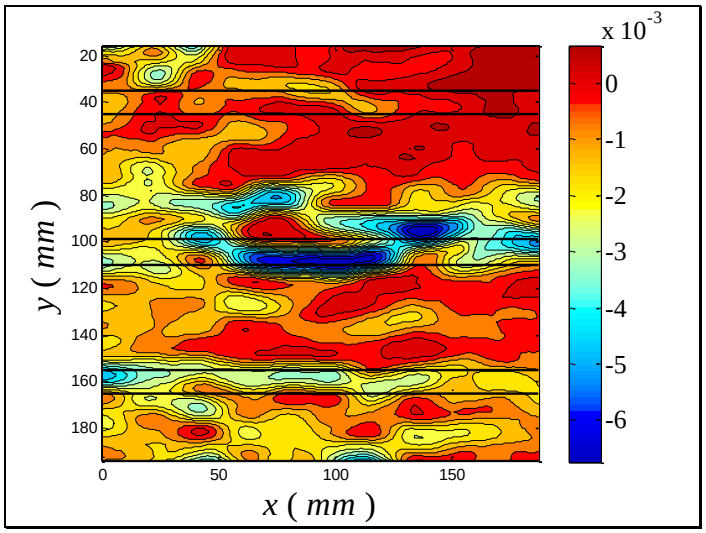

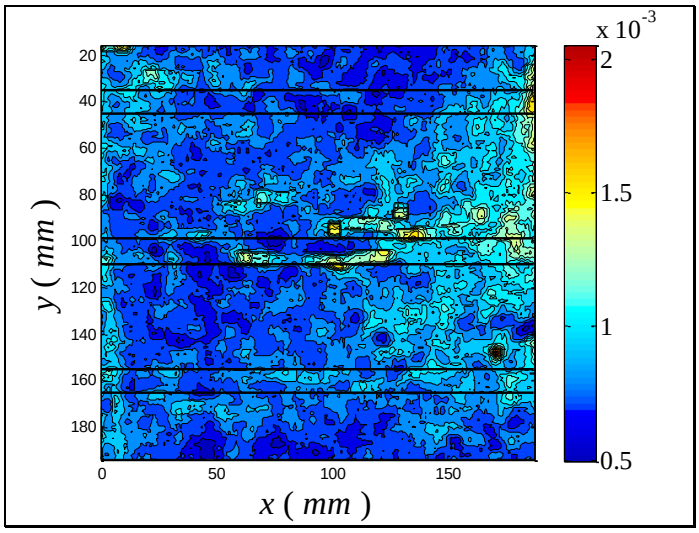

3.1.1.3. Column wrapped 3

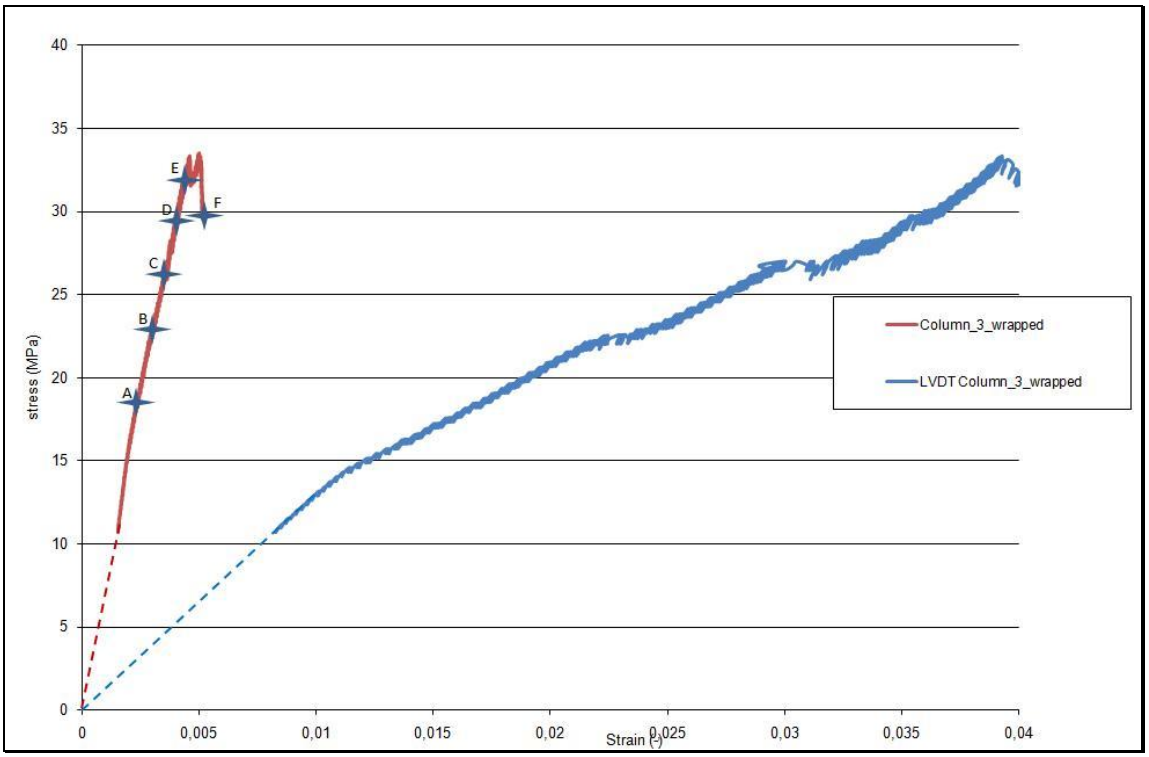

Fig.3.13 – Stress–strain diagram of column wrapped 3

The contour plots of ε_{xx} , ε_{yy} and the correlation factor for all the points in figure are reported below.

- A: 85.14 kips; 18,40 MPa

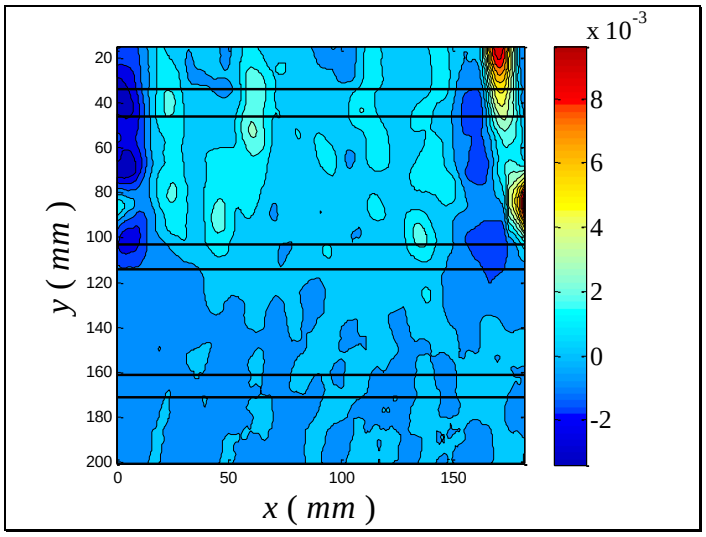

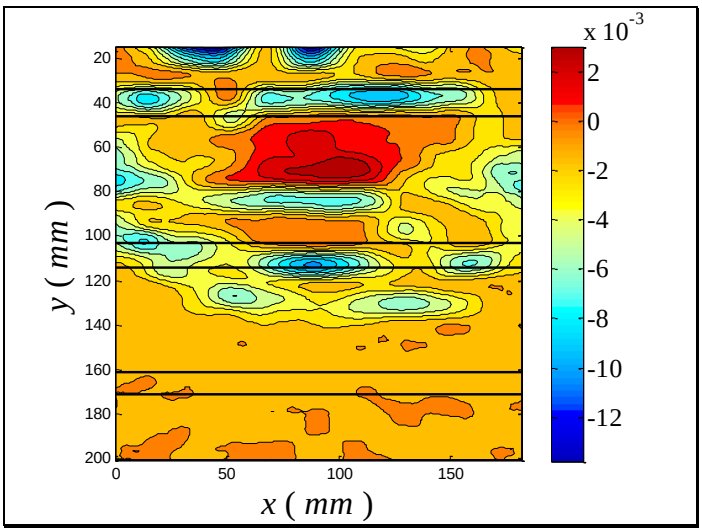

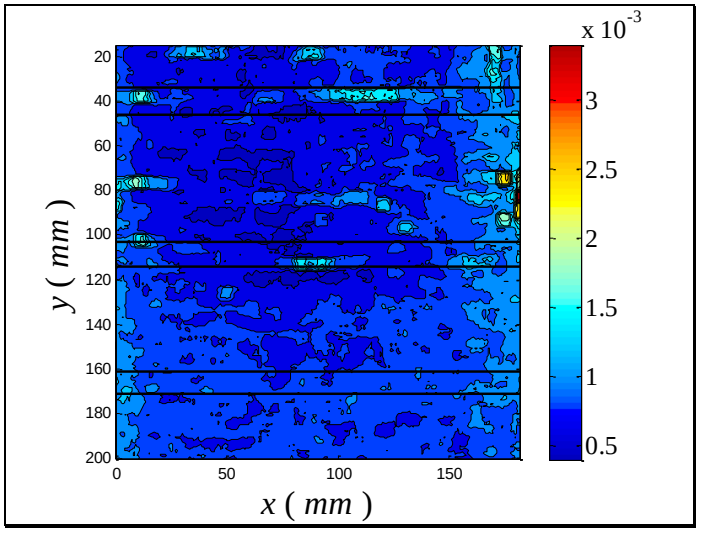

- B: 105.70 kips; 22,86 MPa

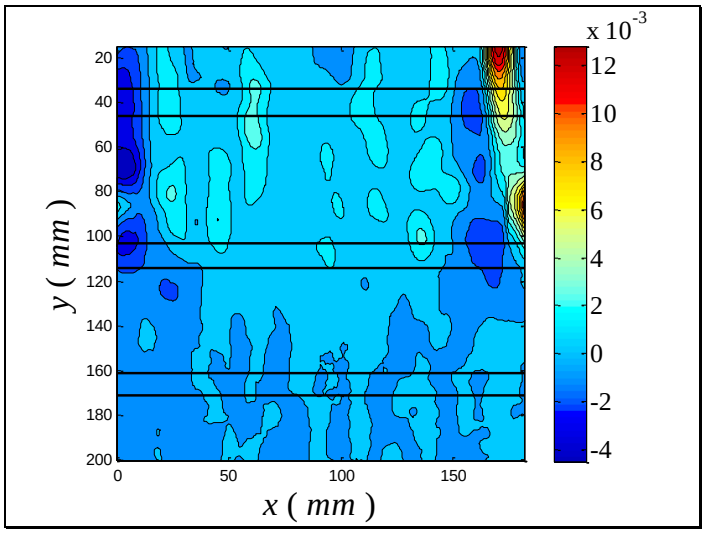

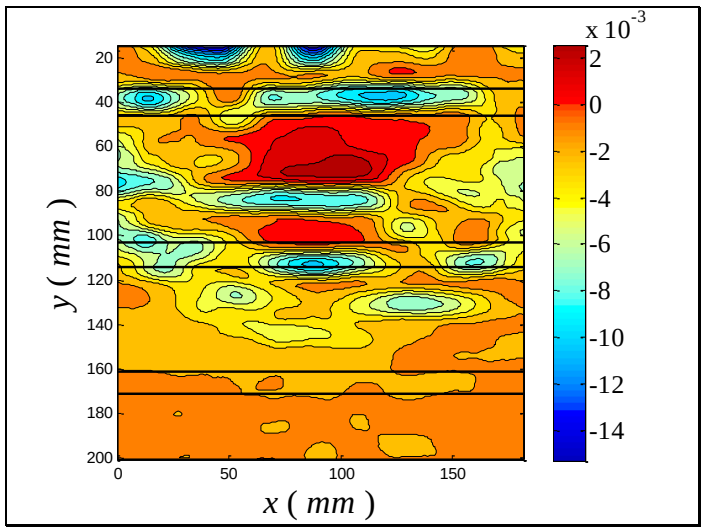

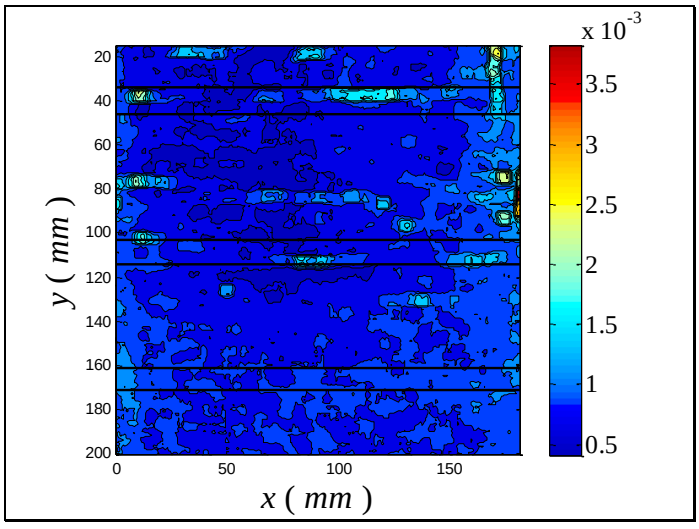

- C: 122.50 kips; 26,49 MPa

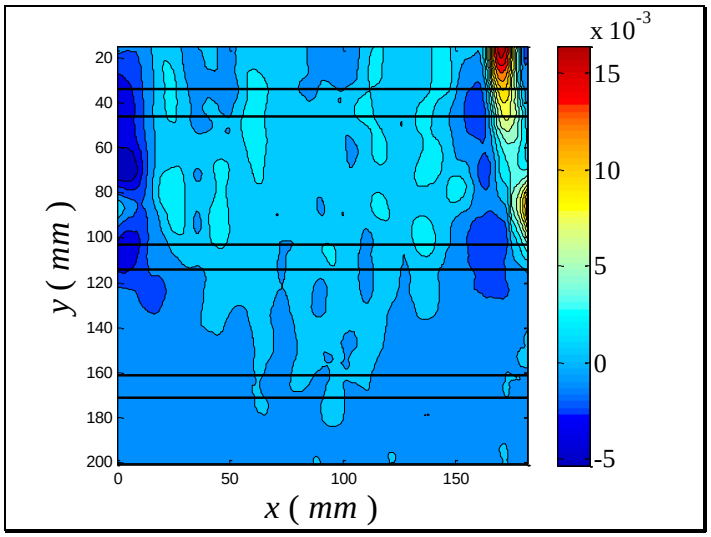

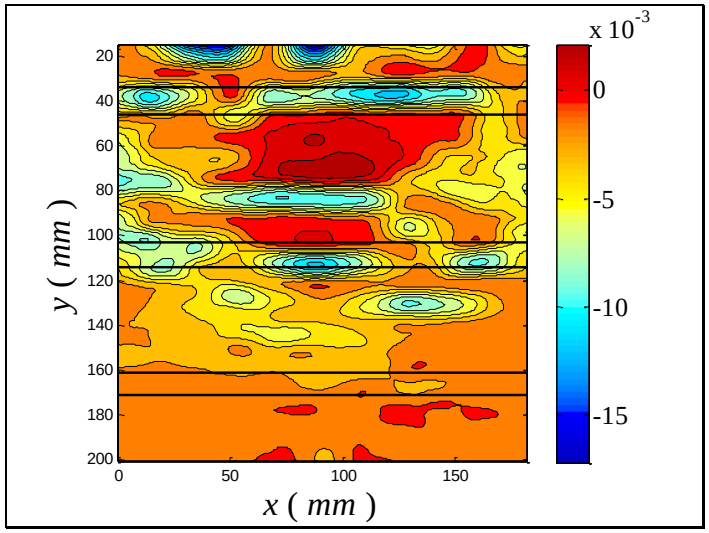

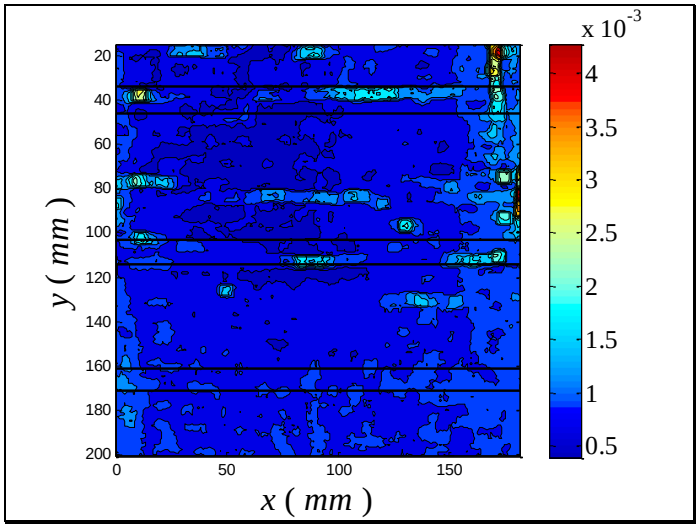

- D: 135.00 kips; 29,19 MPa

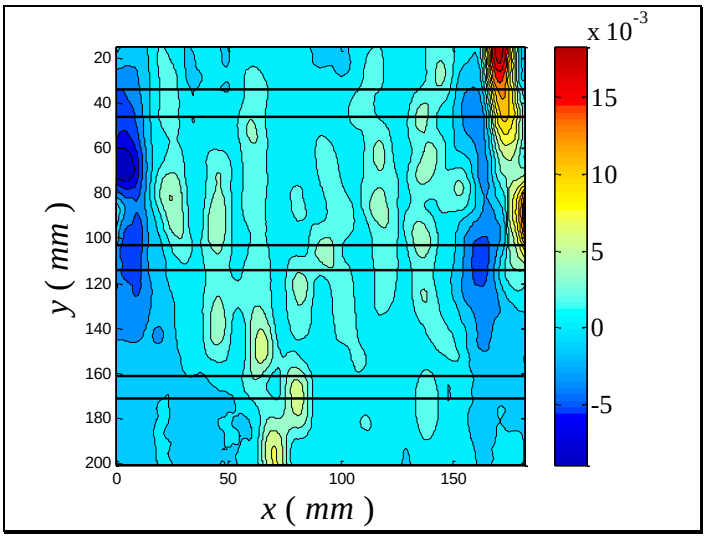

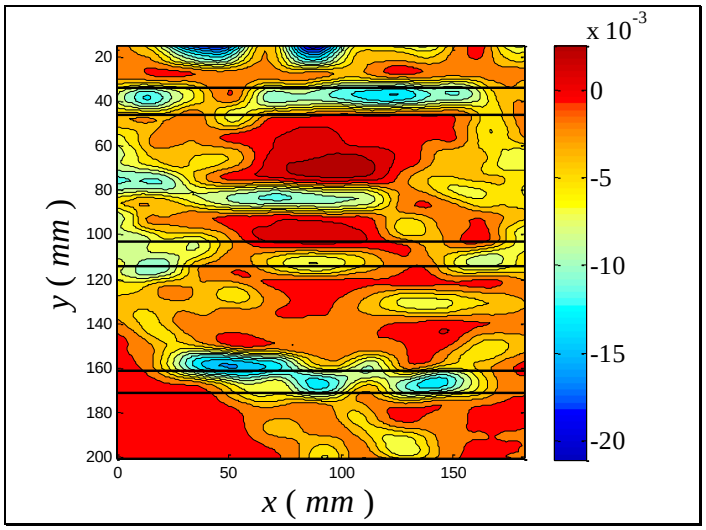

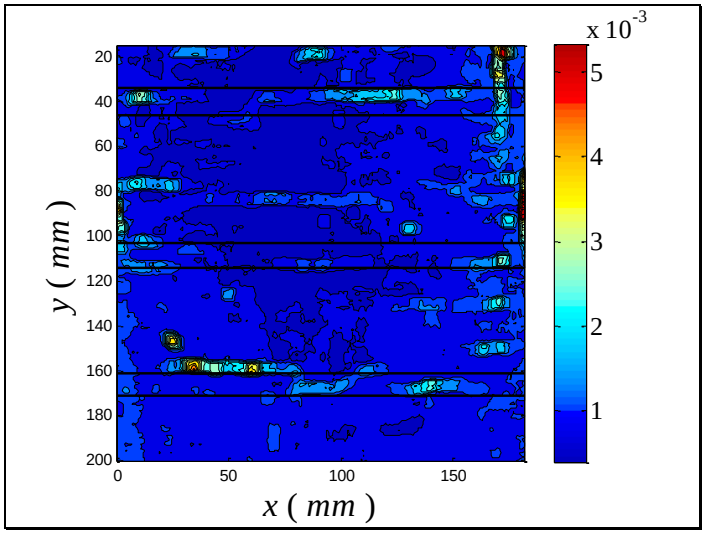

- E: 151.80 kips; 32,83 MPa

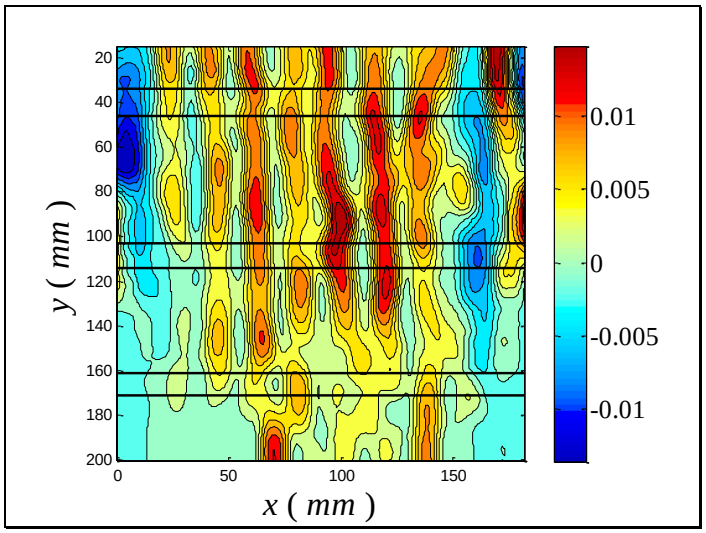

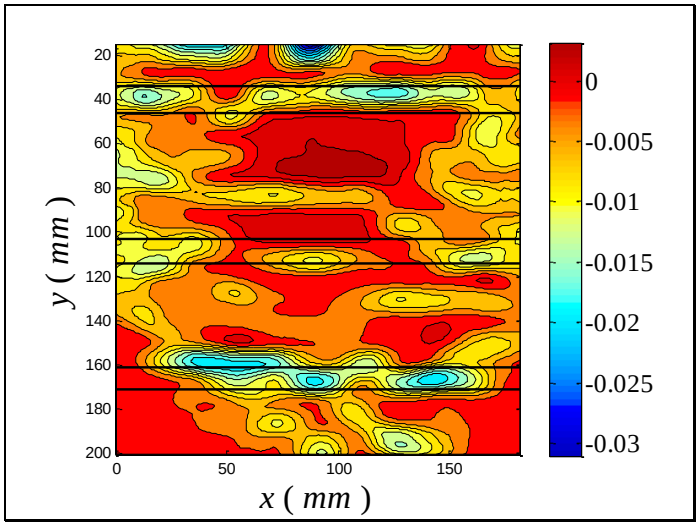

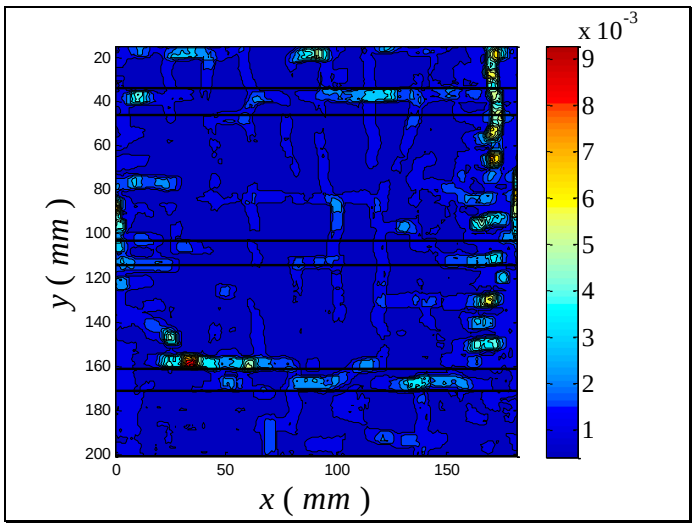

- F: 130.00 kips; 28,11 MPa

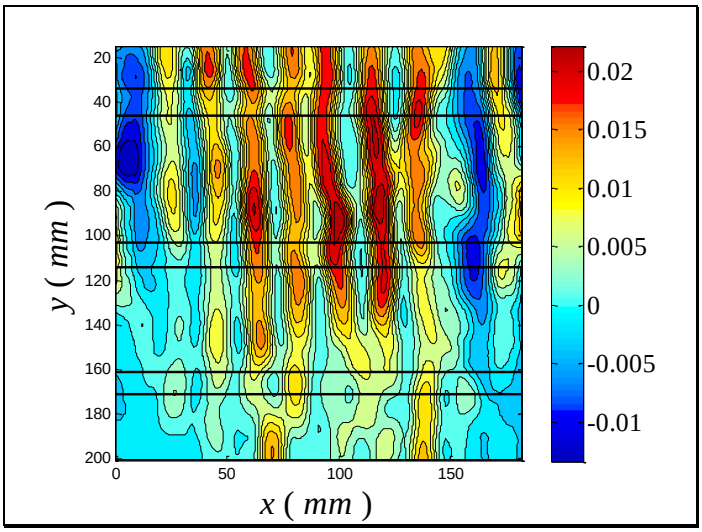

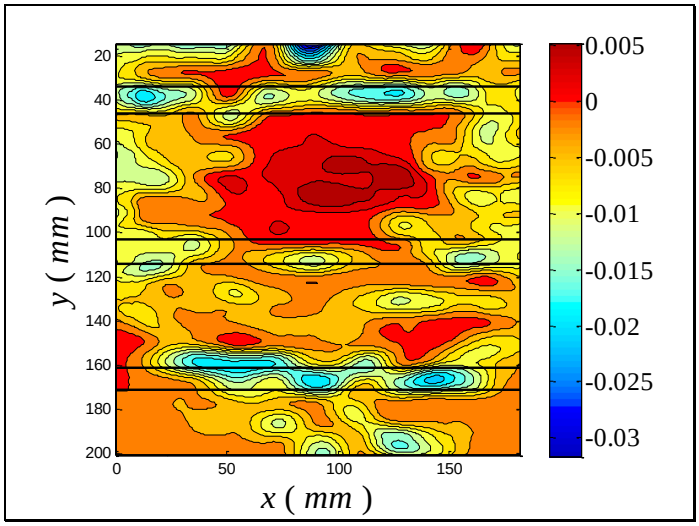

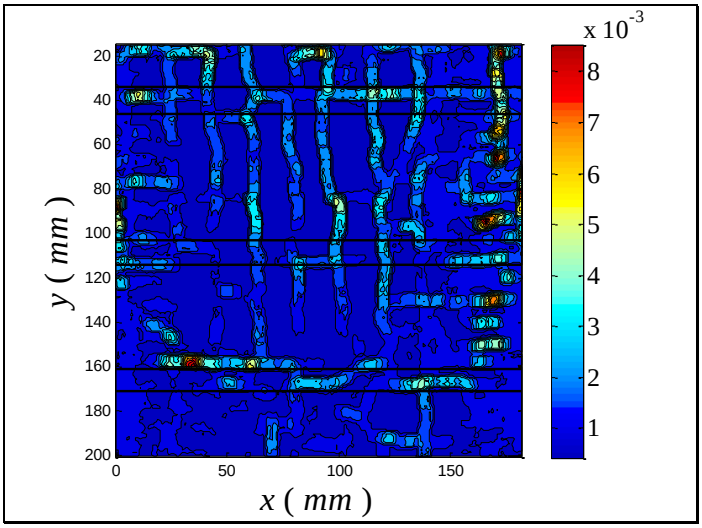

3.1.2. Discussion of result

By examining the stress-strain curves, figure 3.14, and the results given in table 3.1 in terms of strength and ultimate strain, the following observations can be made.

For this configuration FRCM-reinforcement cannot significantly enhance the strength or the deformability of masonry under axial load. This is probably due to the fact that this configuration haven't vertical joints that need to be held together during the test.

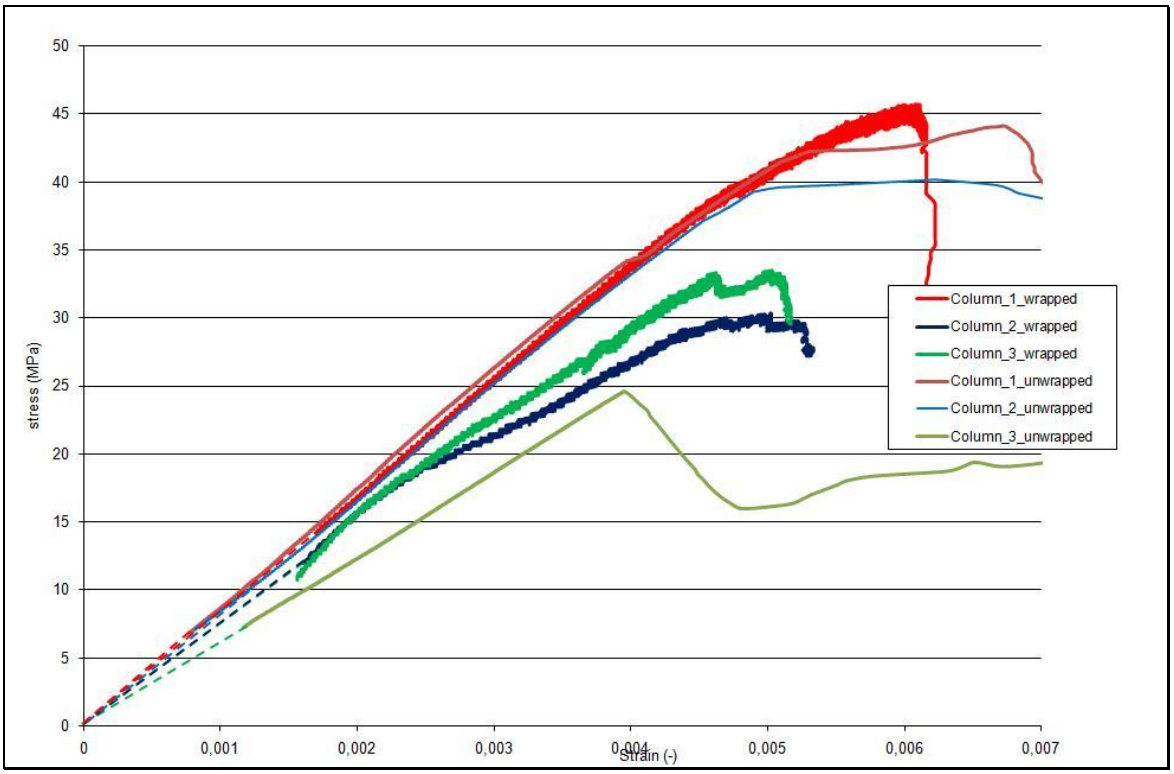

Fig. 3.14 – Stress–strain diagram of wrapped and unwrapped columns compared

The only clear effect of the reinforcement is the holding of the horizontal joints expansion as it can be seen on the DIC pictures.

The response and failure of axially loaded masonry columns confined with FRCM has many characteristics similar to those of concrete because the specimen is close to be considered homogeneous like concrete.

The mortar joints represent a discontinuity of the sections, the reinforcement help the masonry to be considered all homogeneous because help to hold the expansion of the joints.

Hence, the development of a confinement model for this configuration could be based on existing knowledge of and experience with concrete.

For rectangular cross sections, the effectively confined concrete area may be considered to be only a fraction of the overall concrete cross section, figure 3.15.

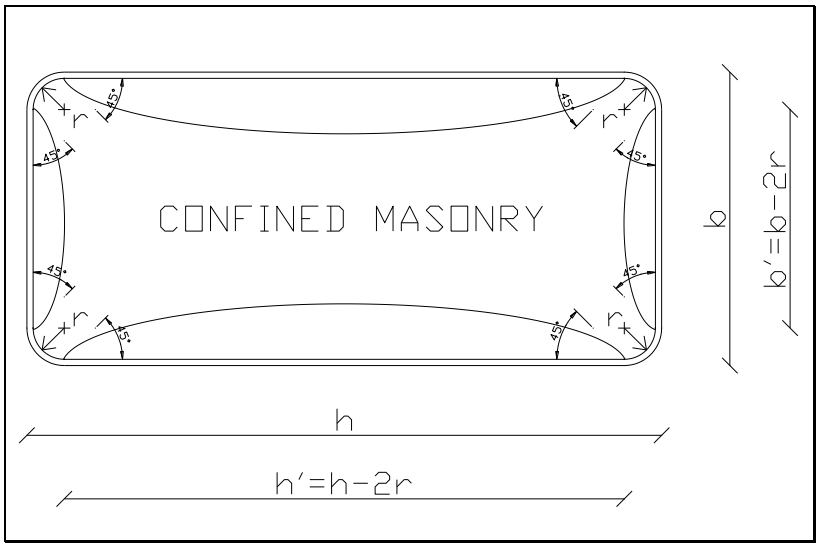

Fig. 3.15 – Effectively confined area in rectangular section columns

The reason for such a behavior lies in the "arch effect" that forms within the cross section. Such an effect depends on the values of the corner radius. [3]

The effectively confined area is assumed to occur within the region where the arching action has been fully developed. The arching action for concrete is represented in the form of a second-degree parabola with an initial tangent slope of 45°. The area within the parabolas is considered as ineffectively confined. [12]

Fig. 3.16 – Arch effect in one specimen after a cut in the middle

Experimental evidences show that the arch effect exist in the brick section but probably the development is not in the form of a second-degree parabola as for the concrete.

In the ε_{yy} is possible to see that in the joints line there is a concentration of the deformation in the central part of the brick caused from the push of the mortar joints on the wrapping.

In all the DIC pictures is clear that after the formation of crack on the wrapping surface there is no more reliabilities on the deformations.

Finally, further studies are required to validate the proposed conclusion and a numerical analysis is required for a complete understanding of the behavior of a wrapped specimen like this under an axial compression test.

CHAPTER 4

BRICK MASONRY WALLS

C H A P T E R 4

BRICK MASONRY WALLS

4.1. Experimental Test Description

In this second part of experimentation we cast three different type of masonry walls using bricks scaled respect with the first ones with a ratio 1:2, figure 4.1.

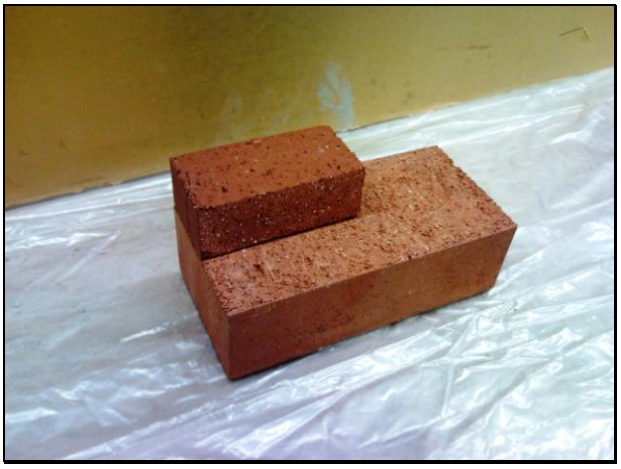

Fig. 4.1 – Brick scaled

A total of 17 model masonry walls specimens were prepared using cut clay bricks with dimensions about of 47 mm width, 30 mm height, and 100 mm length, bonded together with the same mortar used for the other specimens. The cross-sectional area of the specimens was about 100x100 mm with an aspect ratio 1:1 for the first type, figure 4.2.

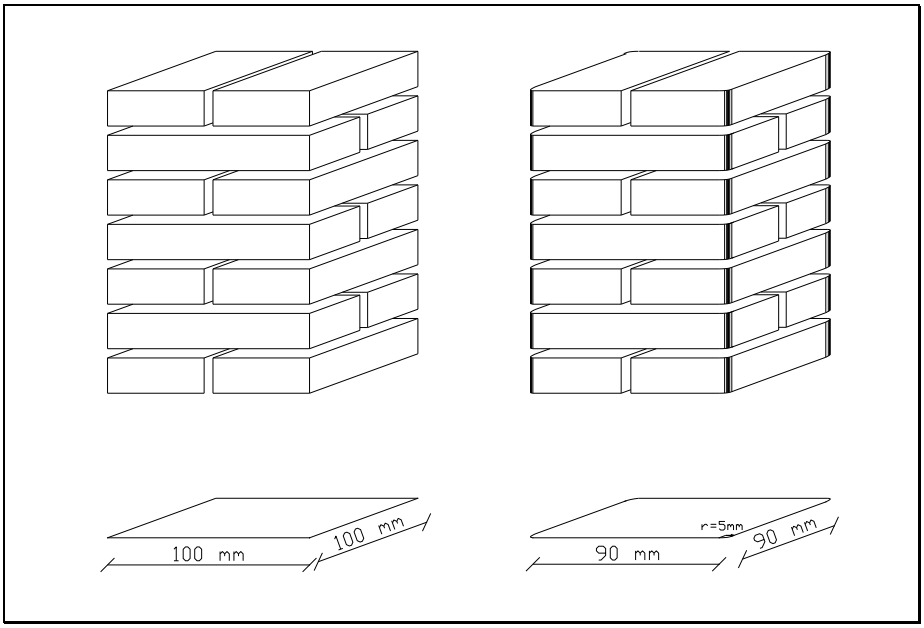

Fig. 4.2 – First model walls

About 100x150 mm with an aspect ratio 1,5:1 for the second type, figure 4.3.

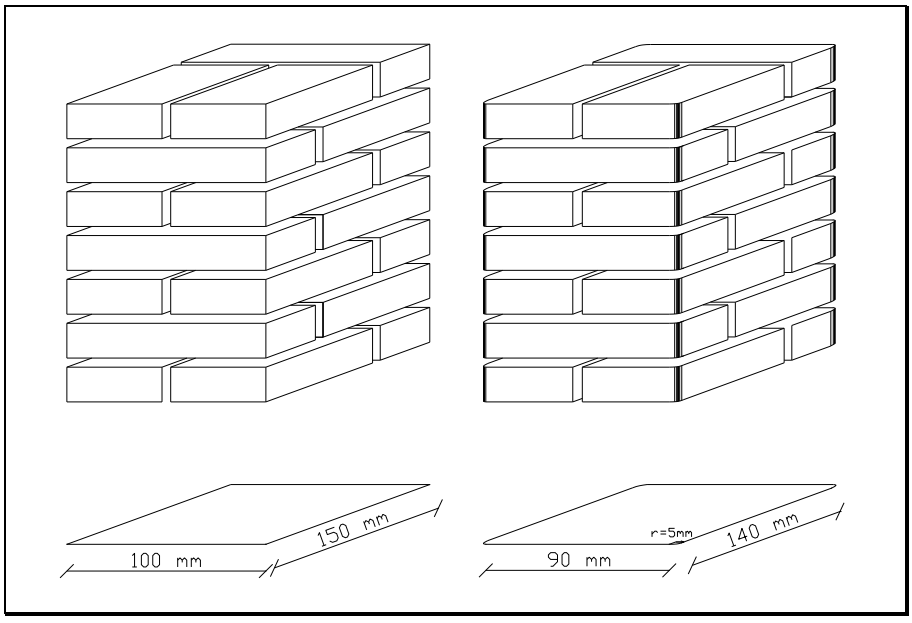

Fig. 4.3 – Second model walls

About 100x200 mm with an aspect ratio 2:1 for the third type, figure 4.4.

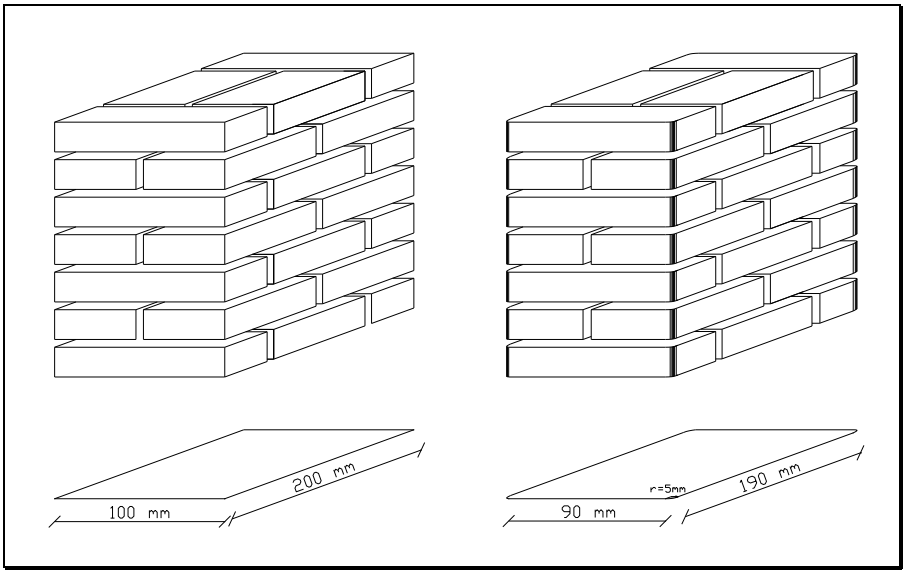

Fig. 4.4 – Third model walls

Each model walls comprised bricks placed in seven rows with six bed joints between, 240 mm height.

The thickness of mortar was, in general, 5 mm.

The corners of 6 specimens, two for each type, were rounded using a grinding machine at a radius of 5 mm. These specimens were wrapped with one layer of Fiber Reinforced Cementitious Matrix (FRCM), an high performance fiber structural reinforcement systems.

Fig. 4.5 – Masonry walls casting

The configurations described above allow investigation of the role of the aspect ratio of the cross section in the effectiveness of FRCM-reinforcing of confined masonry.

4.1.1. Material characterization

Materials characterization was carried out to investigate the mechanical properties of the materials involved in the experimental program.

Three mortar cylinders 150 mm × 75 mm diameter (L/D=2) were cast from the same batch used to cast the specimens used for the tests, figure 4.6.

Fig. 4.6 – Mortar cylinders

Mortar and masonry specimens were demolded 24 hours after casting and subjected to curing at 99% RH until tested.

Cylinders were tested for ultimate strength and elastic modulus using the clip-gauge, is a type of electrical transformer used for measuring linear displacement..

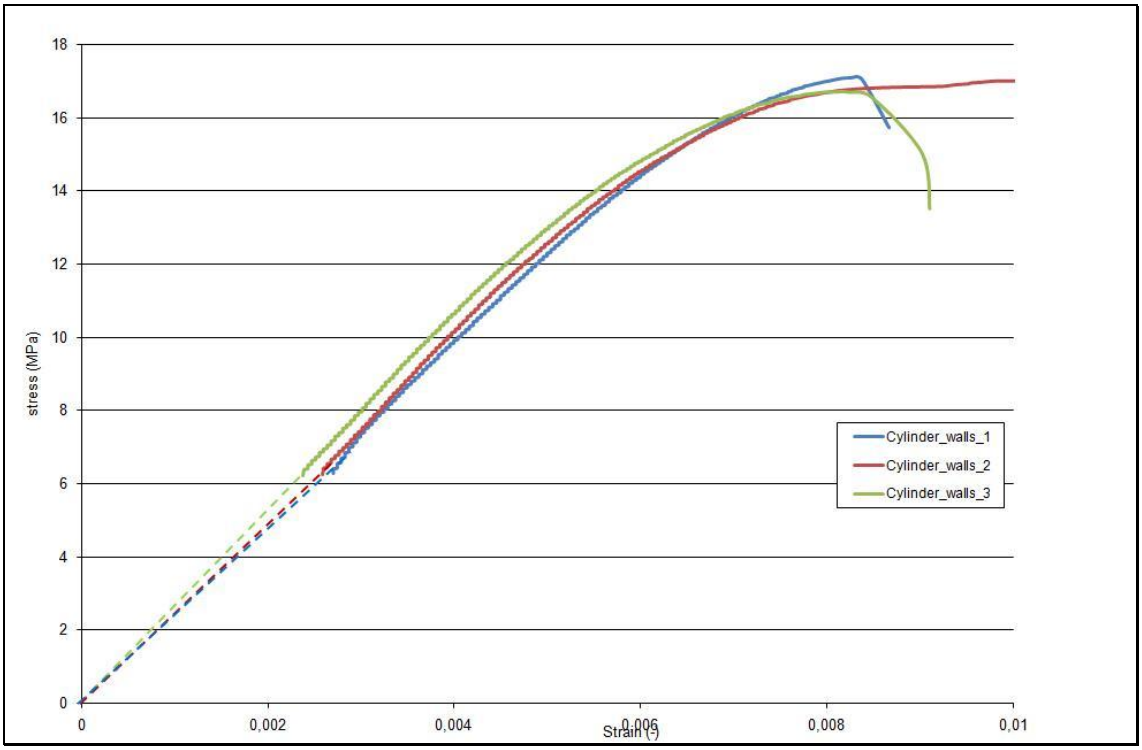

Fig. 4.7 – Stress–strain diagram of mortar cylinders

Specimens notation	**5 precycle (kN)**	**Area (cm^2)**	**Compressive strenght (MPa)**	**Elastic modulus (MPa)**
1	5-27	44,16	17,09	2450
2	5-27	44,16	17,03	2500
3	5-27	44,16	16,70	2625
Load control mode of 1.5 kips/min, about 7 kN/min				

Tab. 4.1 – Summary of test results for mortar cylinder

The average values of the elastic modulus and compression strength for mortar were determined to be 2520 MPa and 16,94 MPa, respectively.

Fig. 4.8 – Failure of cylinder specimens

The bricks were tested for ultimate strength and elastic modulus using the Digital Image Correlation, figure 4.9.

Fig. 4.9 – Brick specimen ready for the DIC

The load was applied perpendicular to the direction along which bricks are normally loaded on 3 half brick specimens, figure 4.10.

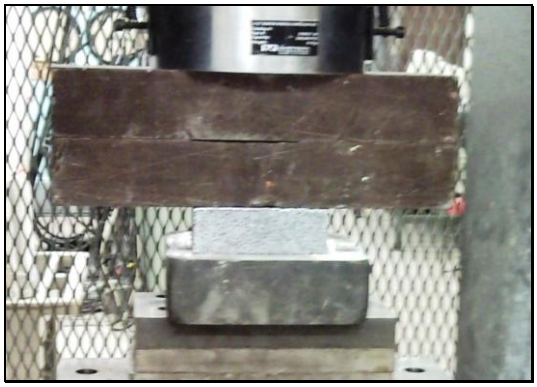

Fig. 4.10 – Brick specimen ready for the test

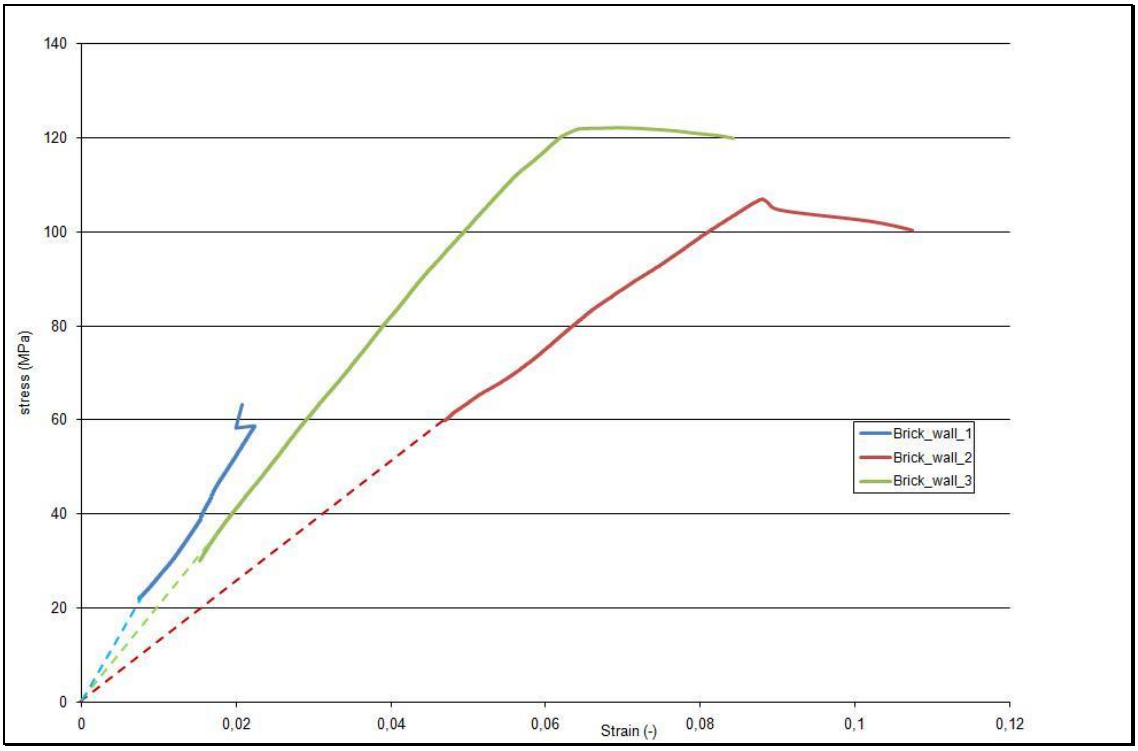

Fig. 4.11 – Stress–strain diagram of brick specimens

Specimens notation	**3 precycle (kN)**	**Area (cm^2)**	**Compressive strenght (MPa)**	**Elastic modulus (MPa)**
1	5-15	90	57,17	2600
2	130-265	90	107,14	1250
3	130-265	90	122,00	2045
Load control mode of 10 kips/min, about 45 kN/min				

Tab. 4.2 – Summary of test results for brick specimens

The average values of the elastic modulus and compression strength for brick were determined to be 5900 MPa and 95.44 MPa, respectively.
In the next chart there is a summary of all the material characterization.

Fig. 4.12 – Failure of brick specimens

Material	Specimen	Properties
Brick	100 x 90 x 55mm	elastic modulus: 5900 MPa; compression strength: 95,44 MPa.
Mortar	Cylinders 150 × 75 mm	elastic modulus: 2520 MPa; compression strength: 16,94 MPa.
Fiber-Reinforced Cementitious Matrix	Supplier	elastic modulus: 270 GPa; tensile stress of the warp per unit of width: 264 kN/m; tensile stress of the weft per unit of width: 66,5 kN/m.

Tab. 4.3 – Material characterization

4.2. Axial Compression Test First Configuration

At least 28 days after the specimens casting, 14 days in curing room at 99% RH and 14 days in the laboratory RH equal to 50% waiting for the reinforcement curing, the walls were tested under axial compression load.

Fig. 4.13 – First configuration masonry wall

Spatially continuous measurements of displacements are obtained using the Digital Image Correlation after the tests, after the preparation of the specimen, figure 4.14.

Fig. 4.14 – First configuration masonry wall ready for the DIC

The objective of testing is to record the axial stress-strain curve and the failure mode of all the masonry specimens, which are subjected to axial loading applied monotonically under a loading control mode in the same compression testing machine used for the other specimens.

Displacements across the 3 central bricks and 2 joints on each specimen were measured using also a Linear Variable Differential Transformer (LVDT) on the left side of the walls attached to the brick surface.

Fig. 4.15 – Square wall ready for the test

4.2.1. Experimental result and failure mode

The main results of the tests are presented in the table 4.4.

Specimens notation	3 precycle (kN)	Maximum load (kN)	Area (cm^2)	Compressive strenght (MPa)	Ultimate machine strain ε
1	20-65	292,59	100	28,63	0,0070
2	20-90	329,86	100	31,95	0,0050
3	20-90	267,68	100	25,93	0,0040
Displacement control mode of 0.008 inch/min, about 0.2 mm/min					

Tab. 4.4 – Summary of test results for square walls unwrapped

The stress-strain diagrams for the first configuration unwrapped specimens are presented in figure 4.16.

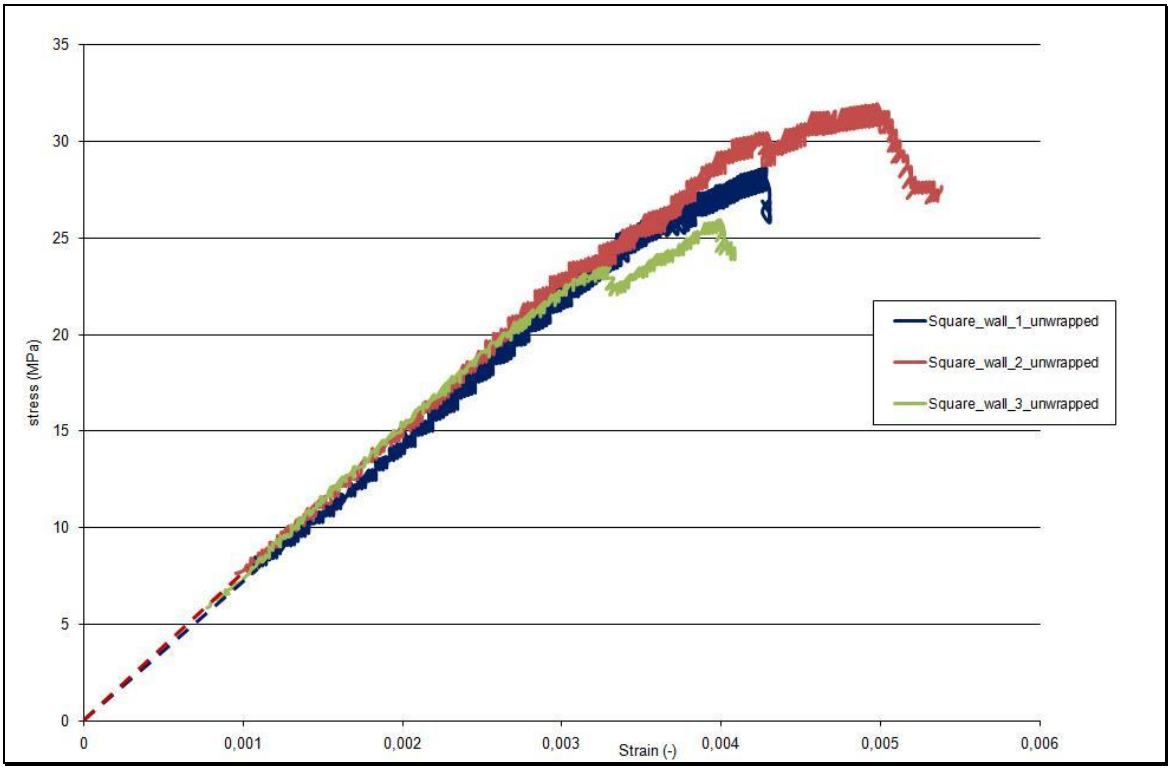

Fig. 4.16 – Stress–strain diagram of square walls unwrapped

It can be observed that in all cases the diagrams are linear up to about 80% of the maximum load.

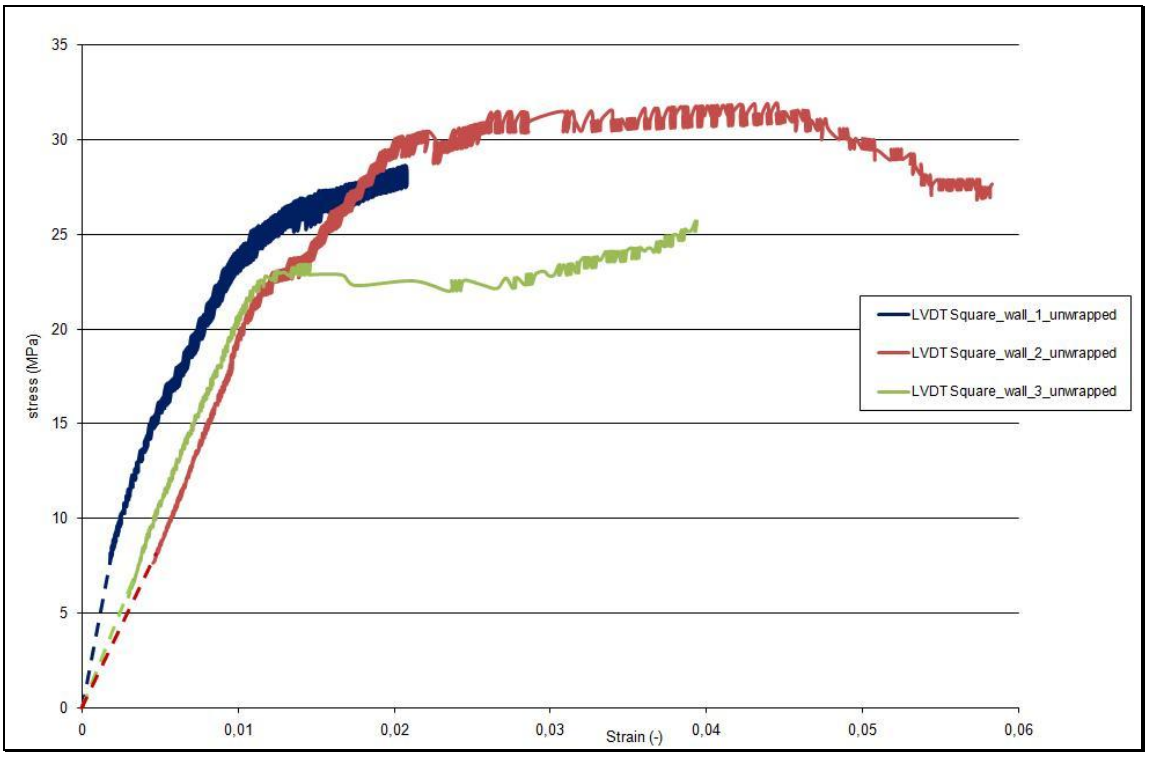

Fig. 4.17 – Stress–LVDTstrain diagram of square walls unwrapped

The control specimens failed in a brittle manner by the formation of vertical cracks through the joints and the bricks in the face that have 4 vertical joints.

Fig. 4.18 – Formation of vertical crack on the wall

After their formation through mortar joints and bricks, vertical cracks became increasingly wide and the masonry between the cracks was crushed.

4.2.1.1.Square wall unwrapped 1

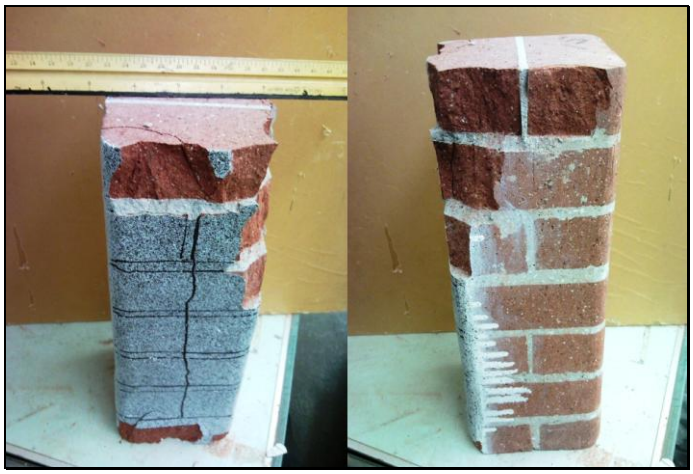

Fig.4.19 – Square wall unwrapped 1

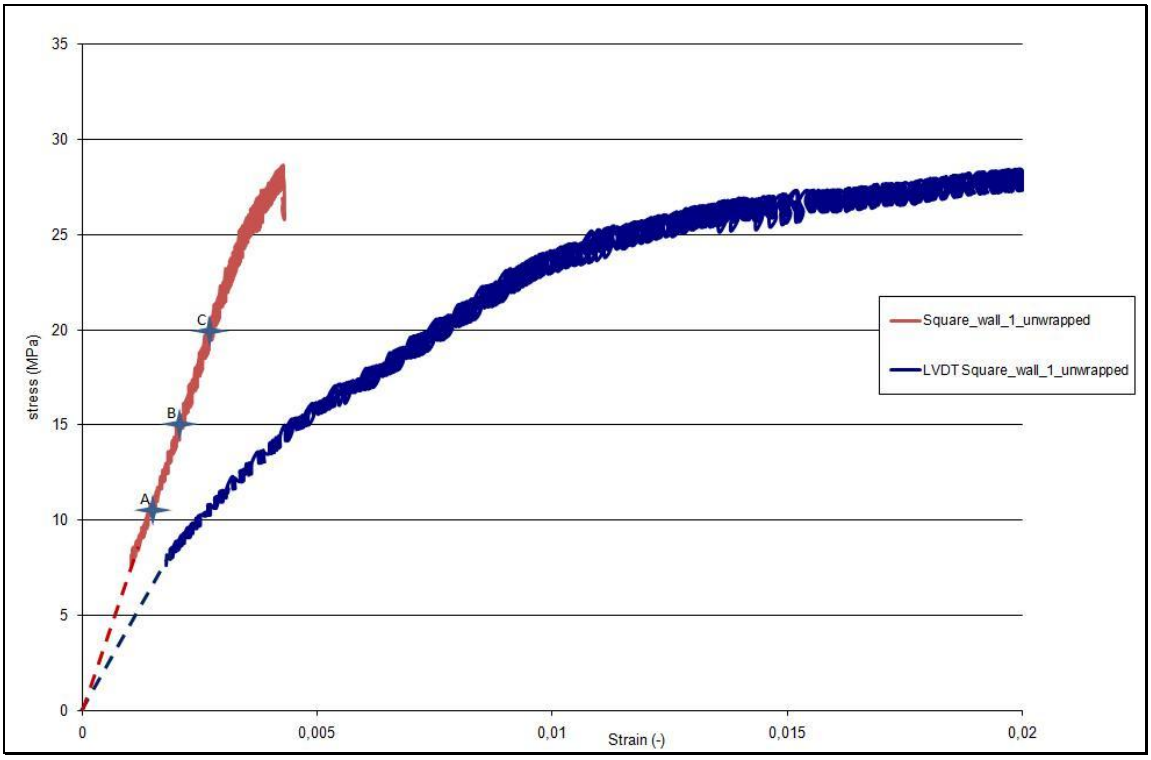

Fig.4.20 – Stress–strain diagram of square wall unwrapped 1

The contour plots of ε_{xx} , ε_{yy} and the correlation factor for all the points in figure are reported below.

- A: 26.10 kips; 11,36 MPa

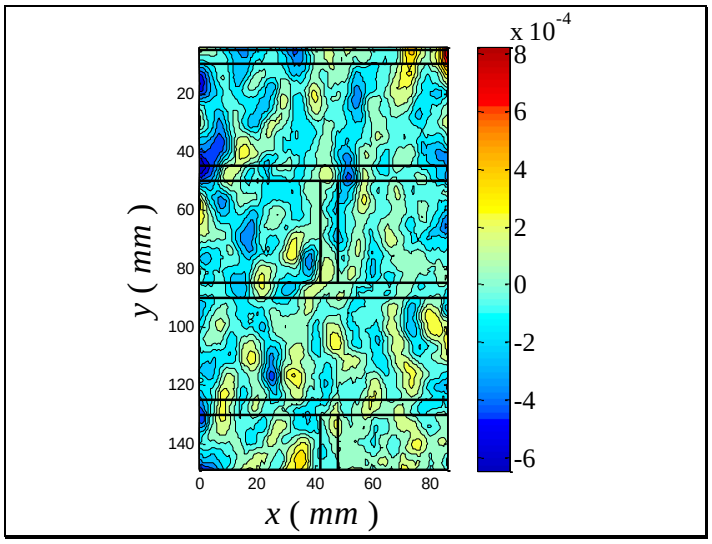

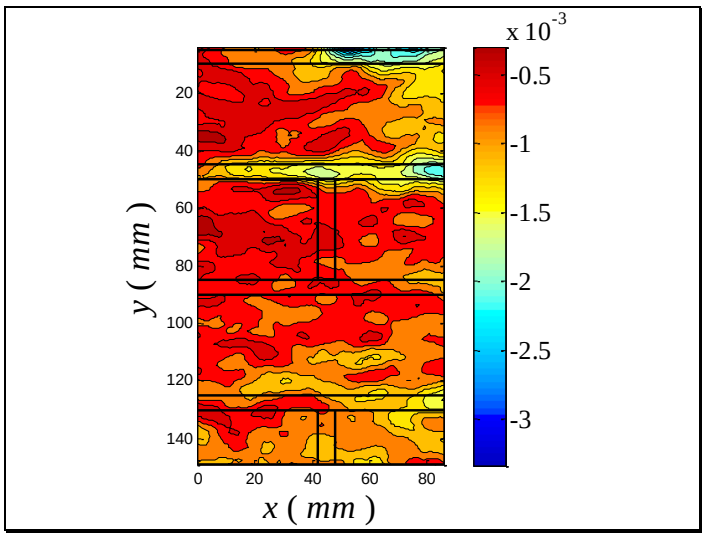

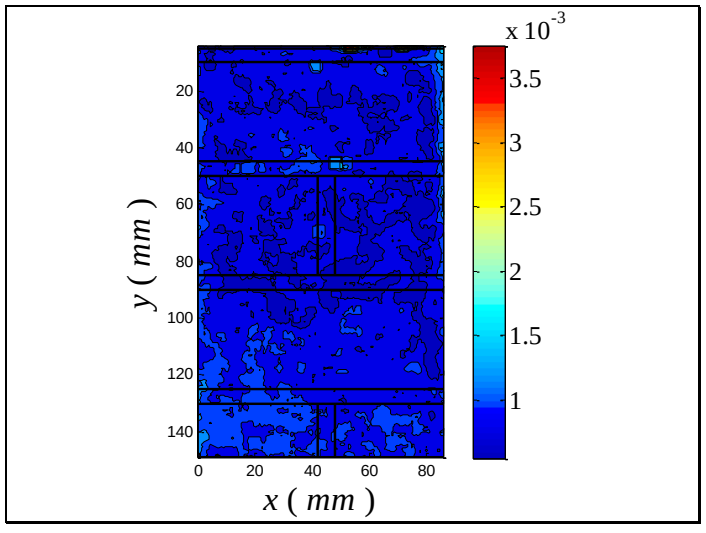

- B: 36.51 kips; 15,89 MPa

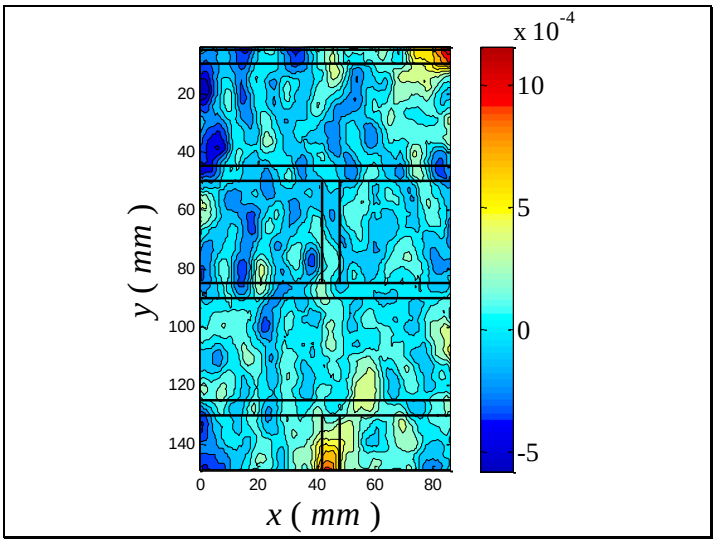

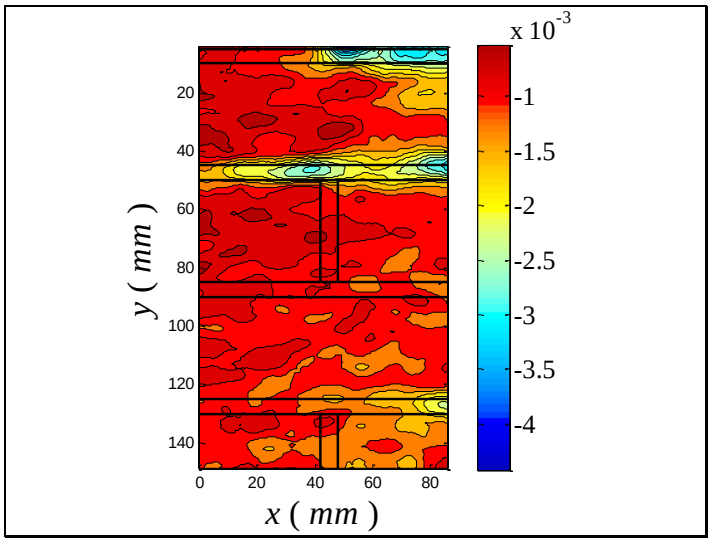

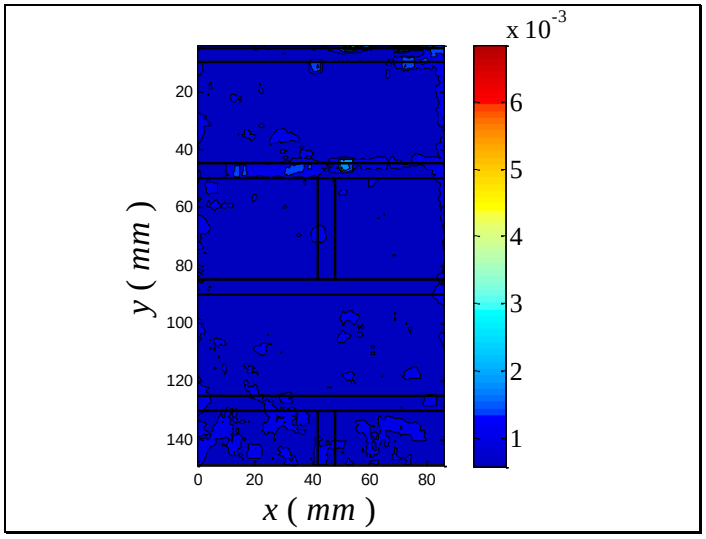

- C: 46.00 kips; 20,02 MPa

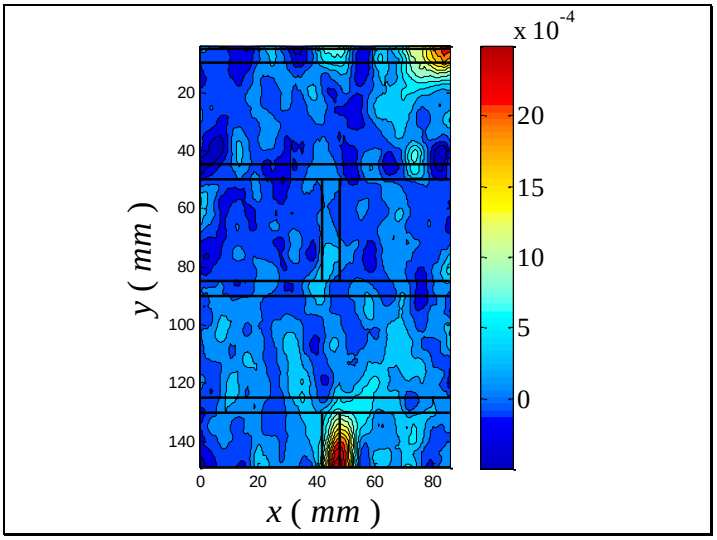

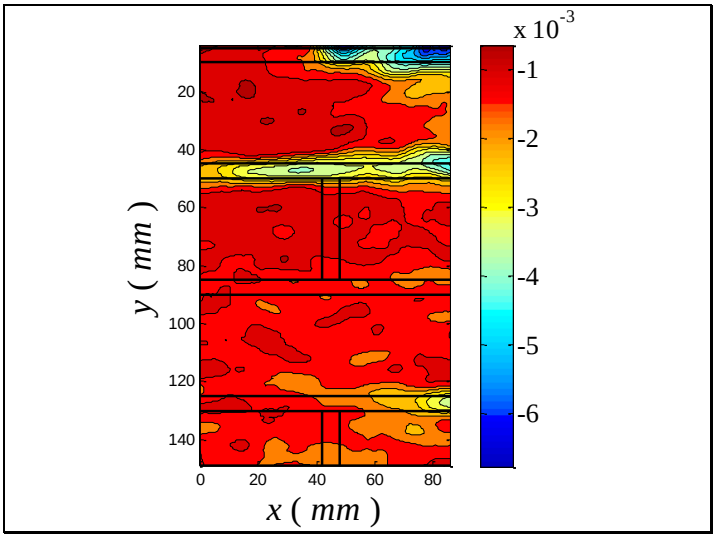

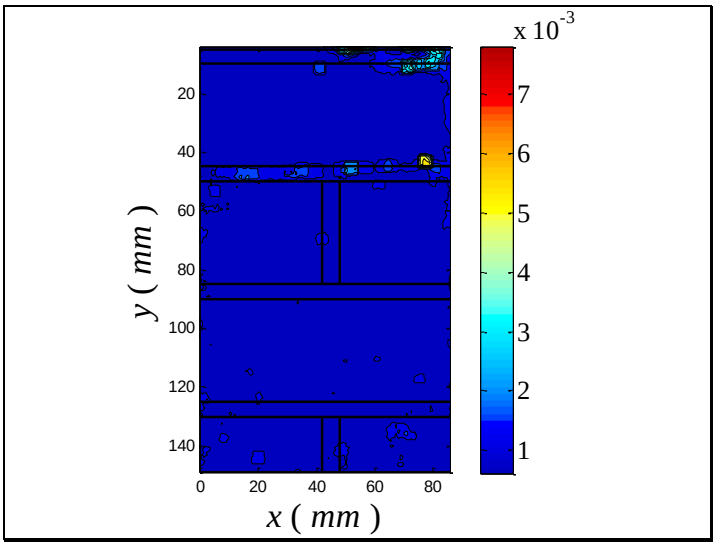

4.2.1.2.Square wall unwrapped 2

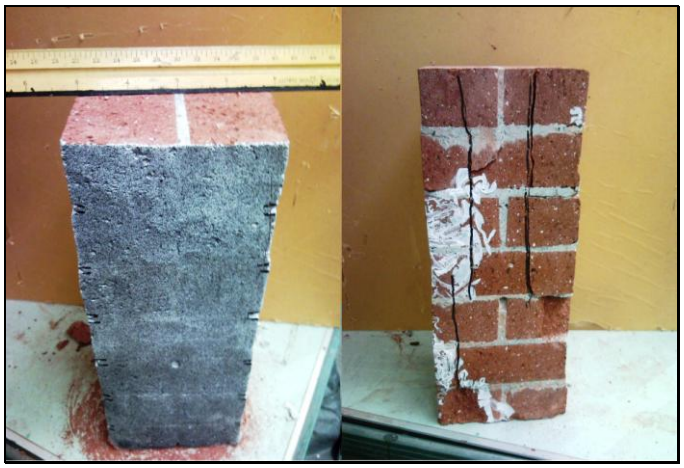

Fig.4.21 – Square wall unwrapped 2

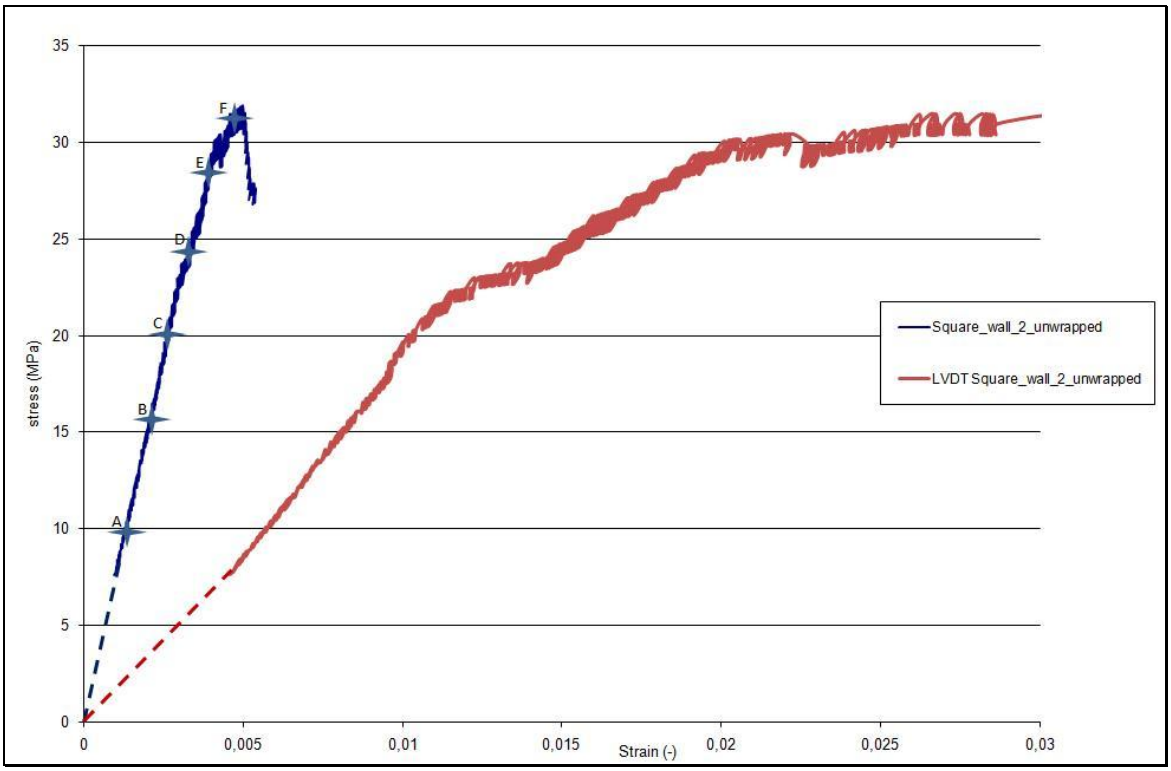

Fig.4.22 – Stress–strain diagram of square wall unwrapped 2

The contour plots of ε_{xx} , ε_{yy} and the correlation factor for all the points in figure are reported below.

- A: 21.50 kips; 9,26 MPa

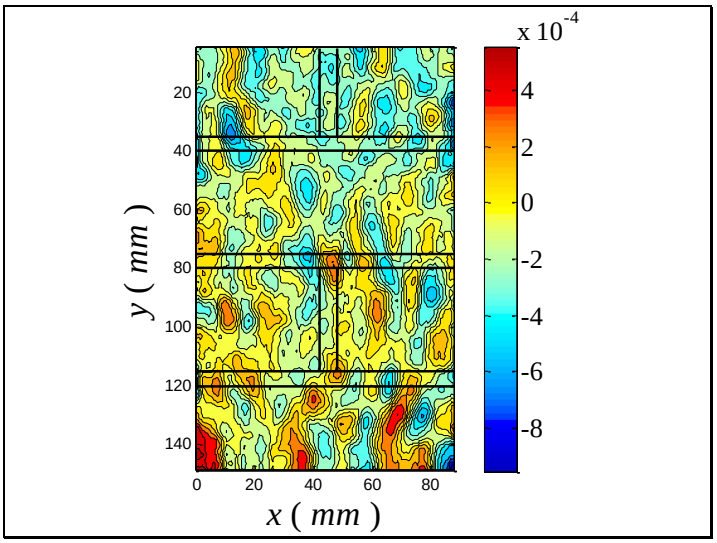

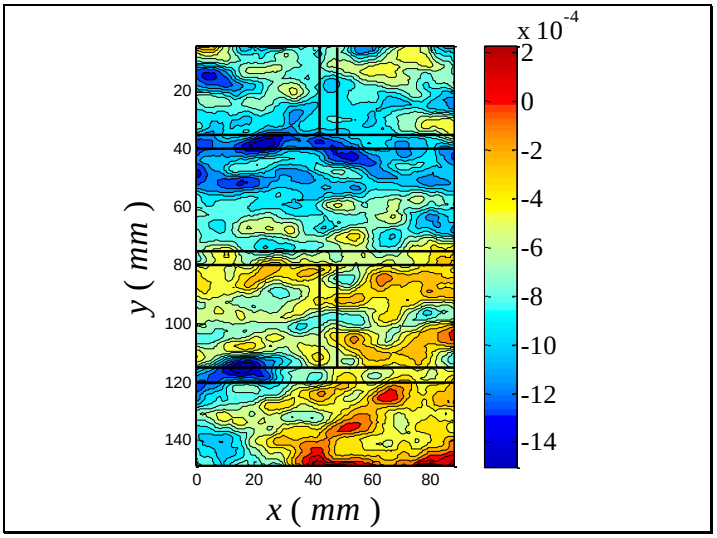

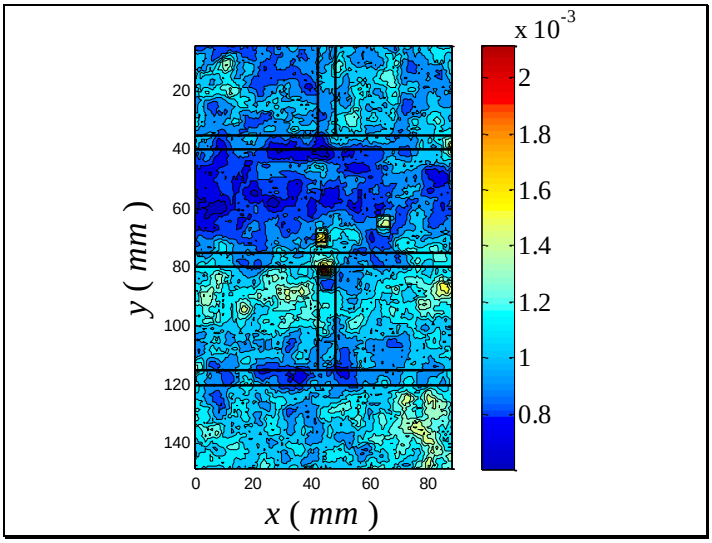

- B: 38.50 kips; 16,59 MPa

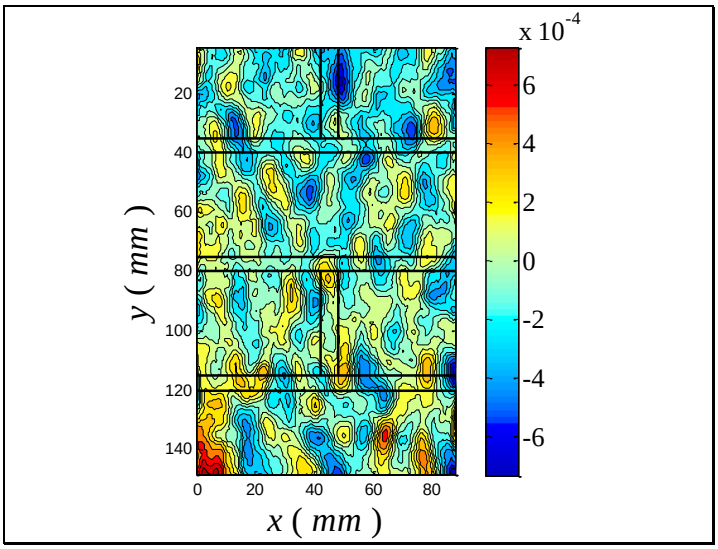

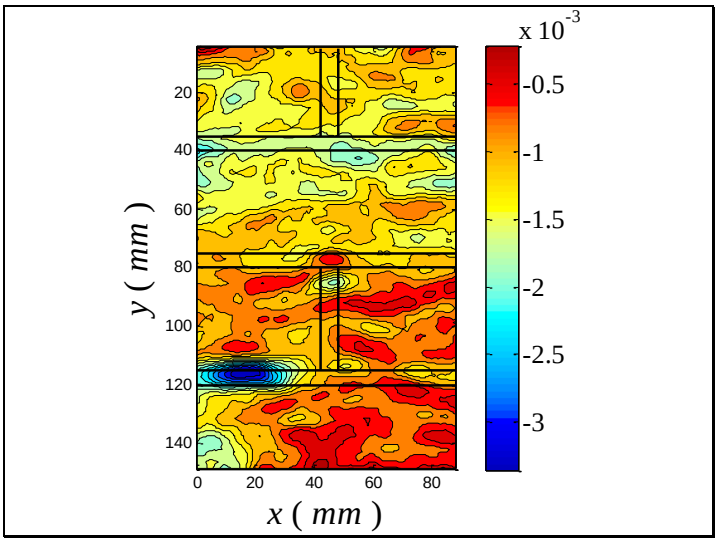

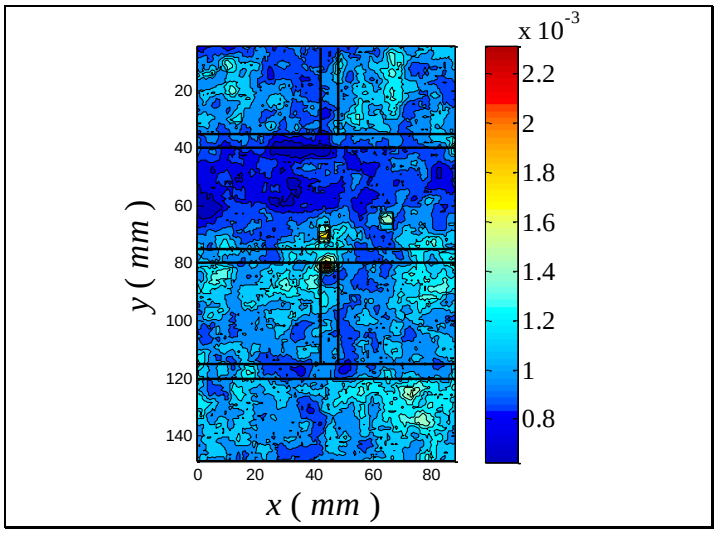

- C: 50.00 kips; 21,55 MPa

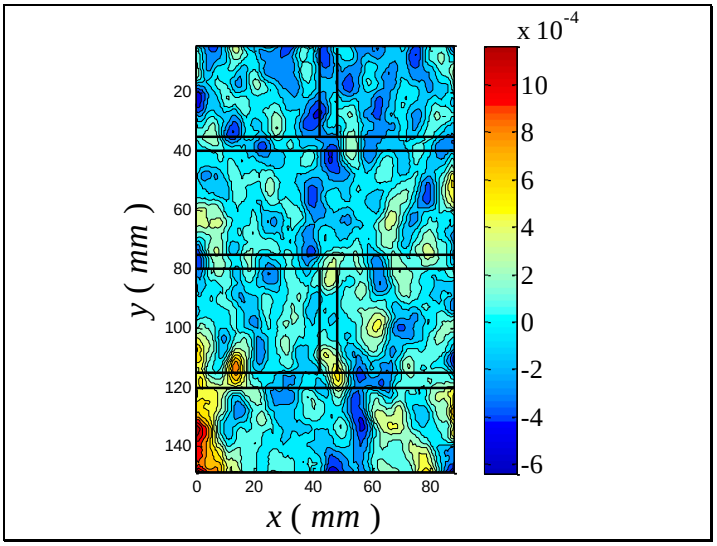

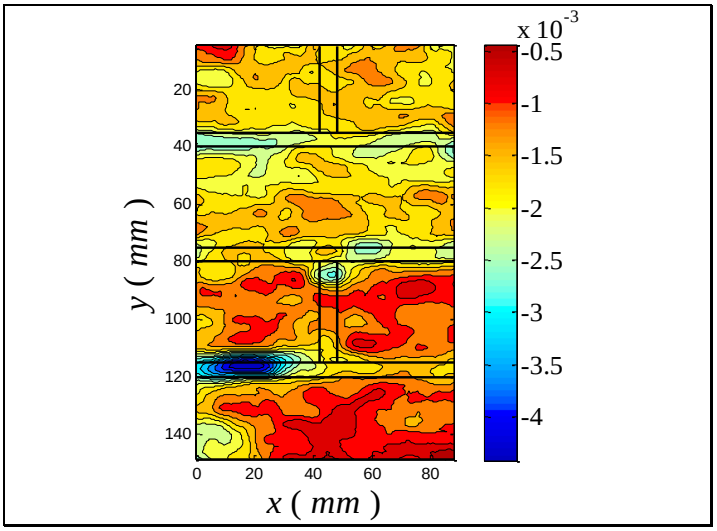

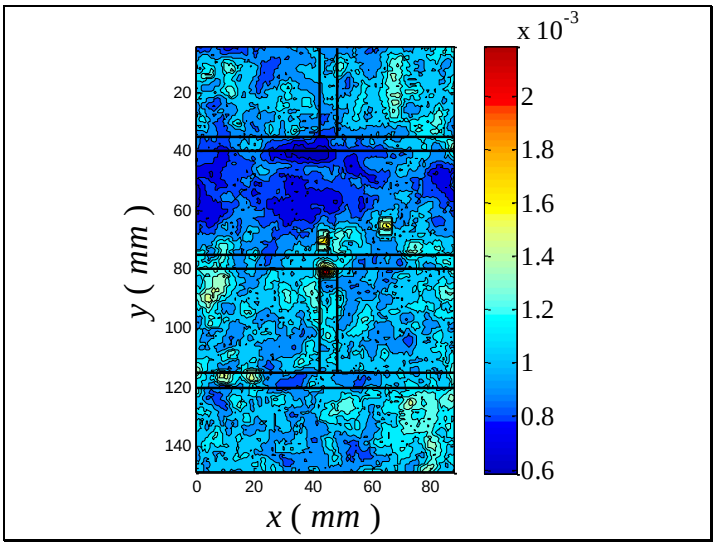

- D: 56.00 kips; 24,13 MPa

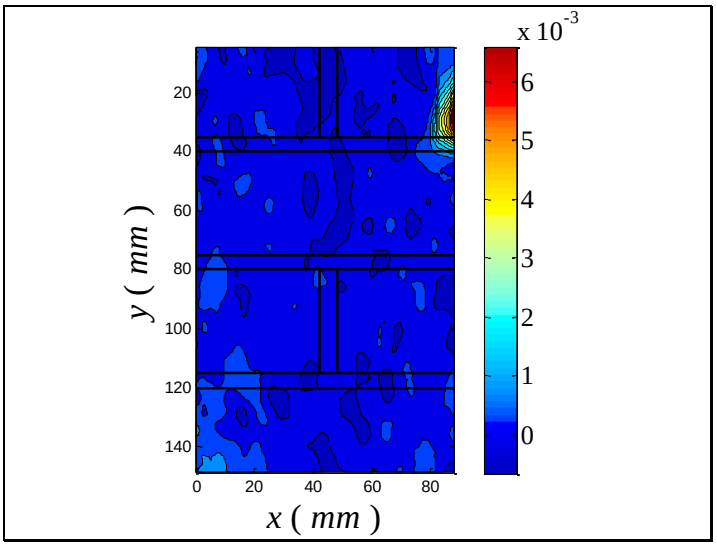

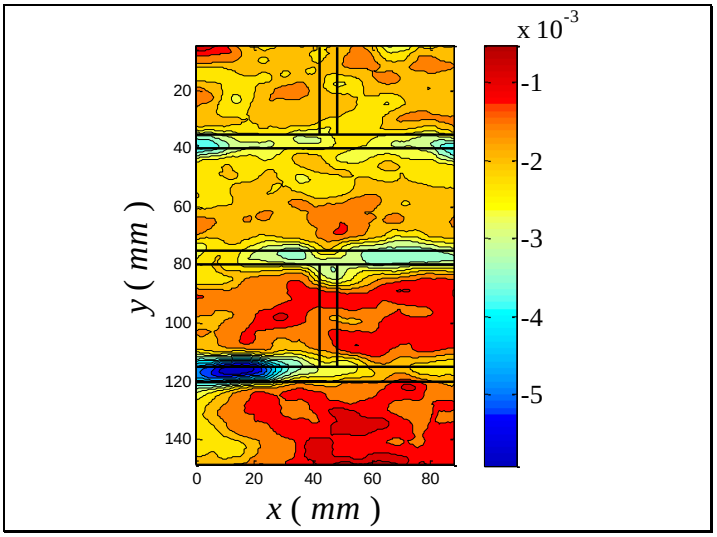

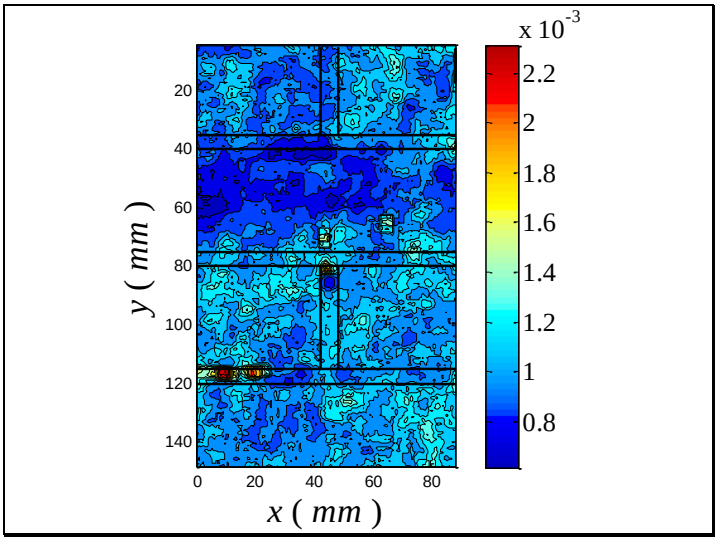

- E: 66.00 kips; 28,44 MPa

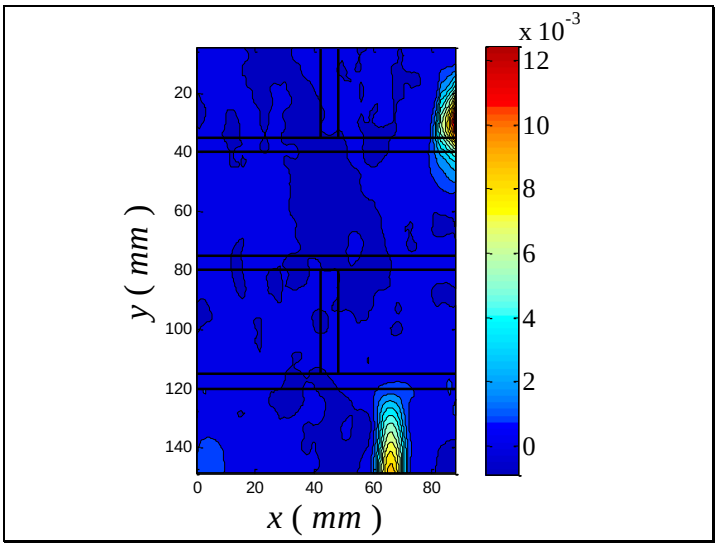

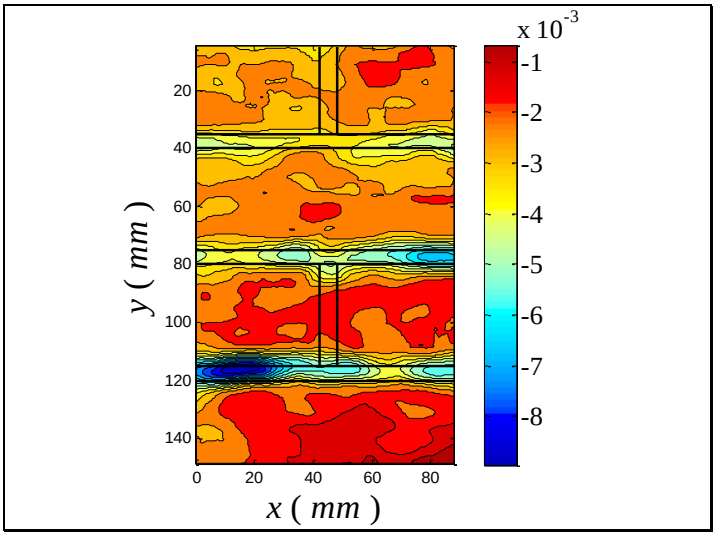

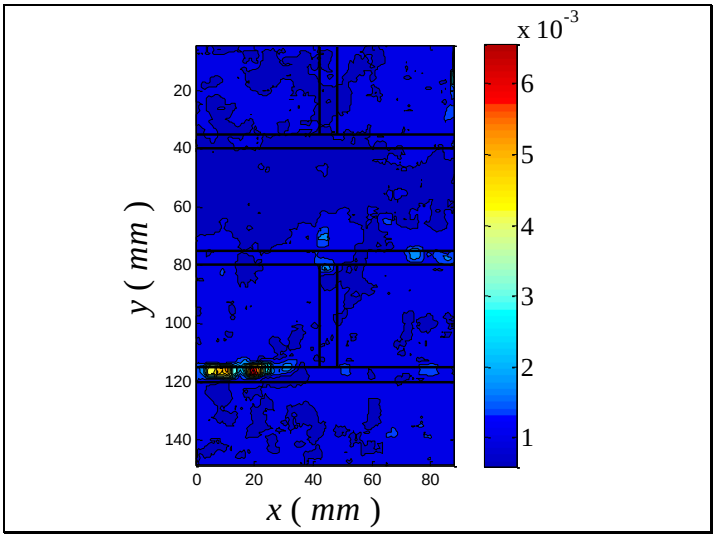

- F: 72.40 kips; 31,20 MPa

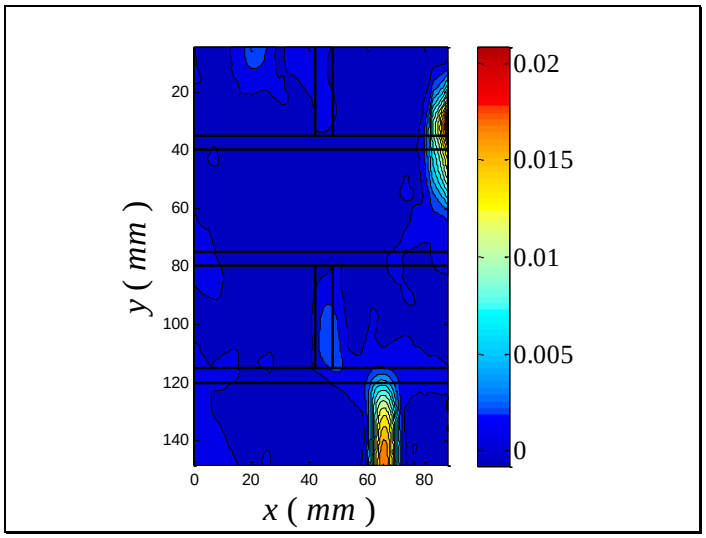

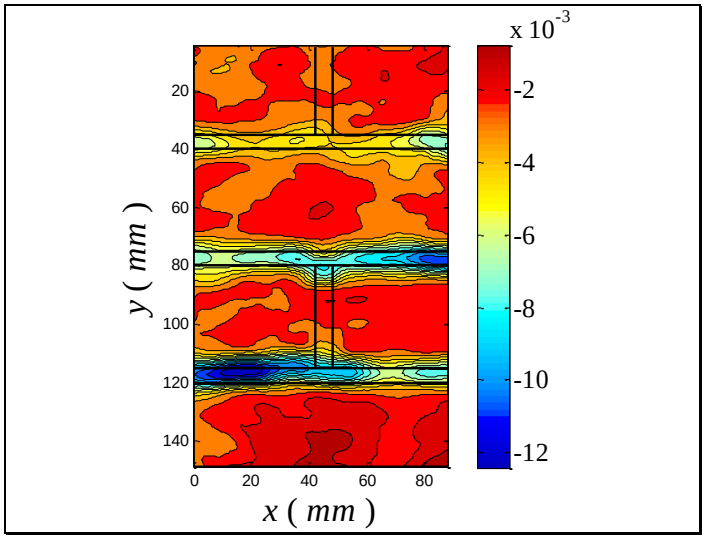

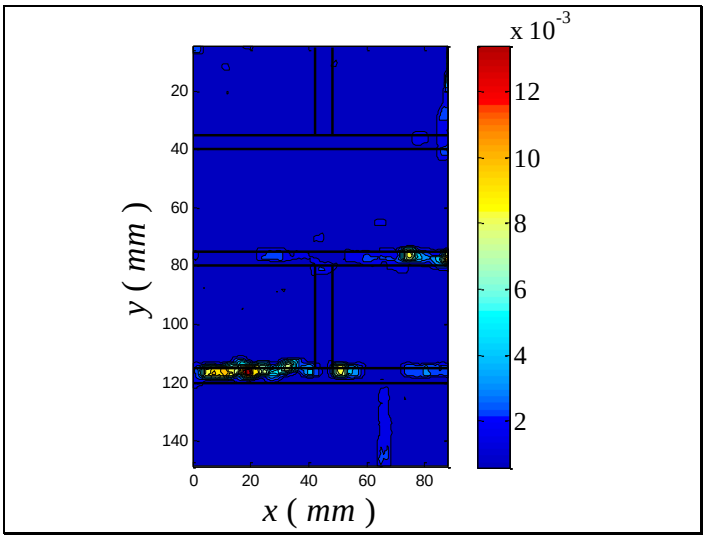

4.2.1.3. Square wall unwrapped 3

Fig.4.23 – Square wall unwrapped 3

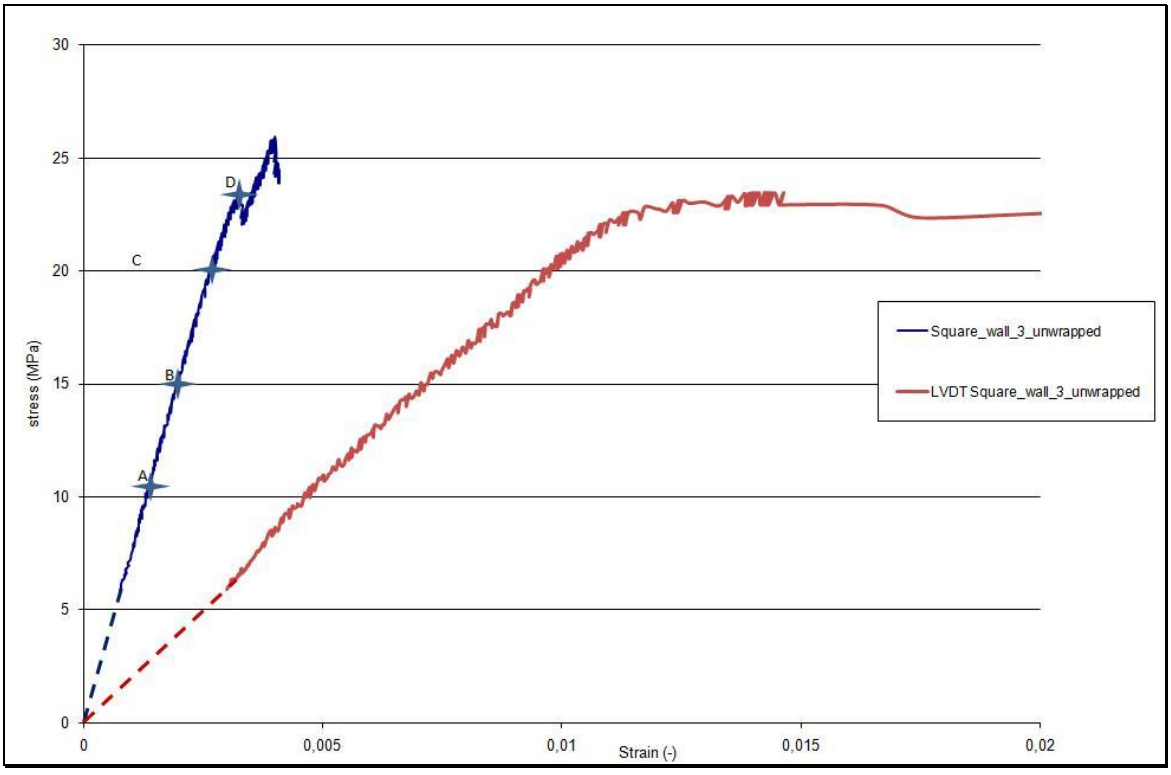

Fig.4.24 – Stress–strain diagram of square wall unwrapped 3

The contour plots of ε_{xx} , ε_{yy} and the correlation factor for all the points in figure are reported below.

- A: 24.90 kips; 10,73 MPa

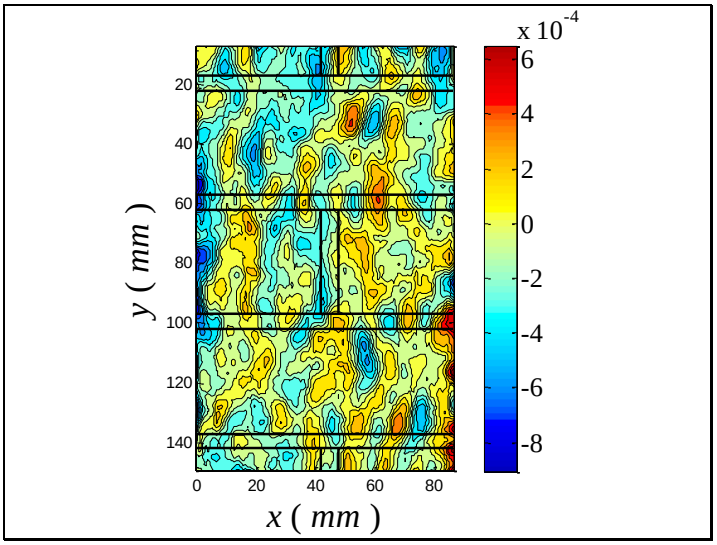

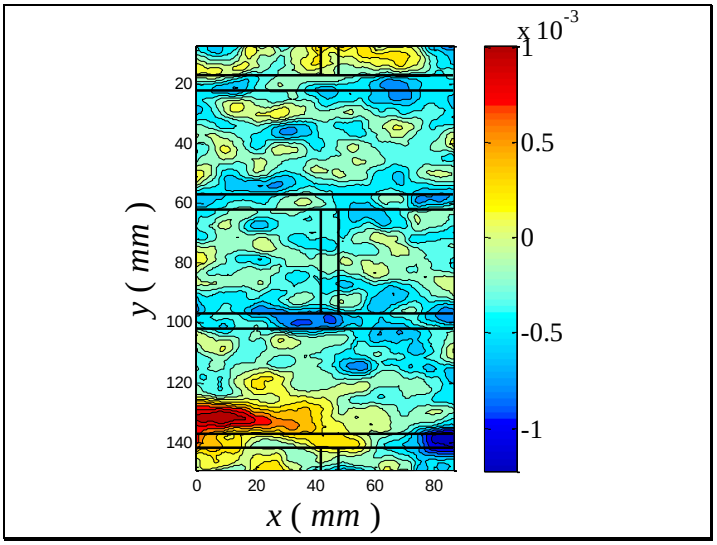

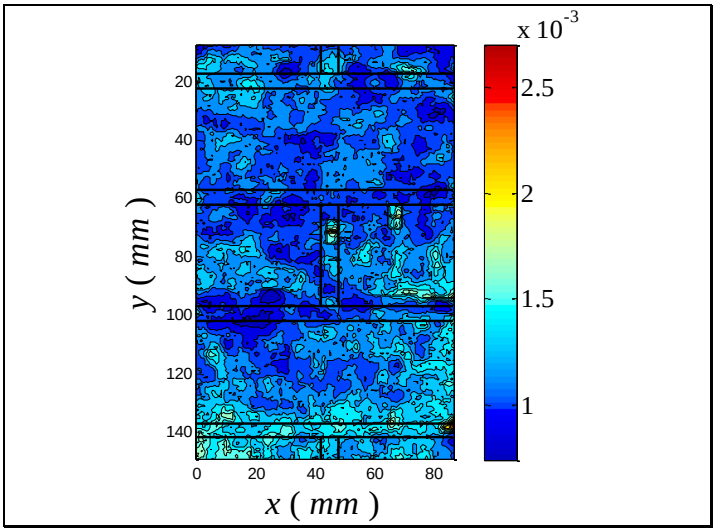

- B: 35.00 kips; 15,08 MPa

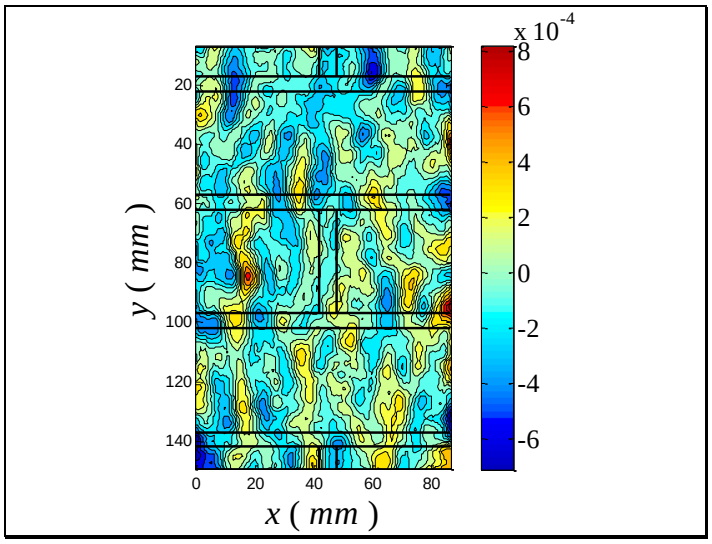

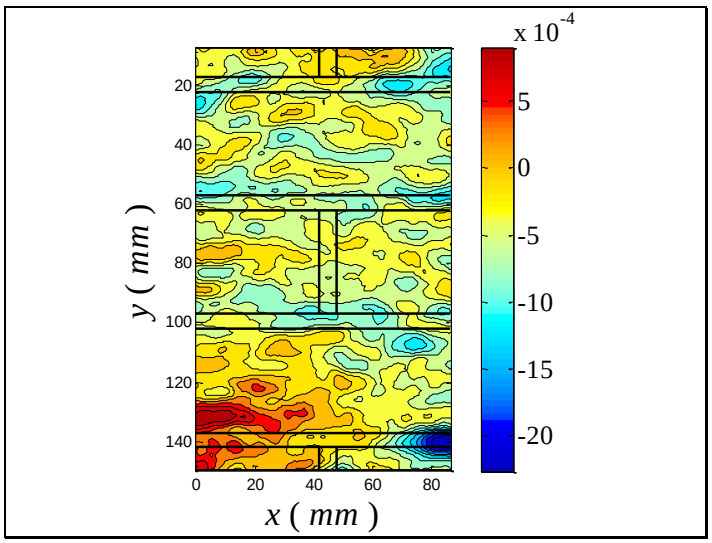

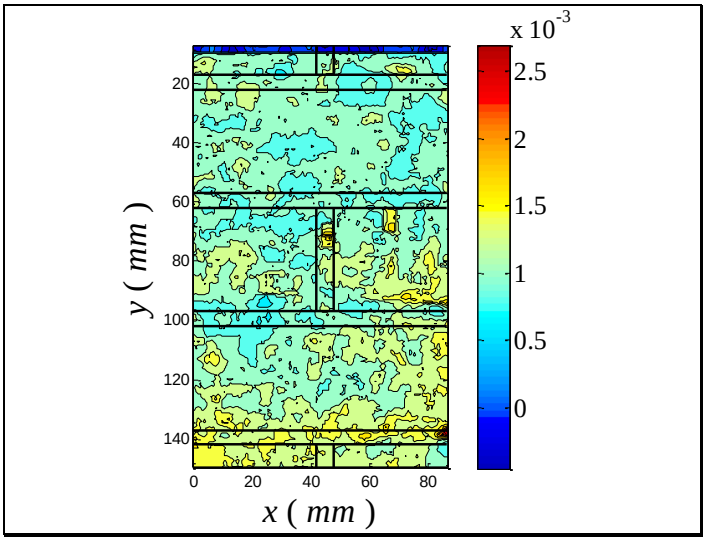

- C: 45.00 kips; 19,39 MPa

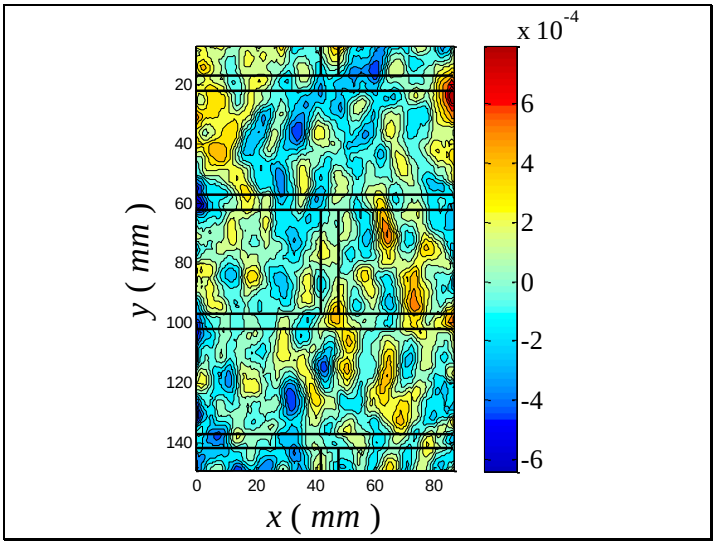

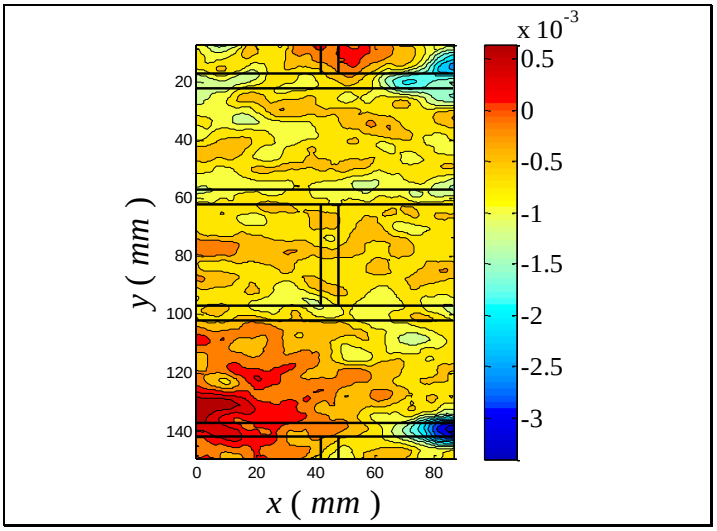

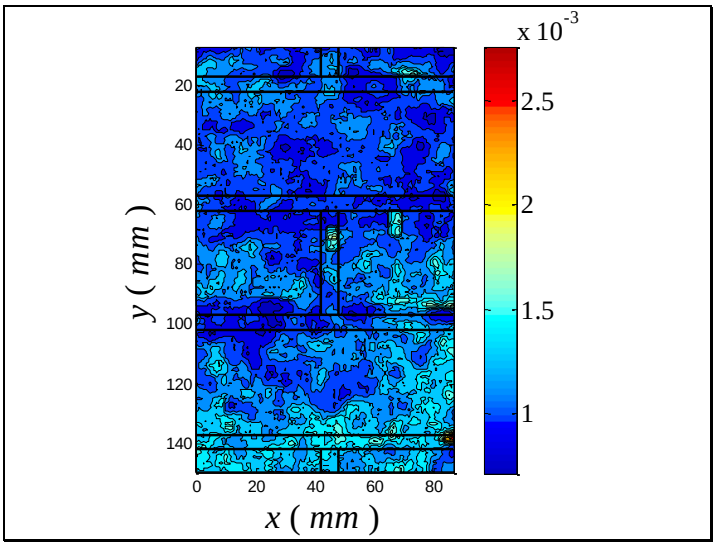

- D: 53.00 kips; 22,84 MPa

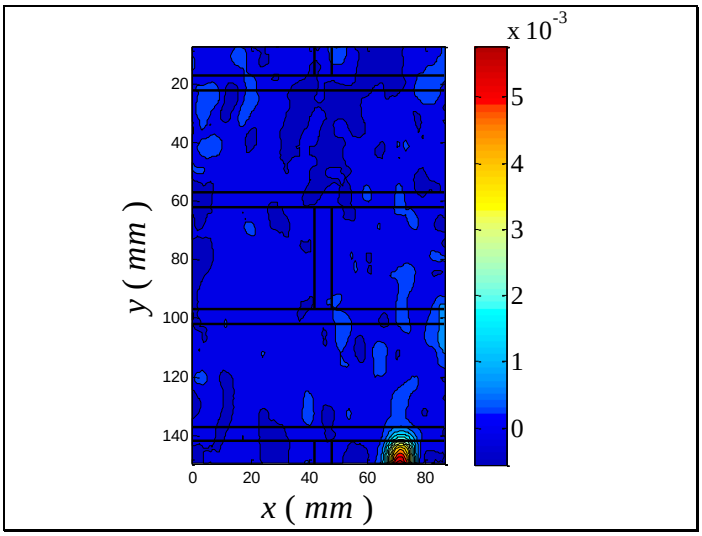

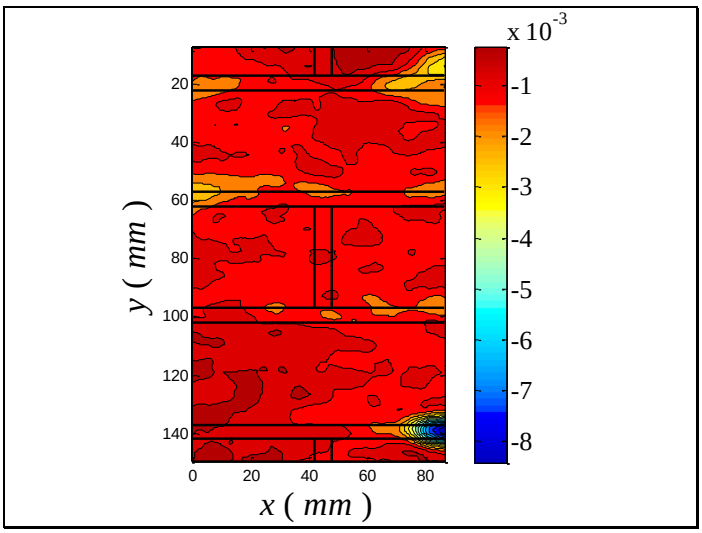

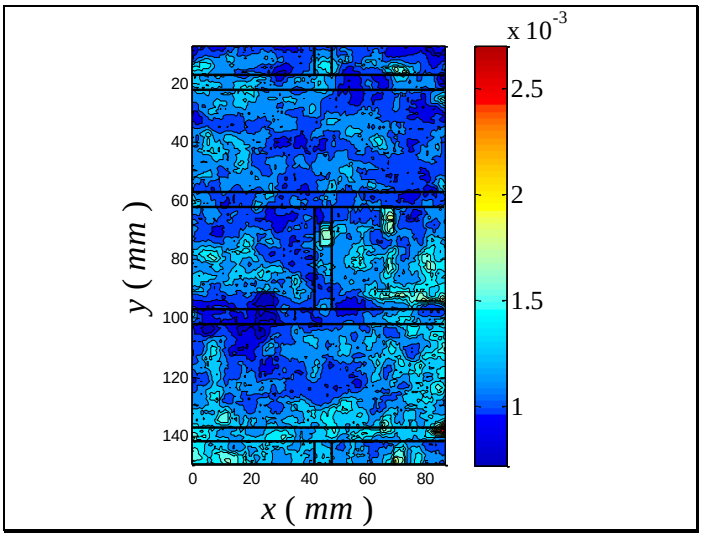

4.2.2. Discussion of result

In general, failure of the test specimens appeared to be initiated by crushing and squeezing of the mortar from the mortar joints followed by vertical splitting of the vertical joints and the bricks, as shown in figure 4.25.

Fig. 4.25 – Vertical splitting of the wall

The main conclusions that can be drawn from the tests on laboratory specimens are as follows.

The compressive strength can also be increased with the use of a reinforcement that increase the lateral confinement holding the mortar joints.

4.3. Axial Compression Test Second Configuration

The same approach was used for the second configuration and at least 28 days after the specimens casting they were tested in compression. Displacements across the 3 central bricks and 2 joints on each specimen were measured using also a Linear Variable Differential Transformer (LVDT) on the left side of the walls attached to the brick surface.

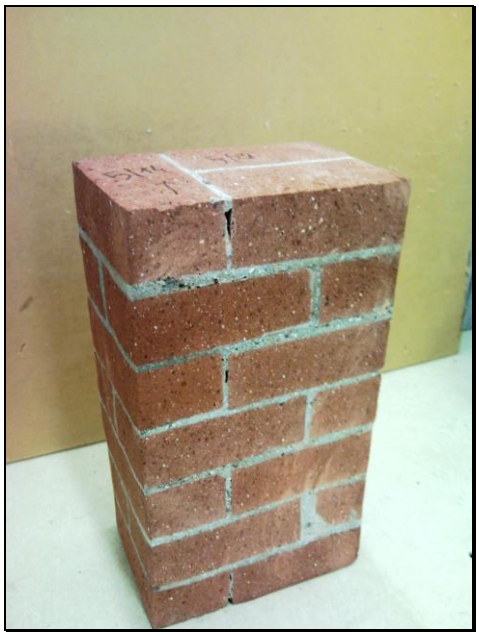

Fig. 4.26 – Second configuration masonry wall

Also for this configuration the specimens face need to be prepared for the DIC with a layer of white paint followed by a layer of a light drops of black paint, figure 4.27.

Fig. 4.27 – Second configuration masonry wall ready for the DIC

4.3.1. Experimental result and failure mode

The main results of the tests are presented in the table 4.5.

Specimens notation	3 precycle (kN)	Maximum load (kN)	Area (cm^2)	Compressive strenght (MPa)	Ultimate machine strain ε
1	15-110	393,79	150	25,65	0,0070
2	65-155	314,88	150	20,34	0,0053
3	65-155	313,96	150	20,28	0,0043
Displacement control mode of 0.008 inch/min, about 0.2 mm/min					

Tab. 4.5 – Summary of test results for rectangular1 walls unwrapped

The stress-strain diagrams for the first configuration unwrapped specimens are presented in figure 4.28.

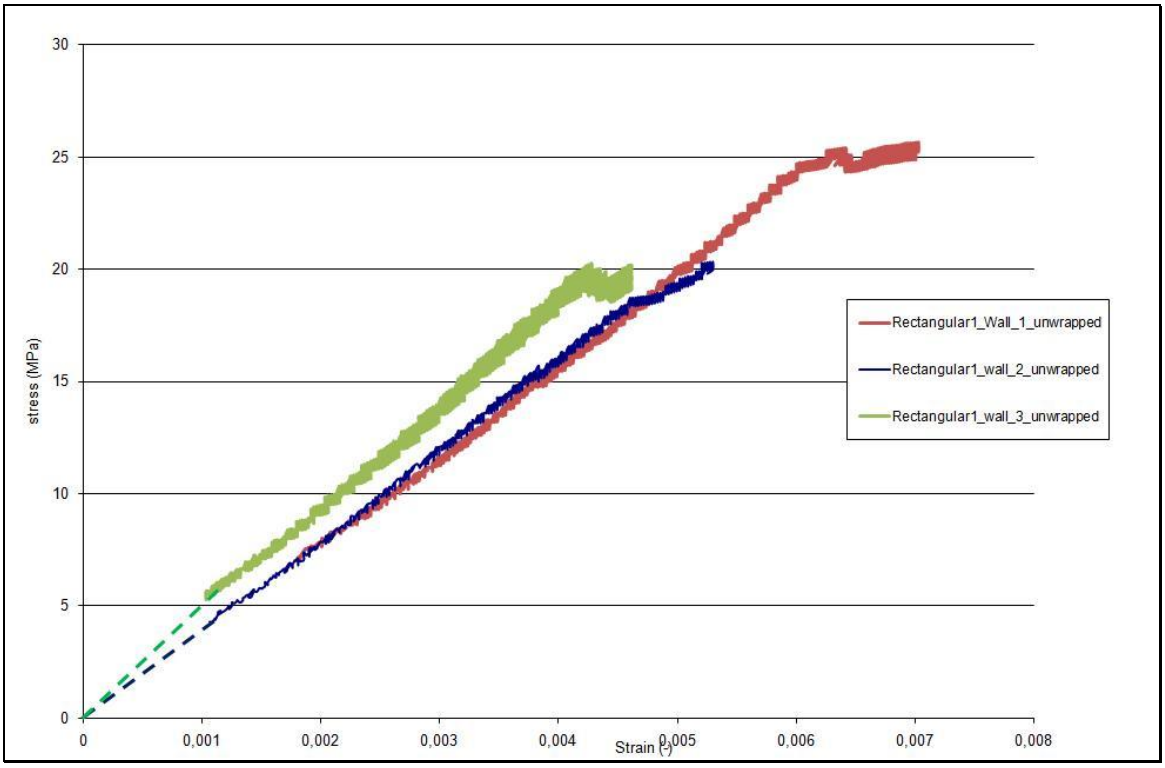

Fig. 4.28 – Stress–strain diagram of rectangular1 walls unwrapped

It can be observed that in all cases the diagrams are linear up to about 80% of the maximum load.

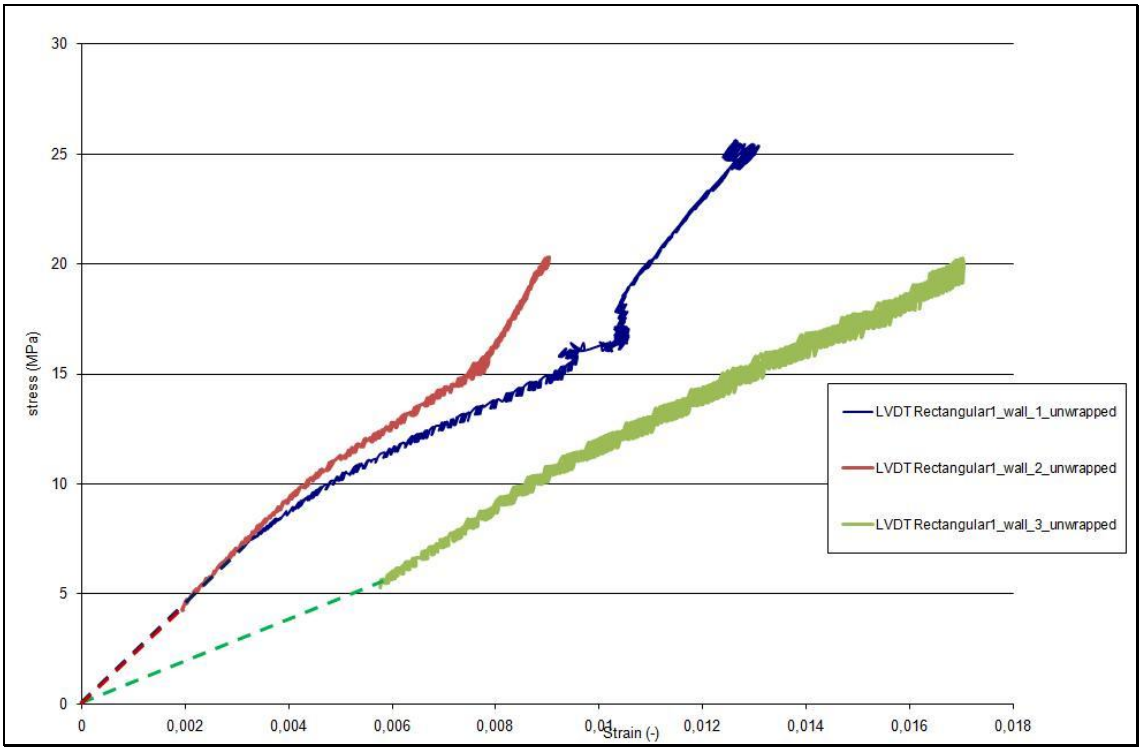

Fig. 4.29 – Stress–LVDTstrain diagram of rectangular1 walls unwrapped

The control specimens failed in a brittle manner by the formation of vertical cracks through the joints and the bricks, in both the face, along the 4 vertical joints side.

After their formation through mortar joints and bricks, vertical cracks became increasingly wide and the masonry between the cracks was crushed with a splitting of the masonry.

4.3.1.1. Rectangular1 wall unwrapped 1

Fig.4.30 – Rectangular1 wall unwrapped 1

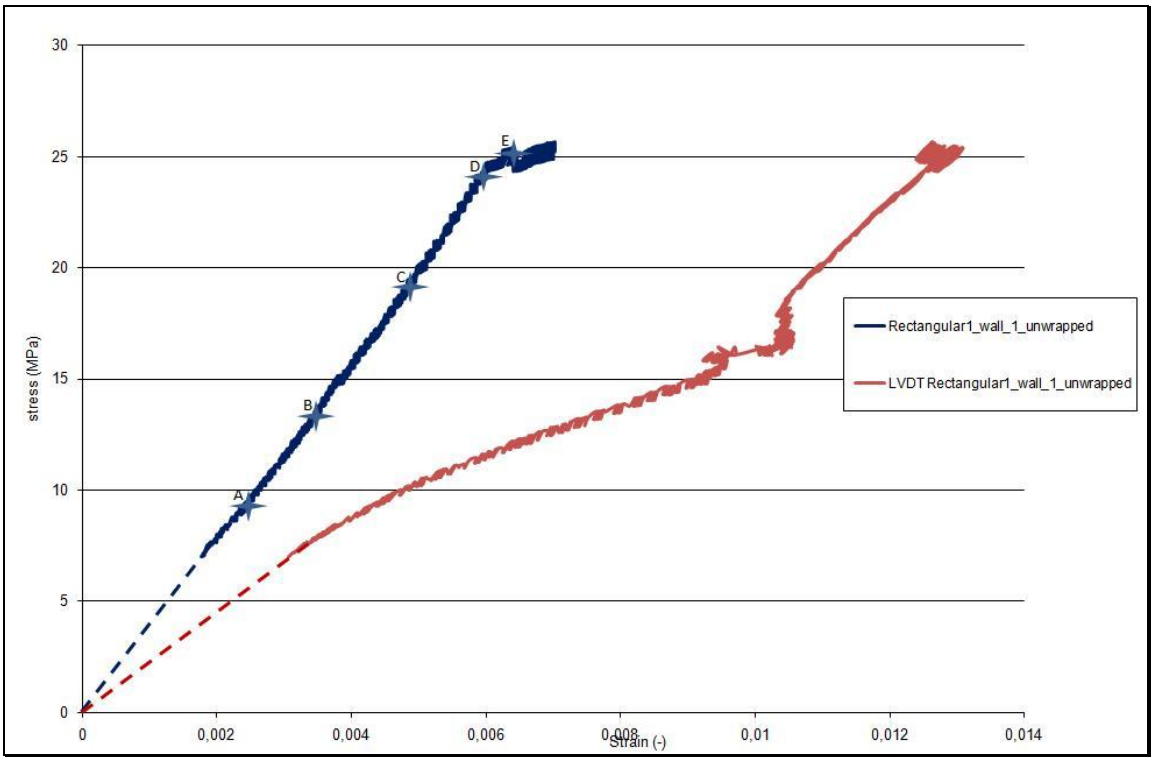

Fig.4.31 – Stress–strain diagram of rectangular1 wall unwrapped 1

The contour plots of ε_{xx} , ε_{yy} and the correlation factor for all the points in figure are reported below.

- A: 31.11 kips; 9,01 MPa

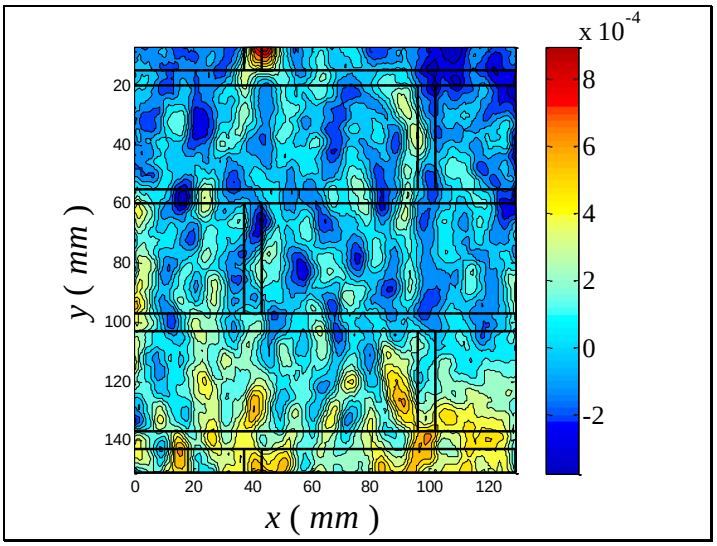

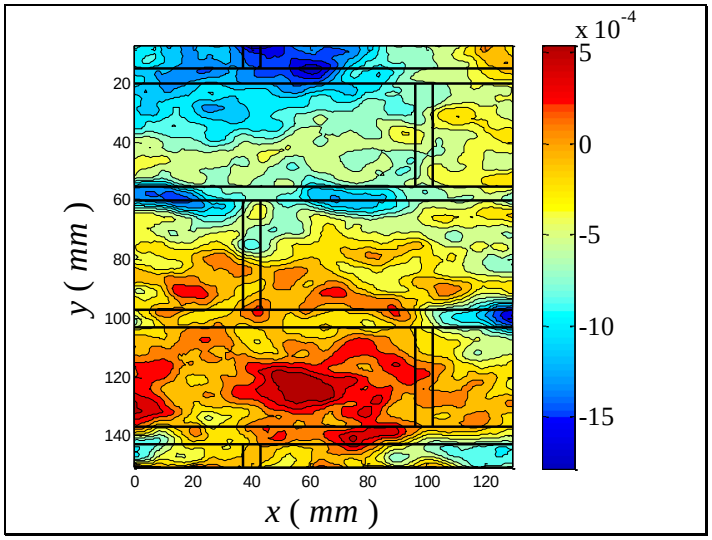

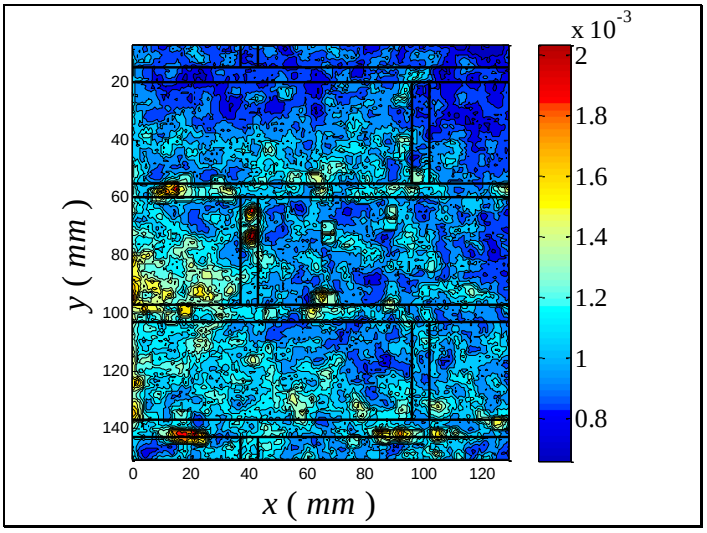

- B: 46.60 kips; 13,50 MPa

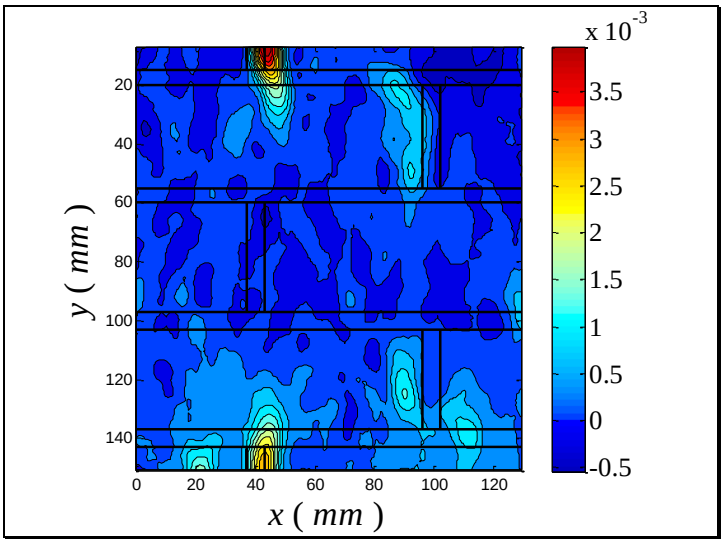

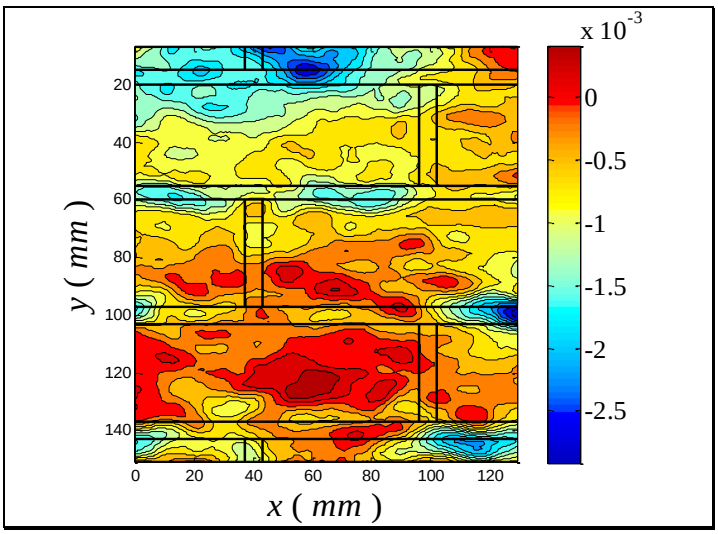

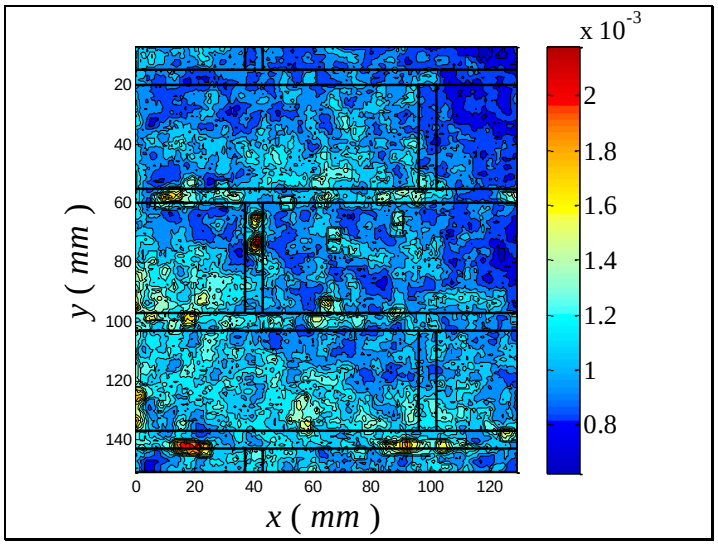

- C: 65.60 kips; 19,00 MPa

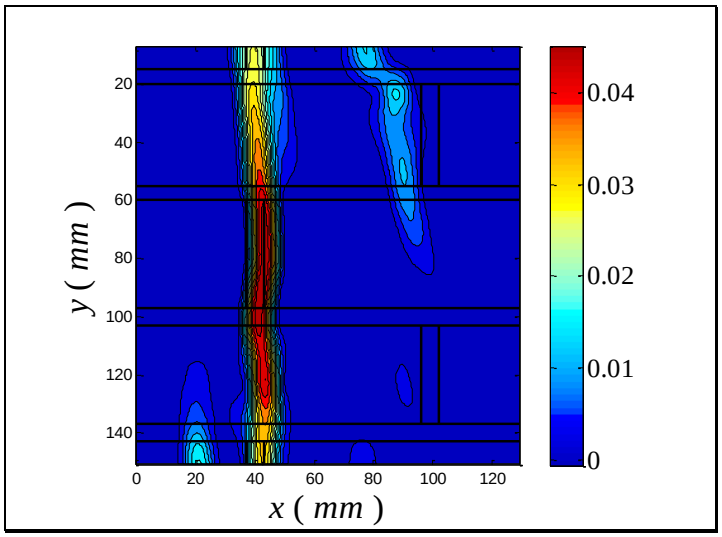

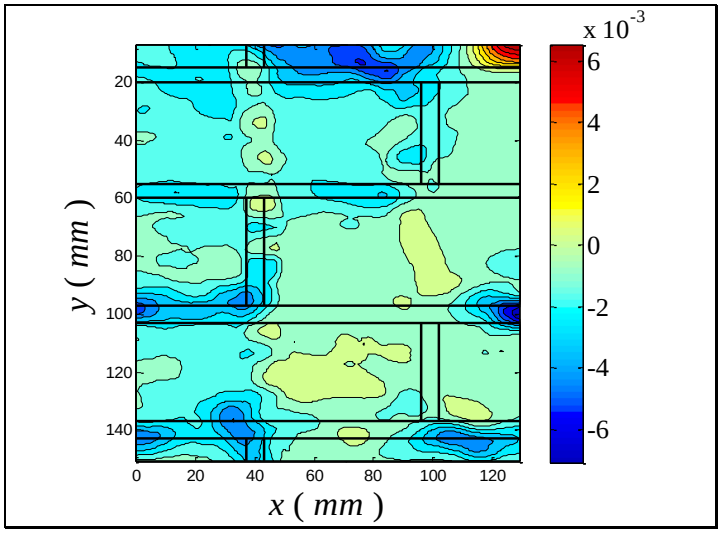

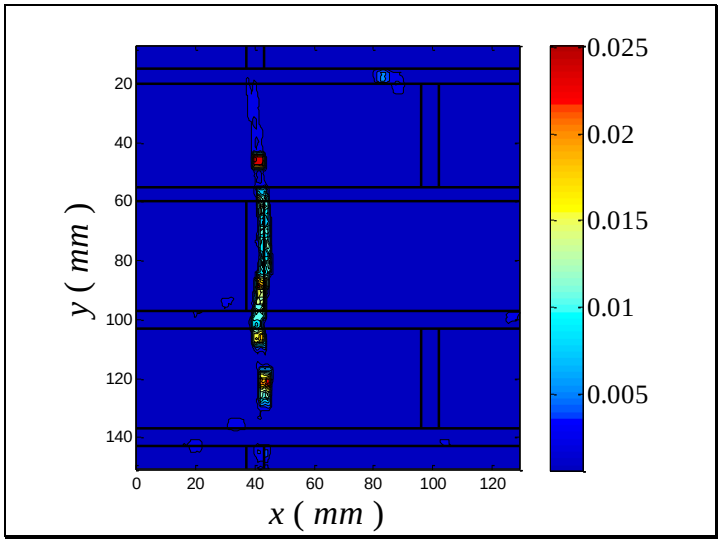

- D: 82.50 kips; 23,90 MPa

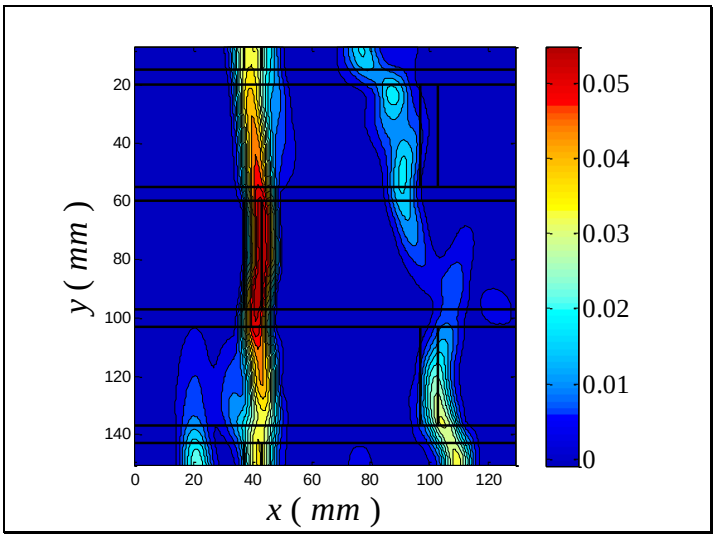

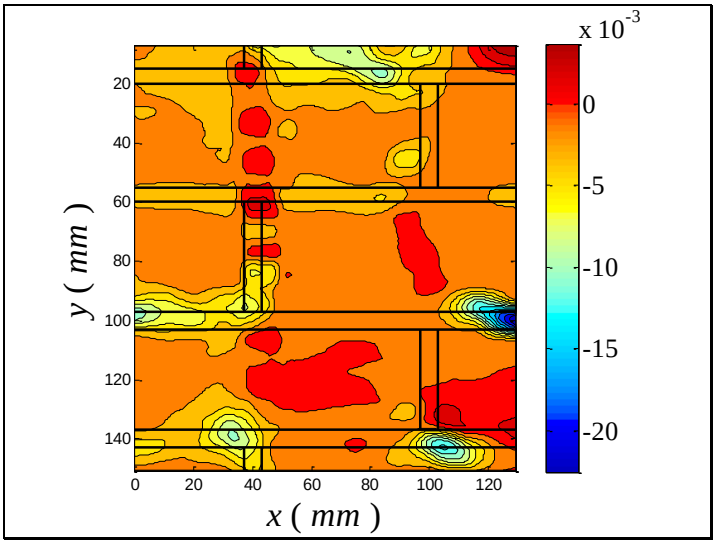

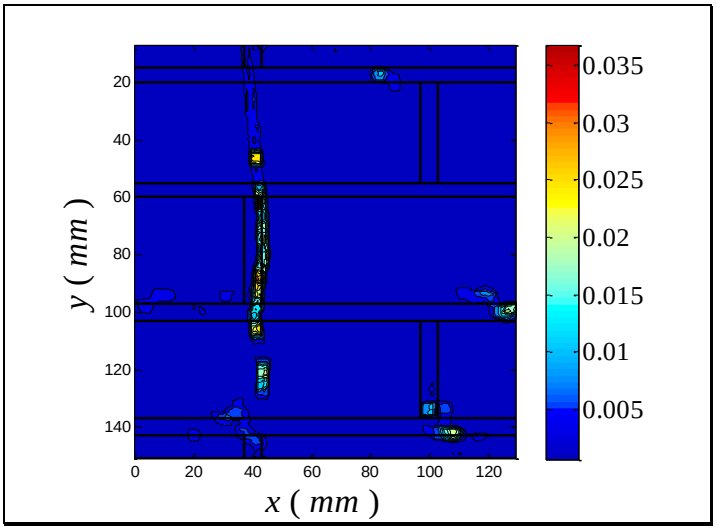

- E: 85.13 kips; 24,66 MPa

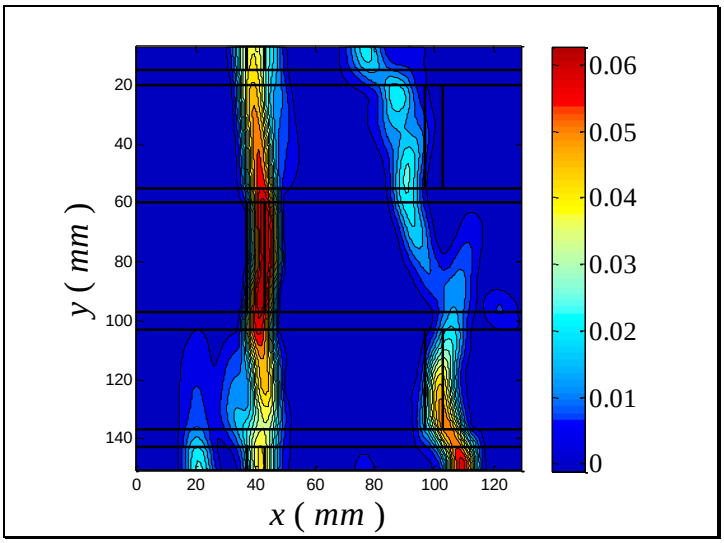

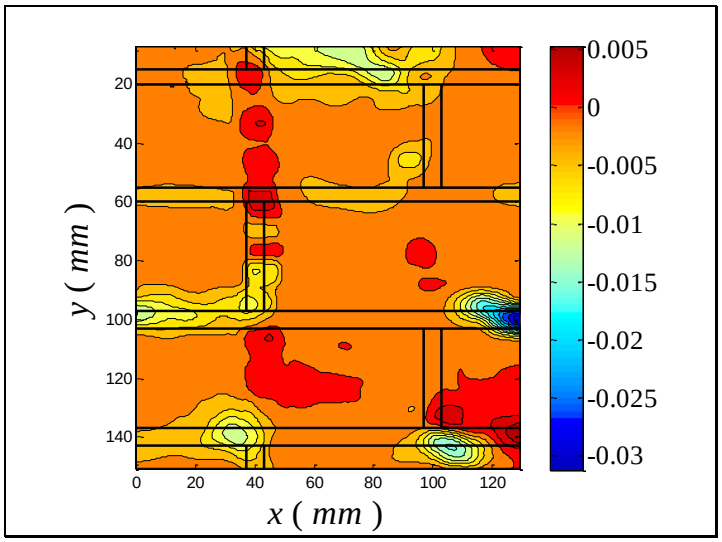

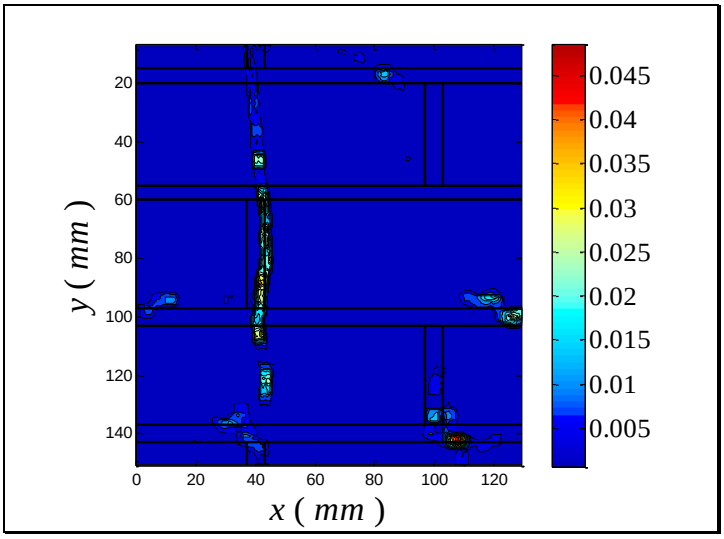

4.3.1.2. Rectangular1 wall unwrapped 2

Fig.4.32 – Rectangular1 wall unwrapped 2

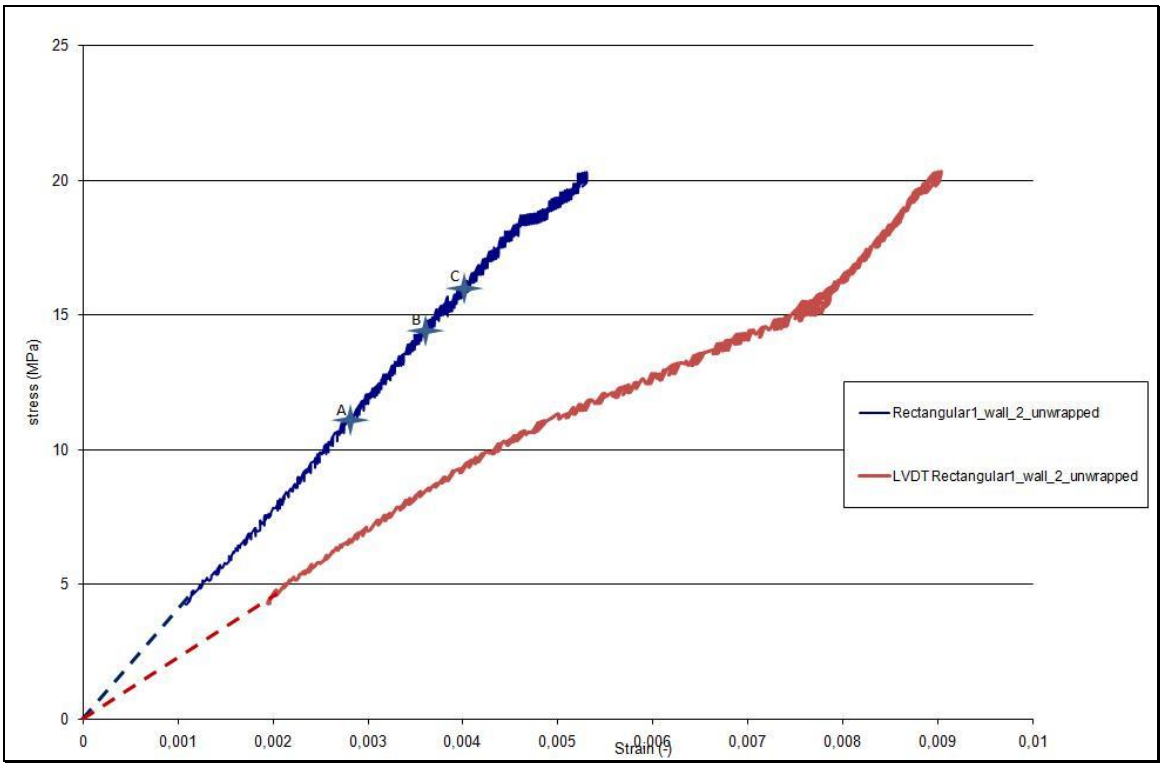

Fig.4.33 – Stress–strain diagram of rectangular1 wall unwrapped 2

The contour plots of ε_{xx} , ε_{yy} and the correlation factor for all the points in figure are reported below.

- A: 39.50 kips; 11,35 MPa

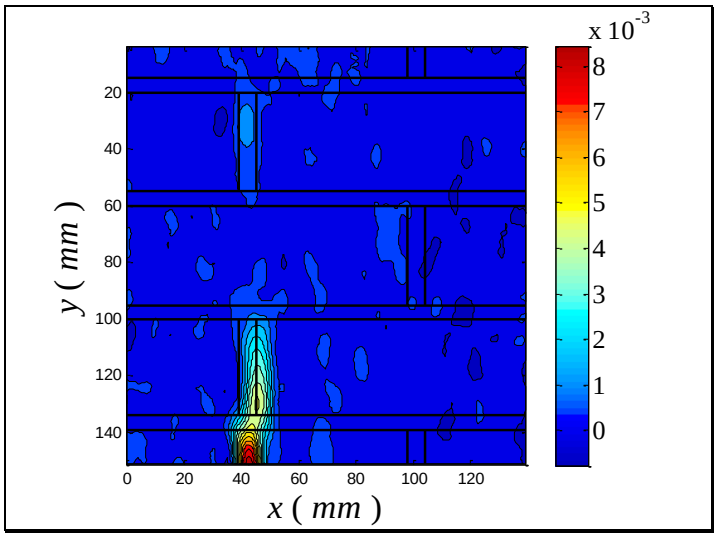

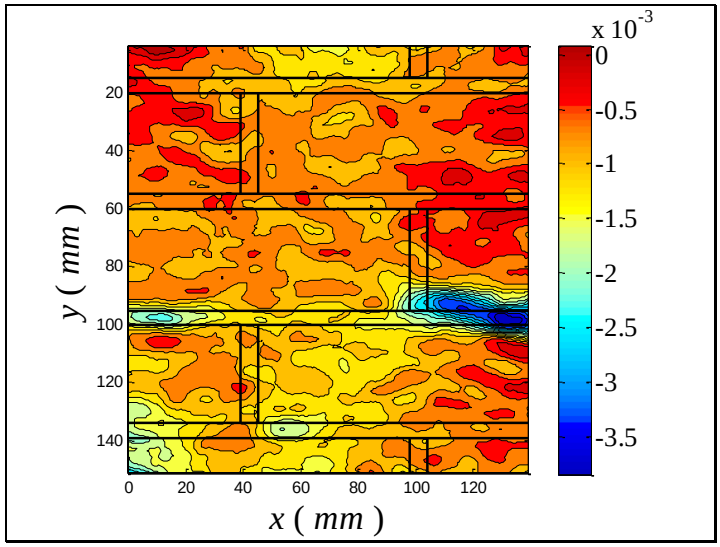

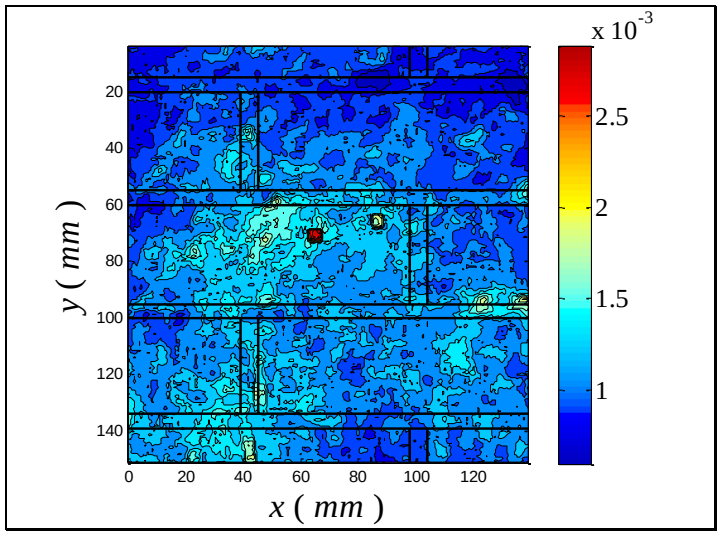

- B: 49.73 kips; 14,29 MPa

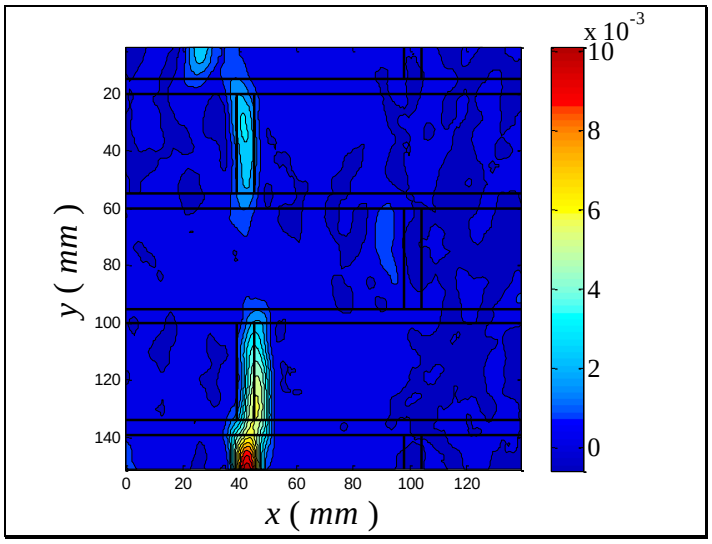

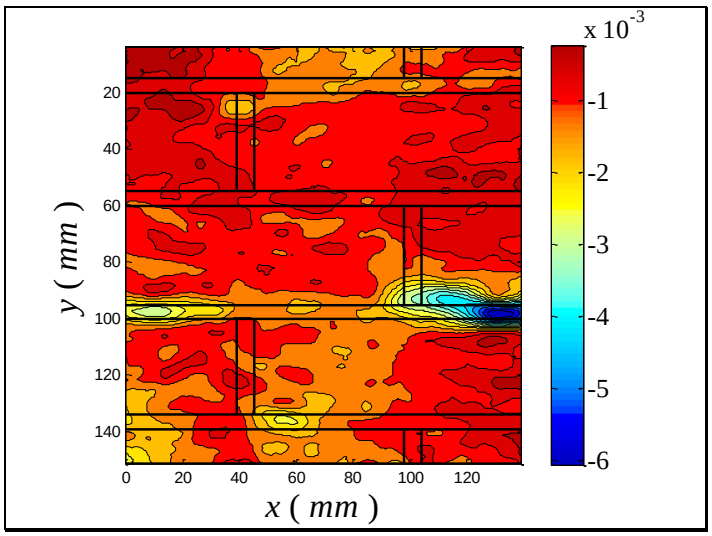

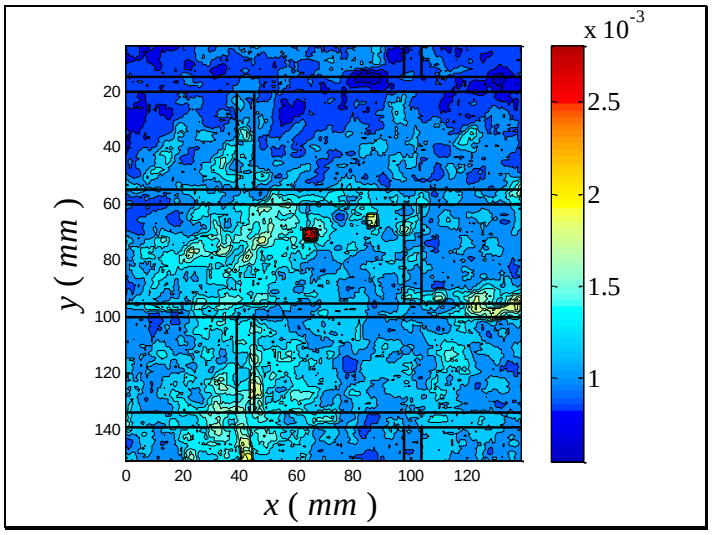

- C: 56.00 kips; 16,08 MPa

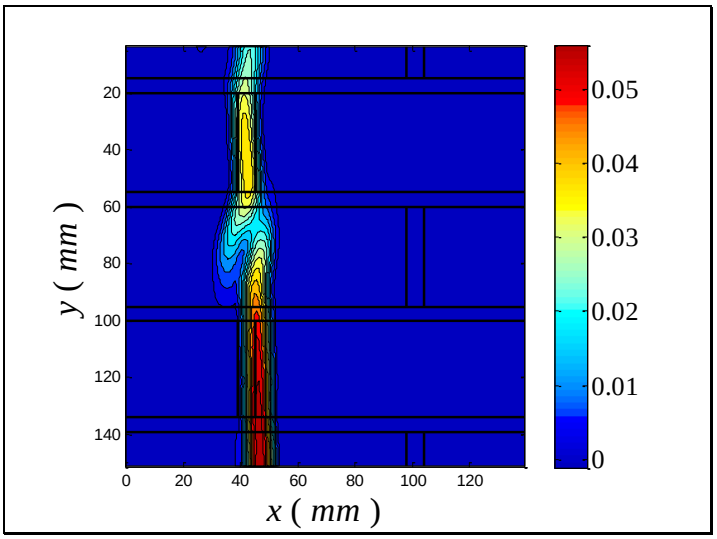

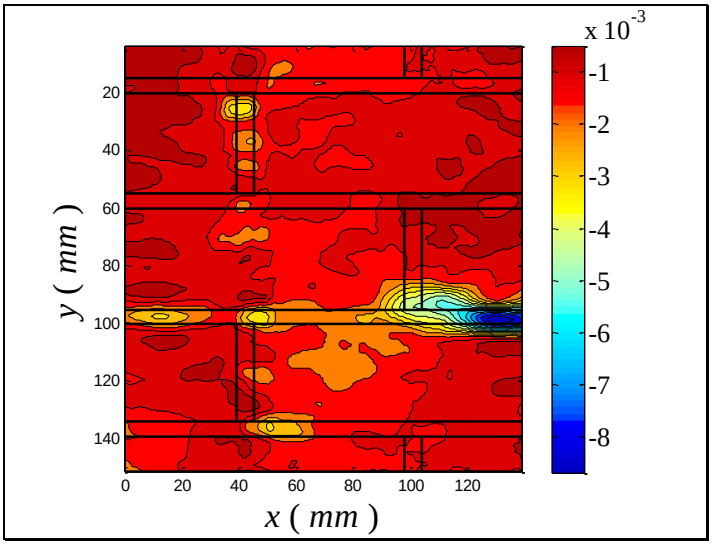

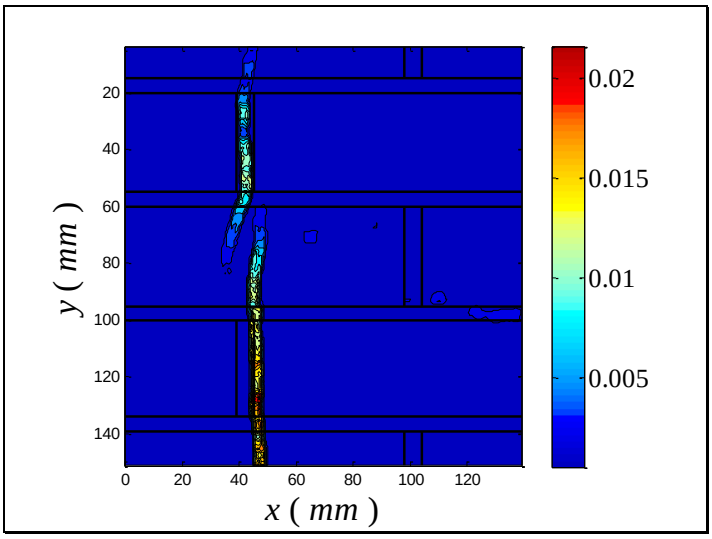

4.3.1.3. Rectangular1 wall unwrapped 3

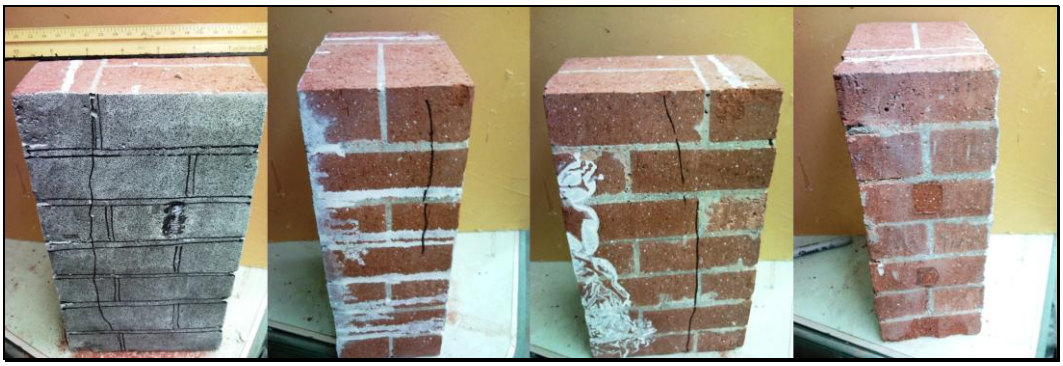

Fig.4.34 – Rectangular1 wall unwrapped 3

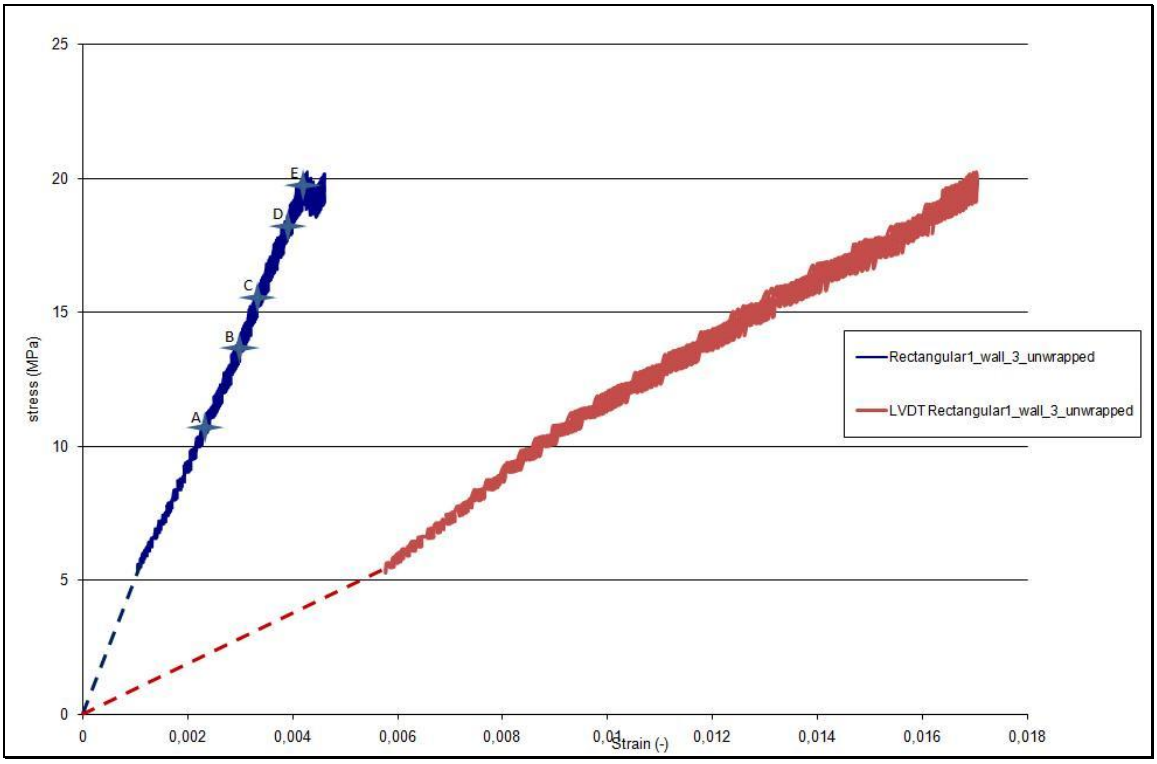

Fig.4.35 – Stress–strain diagram of rectangular1 wall unwrapped 3

The contour plots of ε_{xx} , ε_{yy} and the correlation factor for all the points in figure are reported below.

- A: 38.00 kips; 10,92 MPa

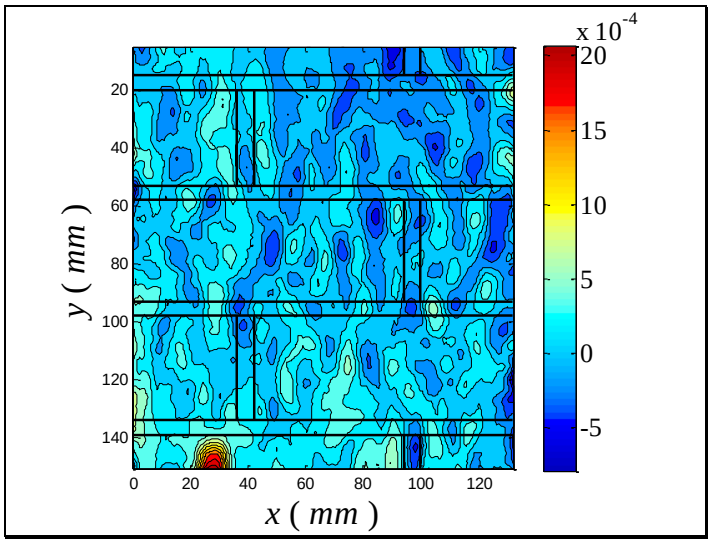

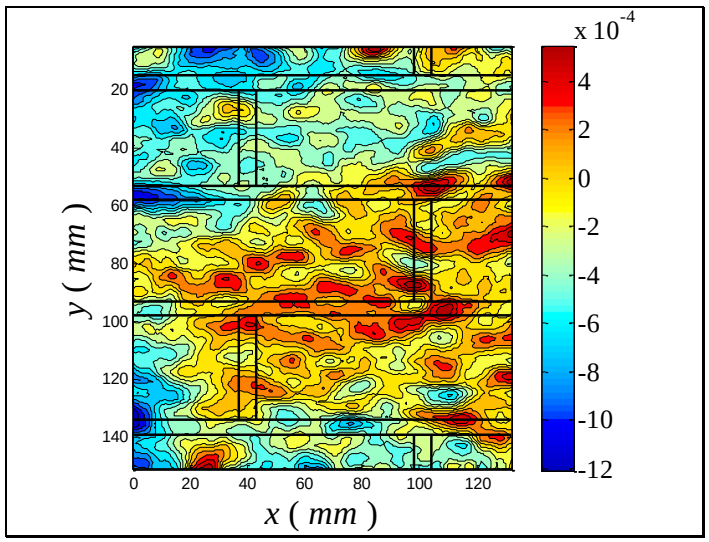

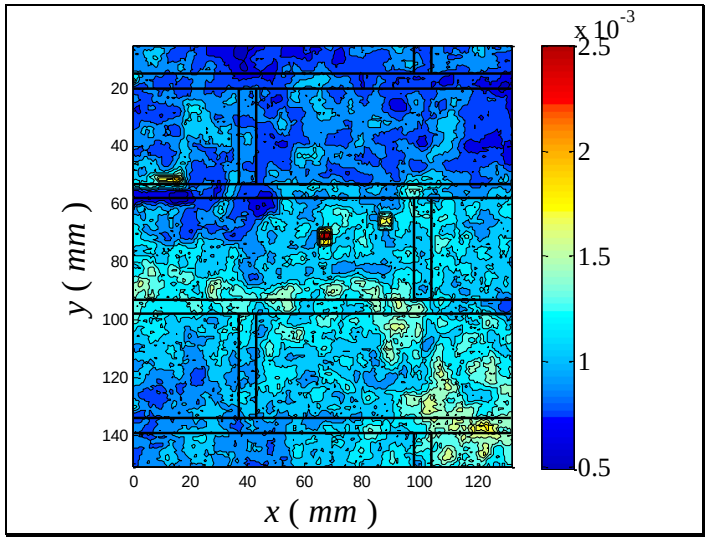

- B: 47.05 kips; 13,52 MPa

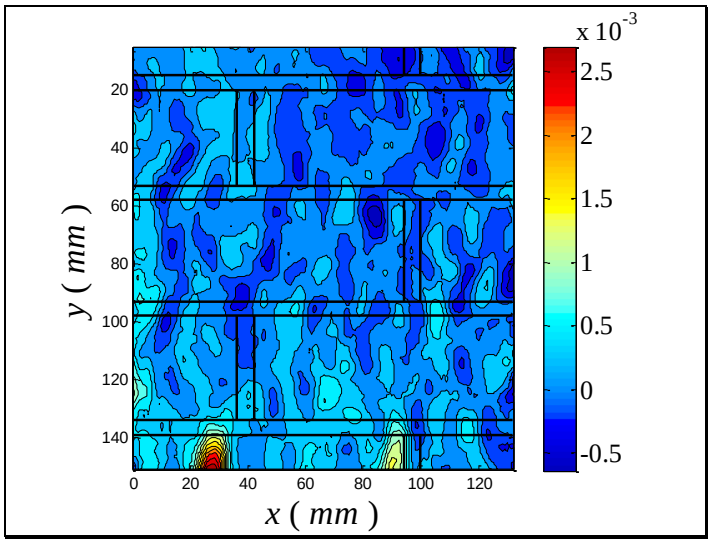

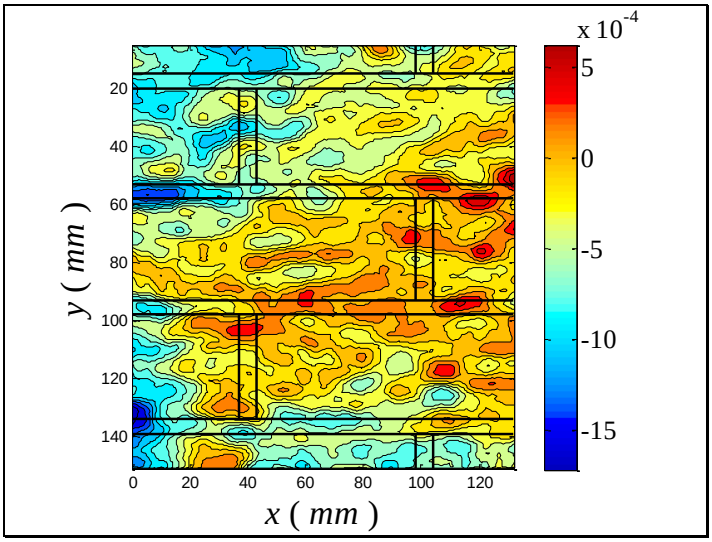

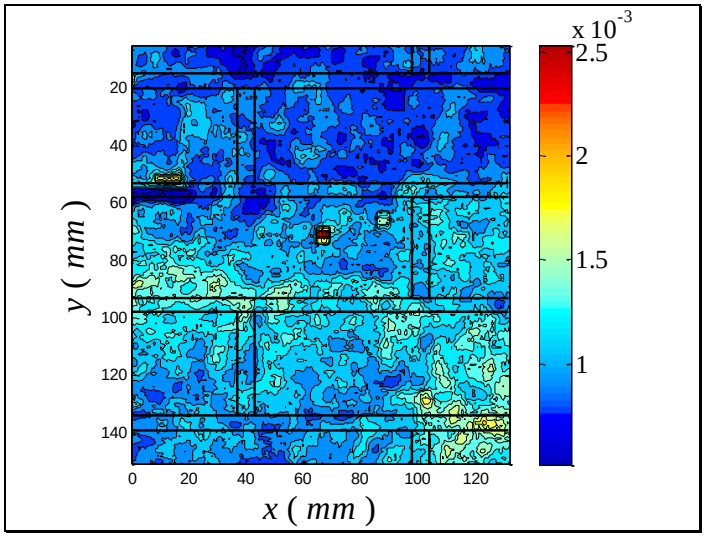

- C: 54.40 kips; 15,43 MPa

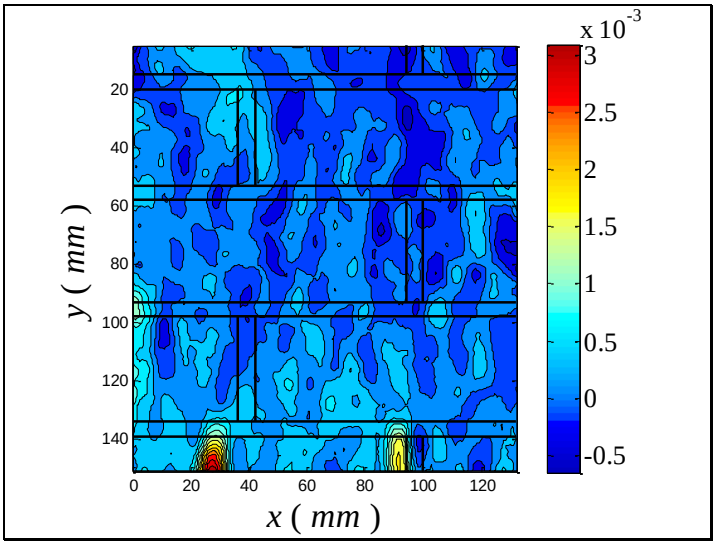

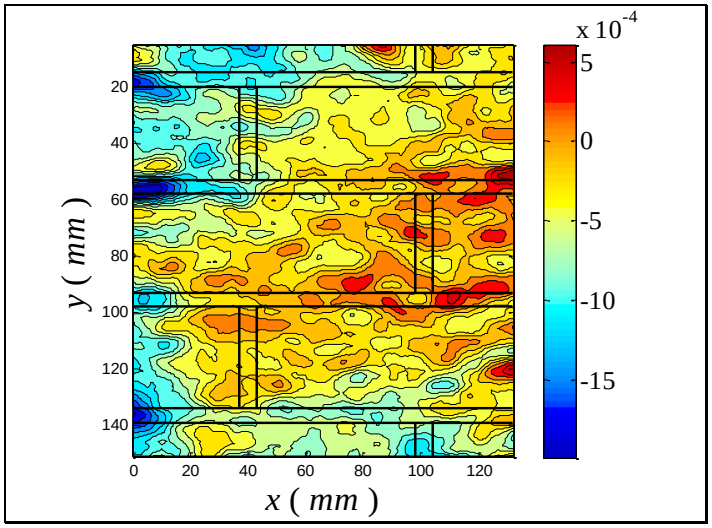

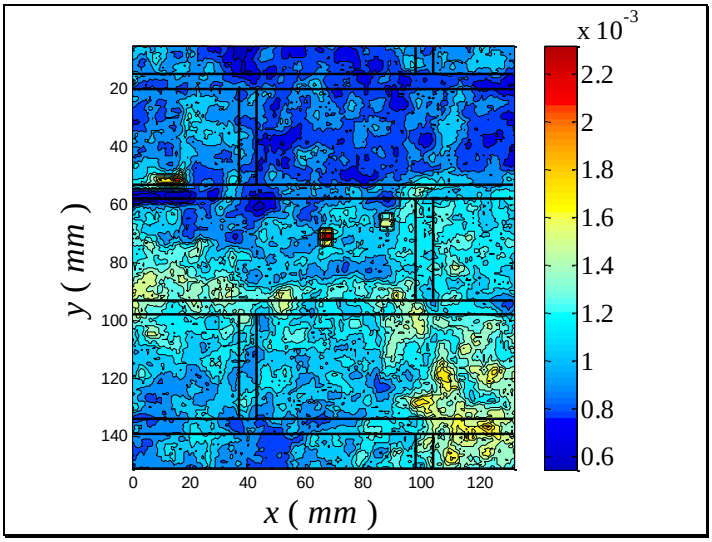

- D: 65.37 kips; 18,78 MPa

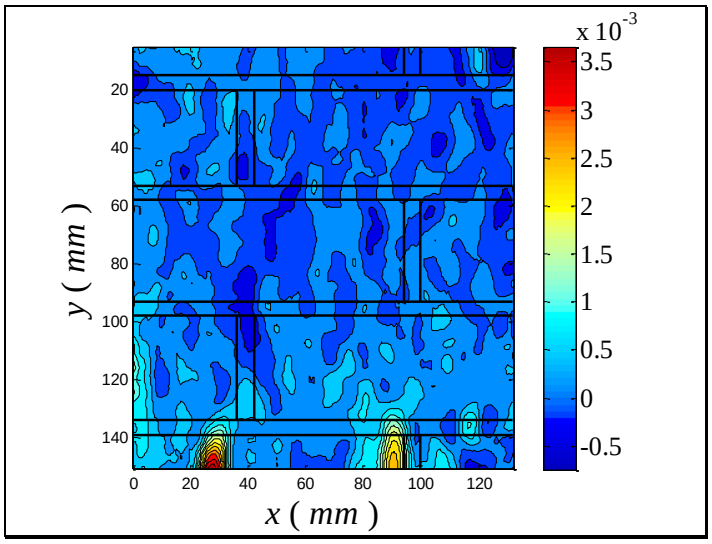

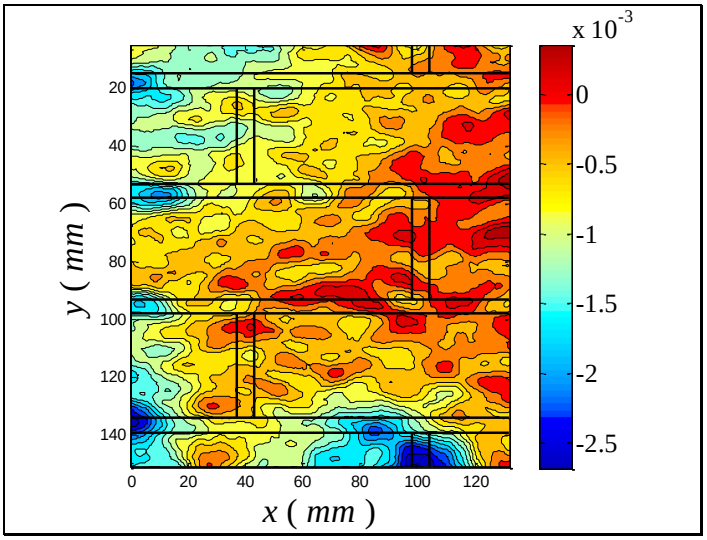

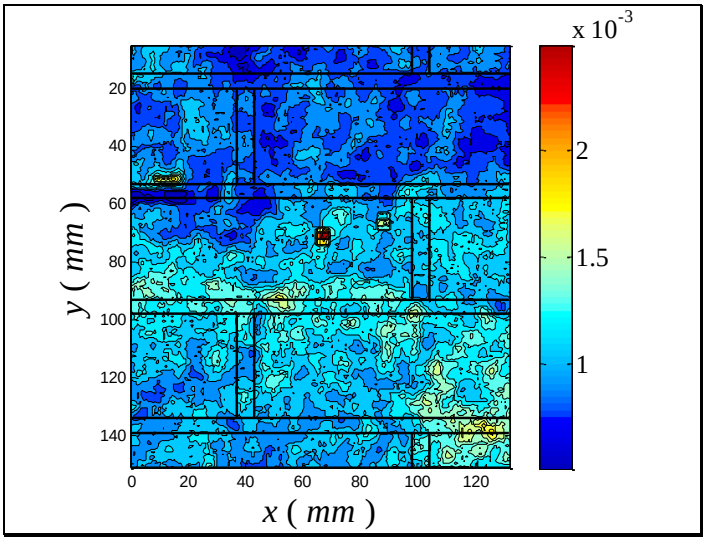

- E: 68.70 kips; 19,74 MPa

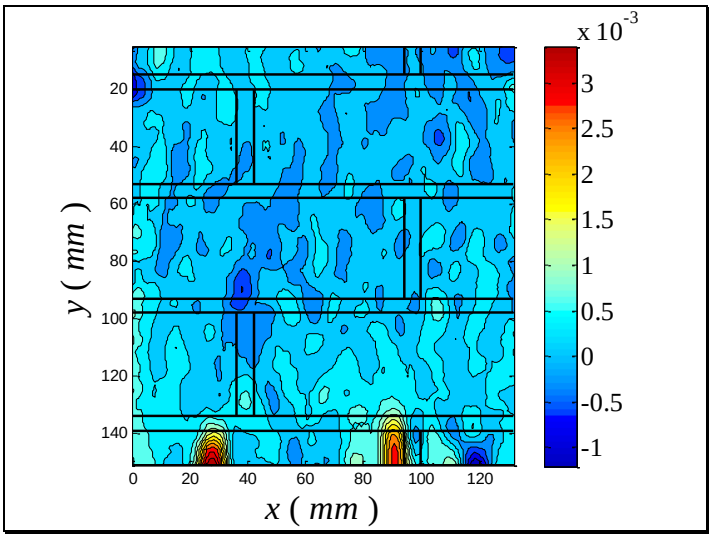

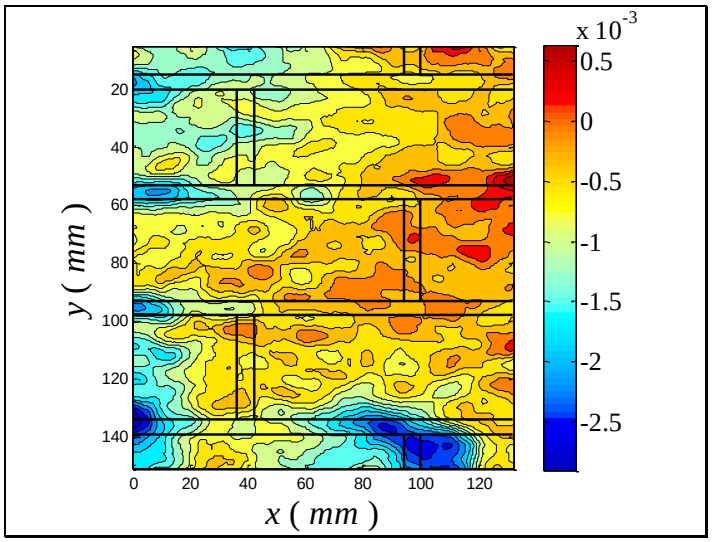

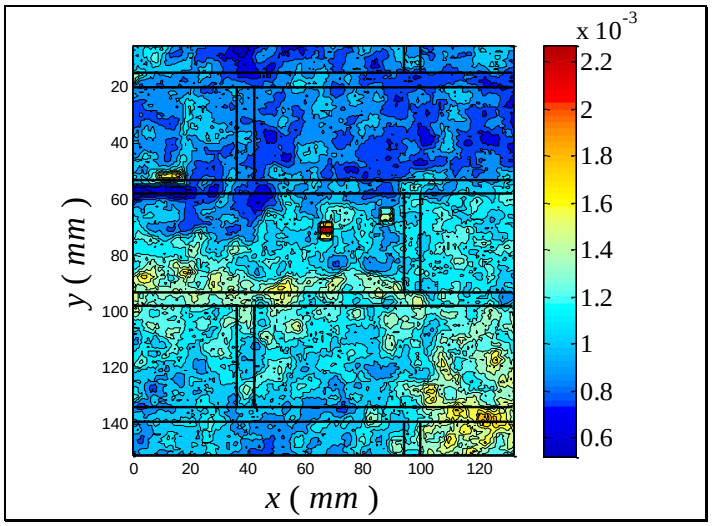

4.3.2. Discussion of result

In general, failure of the test specimens appeared to be initiated by crushing and squeezing of the mortar from the mortar joints followed by vertical splitting of the vertical joints and the bricks, as shown in figure 4.36.

Fig. 4.36 – Vertical splitting of the wall

The same conclusions of the other walls can be drawn, in particular the compressive strength can be increased with the use of a reinforcement that prevents the lateral expansion of the mortar joints.

4.4. Axial Compression Test Third Configuration

As for the last specimen about 28 days after the casting the compression test started on the specimens.

Displacements across the 3 central bricks and 2 joints on each specimen were measured using also a Linear Variable Differential Transformer (LVDT) on the left side of the walls attached to the brick surface.

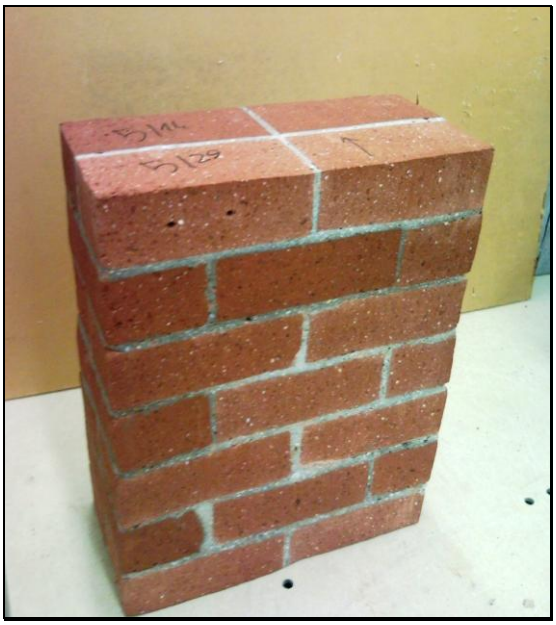

Fig. 4.37 – Third configuration masonry wall

The specimens face need to be prepared for the DIC with a layer of white paint followed by a layer of a light drops of black paint, figure 4.38.

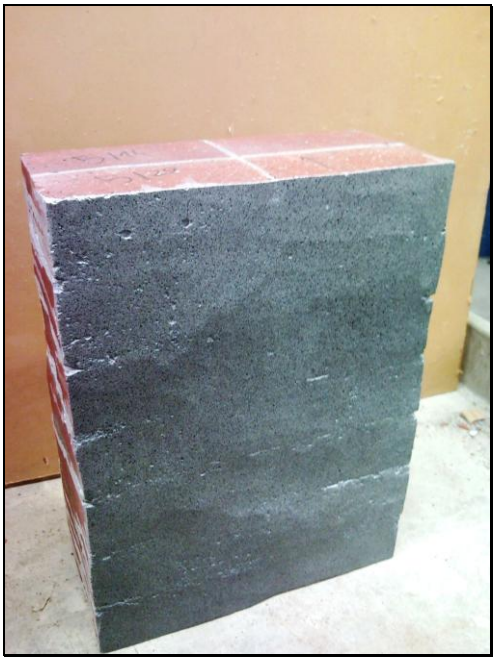

Fig. 4.38 – Third configuration masonry wall ready for the DIC

4.4.1. Experimental result and failure mode

The main results of the tests are presented in the table 4.6.

Specimens notation	3 precycle (kN)	Maximum load (kN)	Area (cm^2)	Compressive strenght (MPa)	Ultimate machine strain ε
1	65-155	224,81	200	10,89	0,0035
2	20-65	122,71	200	5,94	0,0045
3	20-65	208,50	200	10,14	0,0038
Displacement control mode of 0.008 inch/min, about 0.2 mm/min					

Tab. 4.6 – Summary of test results for rectangular2 walls unwrapped

The stress-strain diagrams for the first configuration unwrapped specimens are presented in figure 4.39.

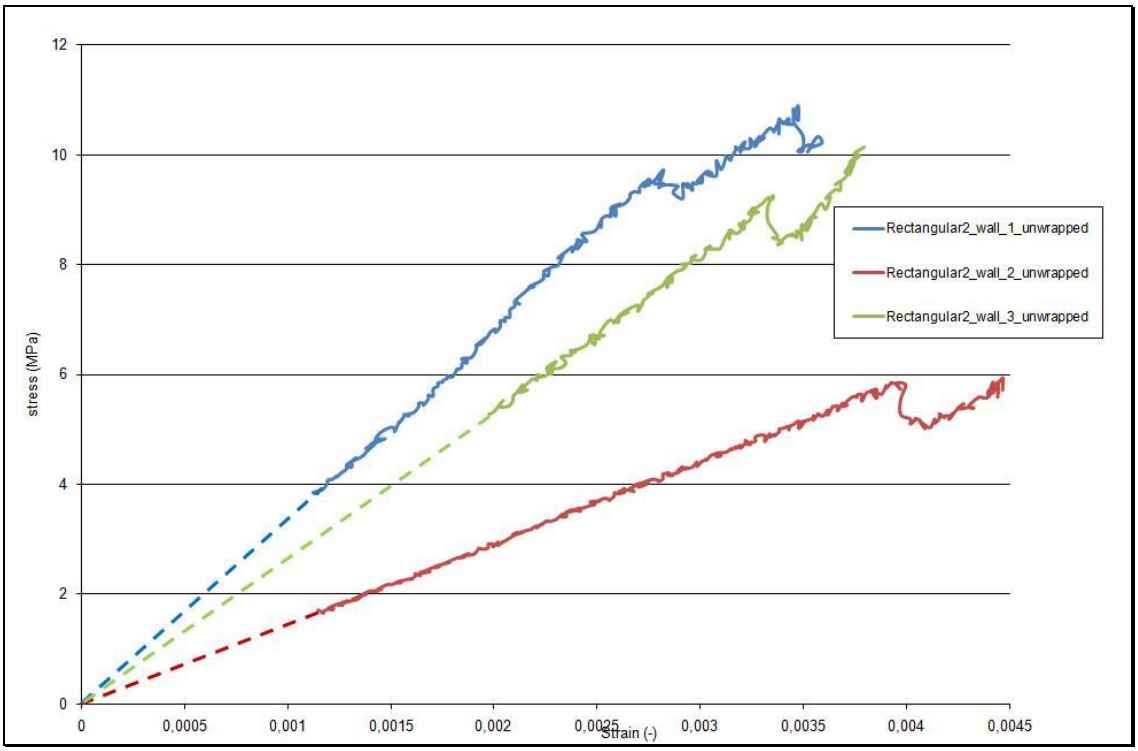

Fig. 4.39 – Stress–strain diagram of rectangular2 walls unwrapped

It can be observed that in all cases the diagrams are linear up to about 80% of the maximum load.

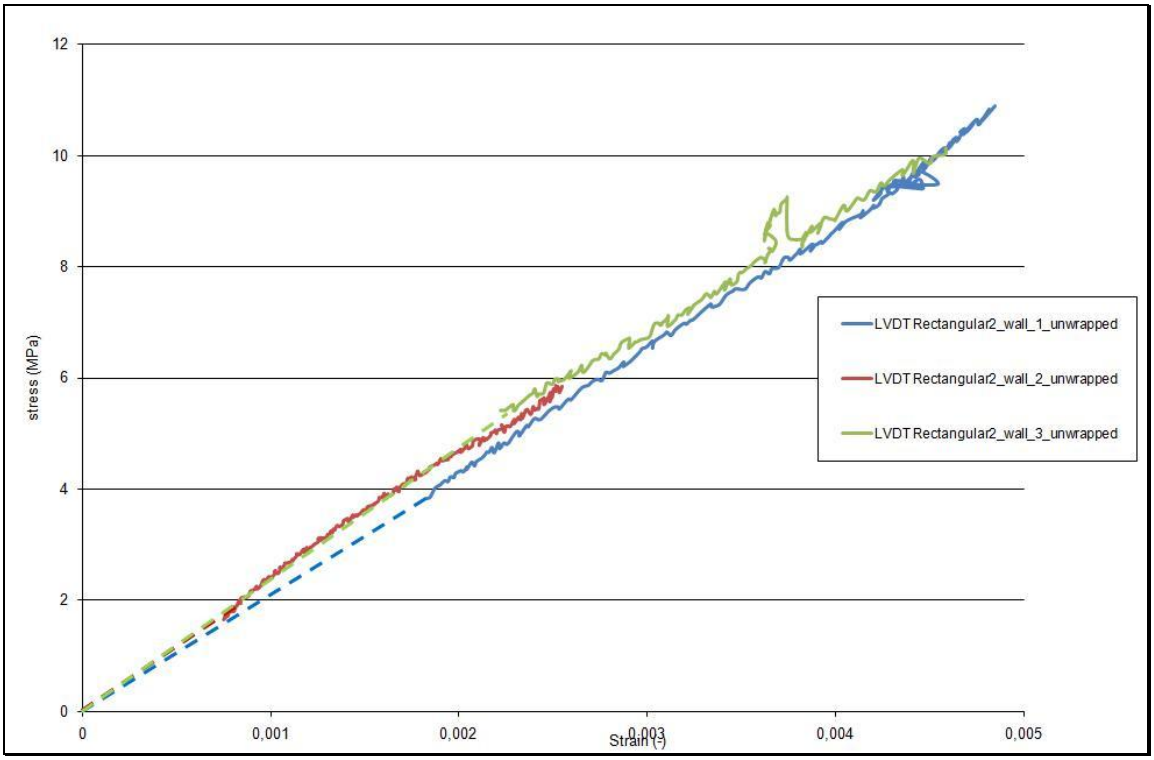

Fig. 4.40 – Stress–LVDTstrain diagram of rectangular2 walls unwrapped

The control specimens failed by the formation of vertical cracks through the joints and the bricks in the middle of both side of the walls along the line of the 4 joints.

After their formation through mortar joints and bricks, vertical cracks became increasingly wide and the masonry between the cracks was crushed with the stop of the tests.

4.4.1.1. Rectangular2 wall unwrapped 1

Fig.4.41 – Rectangular2 wall unwrapped 1

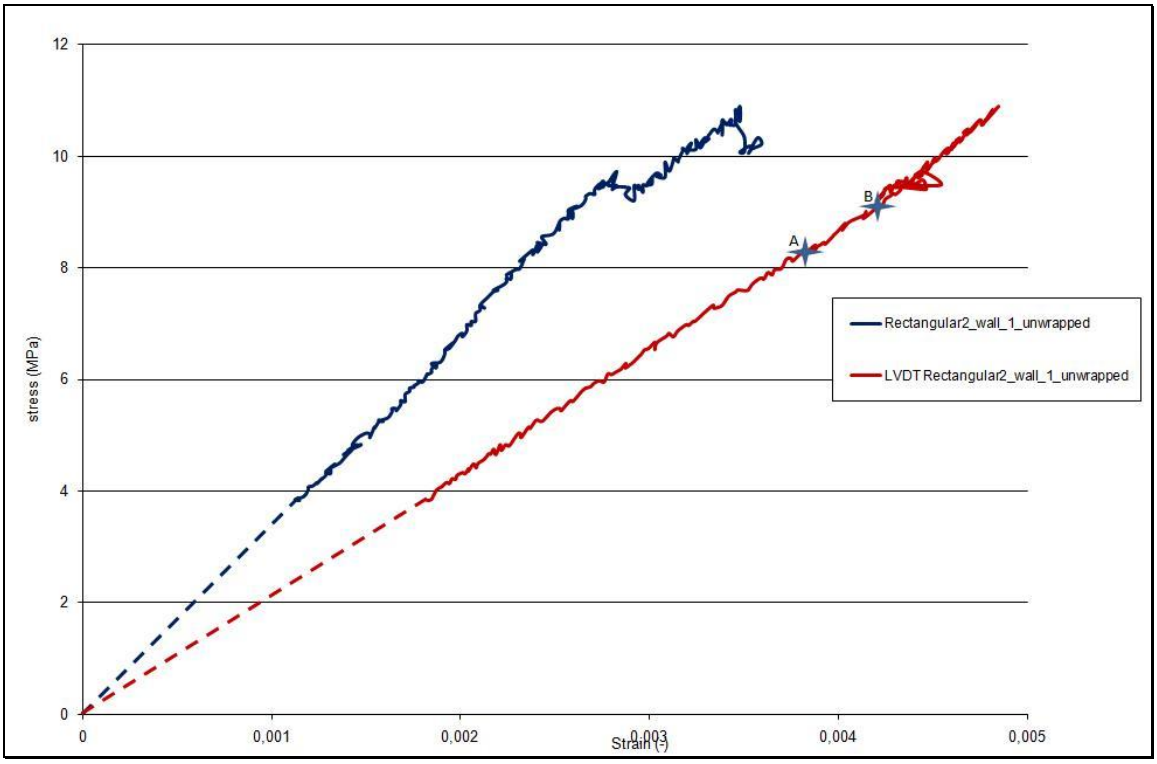

Fig.4.42 – Stress–strain diagram of rectangular2 wall unwrapped 1

The contour plots of ε_{xx} , ε_{yy} and the correlation factor for all the points in figure are reported below.

- A: 39.00 kips; 8,40 MPa

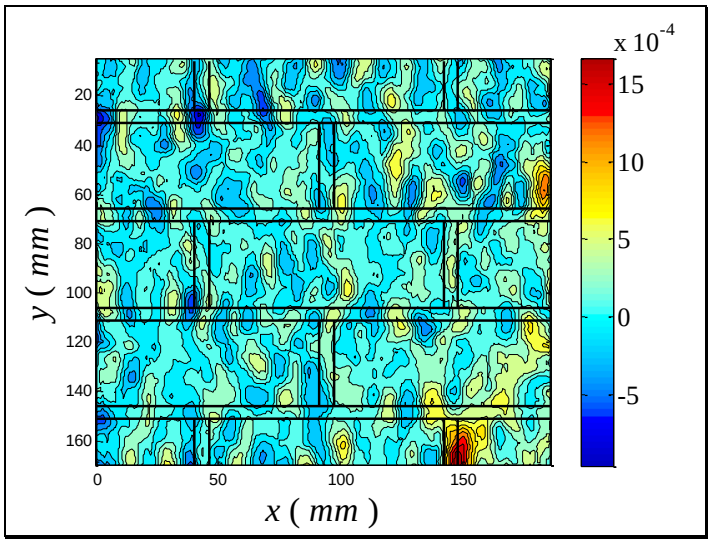

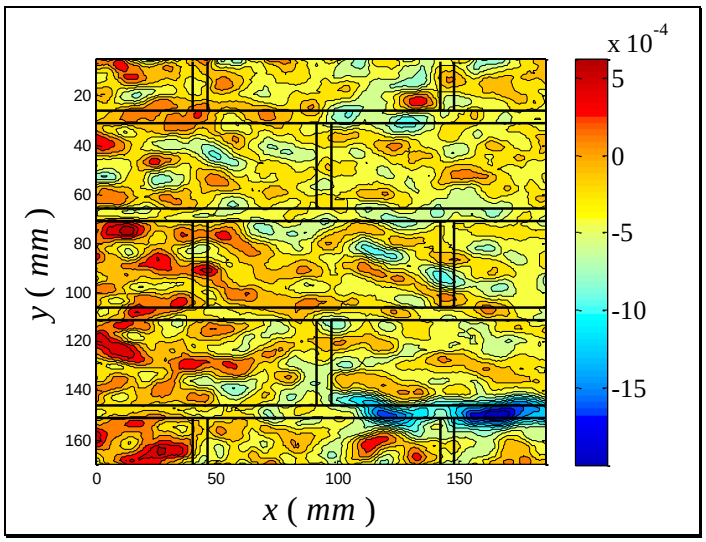

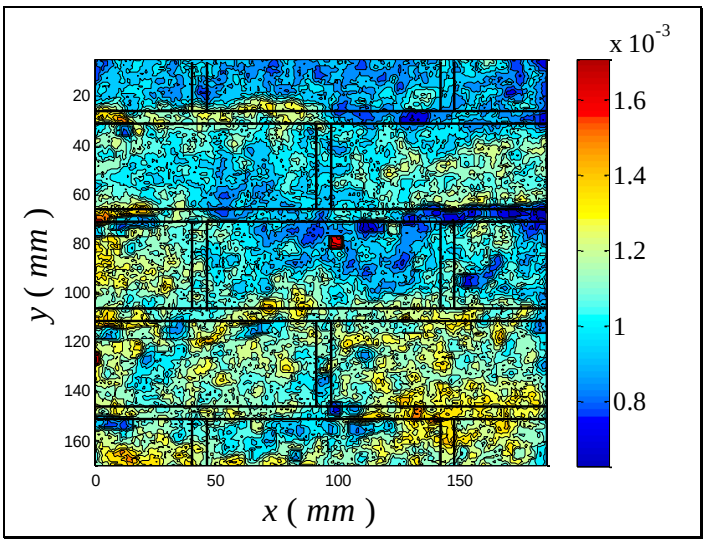

- B: 42.70 kips; 9,20 MPa

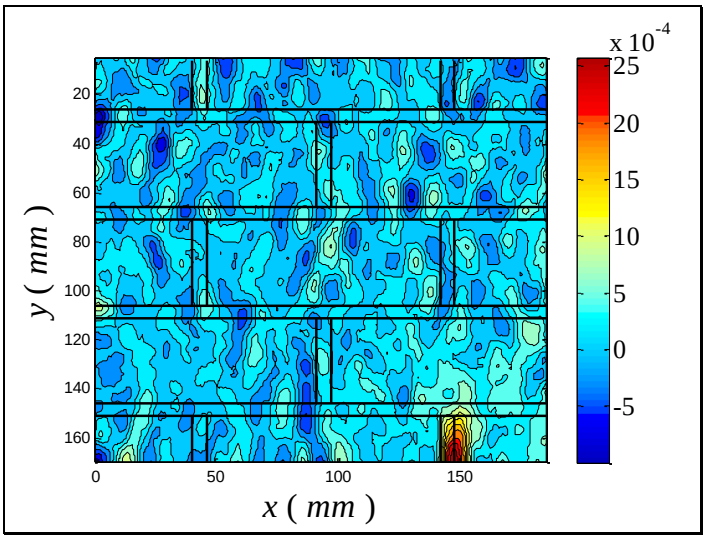

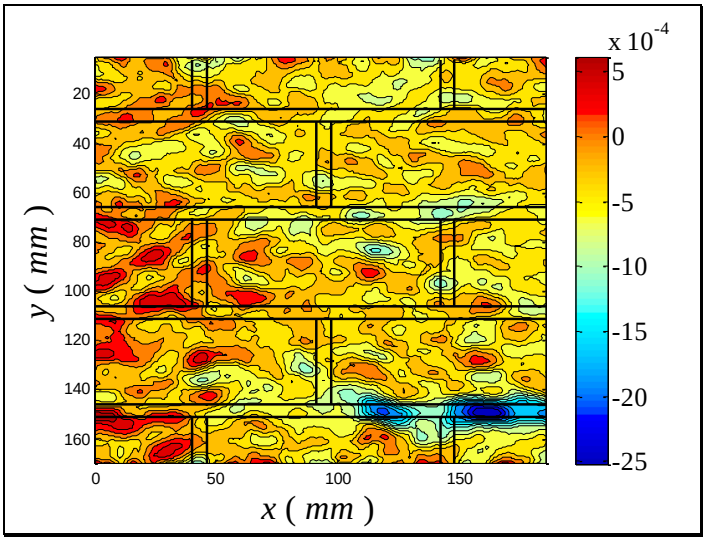

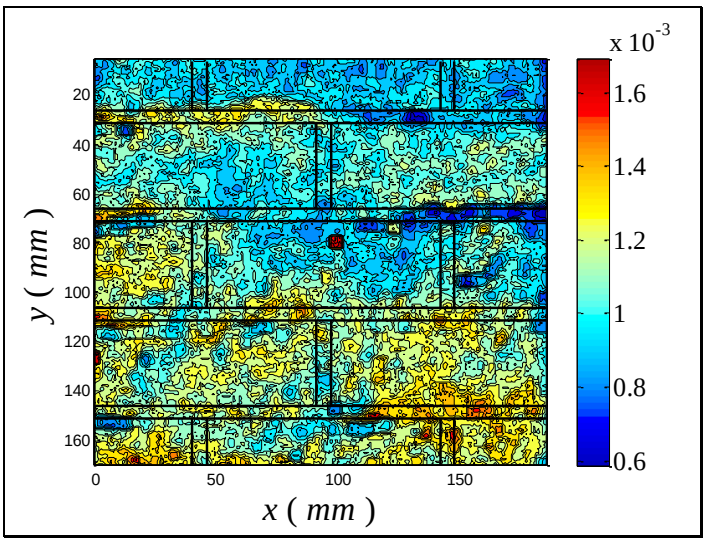

4.4.1.2. Rectangular2 wall unwrapped 2

Fig.4.43 – Rectangular2 wall unwrapped 2

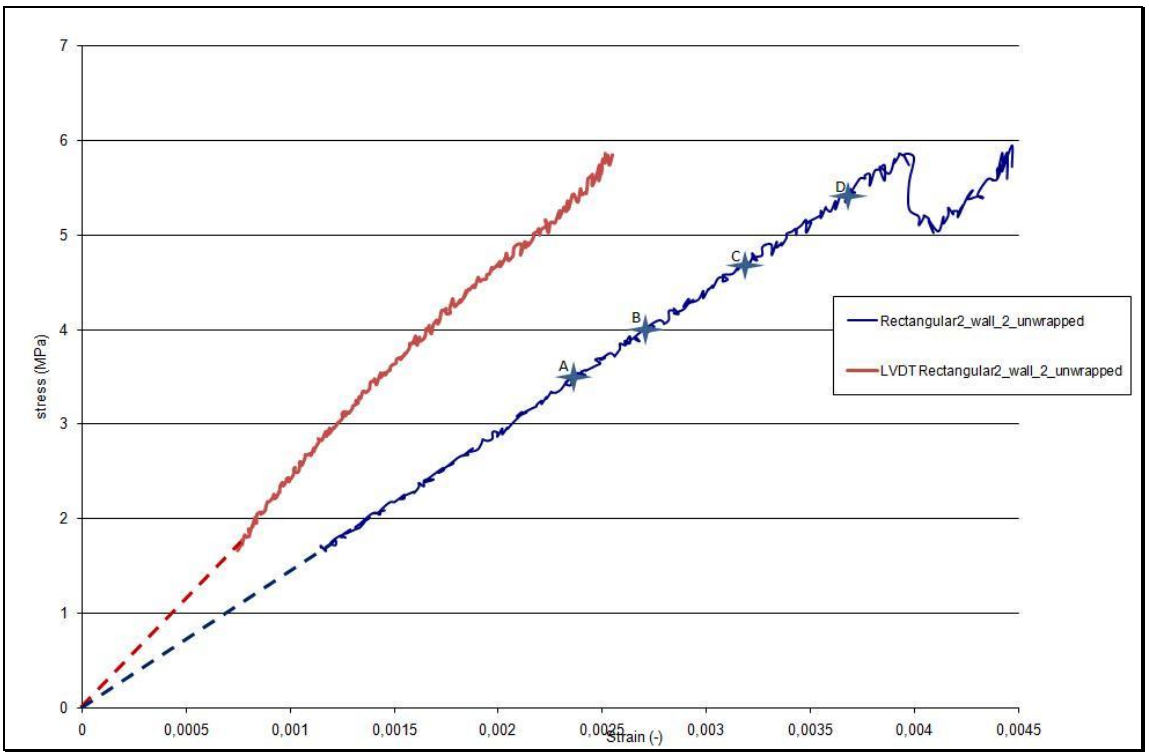

Fig.4.44 – Stress–strain diagram of rectangular2 wall unwrapped 2

The contour plots of ε_{xx} , ε_{yy} and the correlation factor for all the points in figure are reported below.

- A: 16.00 kips; 3,45 MPa

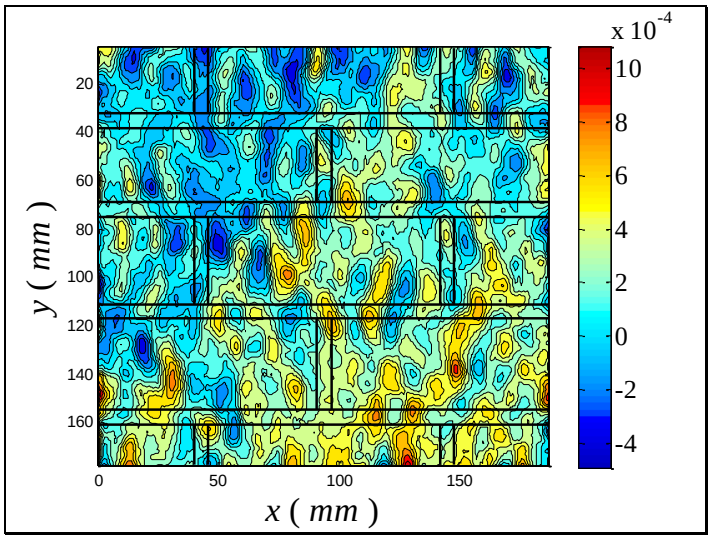

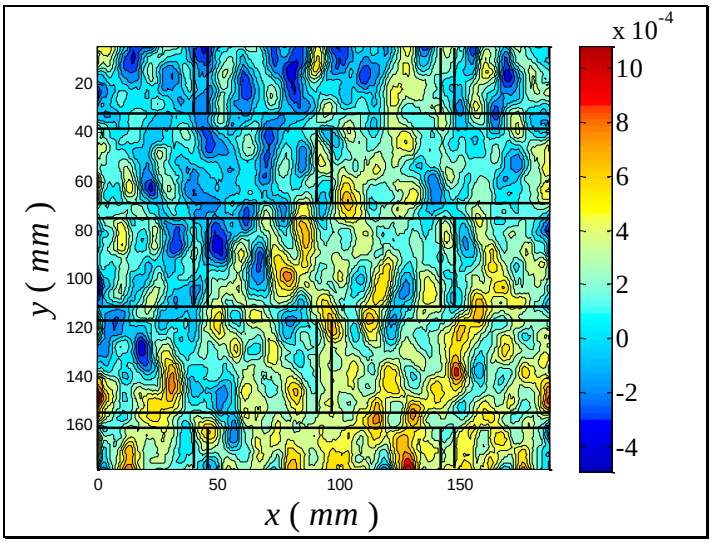

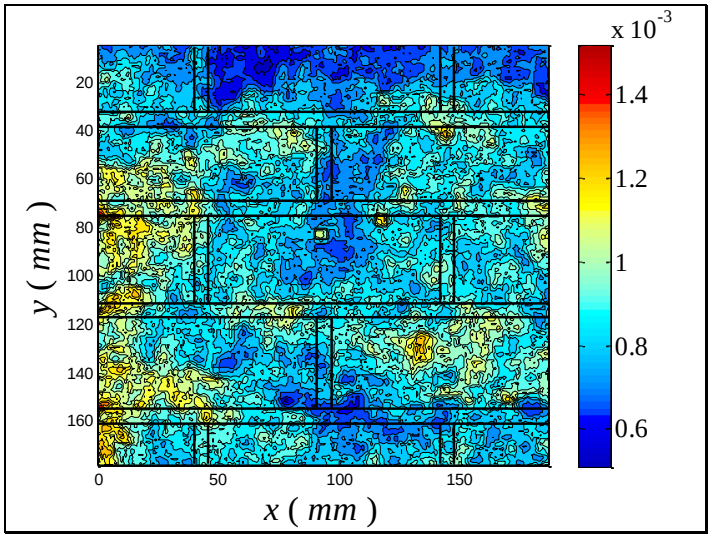

- B: 18.50 kips; 3,99 MPa

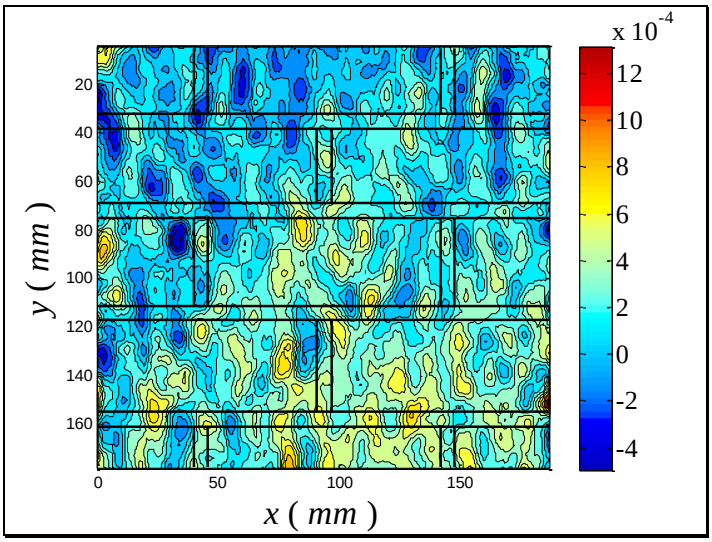

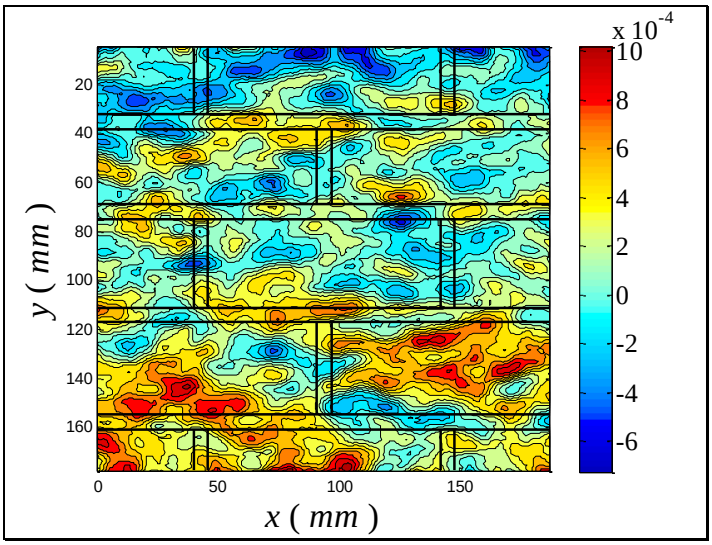

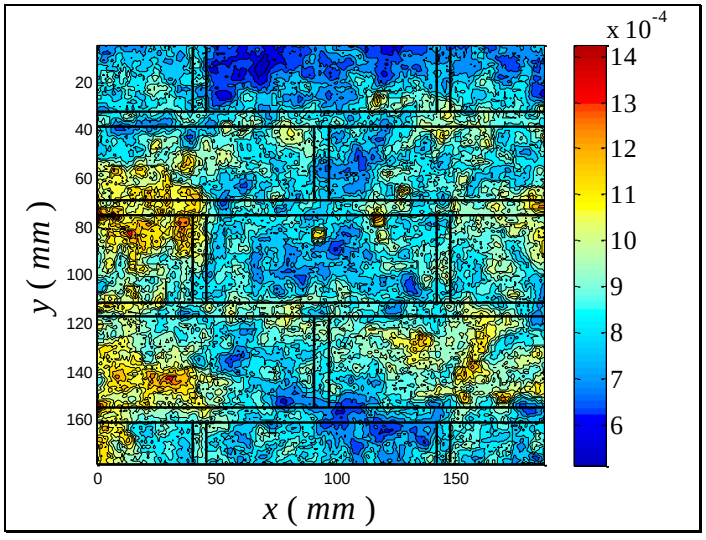

- C: 22.50 kips; 4,84 MPa

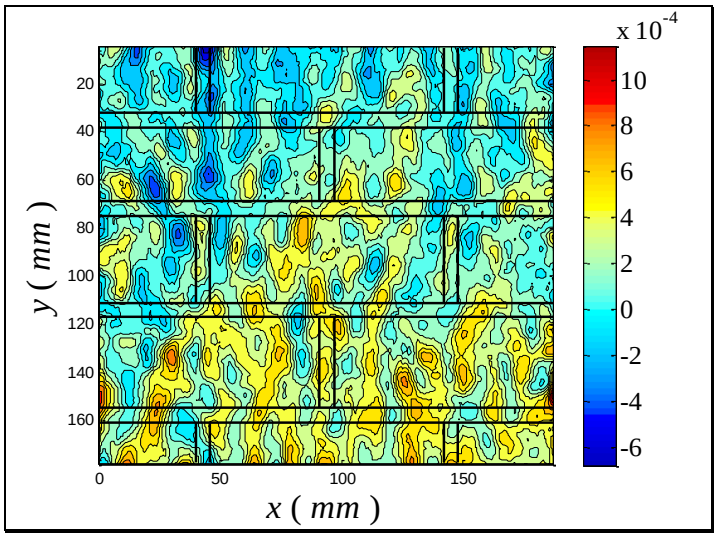

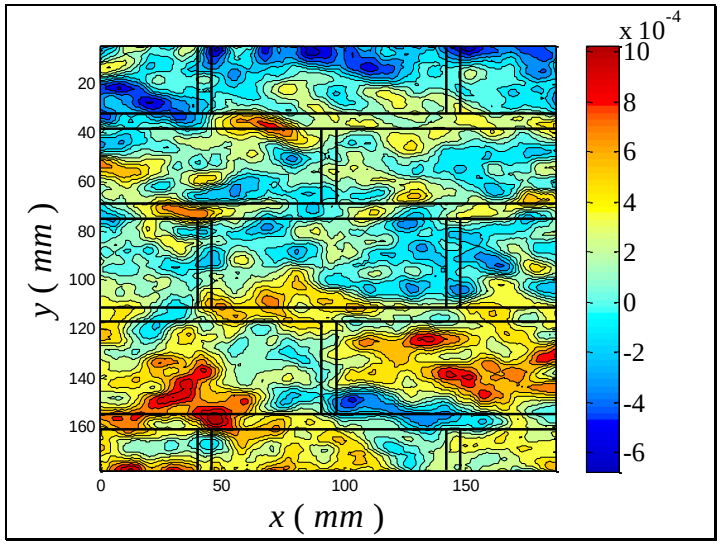

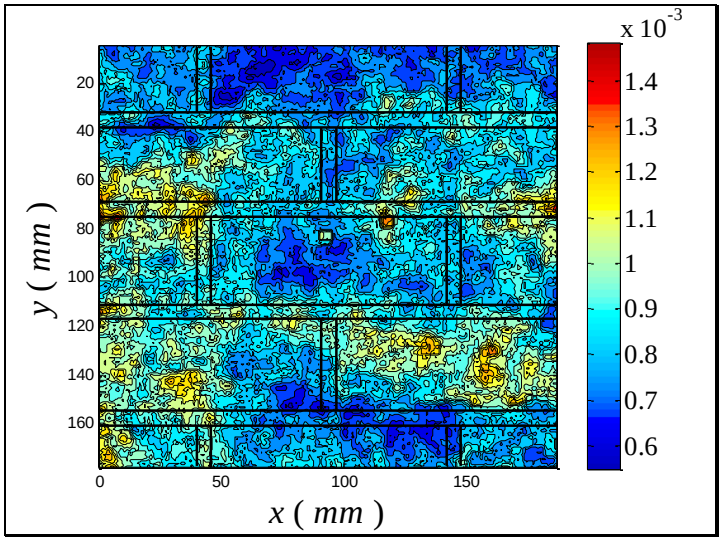

- D: 25.10 kips; 5,41 MPa

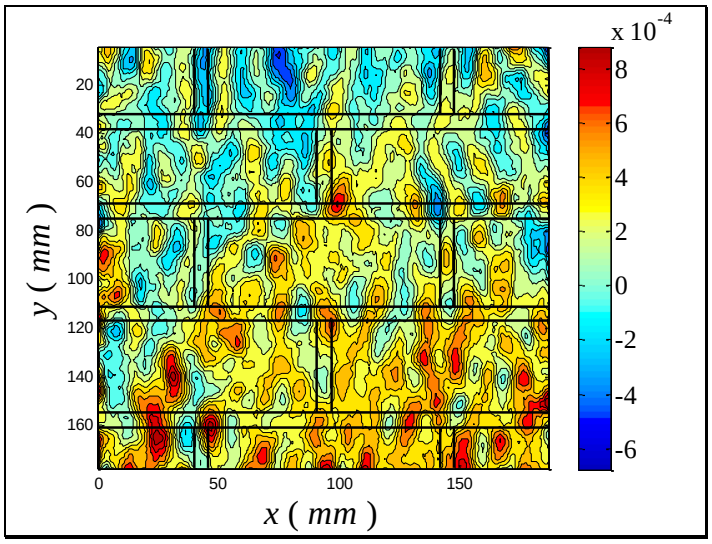

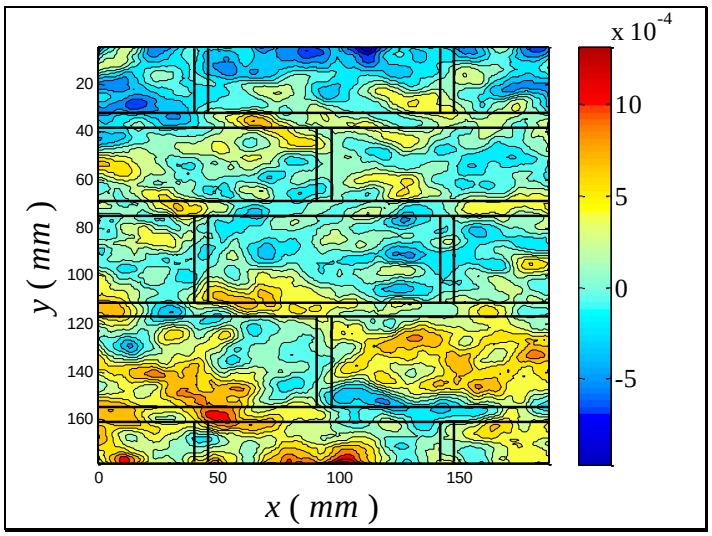

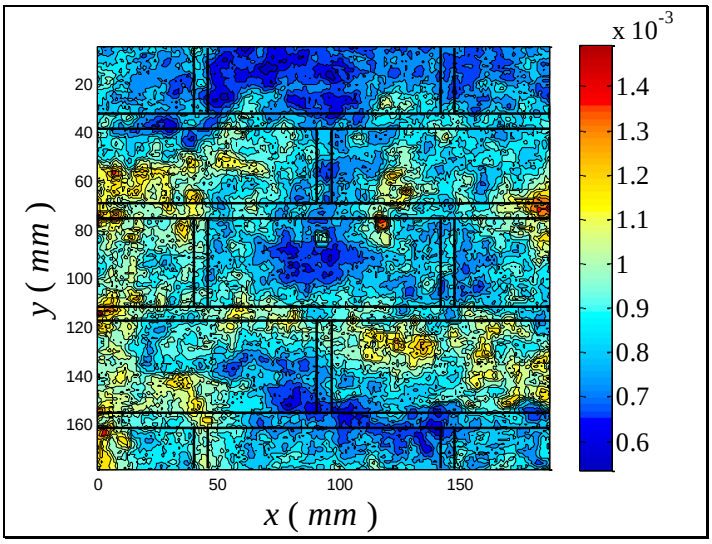

4.4.1.3. Rectangular2 wall unwrapped 3

Fig.4.45 – Rectangular2 wall unwrapped 3

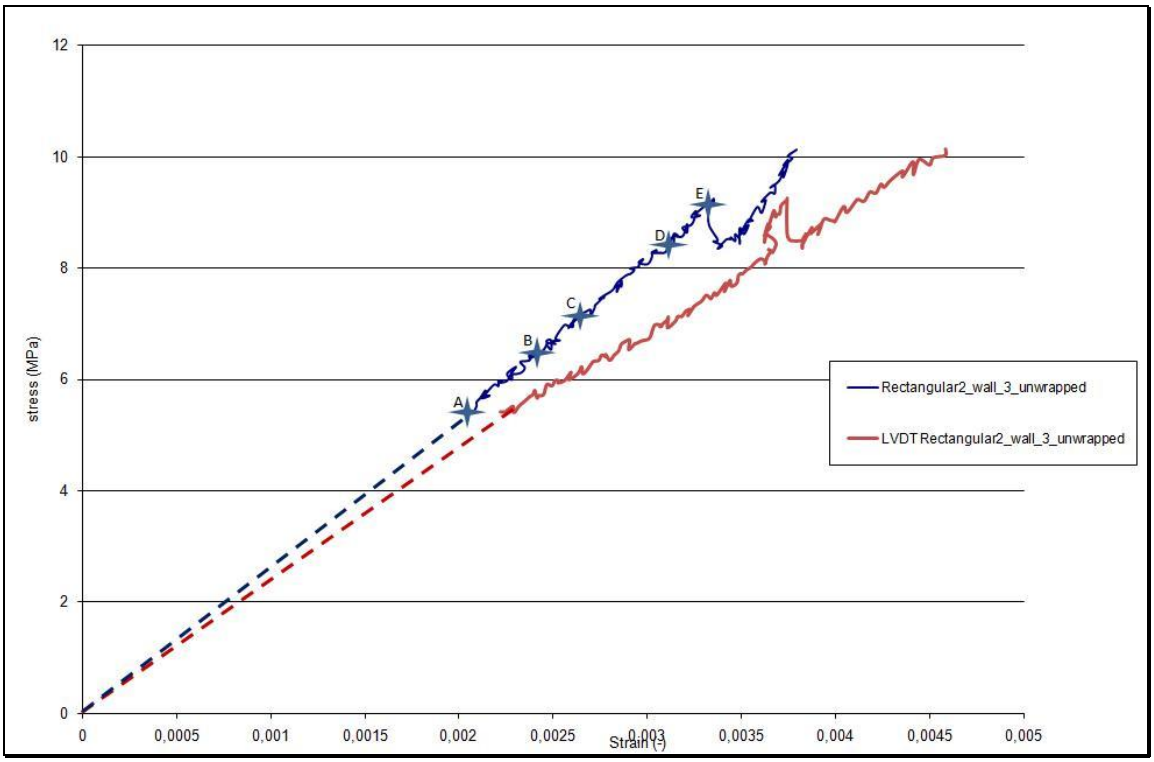

Fig.4.46 – Stress–strain diagram of rectangular2 wall unwrapped 3

DIC pictures are presented with, for all the point marked, in order the ε_{xx} , ε_{yy} and the correlation.

- A: 24.50 kips; 5,30 MPa

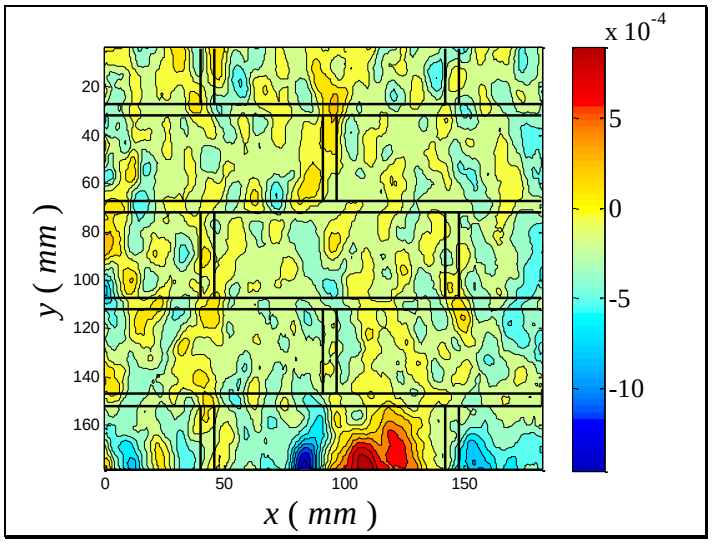

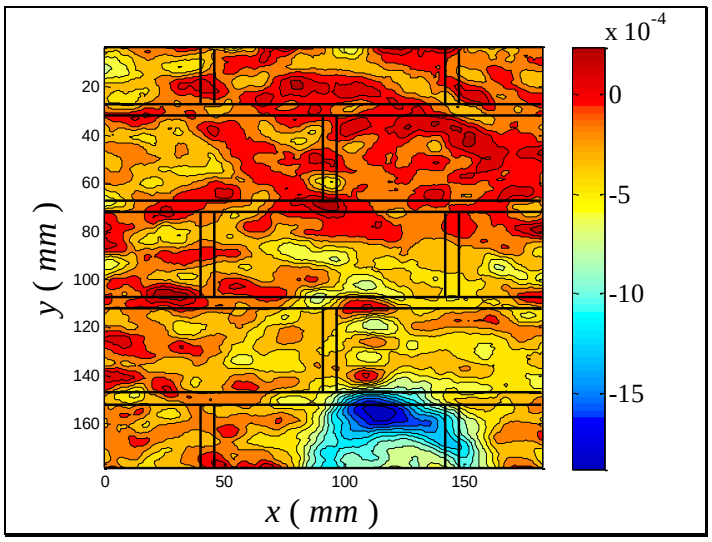

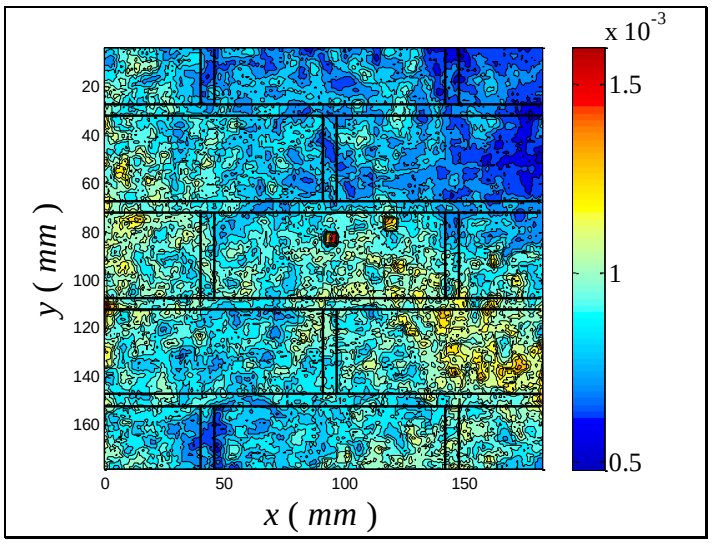

- B: 30.14 kips; 6,52 MPa

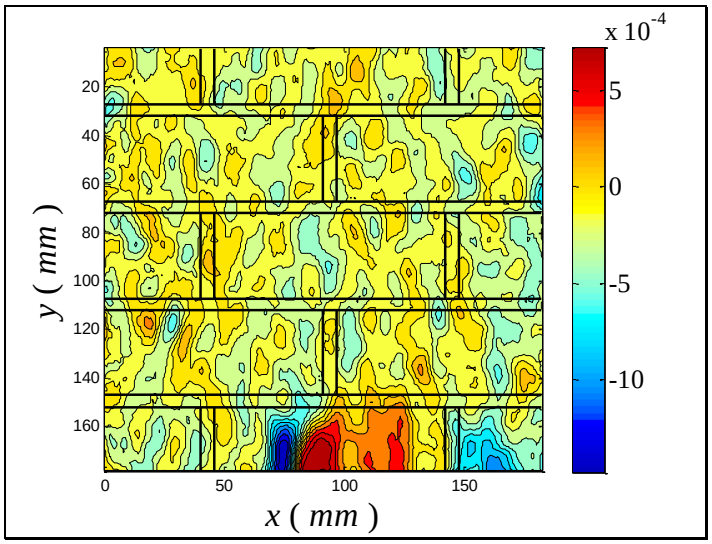

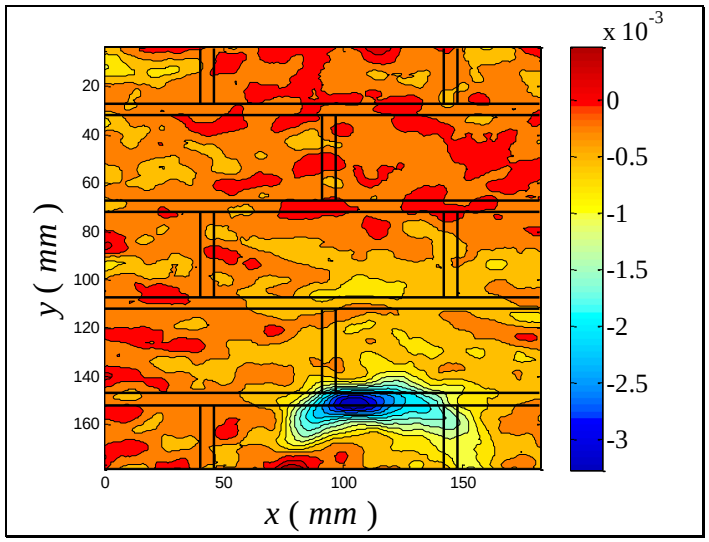

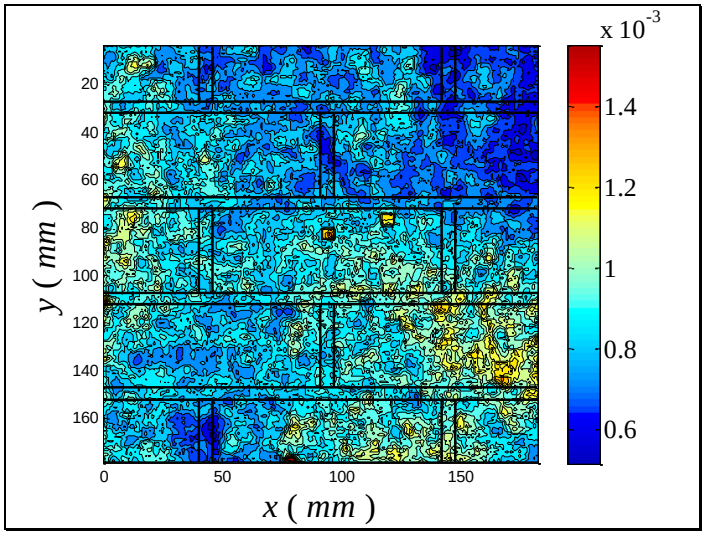

- C: 36.09 kips; 7,80 MPa

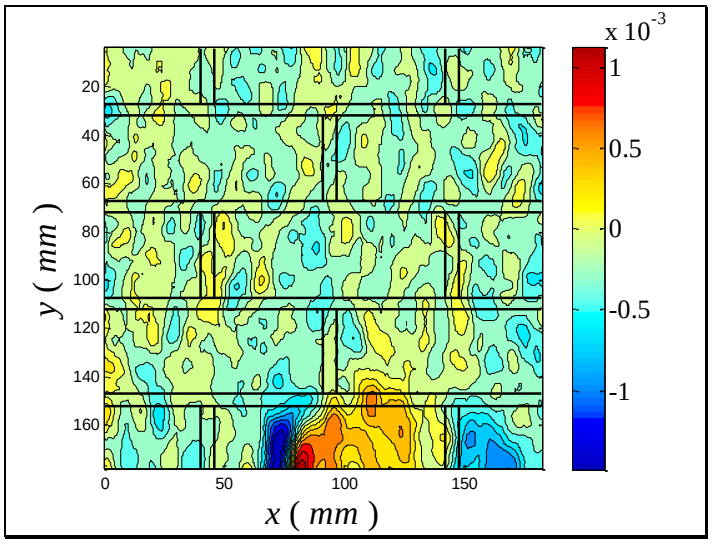

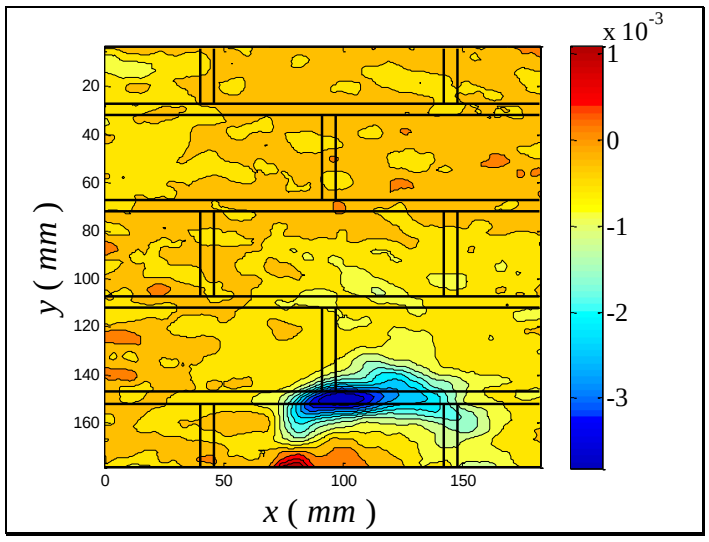

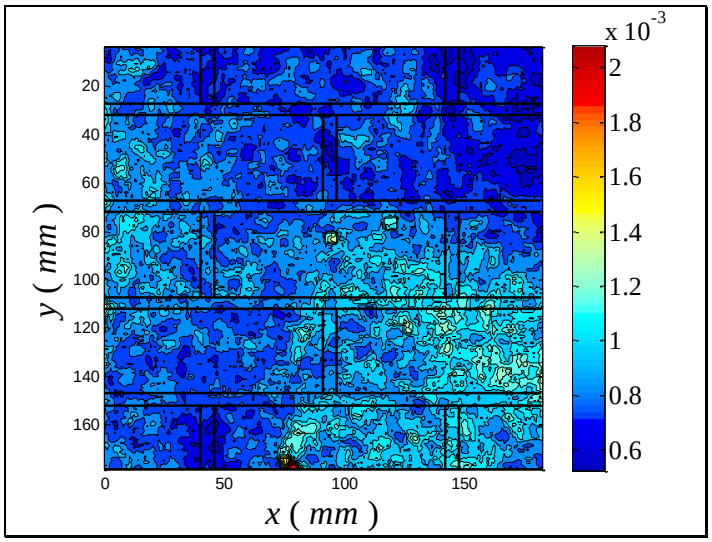

- D: 40.00 kips; 8,65 MPa

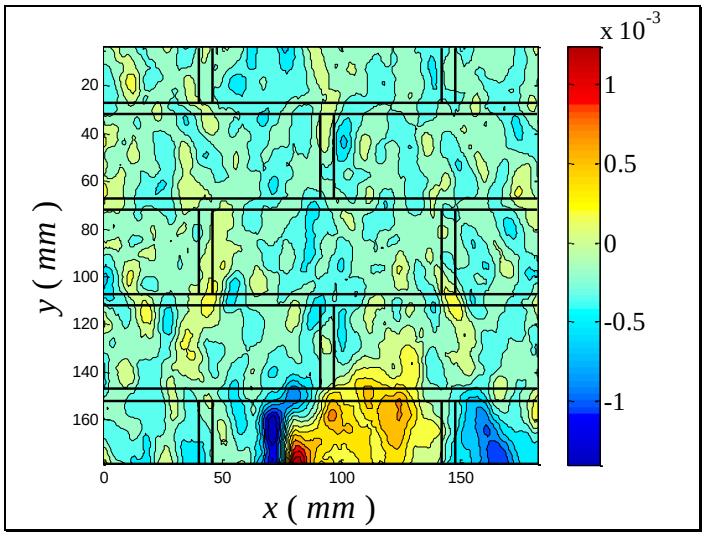

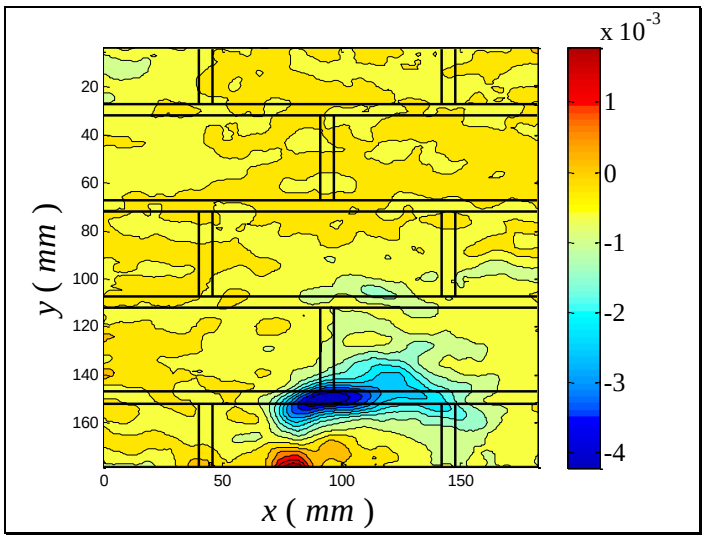

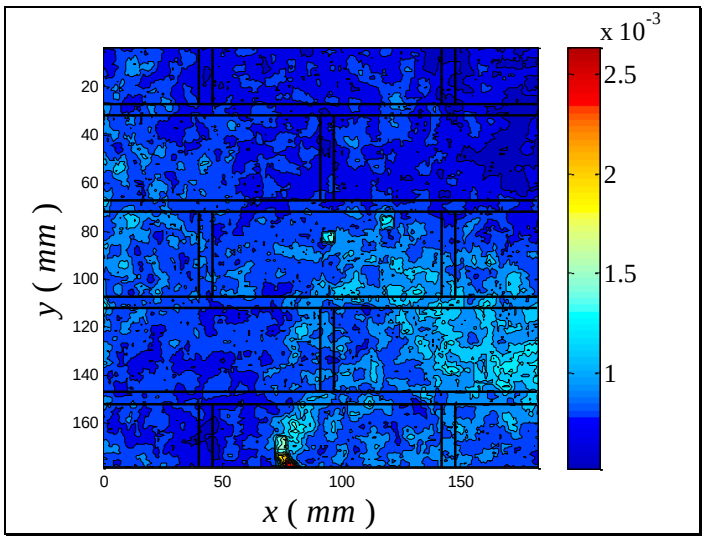

- E: 42.20 kips; 9,13 MPa

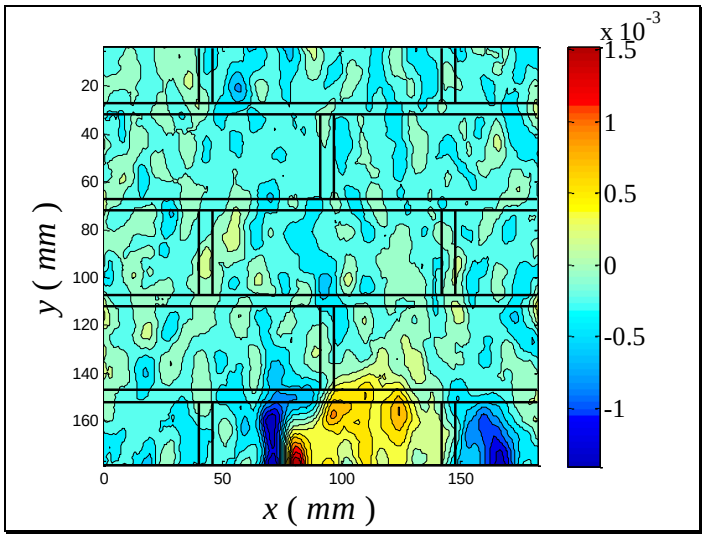

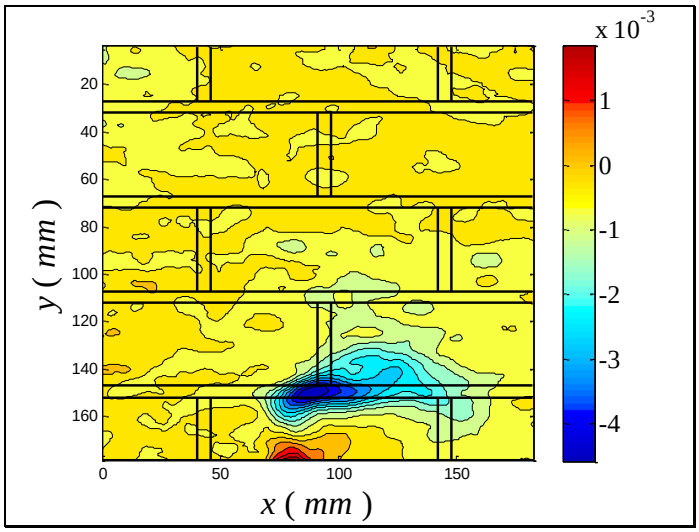

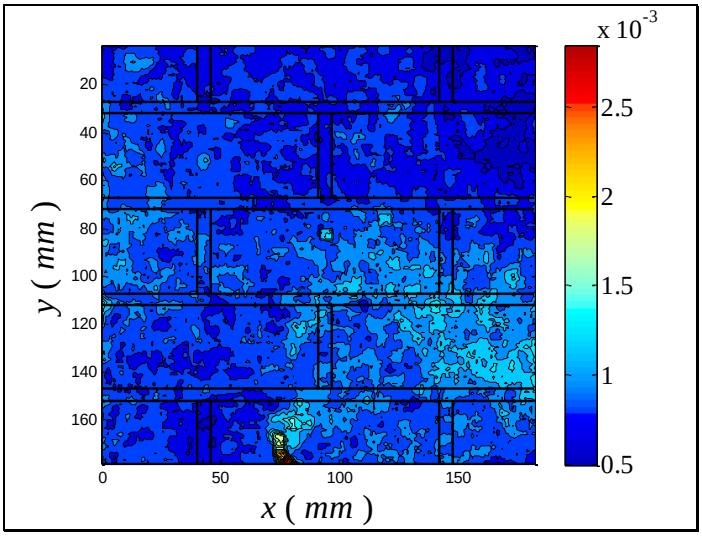

4.4.2. Discussion of result

As the other specimens, failure appeared to be initiated by crushing and squeezing of the mortar from the mortar joints followed by vertical splitting in both side along the preferred line of the 4 joints, as shown in figure 4.47.

In particular in this configuration cracks, as it can be seen in DIC pictures, are not clearly started in the middle of the specimen where there are the 4 joints. There were a lot of cracks distributed on the surface of the masonry until a big crack suddenly started and divide specimens.

After their formation through mortar joints and bricks, vertical cracks became increasingly wide and the masonry between the cracks was crushed.

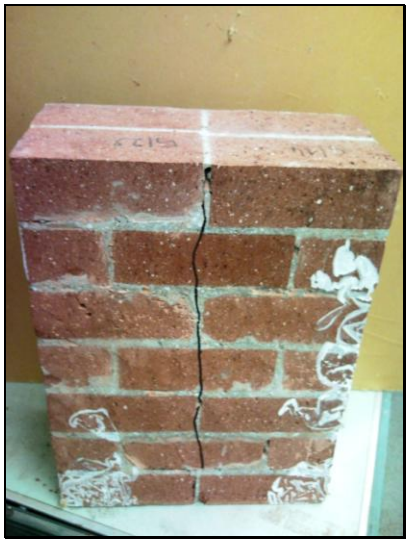

Fig. 4.47 – Vertical splitting of the wall

The same conclusions of the other walls can be drawn, in particular the compressive strength can be increased with the use of a reinforcement that contain, after the crack of the vertical joint, the lateral expansion of the specimen increasing the load-carrying capacity.

CHAPTER 5

FRCM-REINFORCED BRICK MASONRY WALLS

C H A P T E R 5

FRCM-REINFORCED BRICK MASONRY WALLS

5.1. Axial Compression Test First Configuration

Composite materials are getting more and more common for strengthening existing members and structures; Fiber-Reinforced Cementitious Matrix (FRCM) materials have been more recently proposed especially for strengthening masonry members. In the present chapter, the results of an experimental campaign carried out on brick masonry walls in different configurations strengthened by this cement-based composite are reported and commented.

Before wrapping all the corner of the specimens were rounded using a grinding machine at a radius of 10 mm, figure 5.1.

Fig. 5.1 – First configuration masonry wall with rounded corners

The specimens were wrapped with one layer of Fiber Reinforced Cementitious Matrix (FRCM), an high performance fiber structural

reinforcement systems. Initially a layer of a stabilized inorganic matrix designed to connect the mesh with the substrate was applied on the surface of each specimen, figure 5.2, and then a PBO mesh was applied with the fibers in the hoop direction, figure 5.3.

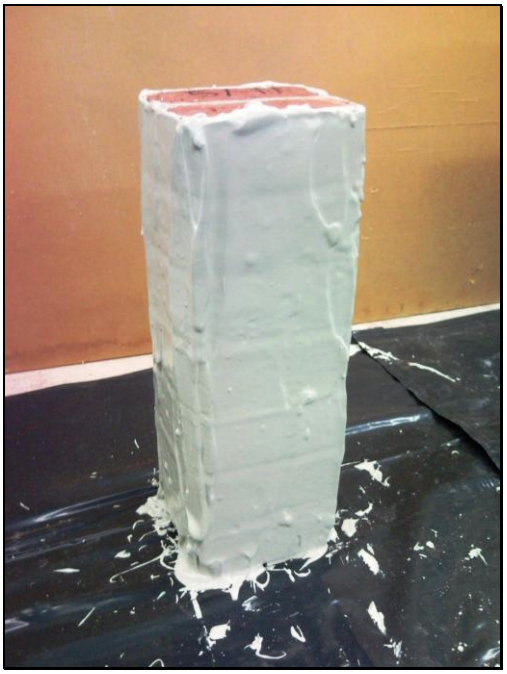

Fig. 5.2 – Epoxy resin application on the masonry surface

Fig. 5.3 – First configuration masonry wall wrapping

The finishing end of the mesh overlapped the starting end by approximately 100 mm.

After the wrapping all the fibers were covered with the same cementitious inorganic matrix used before, figure 5.4.

Fig. 5.4 – First configuration masonry wall after the complete wrapping

Curing of the wrapping took place after curing of the masonry specimens, at least 14 days, and testing started approximately one month after the casting of the walls.

The specimens face need to be prepared for the DIC with a layer of white paint followed by a layer of a light drops of black paint, figure 5.5.

Fig. 5.5 – First configuration masonry wall ready for the DIC

Displacements of the central section on each specimen were measured using also a Linear Variable Differential Transformer (LVDT) on the left side of the columns attached to the wrapping surface.

5.1.1. Experimental result and failure mode

The main results of the tests are presented in the table 5.1.

Specimens notation	3 precycle (kN)	Maximum load (kN)	Area (cm^2)	Compressive strenght (MPa)	Ultimate machine strain ε
1	20-90	346,73	99,14	33,93	0,0062
2	45-110	422,36	99,14	41,33	0,0059
3	45-110	340,97	99,14	34,23	0,0015
Displacement control mode of 0.008 inch/min, about 0.2 mm/min					

Tab. 5.1 – Summary of test results for square walls wrapped

The stress-strain diagrams for the first configuration wrapped specimens are presented in figure 5.6.

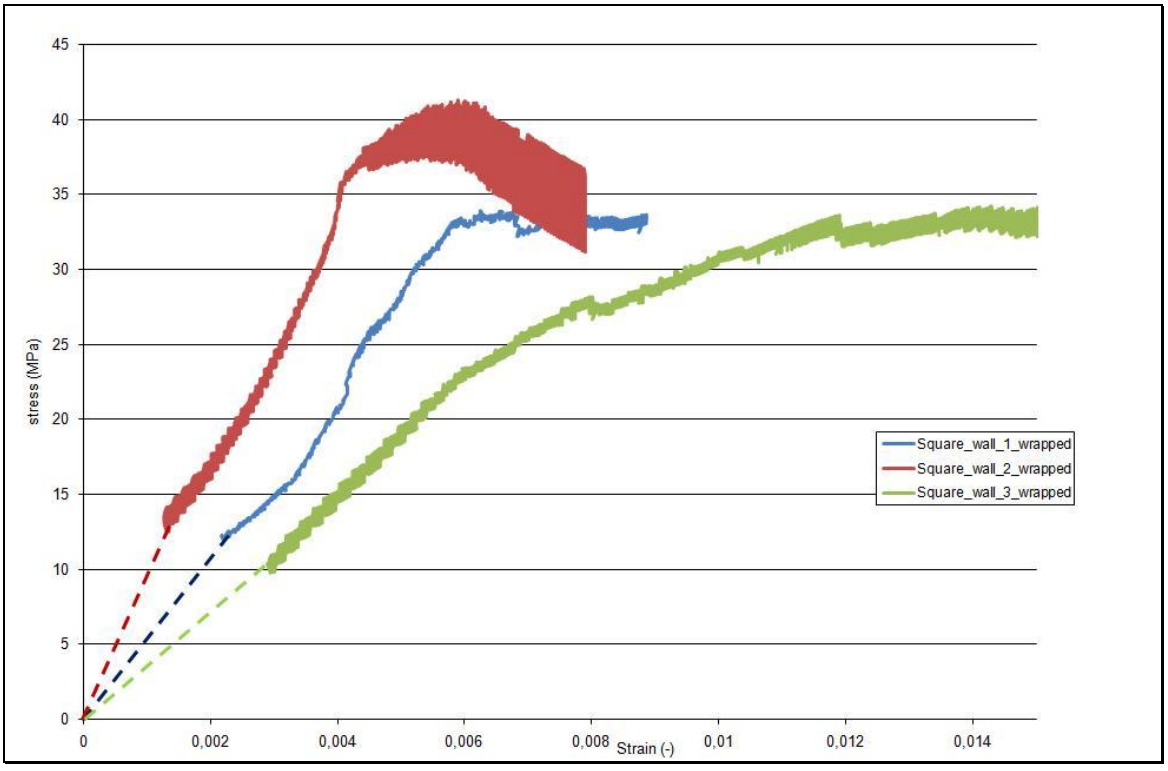

Fig. 5.6 – Stress–strain diagram of square walls wrapped

It can be observed that in all cases the diagrams are linear up to about 80% of the maximum load.

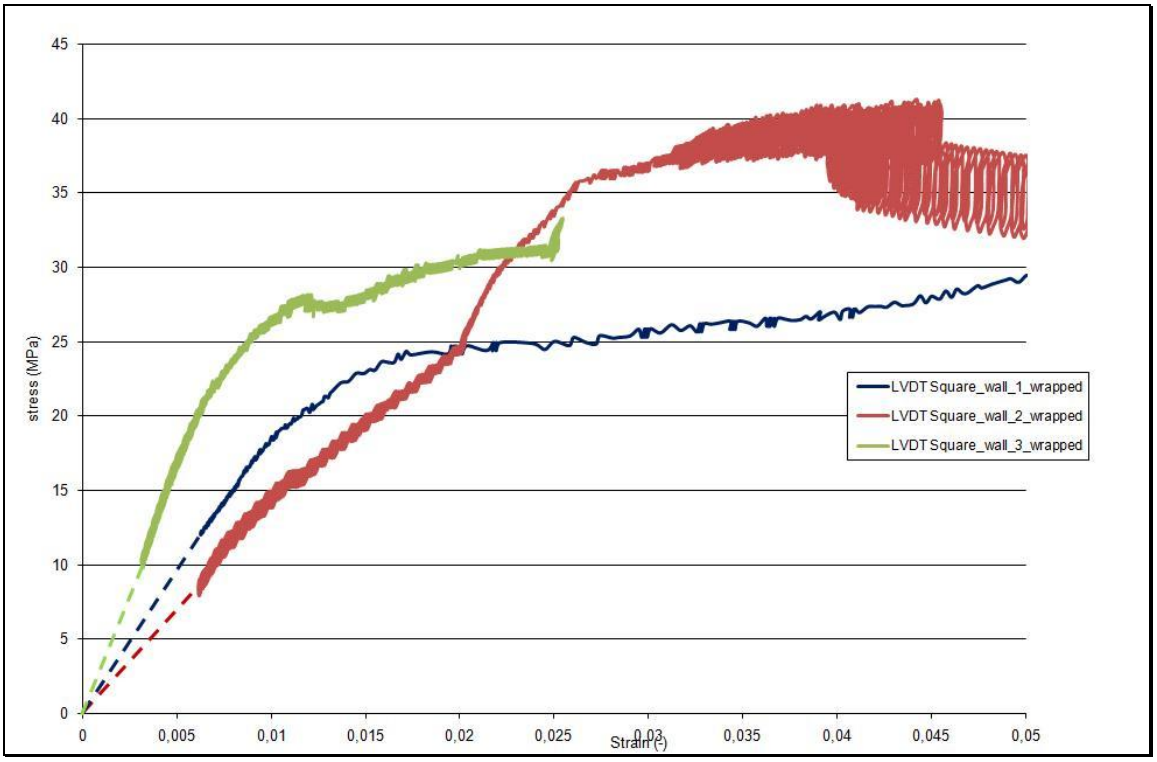

Fig. 5.7 – Stress–LVDTstrain diagram of square walls wrapped

The control specimens failed by the formation of vertical cracks through the joints and the bricks in the middle of the face with 4 mortar joints, it can be seen in the picture of the digital image correlation.

After the crack of the vertical joints the reinforcement begins to work keeping the bricks together and attributing to the masonries a ductility that otherwise it hasn't.

At the end, vertical cracks became increasingly wide, up to unthread the reinforcement on the overlap in the back of the specimens.

5.1.1.1. Square wall wrapped 1

Fig.5.8 – Square wall wrapped 1

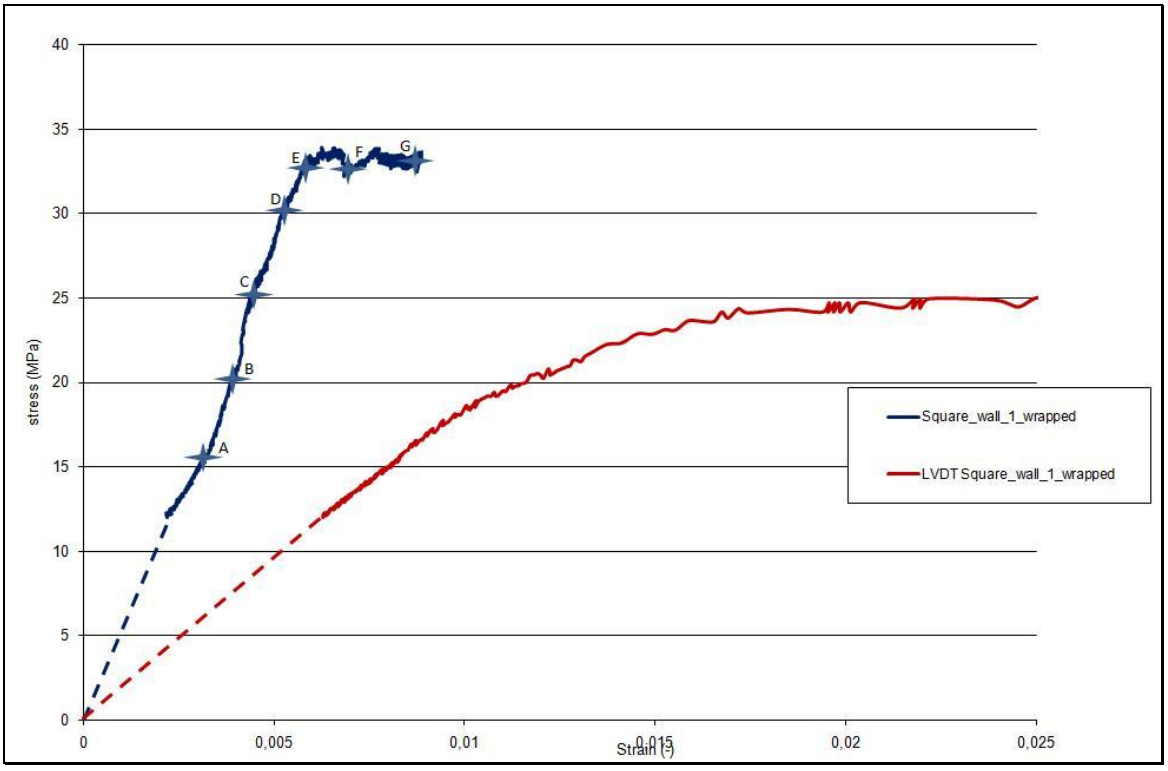

Fig.5.9 – Stress–strain diagram of square wall wrapped 1

The contour plots of ε_{xx} , ε_{yy} and the correlation factor for all the points in figure are reported below.

- A: 37.00 kips; 16,10 MPa

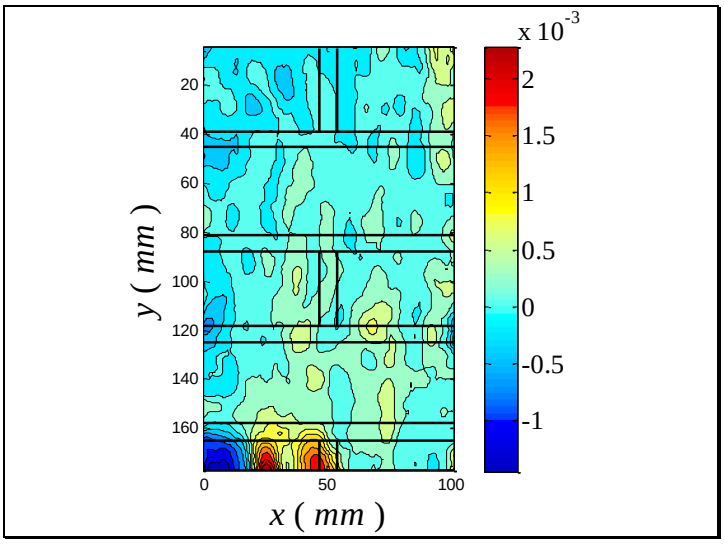

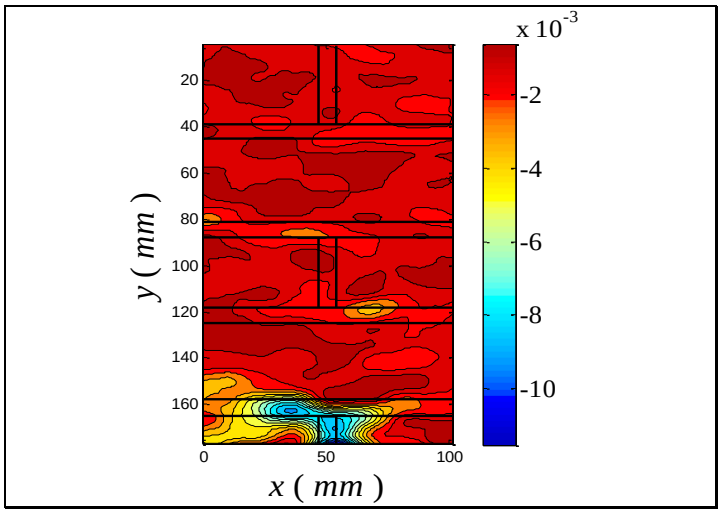

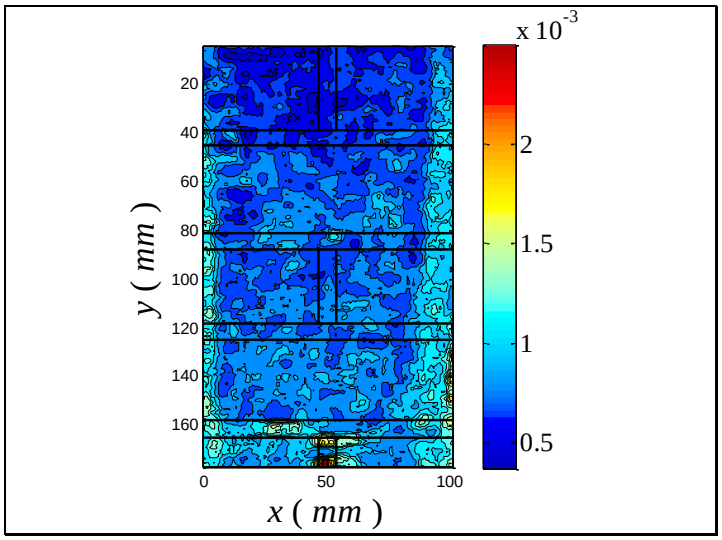

- B: 47.11 kips; 20,50 MPa

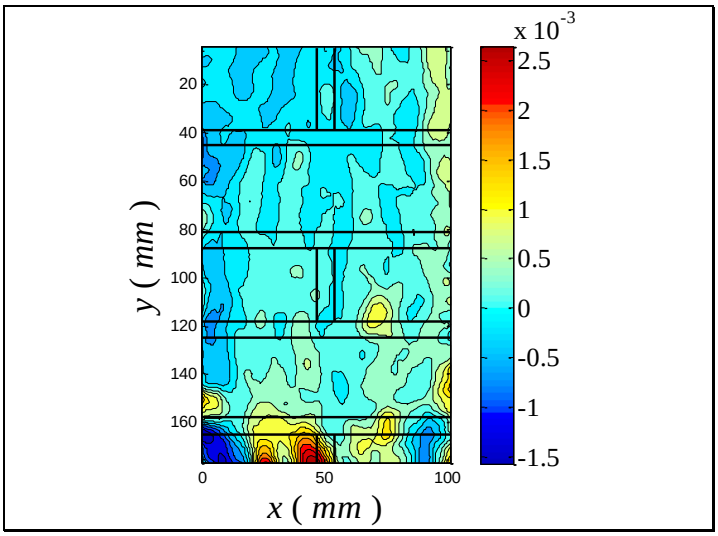

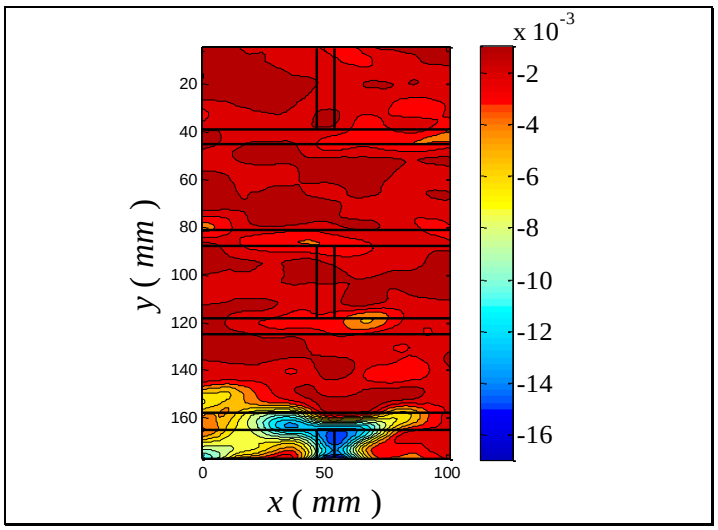

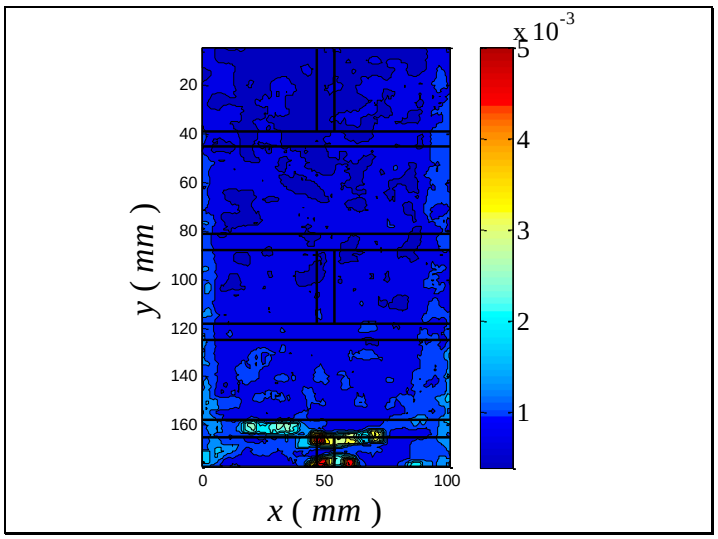

- C: 58.70 kips; 25,55 MPa

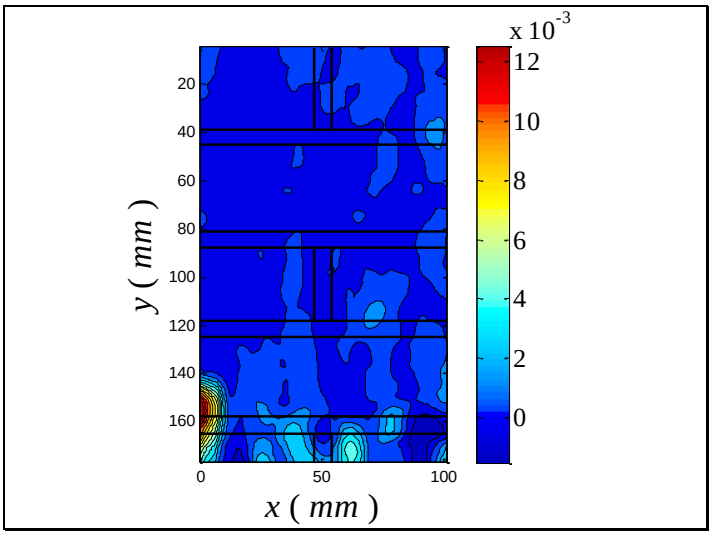

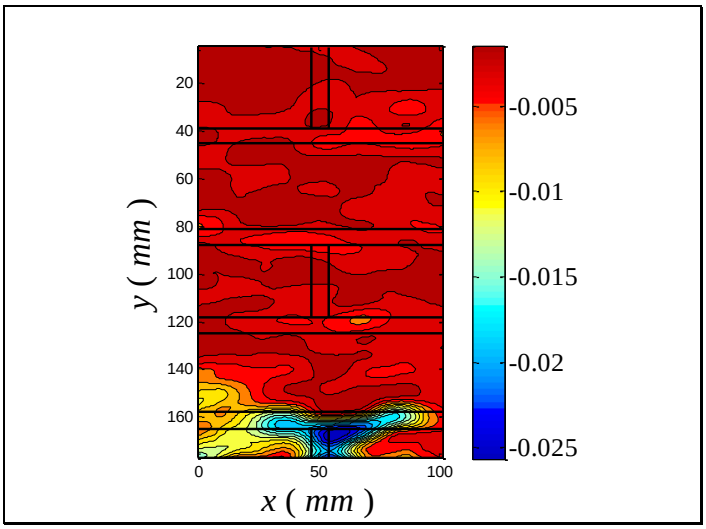

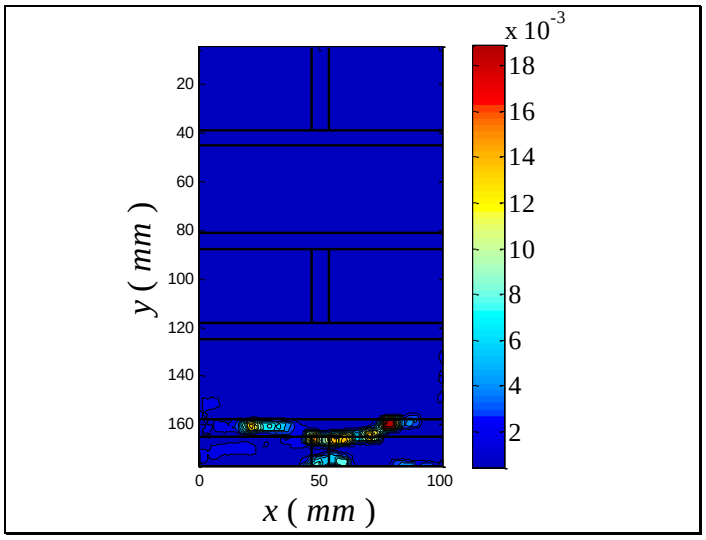

- D: 69.10 kips; 30,08 MPa

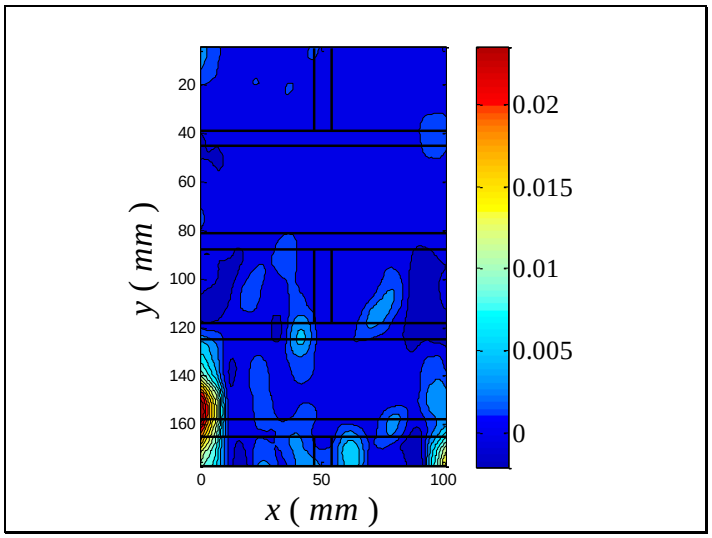

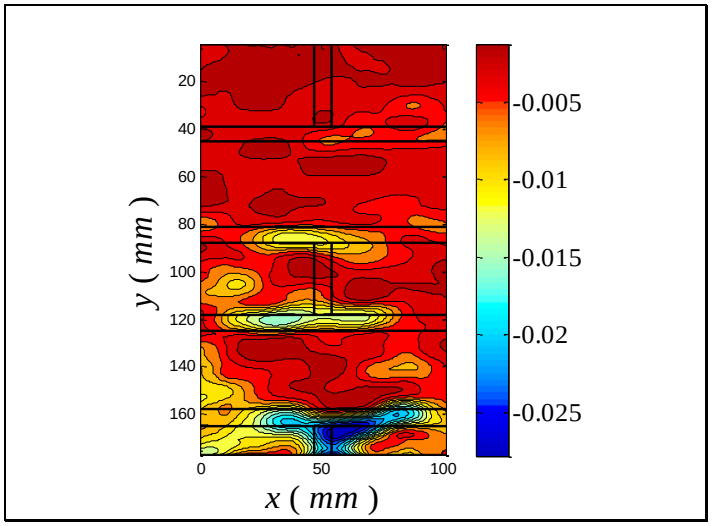

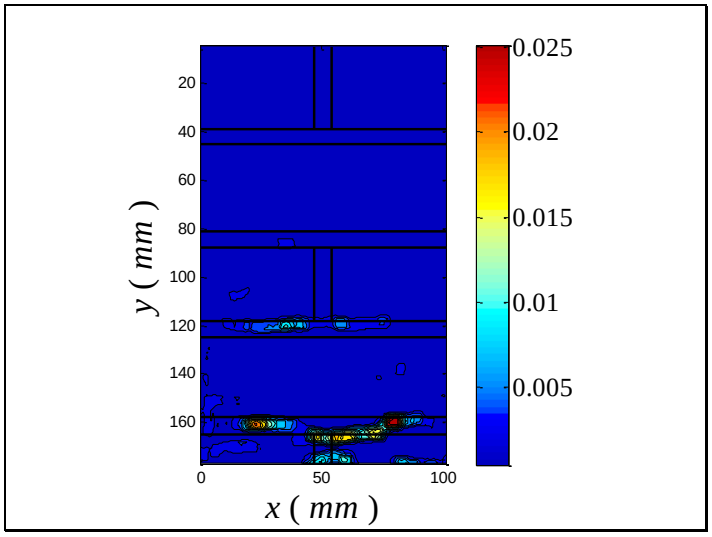

- E: 76.20 kips; 33,17 MPa

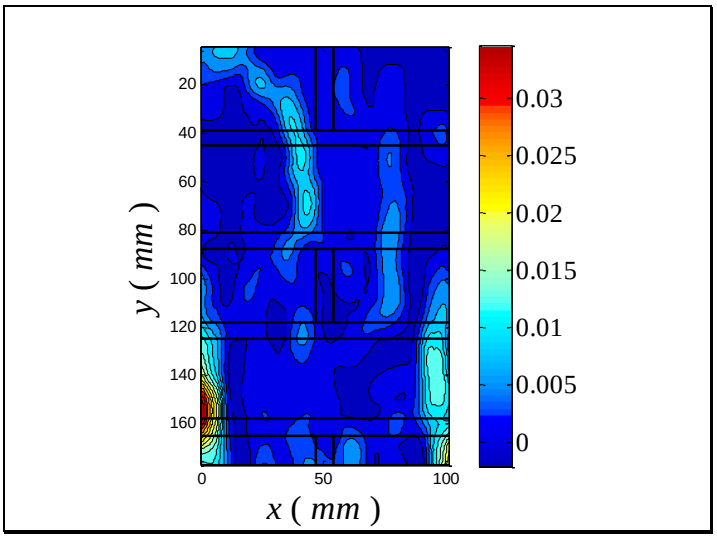

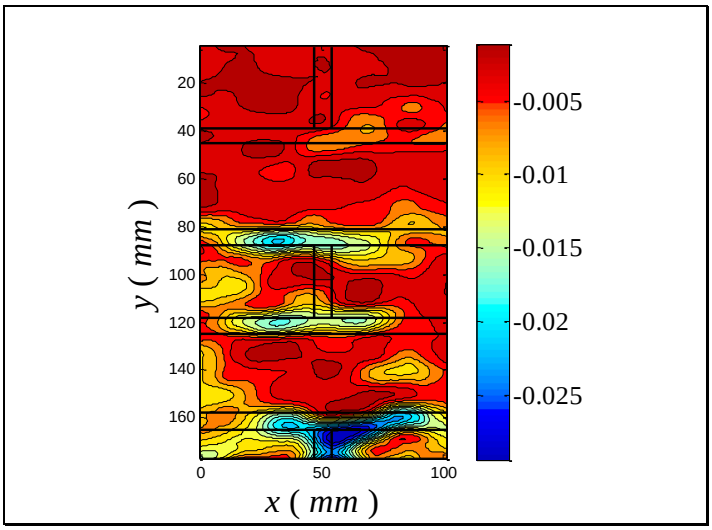

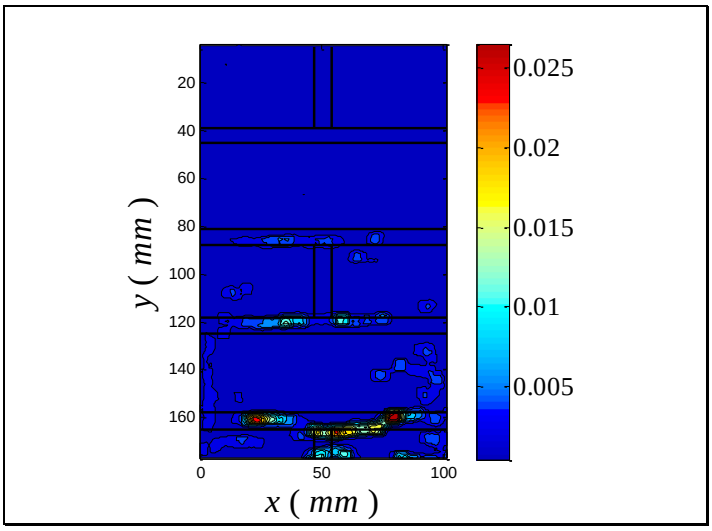

- F: 75.50 kips; 32,86 MPa

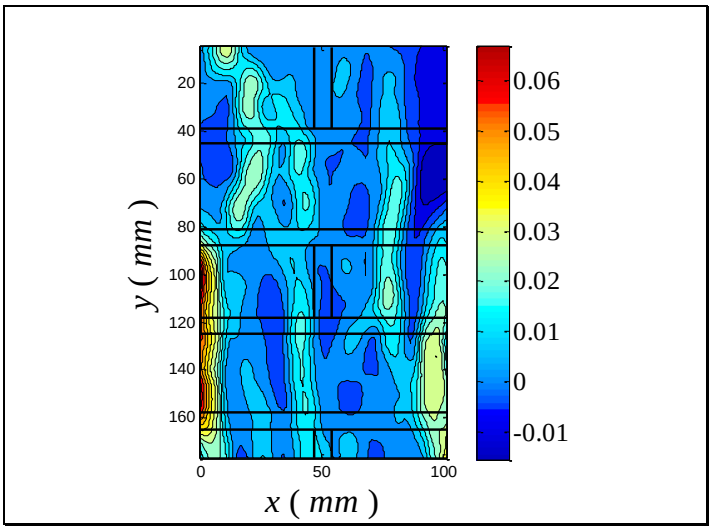

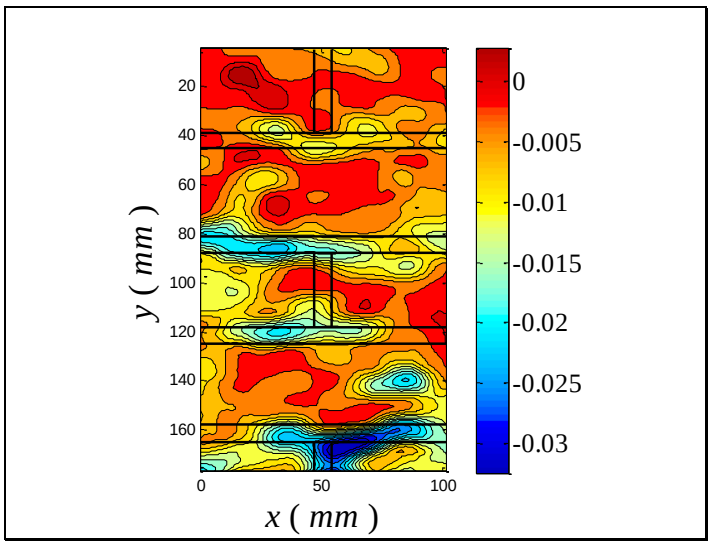

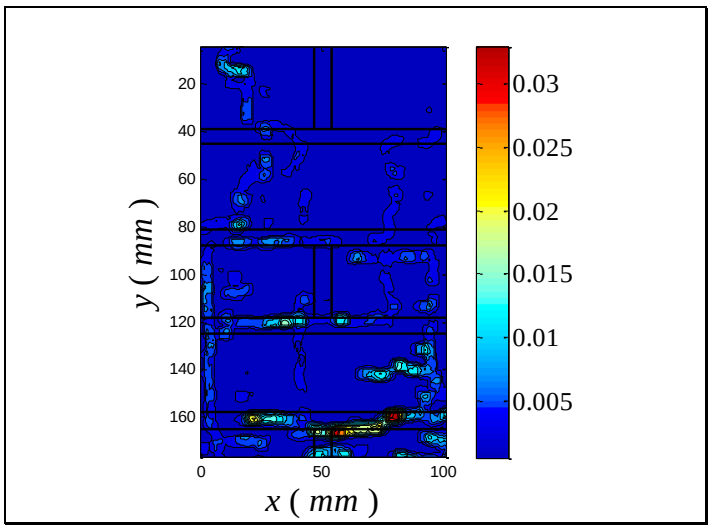

- G: 77.00 kips; 33,51 MPa

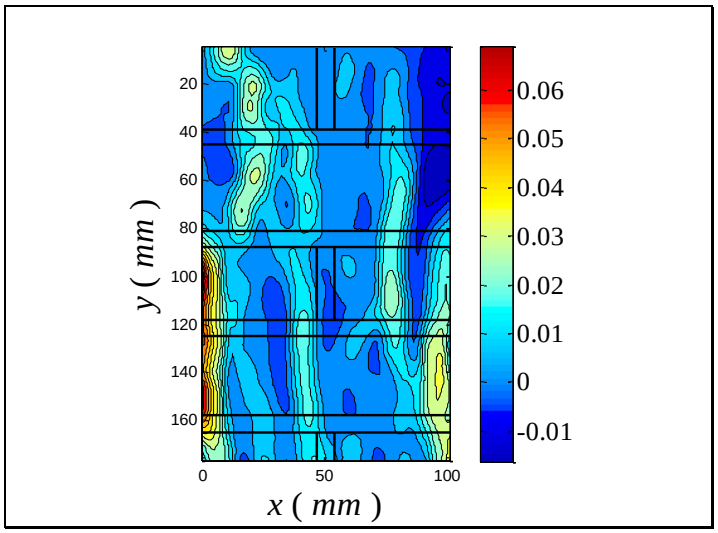

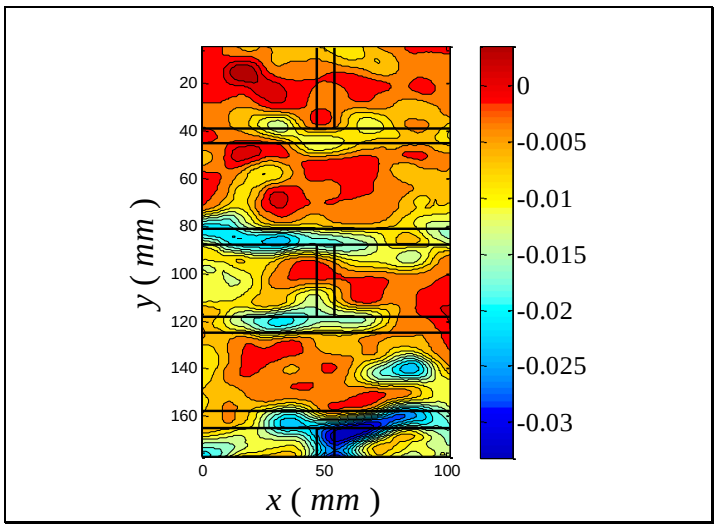

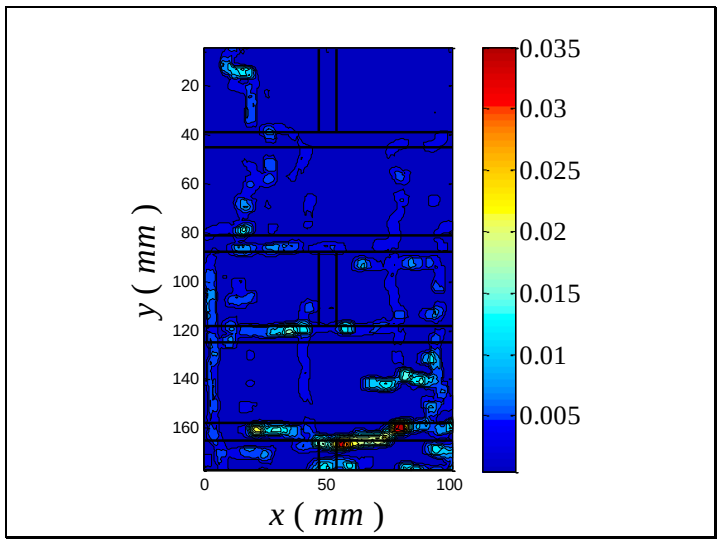

5.1.1.2.Square wall wrapped 2

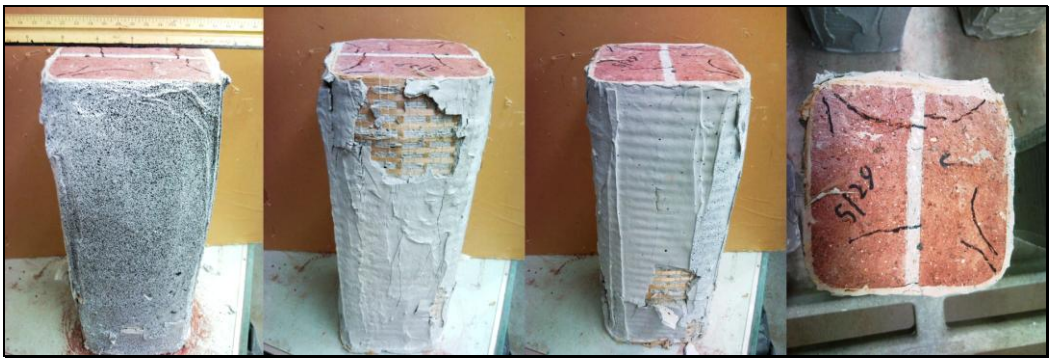

Fig.5.10 – Square wall wrapped 2

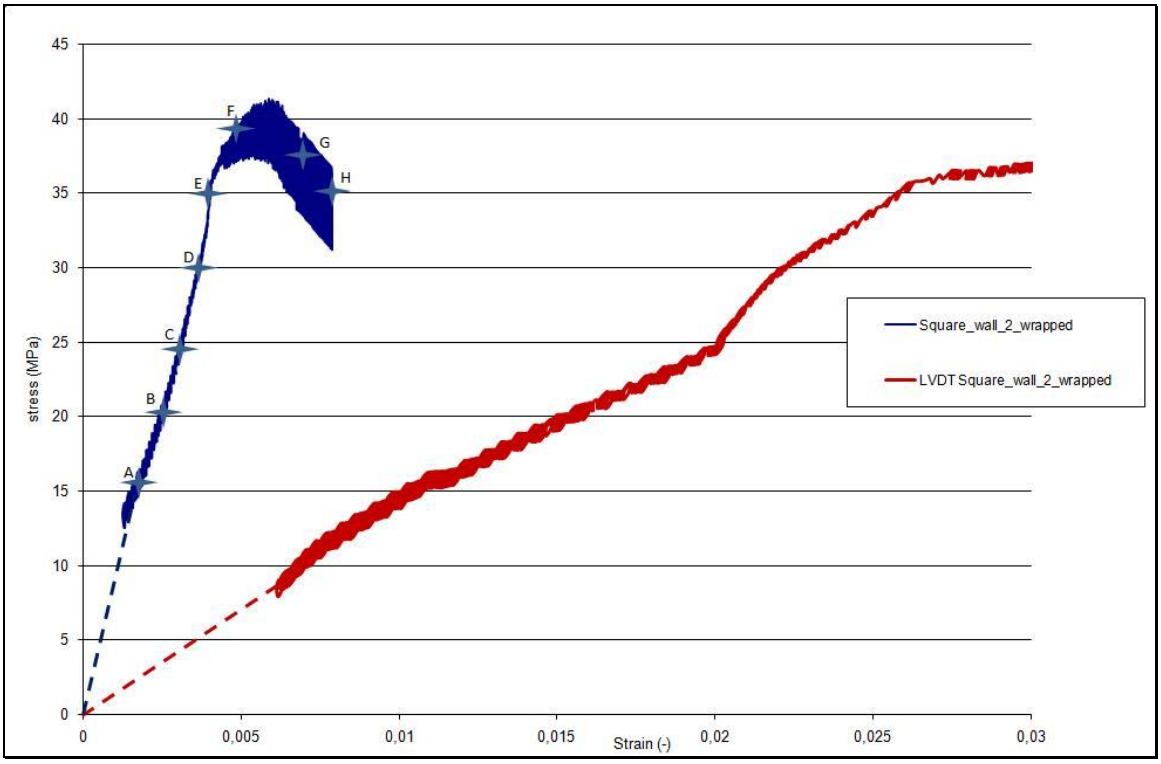

Fig.5.11 – Stress–strain diagram of square wall wrapped 2

The contour plots of ε_{xx} , ε_{yy} and the correlation factor for all the points in figure are reported below.

- A: 36.60 kips; 15,93 MPa

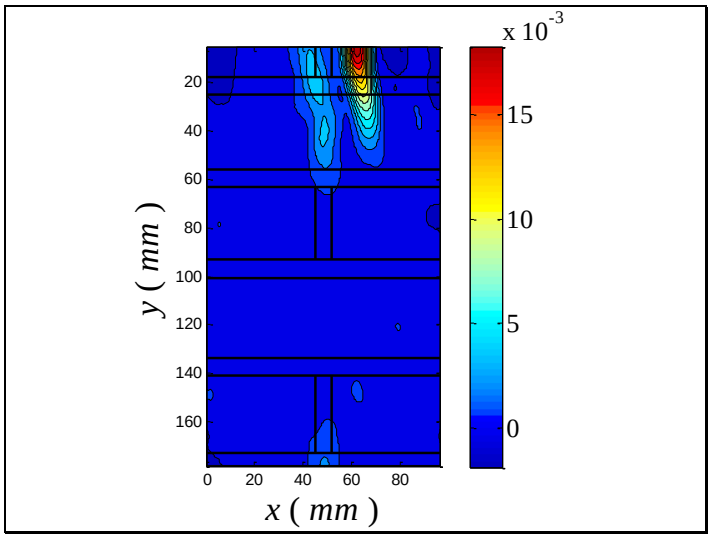

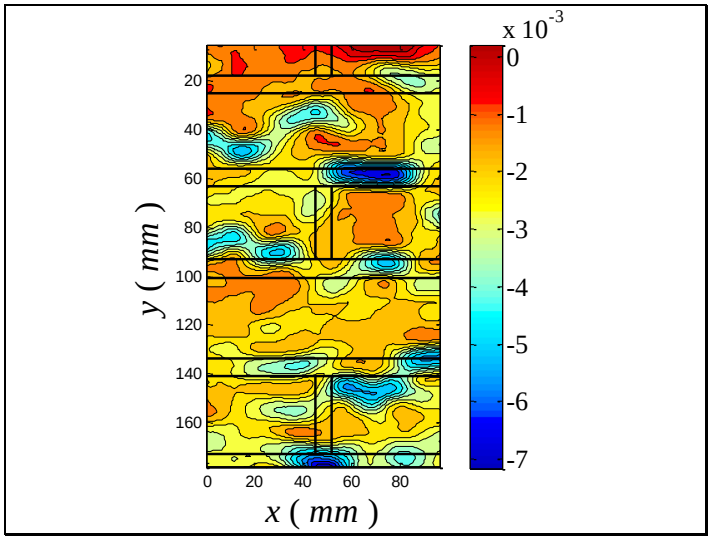

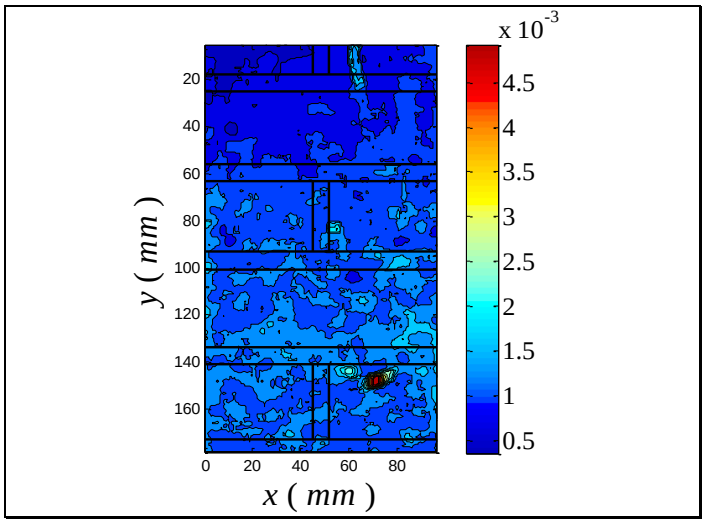

- B: 46.27 kips; 20,14 MPa

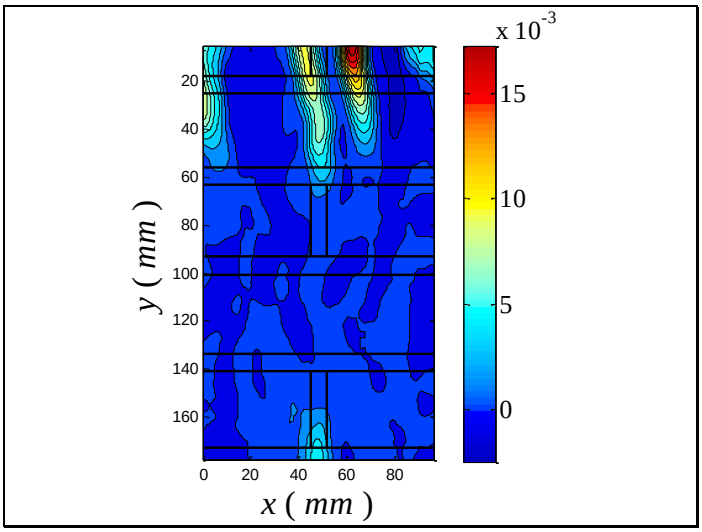

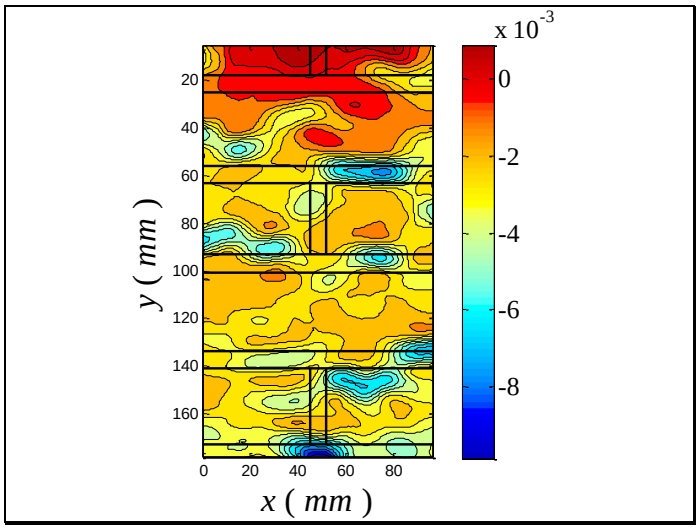

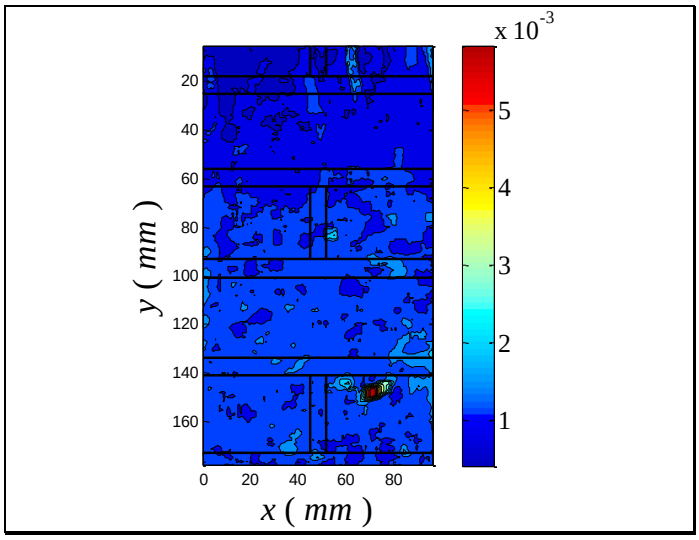

- C: 56.13 kips; 24,43 MPa

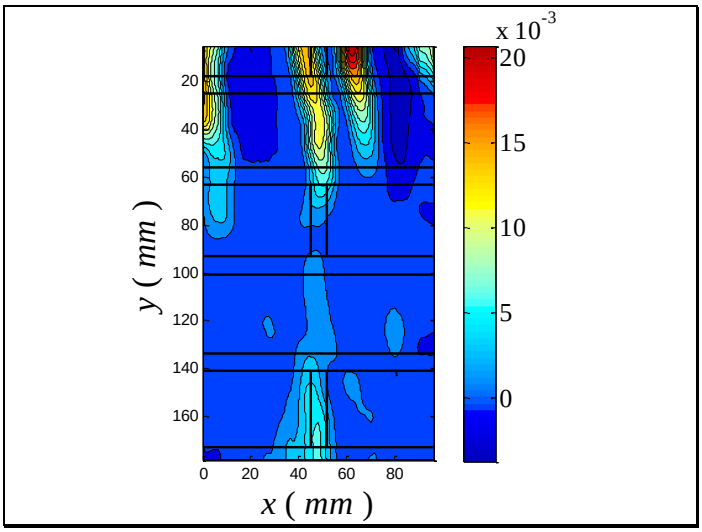

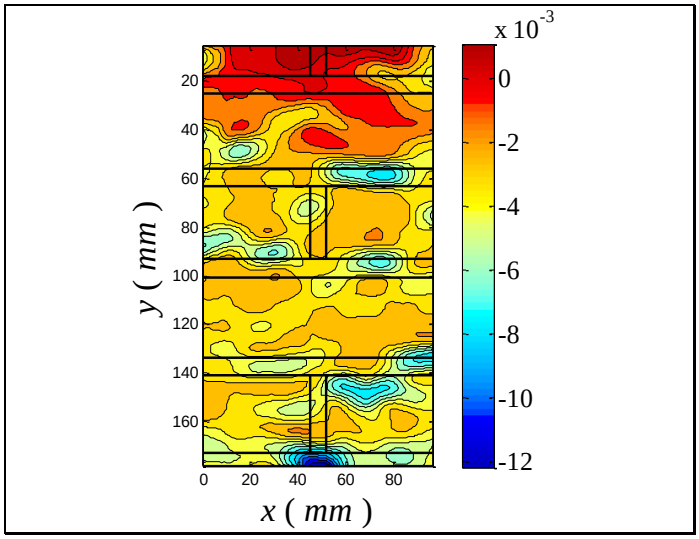

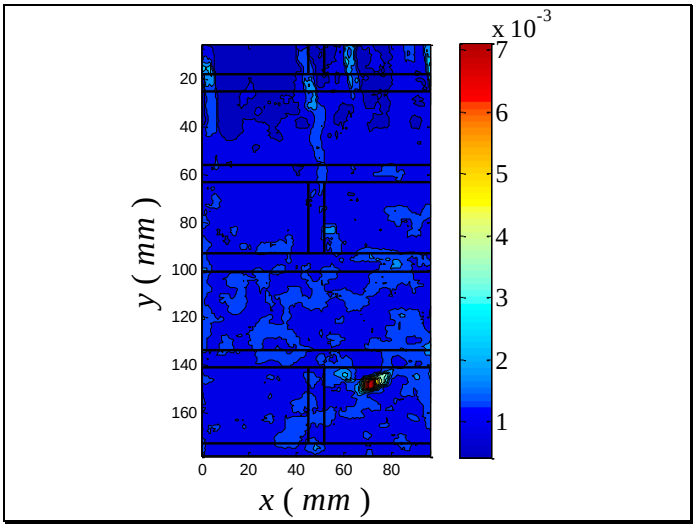

- D: 69.00 kips; 30,03 MPa

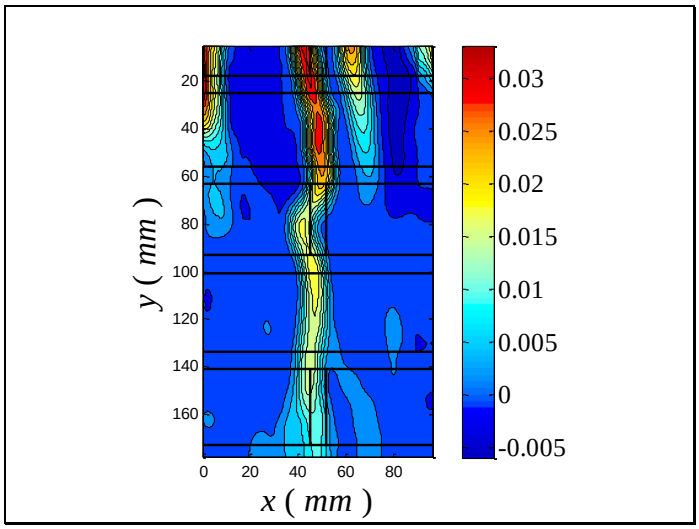

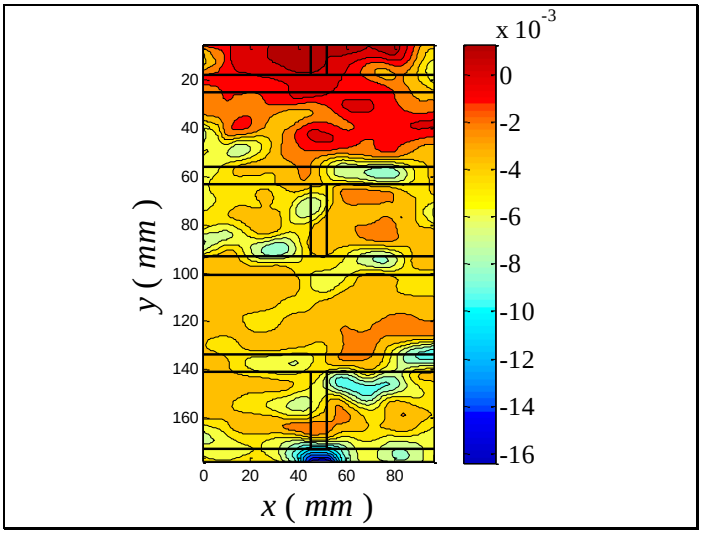

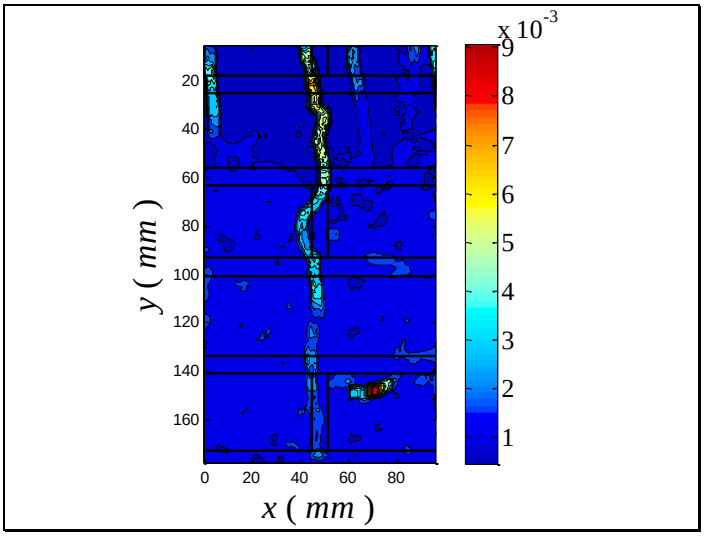

- E: 80.60 kips; 35,08 MPa

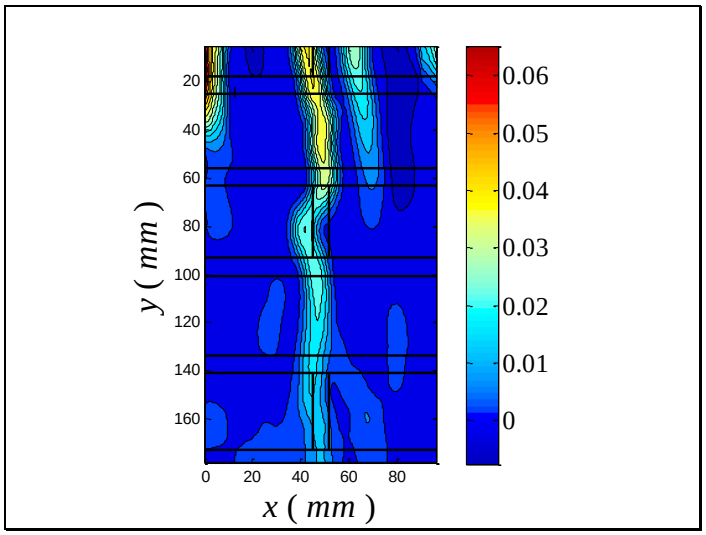

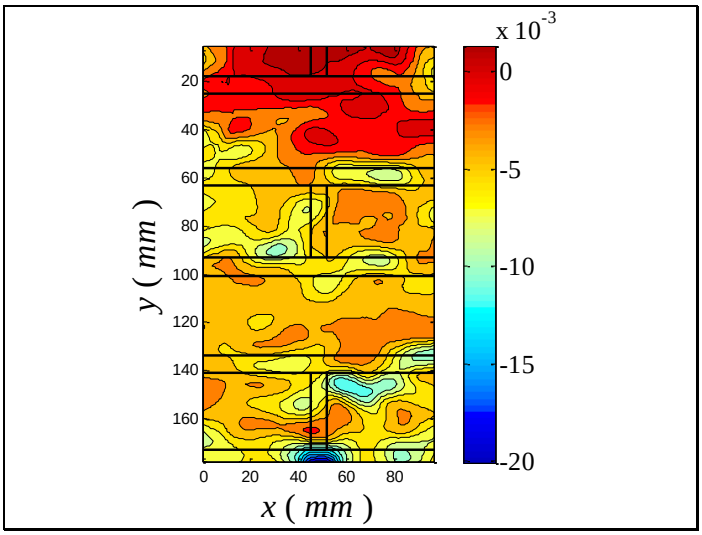

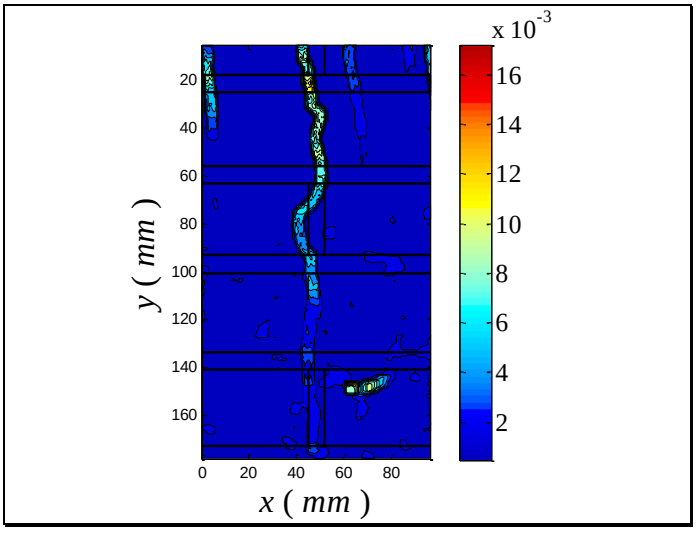

- F: 90.00 kips; 39,17 MPa

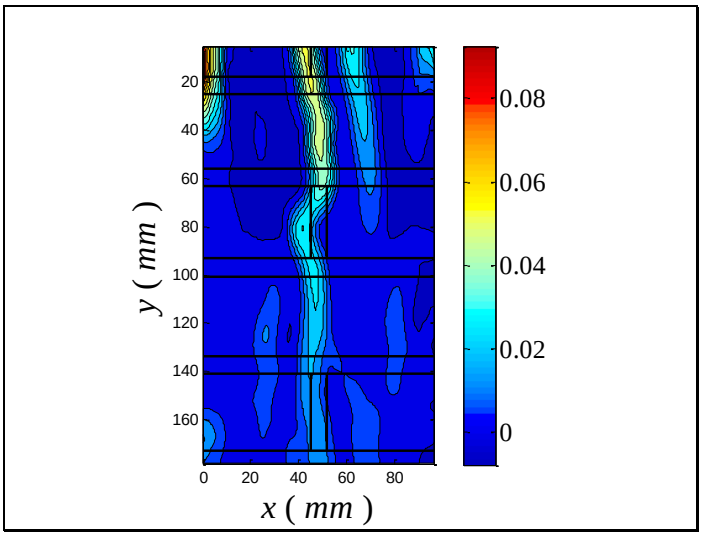

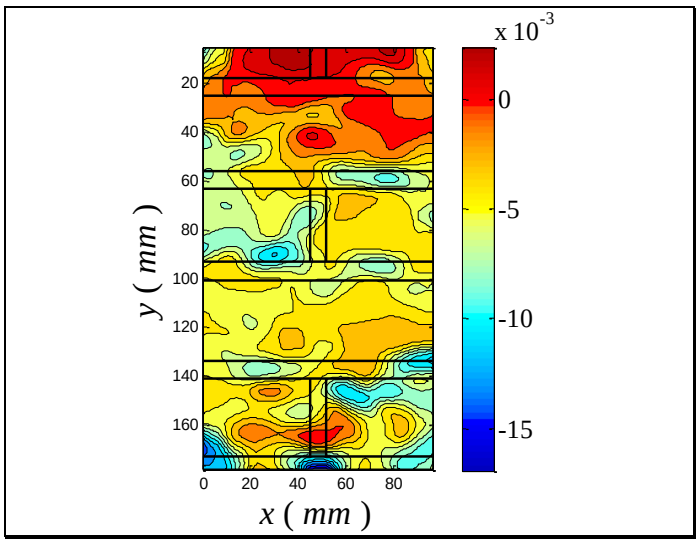

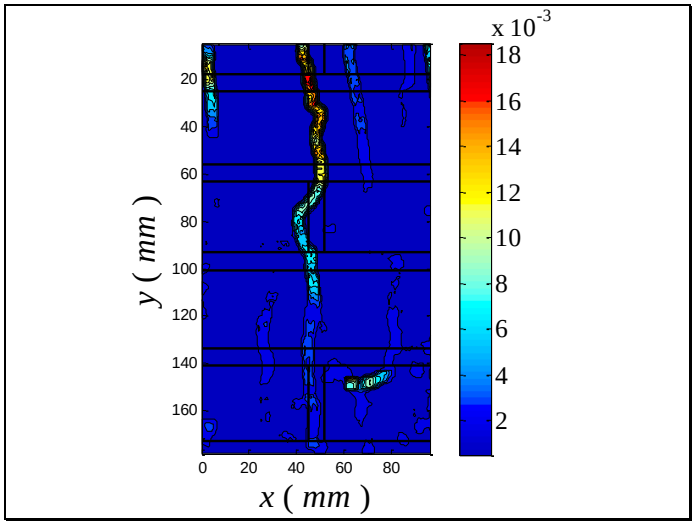

- G: 83.00 kips; 36,13 MPa

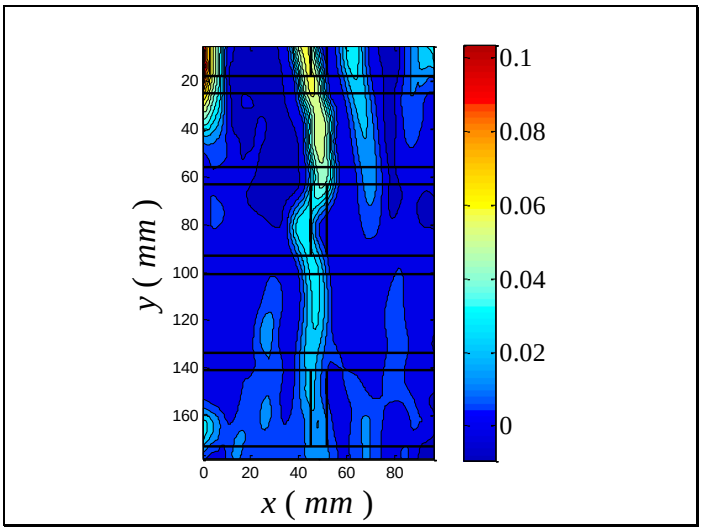

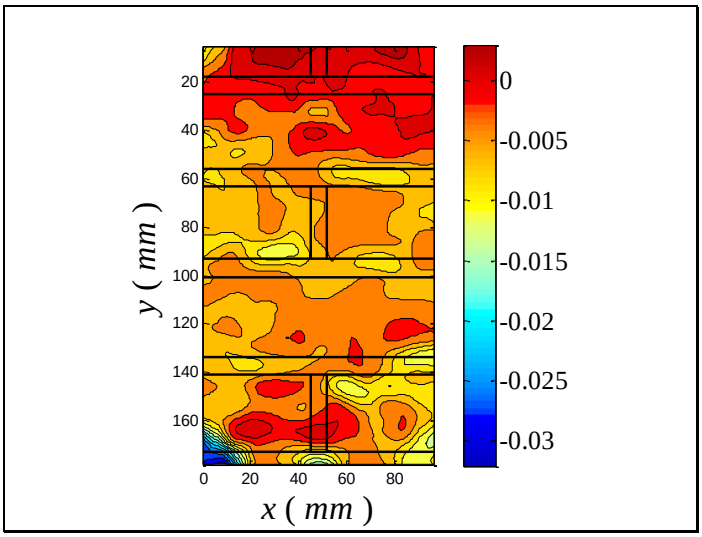

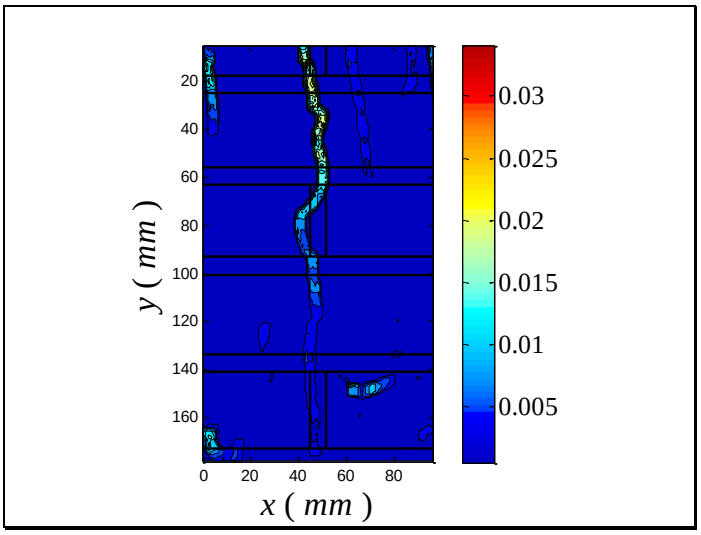

- H: 81.00 kips; 35,26 MPa

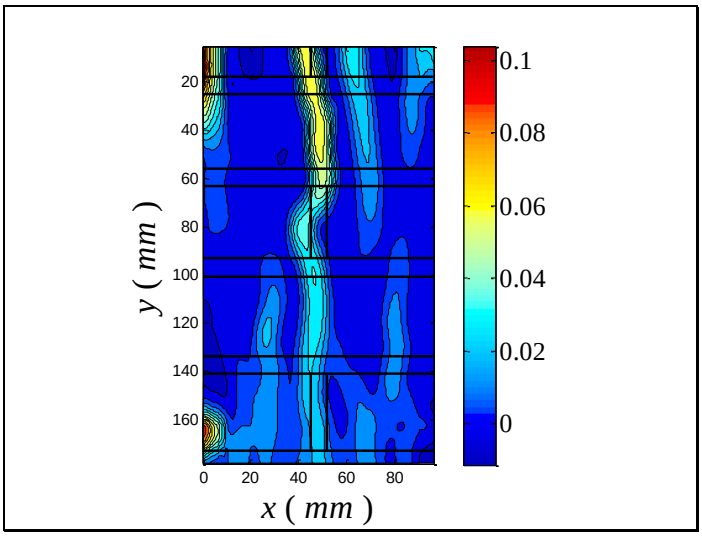

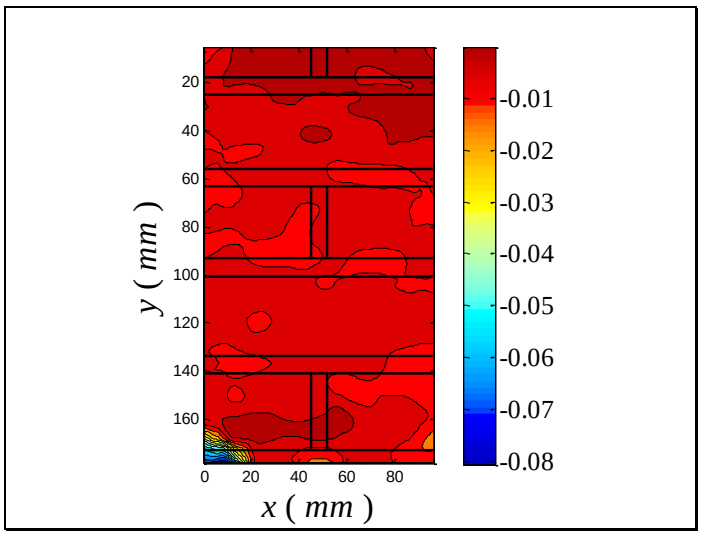

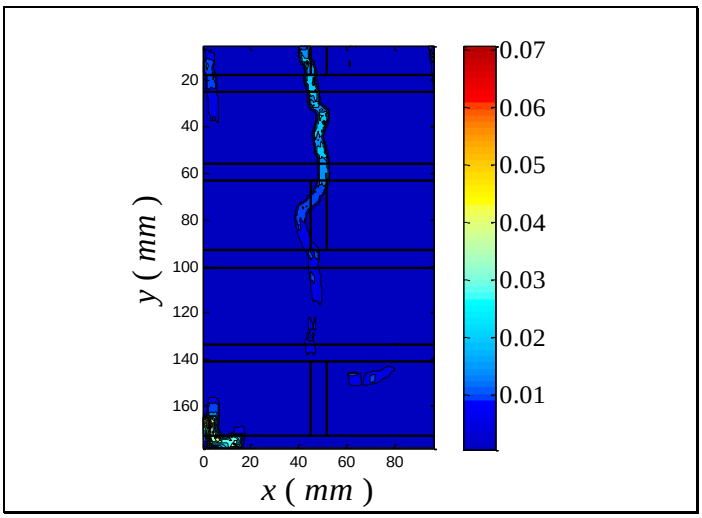

5.1.1.3. Square wall wrapped 3

Fig.5.12 – Square wall wrapped 3

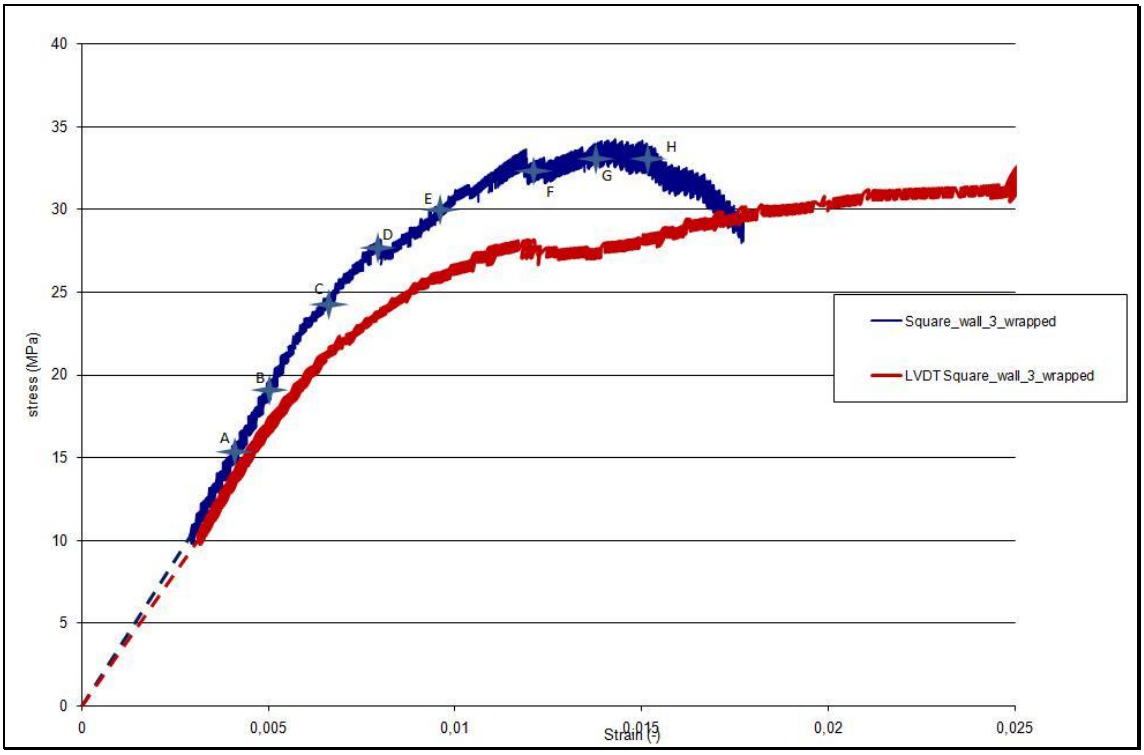

Fig.5.13 – Stress–strain diagram of square wall wrapped 3

The contour plots of ε_{xx} , ε_{yy} and the correlation factor for all the points in figure are reported below.

- A: 35.76 kips; 15,56 MPa

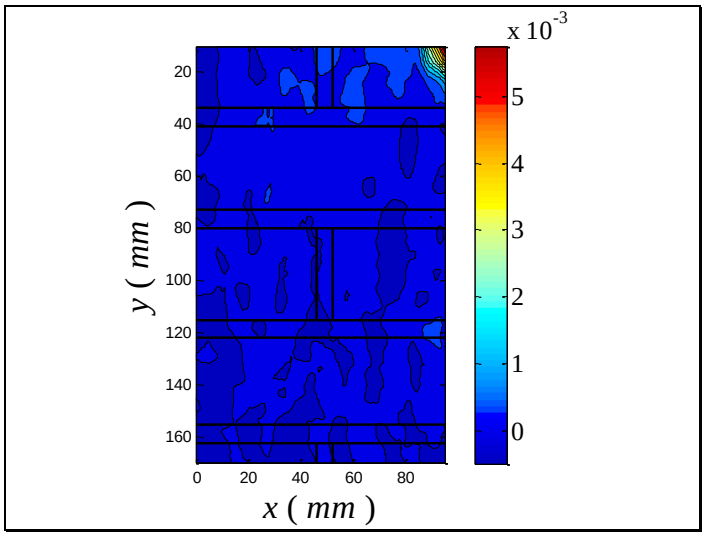

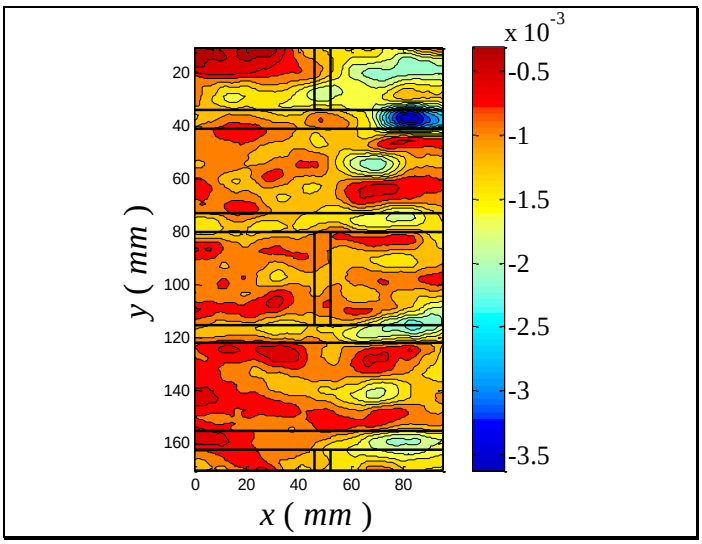

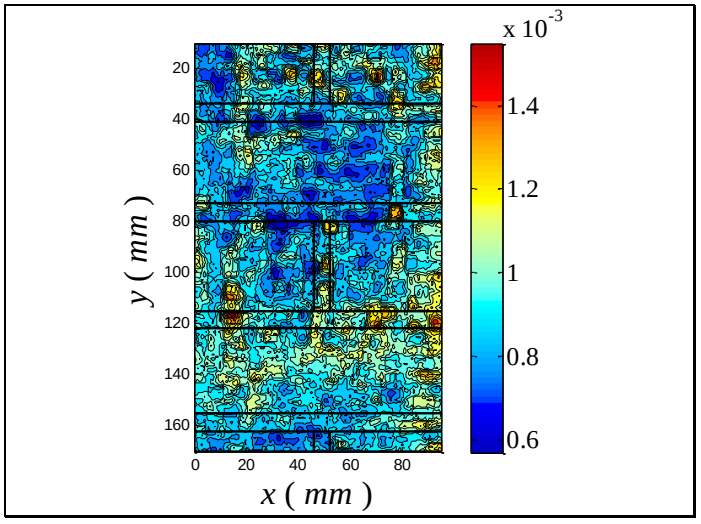

- B: 43.93 kips; 19,12 MPa

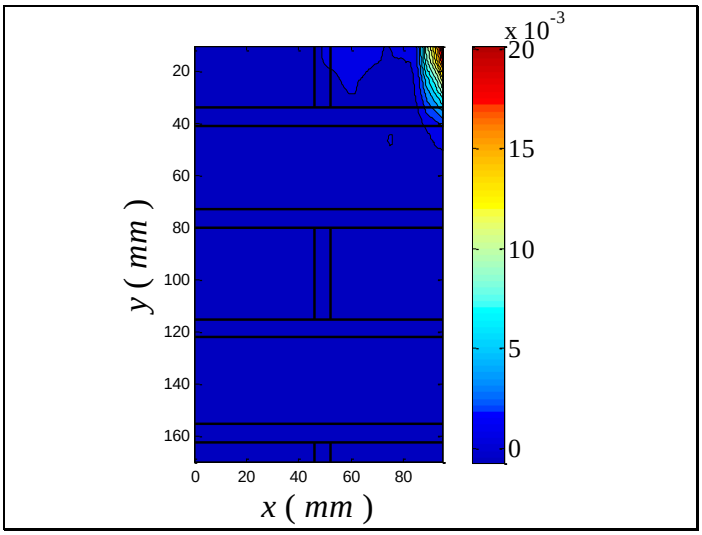

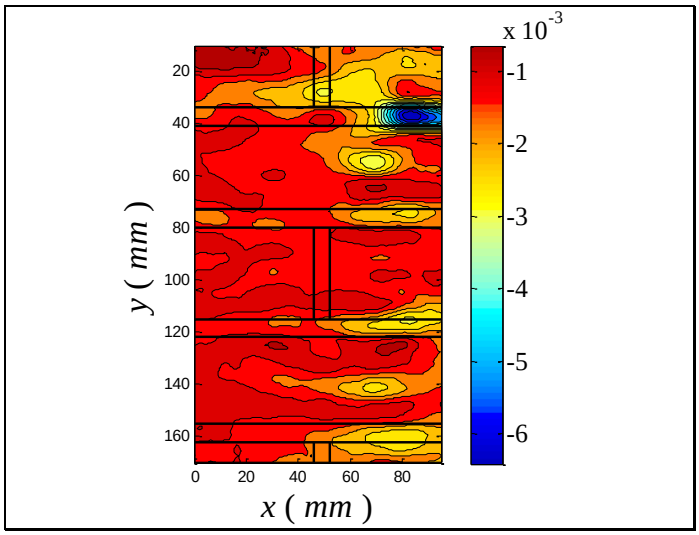

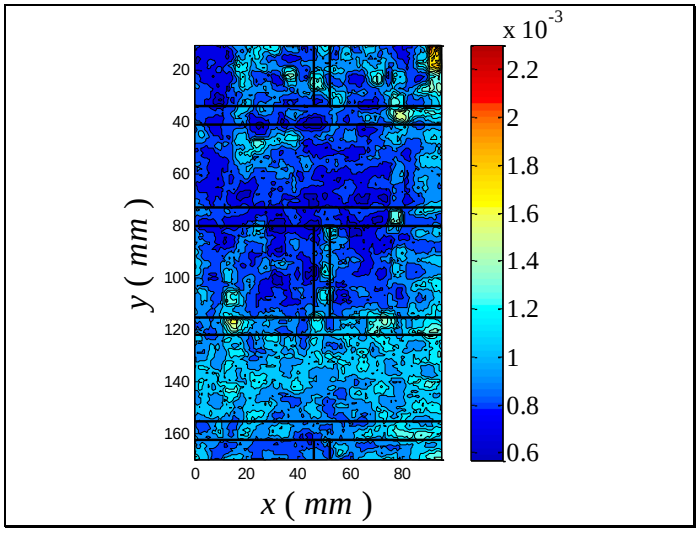

- C: 56.26 kips; 24,49 MPa

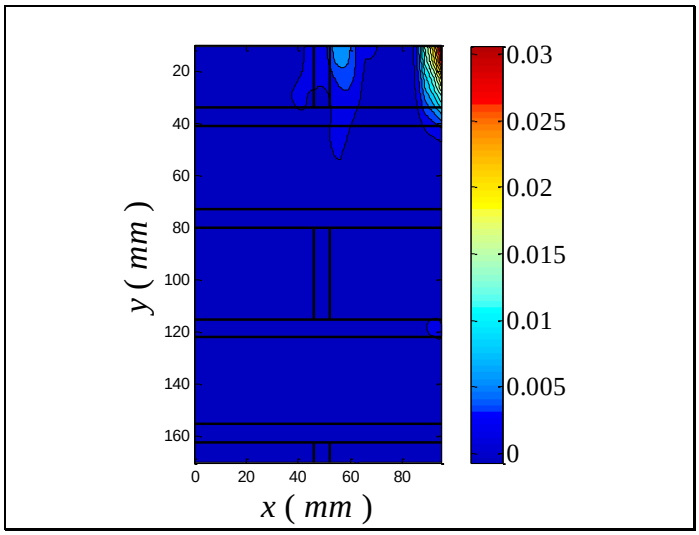

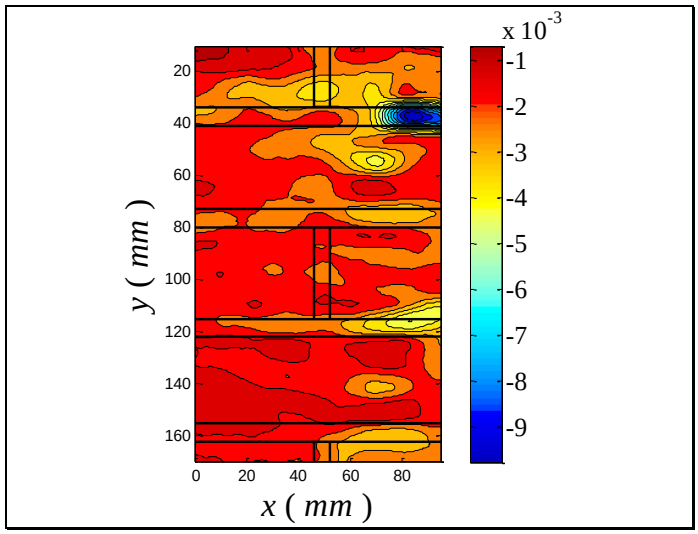

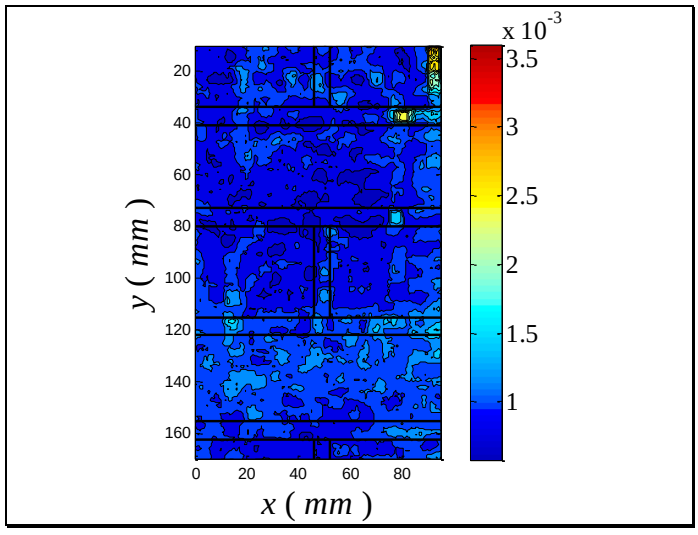

- D: 64.80 kips; 28,20 MPa

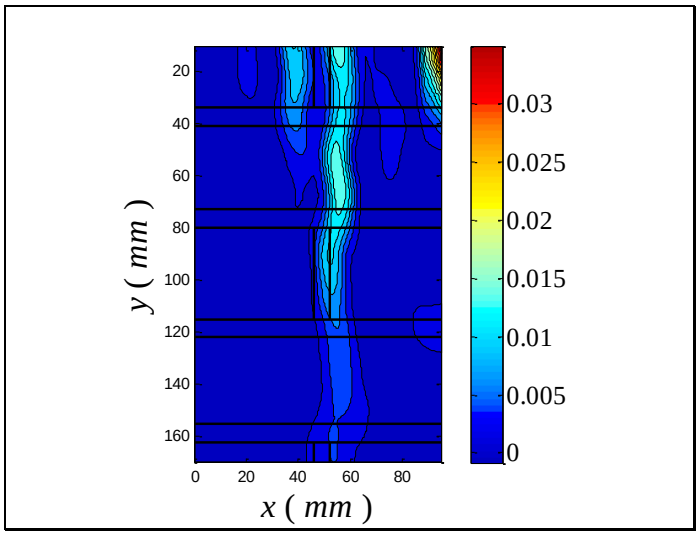

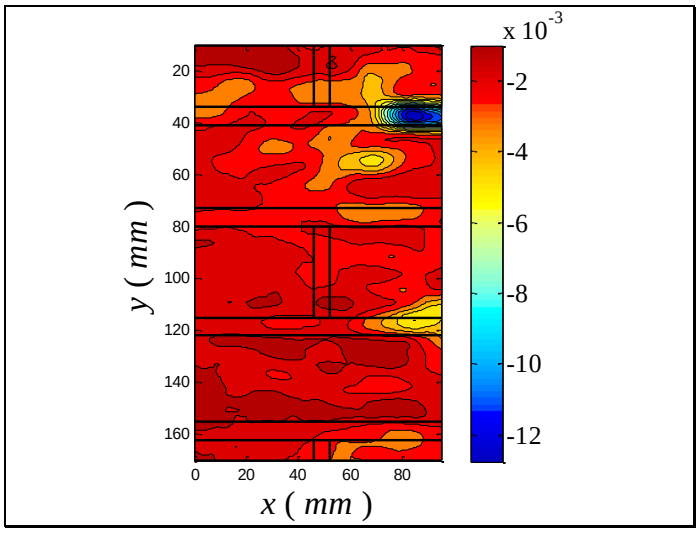

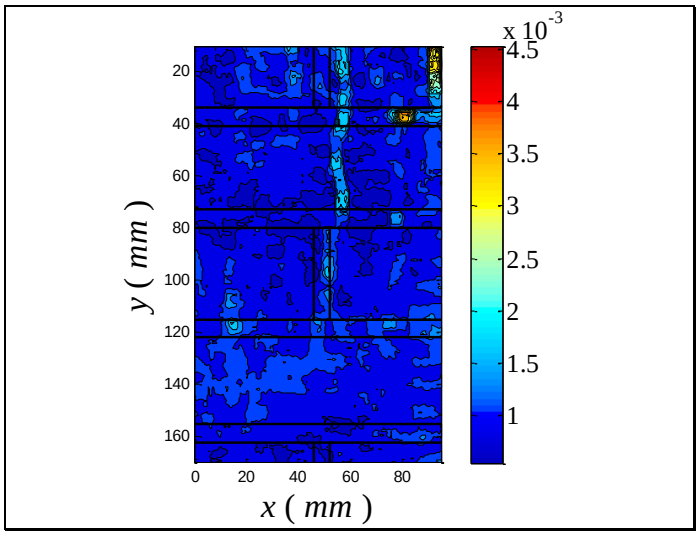

- E: 70.00 kips; 30,47 MPa

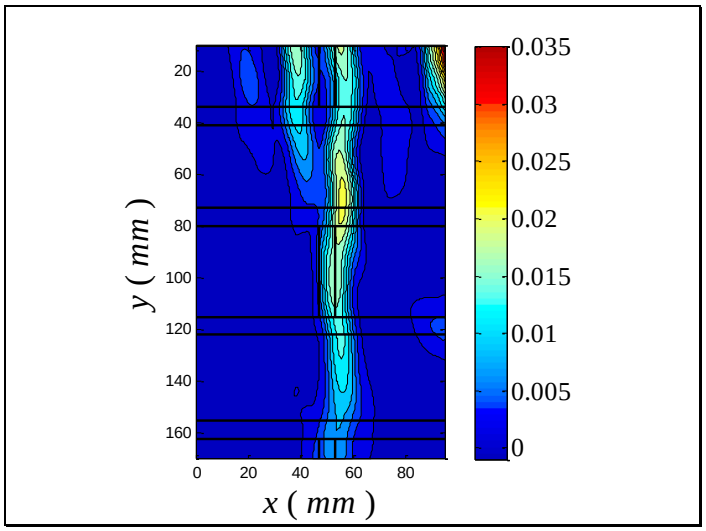

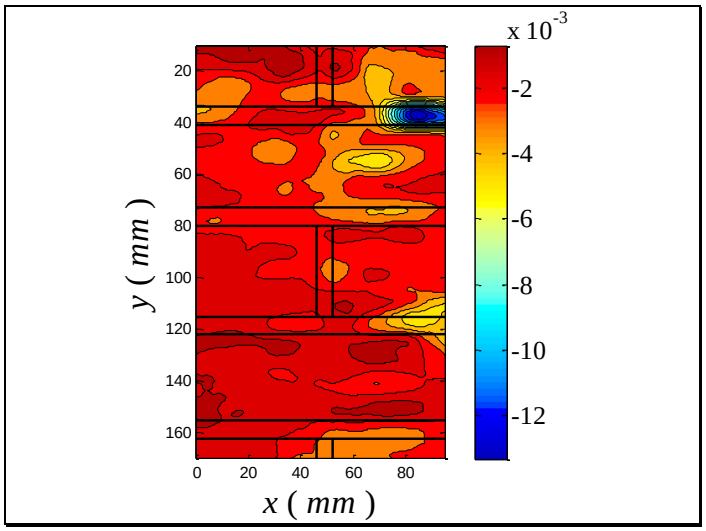

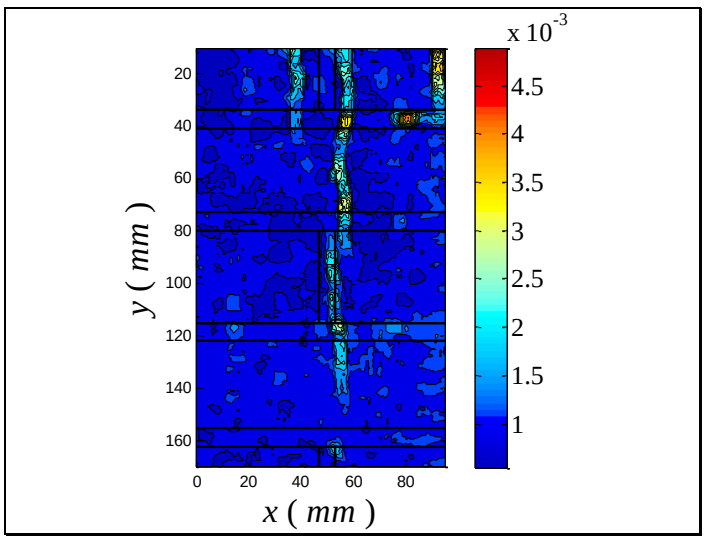

- F: 73.00 kips; 31,77 MPa

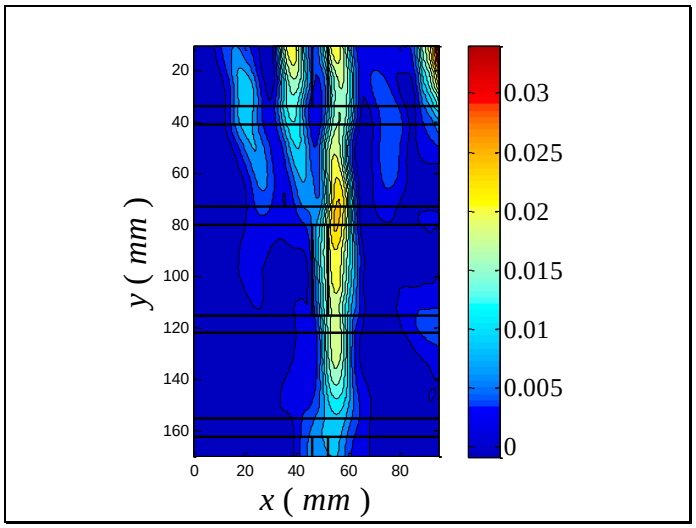

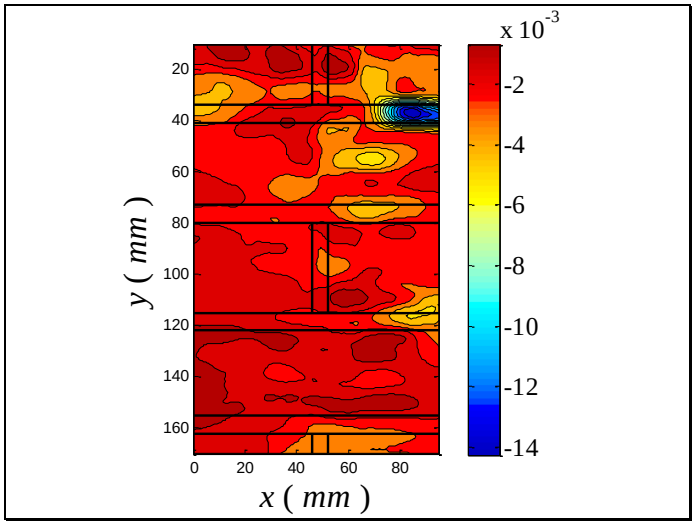

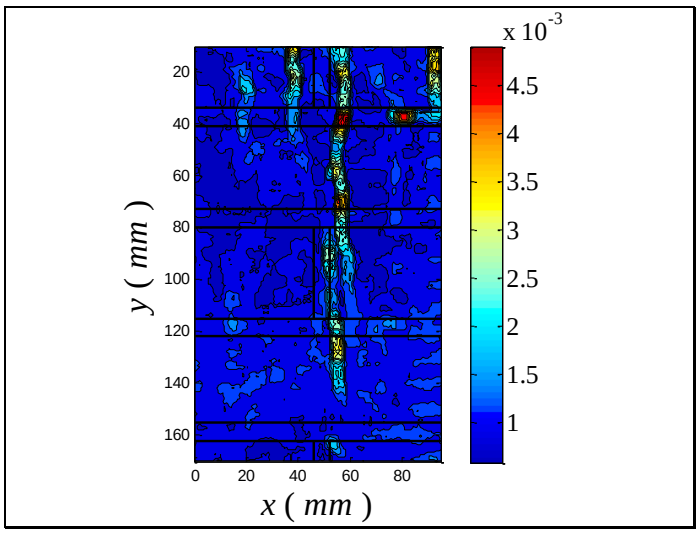

- G: 73.25 kips; 31,88 MPa

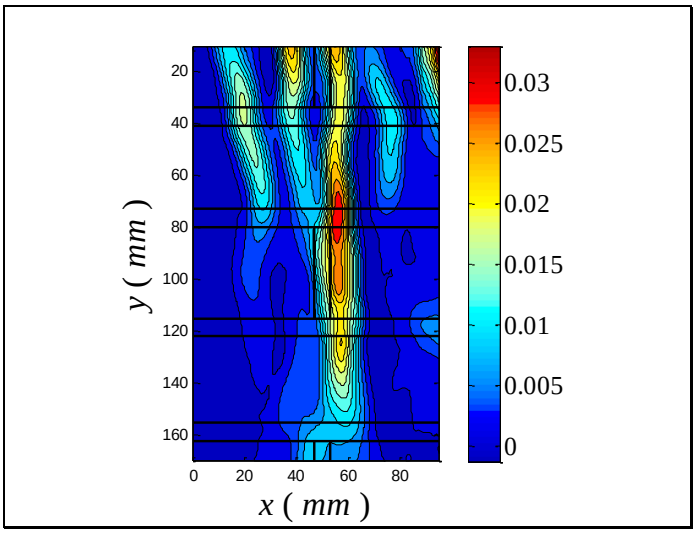

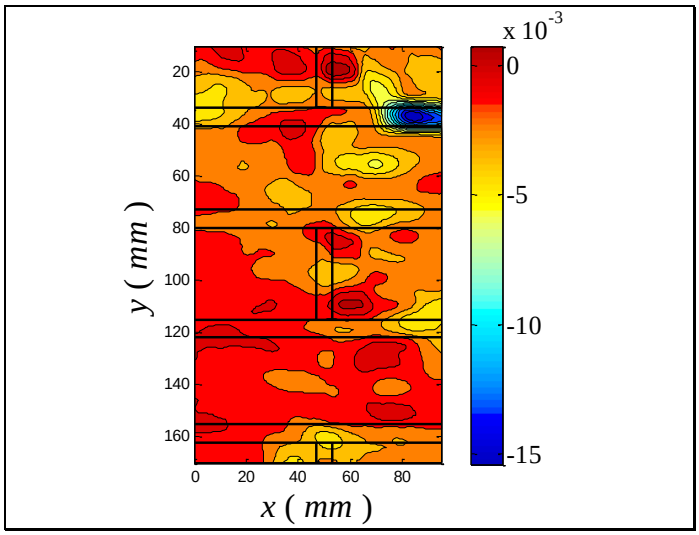

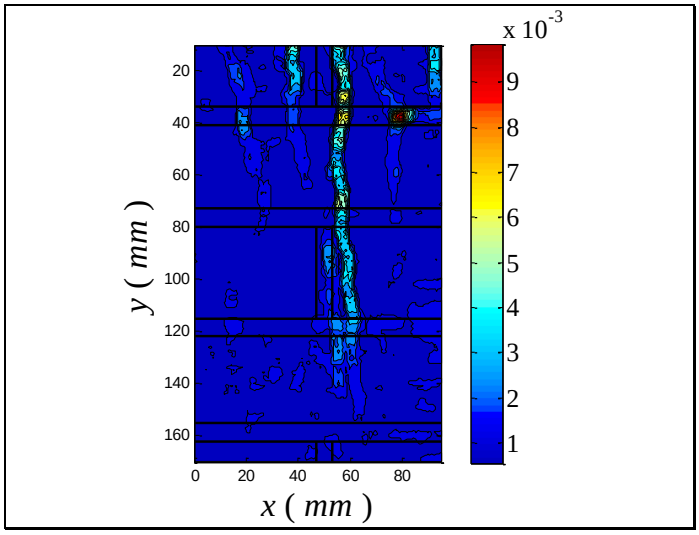

- H: 75.30 kips; 32,77 MPa

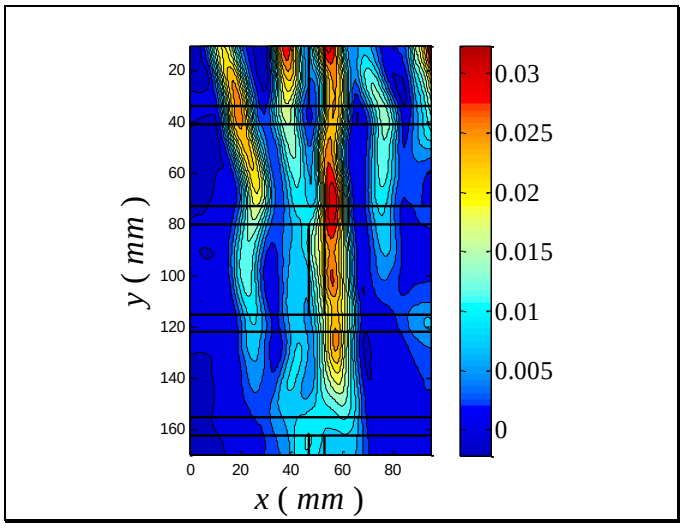

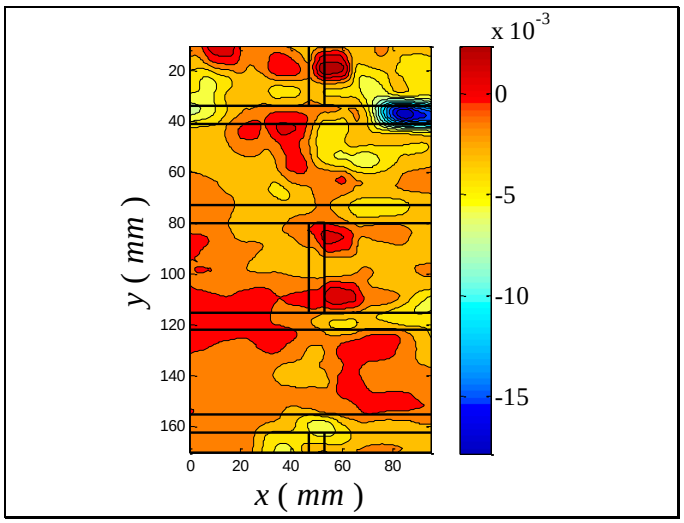

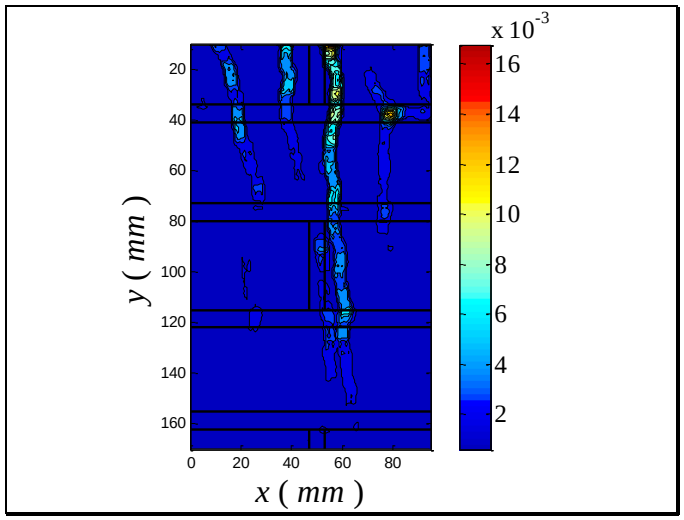

5.1.2. Discussion of result

In general, in the first phase failure of the test specimens appeared to be initiated by crushing and squeezing of the mortar from the mortar joints followed by vertical splitting of the bricks.

Immediately the reinforcement begins to work containing the expansion of the mortar and the bricks and increasing the load-carrying capacity of the masonry.

The next figure shown the developing of the arch effect on the section after cutting in the middle the specimens.

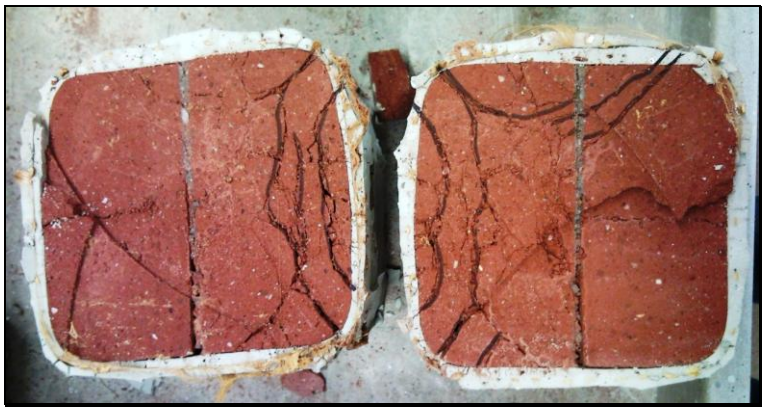

Fig. 5.14 – Section of square wall wrapped 1

Fig. 5.15 – Section of square wall wrapped 2

Fig. 5.16 – Section of square wall wrapped 3

The main conclusions that can be drawn from the tests on laboratory specimens are as follows.

The arch effect is not modified by the presence of vertical joints in this configuration. After the cut in the middle of the specimens it's clear the presence of cracks that follow the development of the arch effect in both the side of the masonry.

The effectively confined area is assumed as the region where the arching action has been fully developed, figure 5.17.

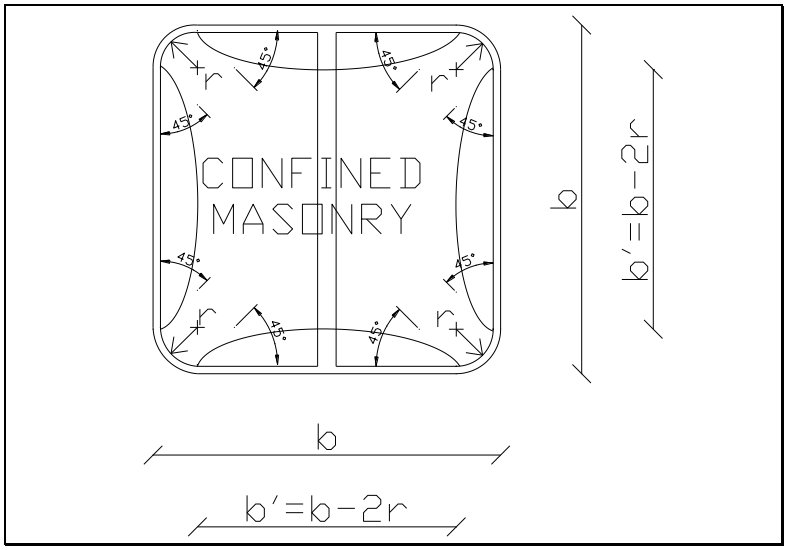

Fig. 5.17 – Effectively confined masonry in square section walls

The critical point continued to be the mortar joints, horizontal and vertical as it is shown in the DIC picture.

The compressive strength of masonry is not really increased with the use of the FRCM in this configuration. Approximately no more than 20% of the unwrapped strength.

The true increase is visible in the strain that is improved more of 50% as it's clear in figure 5.18 and 5.19.

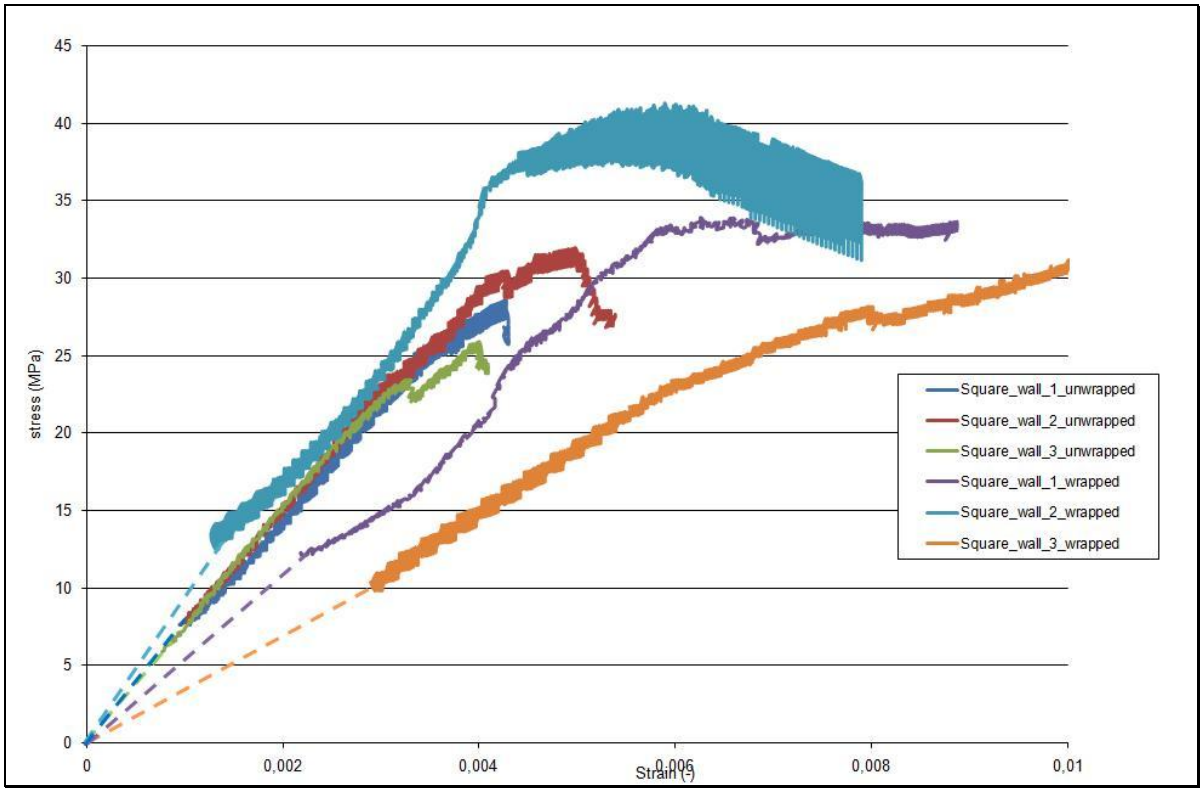

Fig. 5.18 – Stress–strain diagram of square walls wrapped and unwrapped compared

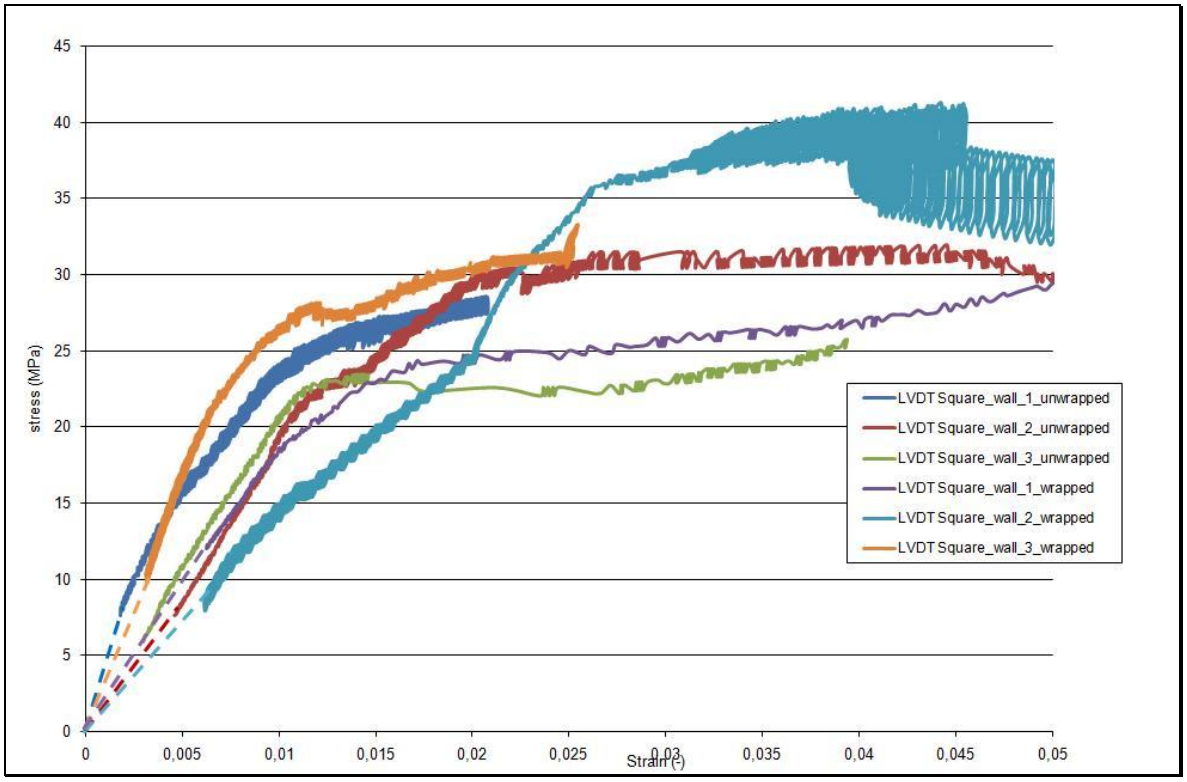

Fig. 5.19 – Stress–LVDTstrain diagram of square walls wrapped and unwrapped compared

5.2. Axial Compression Test Second Configuration

Also for this configuration 14 days before testing all the corner were rounded using a grinding machine at a radius of 10 mm, figure 5.20.

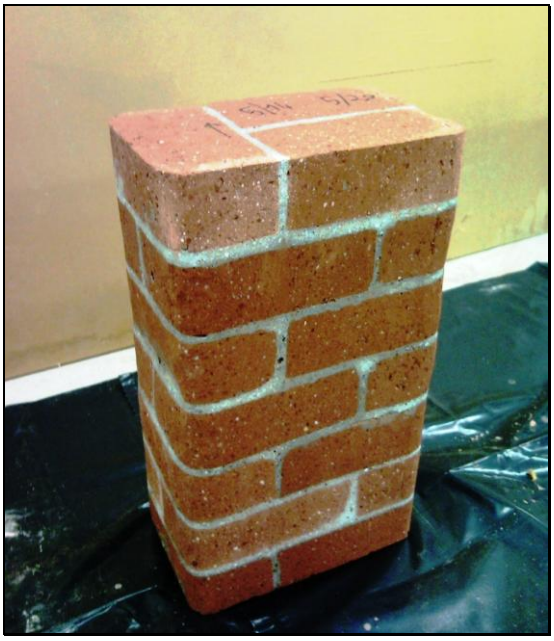

Fig. 5.20 – Second configuration masonry wall with rounded corners

After this operation the specimens were wrapped with one layer of Fiber Reinforced Cementitious Matrix (FRCM).

Initially we putted on a layer of stabilized inorganic matrix and after the kevlar mesh, figure 5.21.

Fig. 5.21 – Second configuration masonry wall wrapping

At the end we covered with the same cementitious inorganic matrix the fibers, with the finishing end of the mesh overlapping the starting end by approximately 100 mm.

Fig. 5.22 – Second configuration masonry wall after the complete wrapping

The smooth surface on the opposite side of the overlapping need to be prepared for the DIC with the usual layer of white and light drops black paint, figure 5.23.

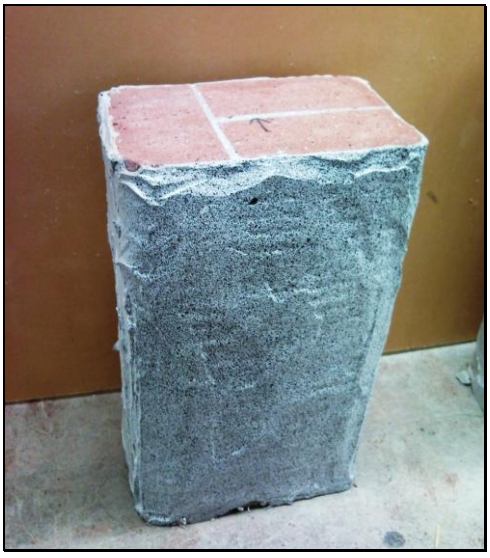

Fig. 5.23 – Second configuration masonry wall ready for the DIC

Displacements of the central section on each specimen were measured using also a Linear Variable Differential Transformer (LVDT) on the left side of the columns attached to the wrapping surface, as it's show in the pictures of the specimens.

5.2.1. Experimental result and failure mode

The main results of the tests are presented in the table 5.2.

Specimens notation	3 precycle (kN)	Maximum load (kN)	Area (cm^2)	Compressive strenght (MPa)	Ultimate machine strain ε
1	45-110	591,46	149,14	38,52	0,0148
2	65-135	576,17	149,14	37,52	0,0144
3	65-135	585,29	149,14	38,12	0,0077
Displacement control mode of 0.008 inch/min, about 0.2 mm/min					

Tab. 5.2 – Summary of test results for rectangular1 walls wrapped

The stress-strain diagrams for the first configuration wrapped specimens are presented in figure 5.24.

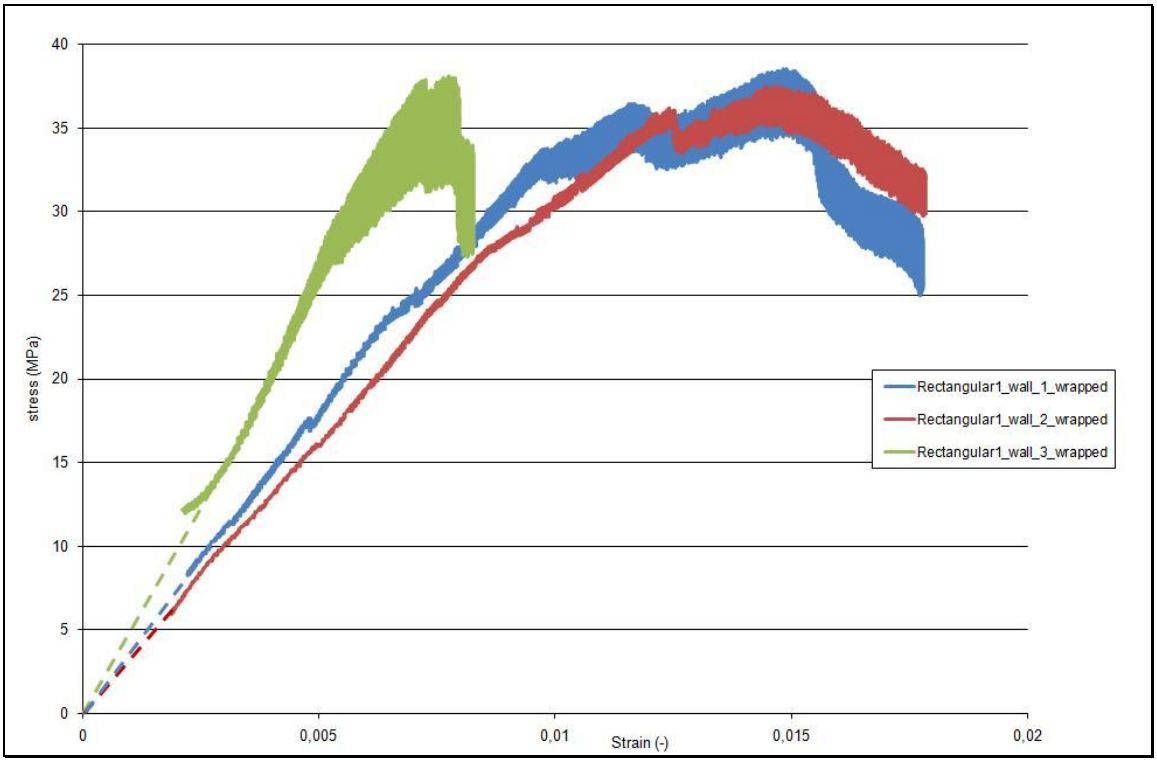

Fig. 5.24 – Stress–strain diagram of rectangular1 walls wrapped

It can be observed that in all cases the diagrams are linear up to about 80% of the maximum load.

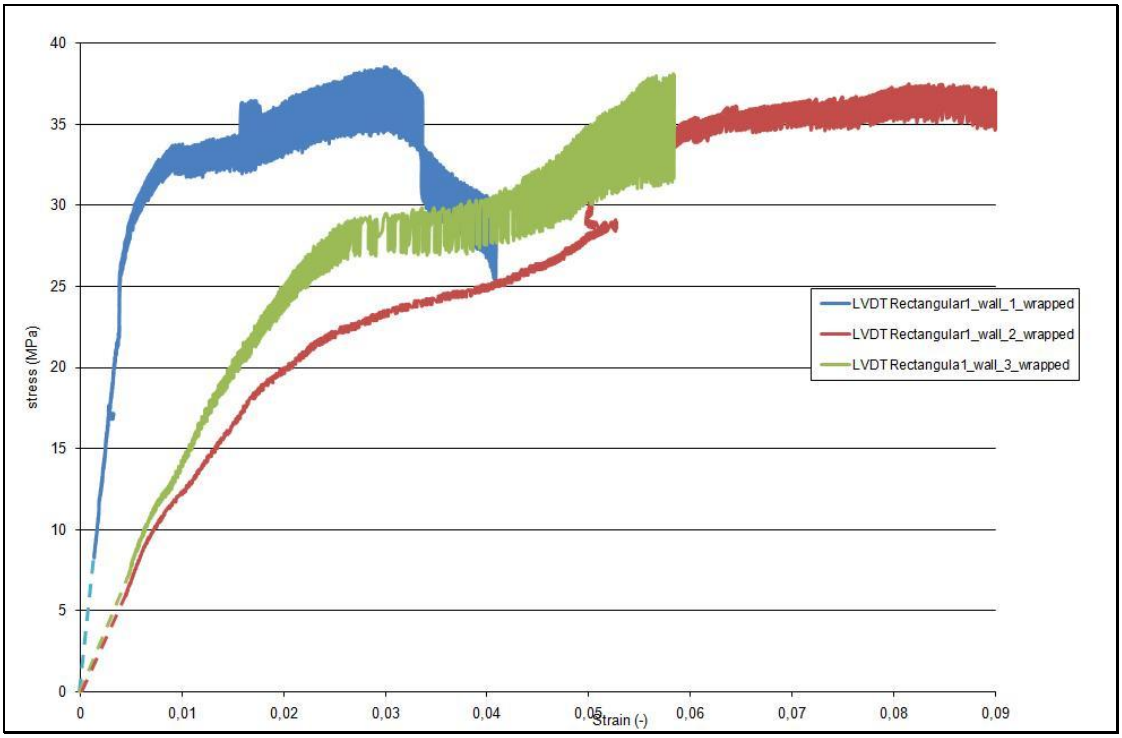

Fig. 5.25 – Stress–LVDTstrain diagram of rectangular1 walls wrapped

The DIC pictures show that almost all the tests failed by the formation of vertical cracks through the joints and the bricks along the side with 4 mortar joints.

After the crack of the vertical joints the pressure of brick and in particular of the joints start and the reinforcement begins to work increasing the ductility of the specimens.

The interaction of the vertical and horizontal joints is clear on the ε_{yy} pictures for this configuration.

Finally, vertical cracks became increasingly wide, up to unthread the reinforcement on the overlap in the back of the specimens, as in the other configuration.

5.2.1.1. Rectangular1 wall wrapped 1

Fig.5.26 – Rectangular1 wall wrapped 1

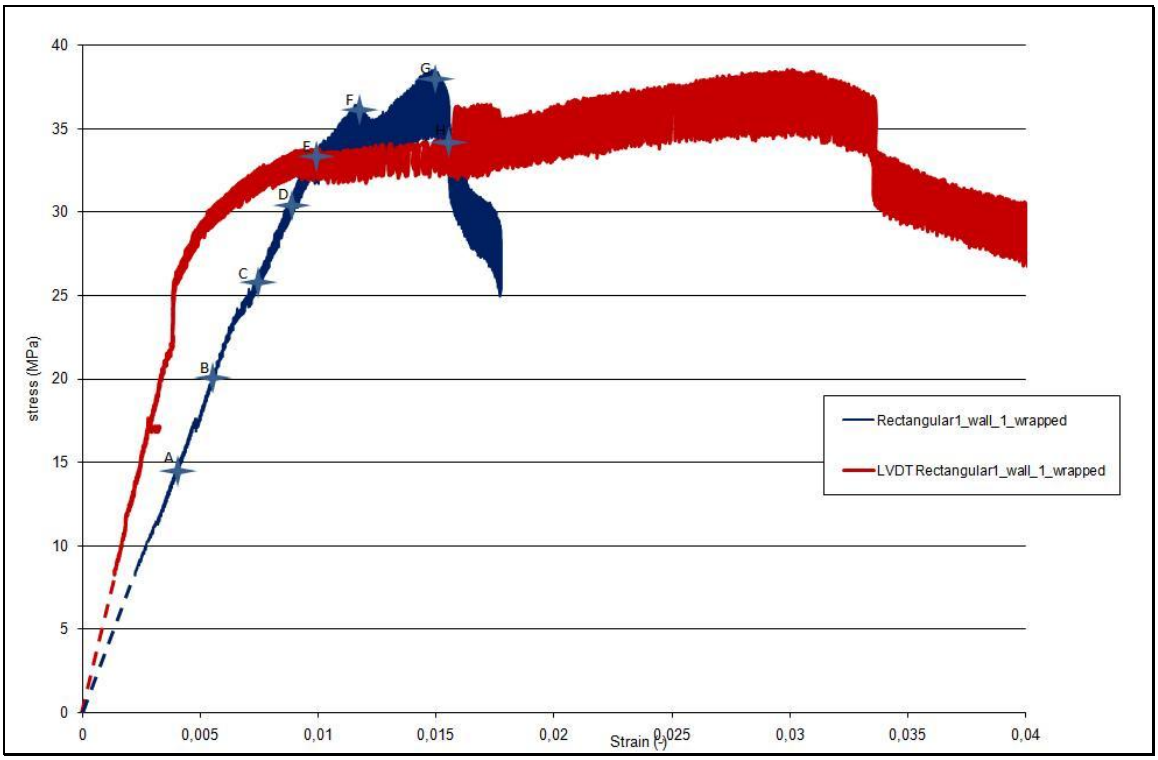

Fig.5.27 – Stress–strain diagram of rectangular1 wall wrapped 1

The contour plots of ε_{xx} , ε_{yy} and the correlation factor for all the points in figure are reported below.

- A: 50.00 kips; 14,48 MPa

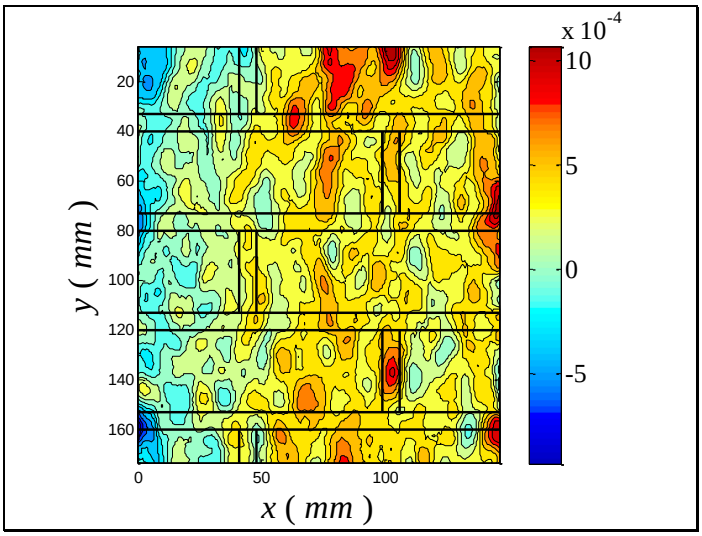

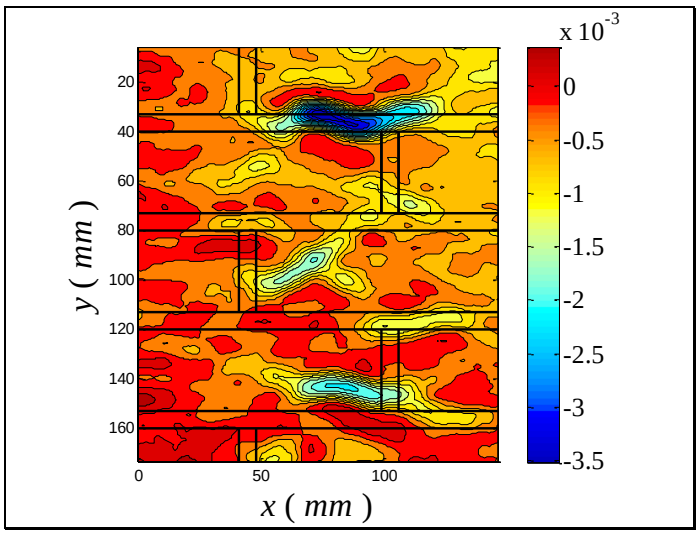

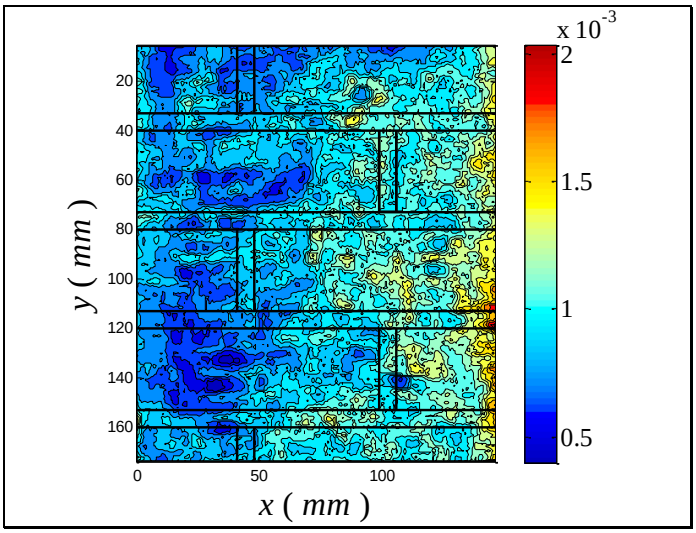

- B: 69.99 kips; 20,27 MPa

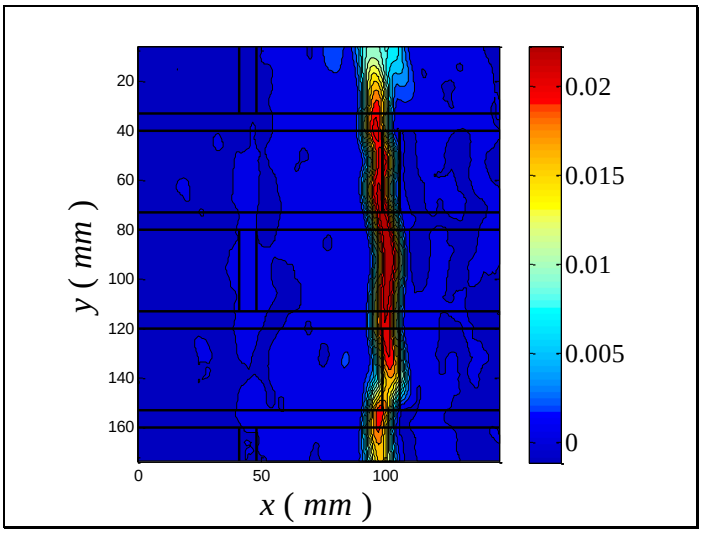

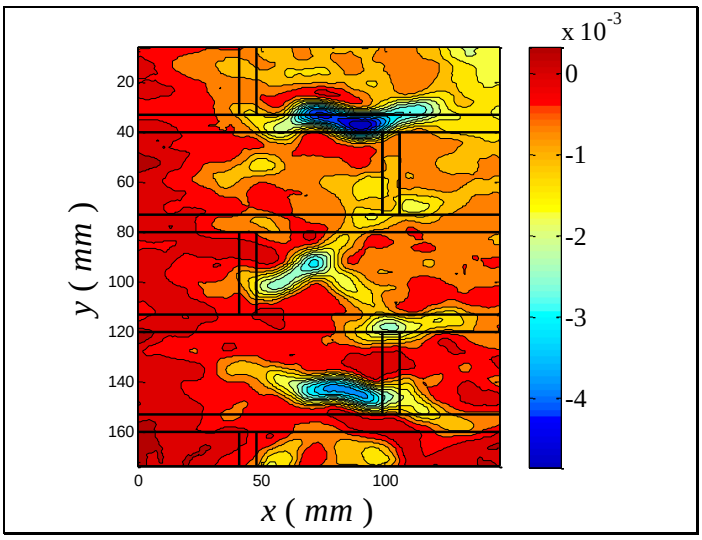

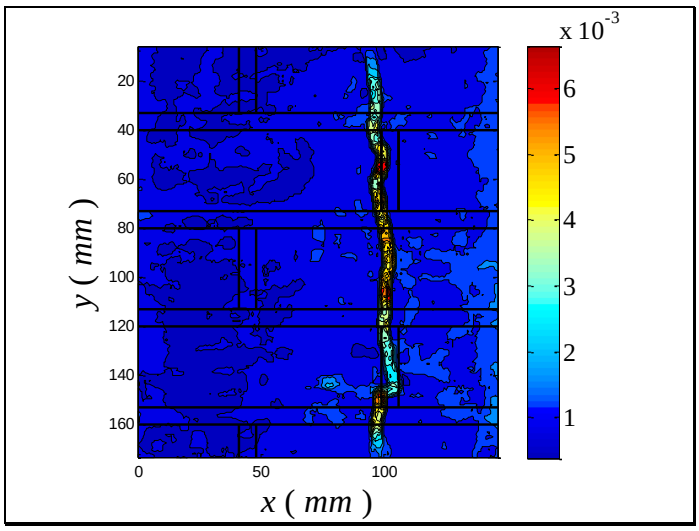

- C: 90.03 kips; 26,08 MPa

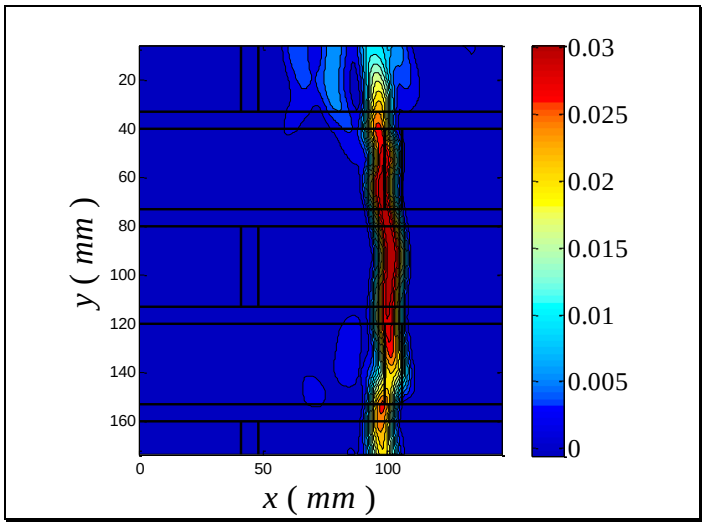

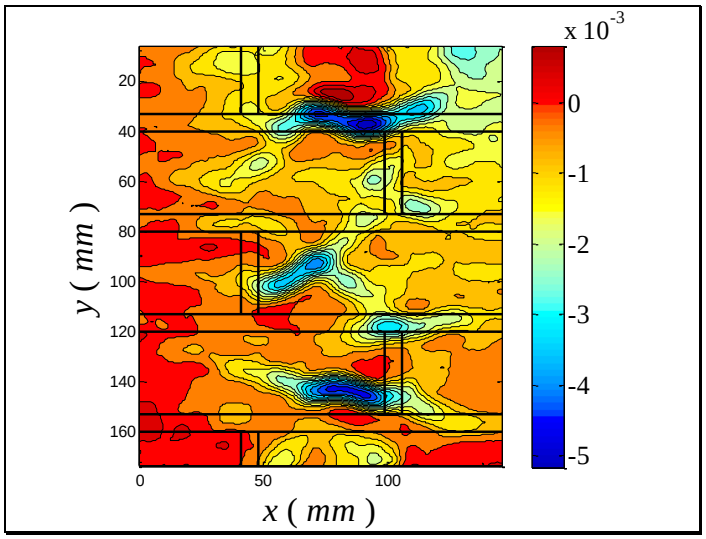

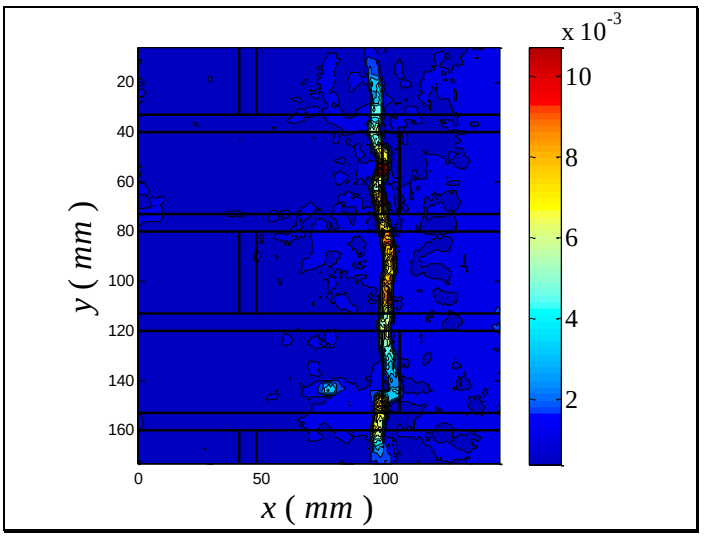

- D: 106.70 kips; 30,91 MPa

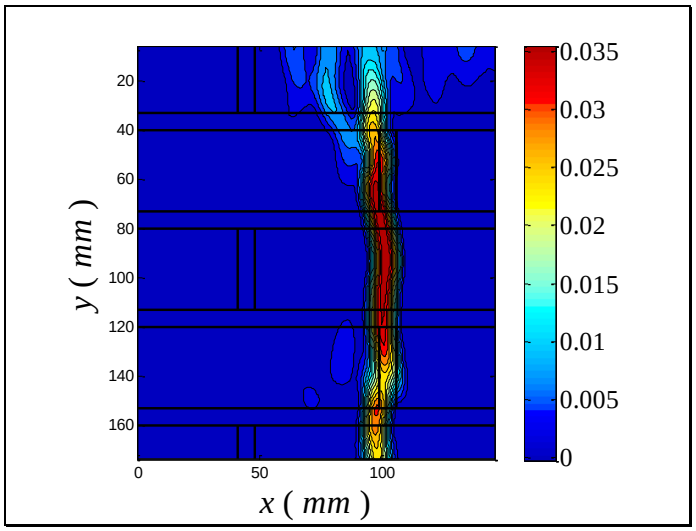

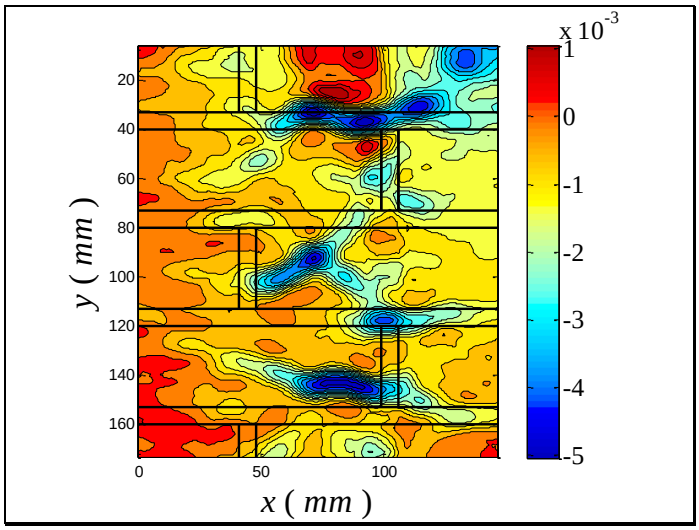

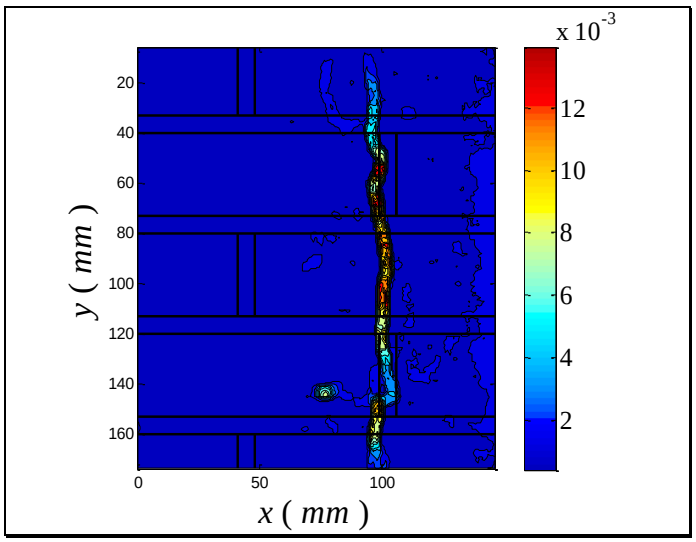

- E: 114.00 kips; 33,02 MPa

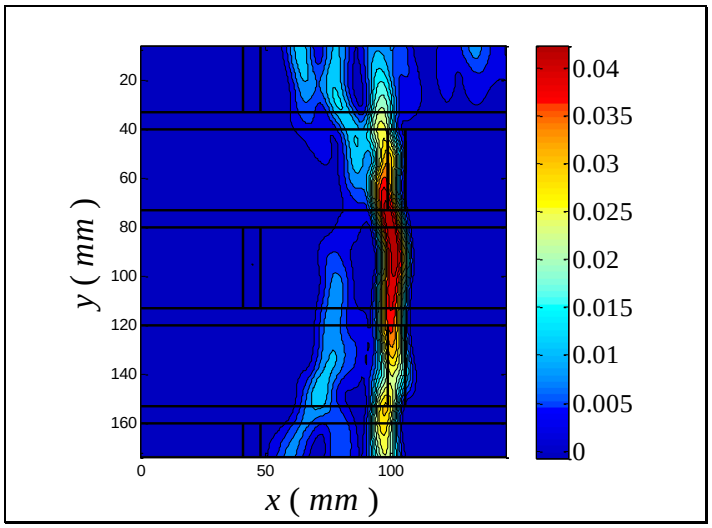

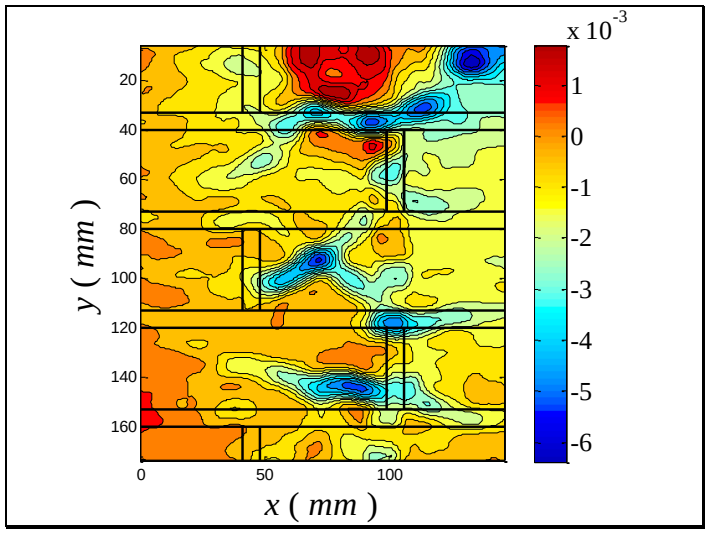

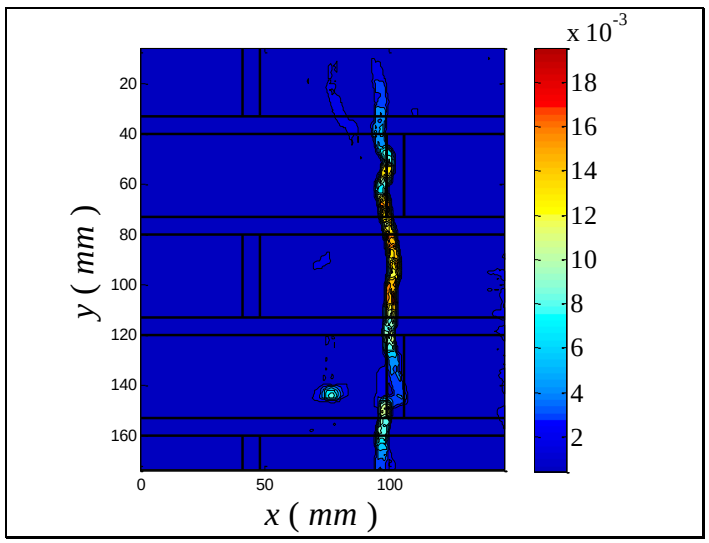

- F: 123.10 kips; 35,66 MPa

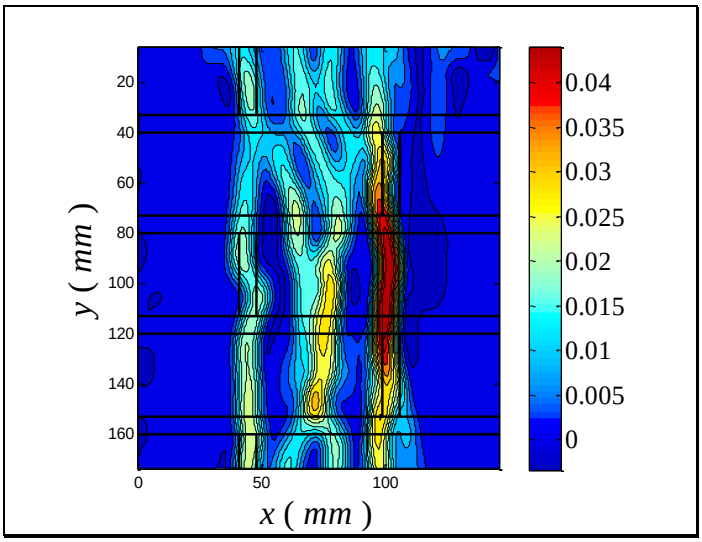

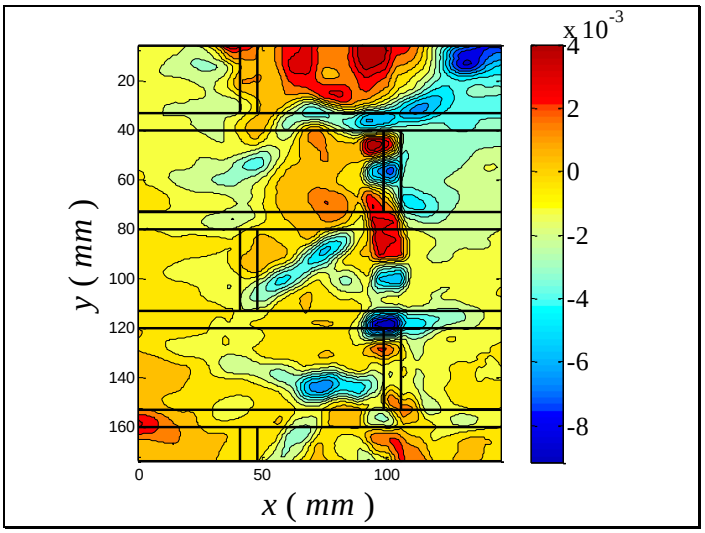

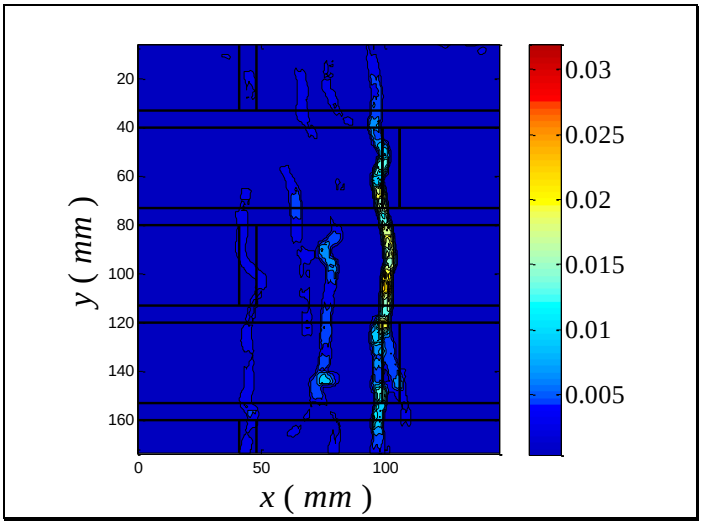

- G: 128.00 kips; 37,08 MPa

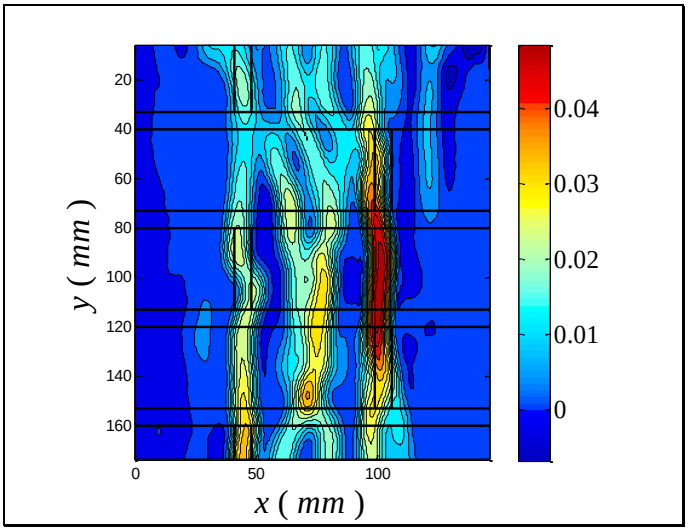

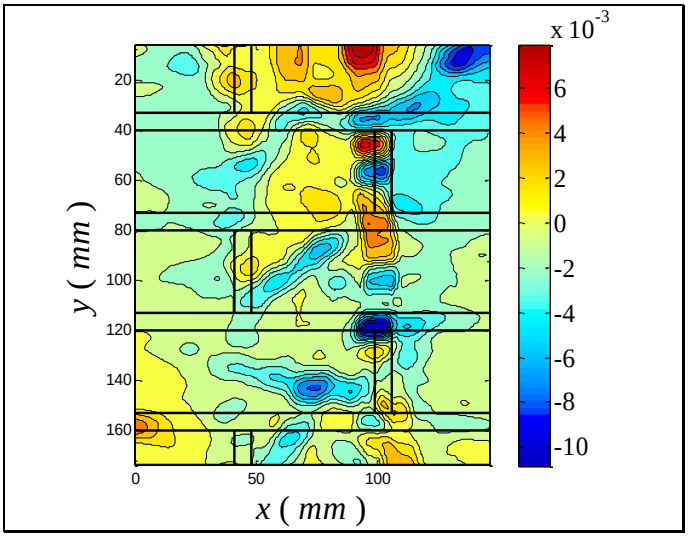

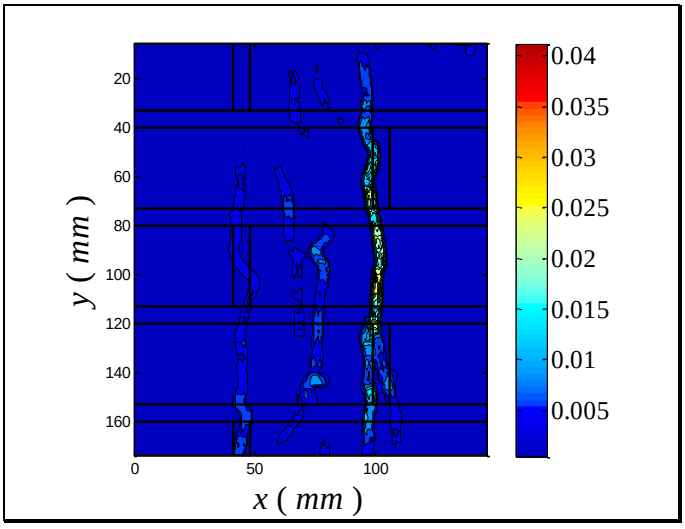

- H: 118.00 kips; 34,18 MPa

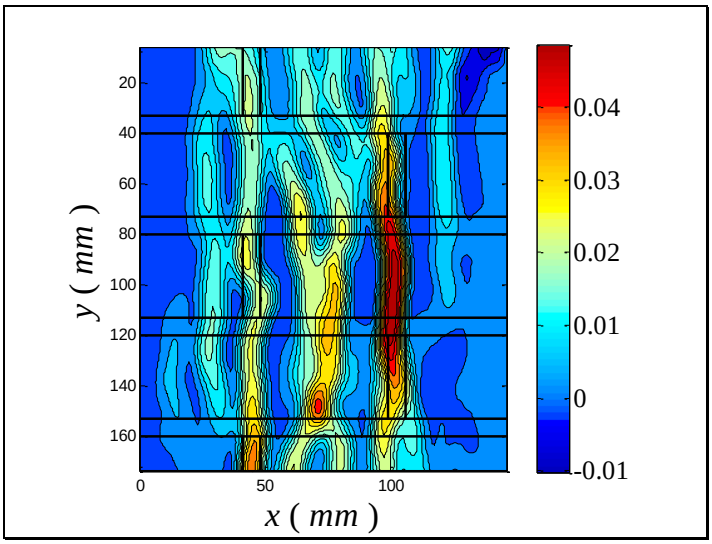

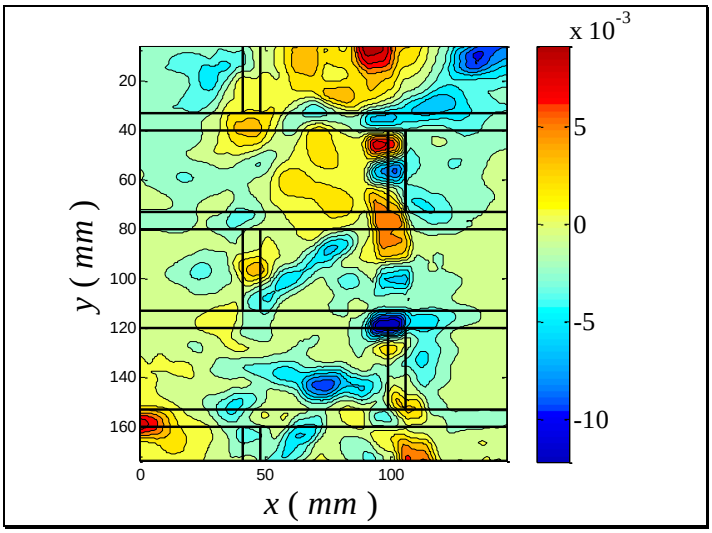

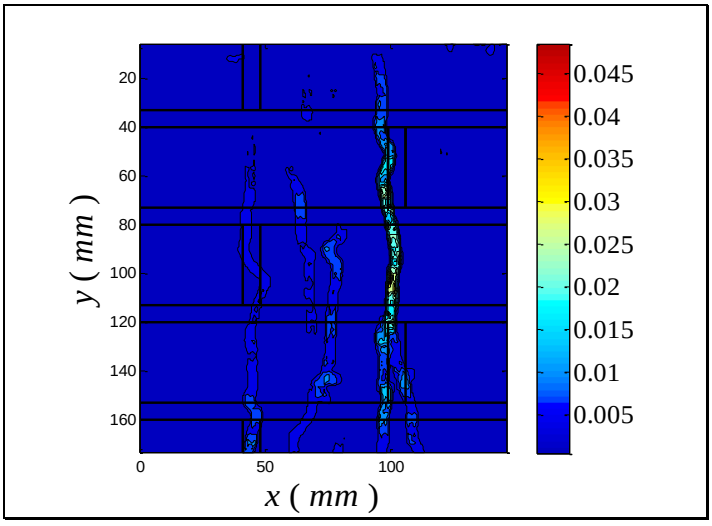

5.2.1.2. Rectangular1 wall wrapped 2

Fig.5.28 – Rectangular1 wall wrapped 2

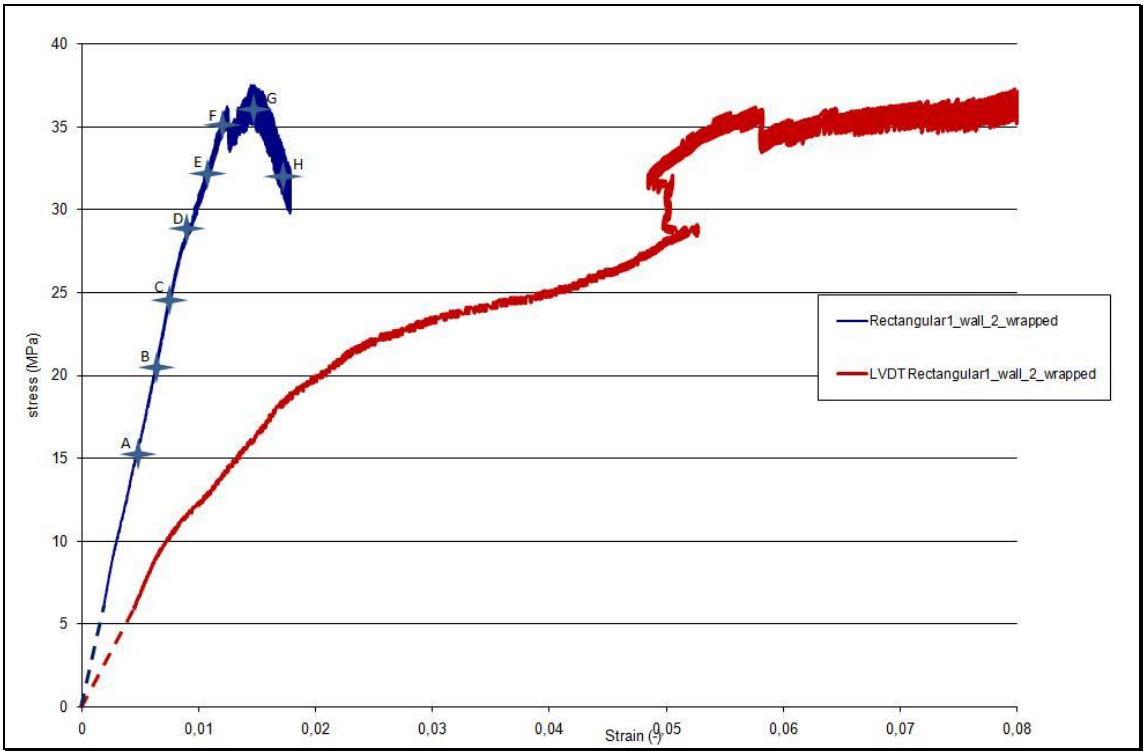

Fig.5.29 – Stress–strain diagram of rectangular1 wall wrapped 2

The contour plots of ε_{xx} , ε_{yy} and the correlation factor for all the points in figure are reported below.

- A: 55.00 kips; 15,93 MPa

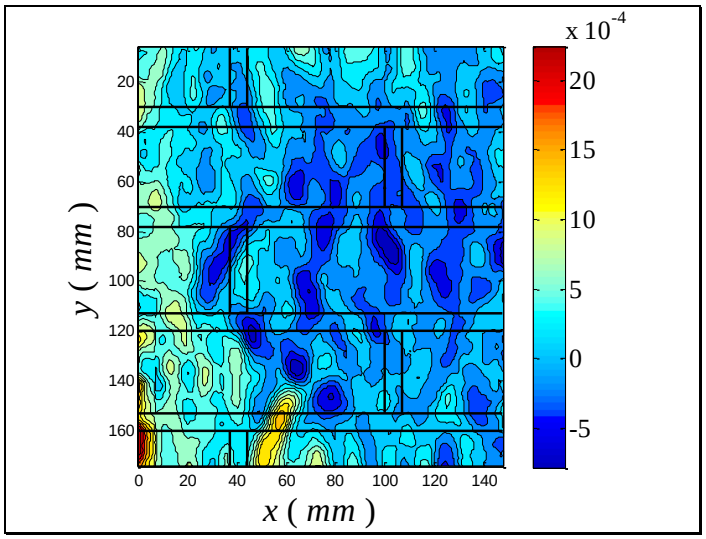

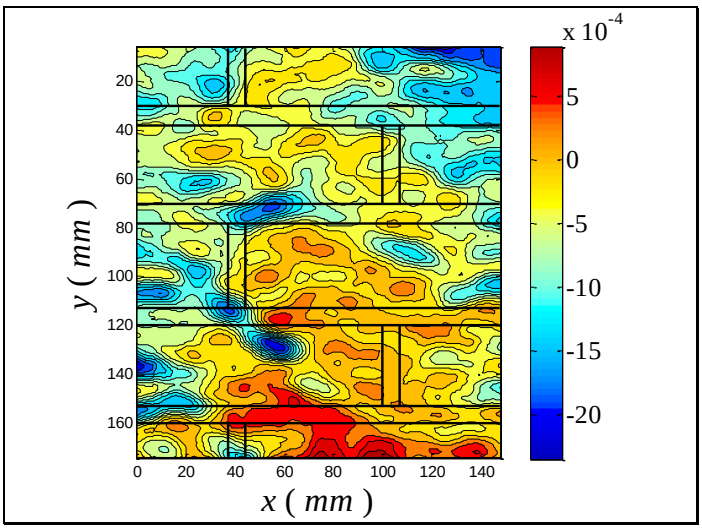

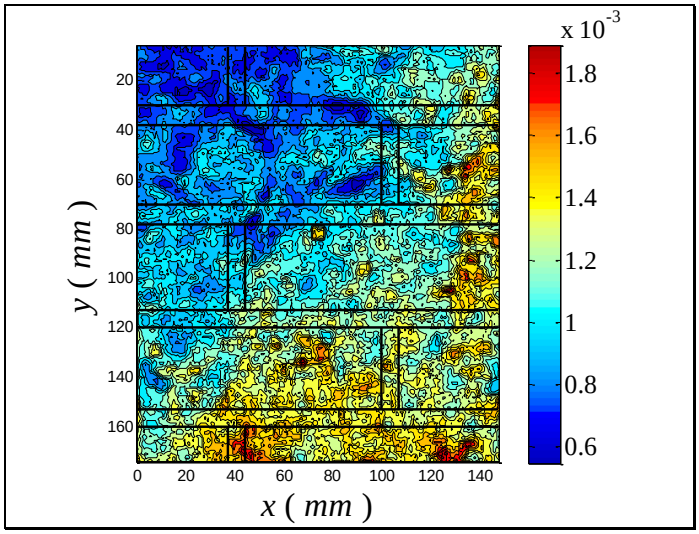

- B: 71.20 kips; 20,63 MPa

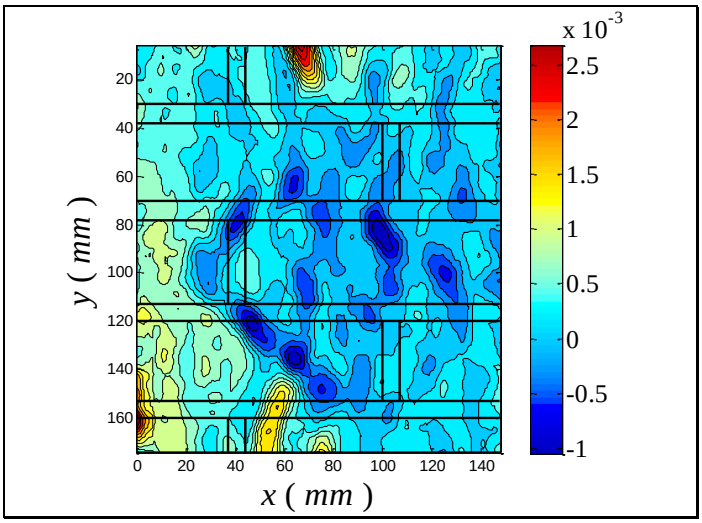

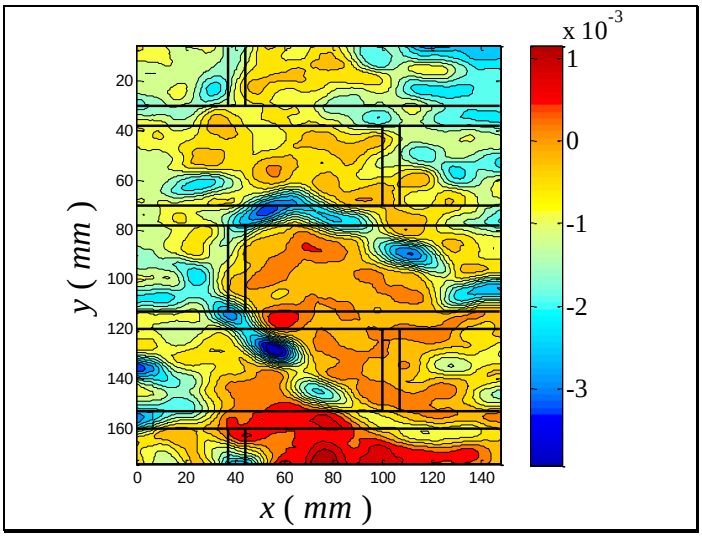

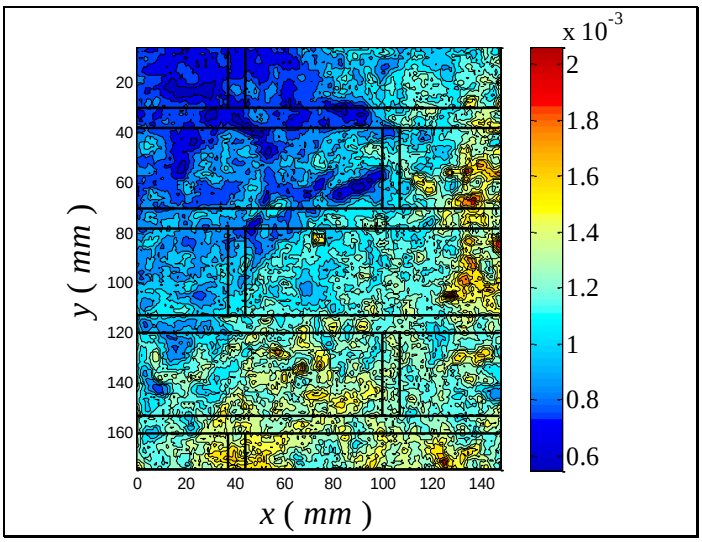

- C: 85.02 kips; 24,63 MPa

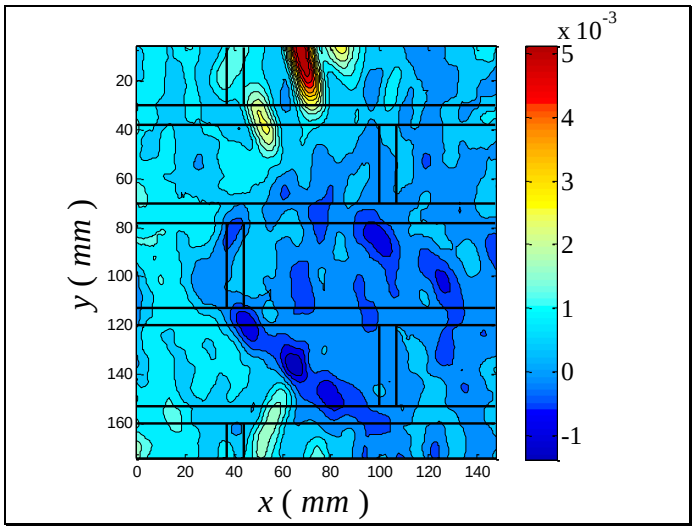

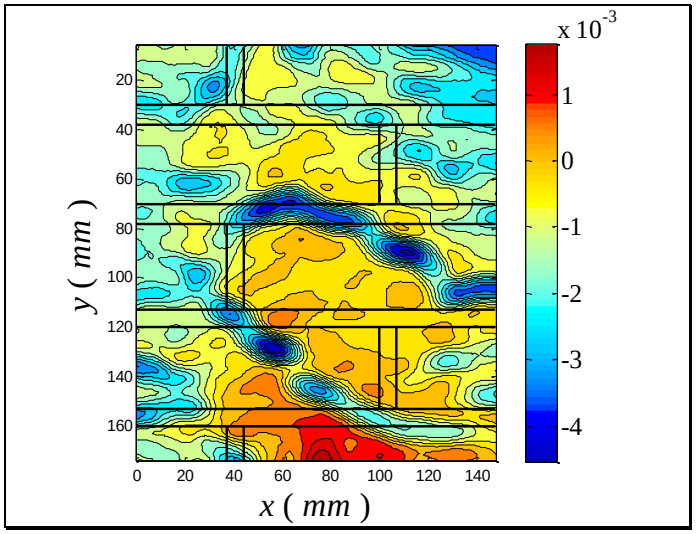

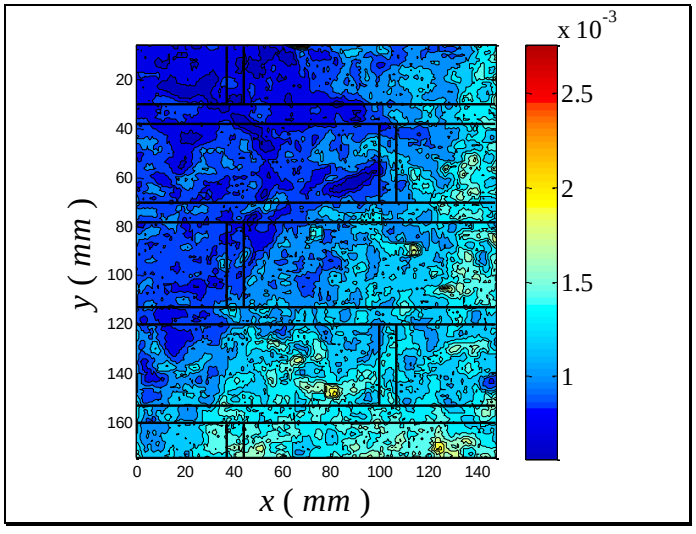

- D: 99.53 kips; 28,83 MPa

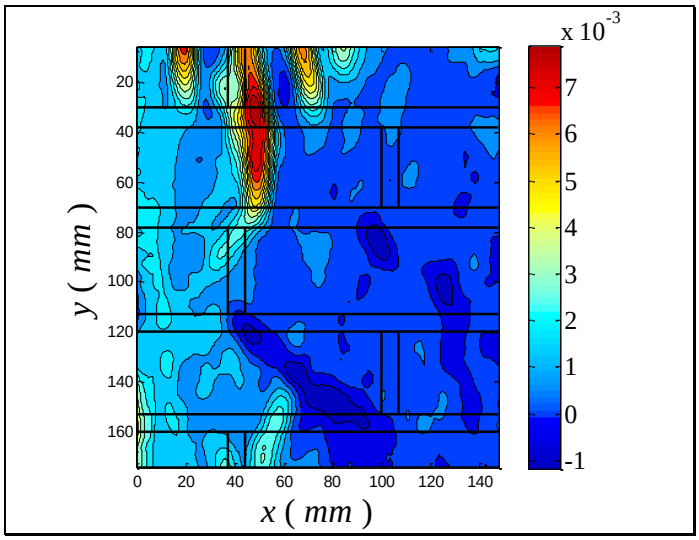

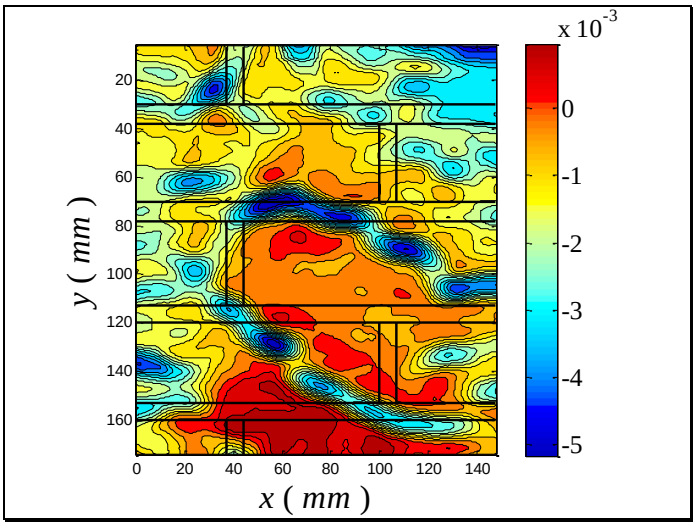

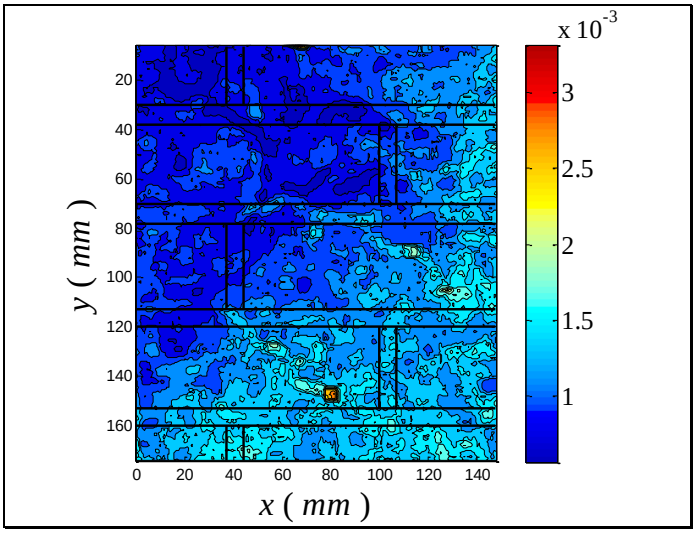

- E: 109.40 kips; 31,69 MPa

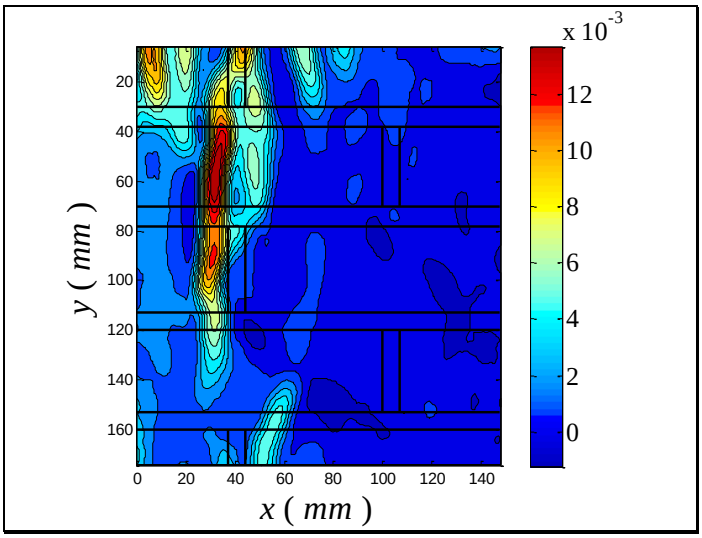

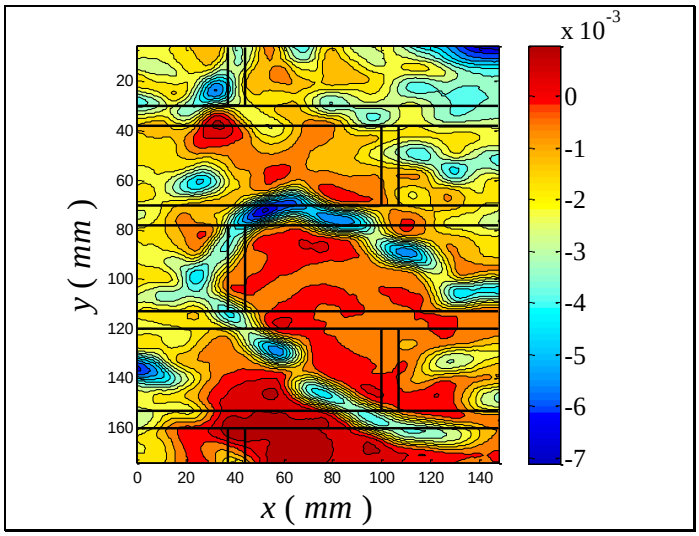

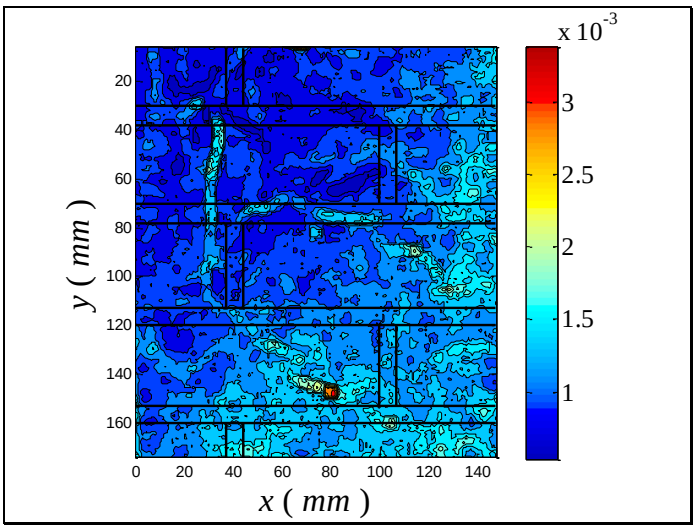

- F: 118.60 kips; 34,36 MPa

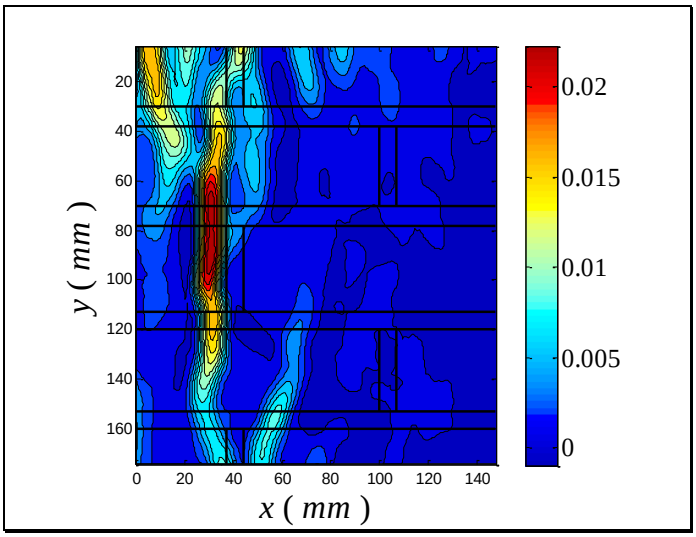

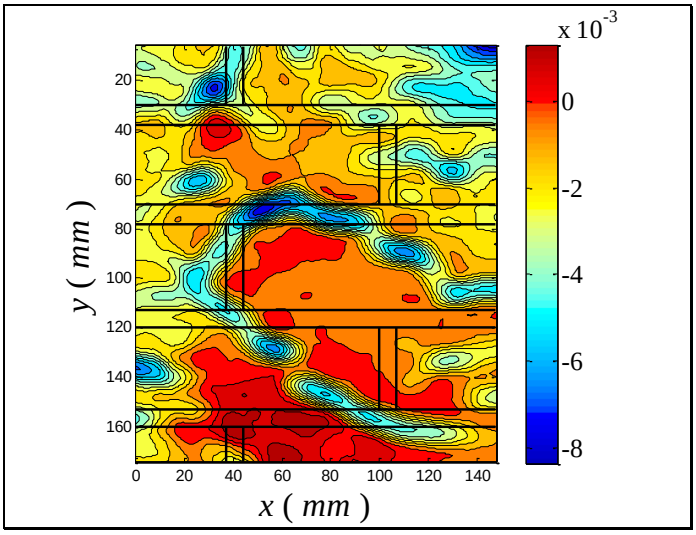

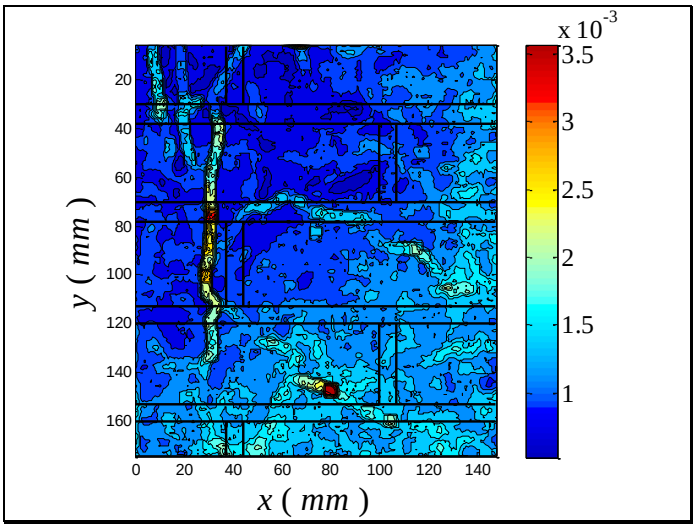

- G: 125.00 kips; 36,21 MPa

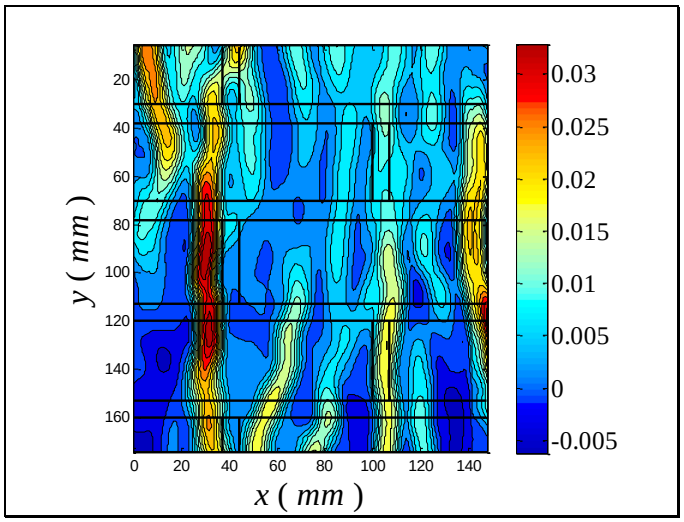

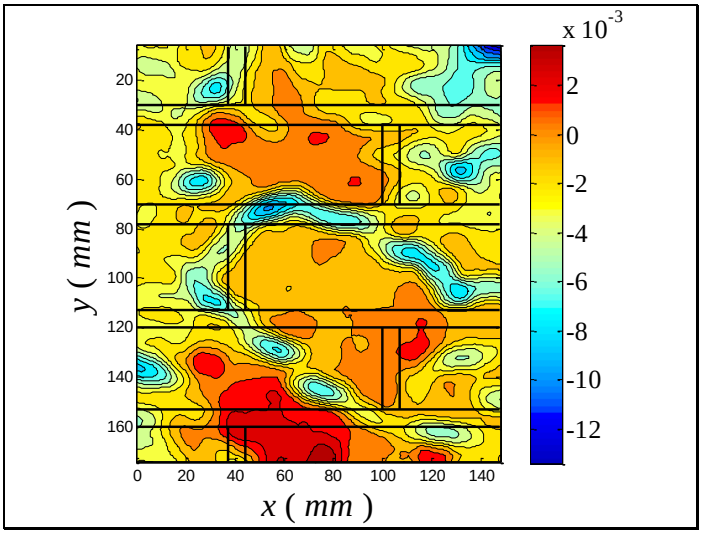

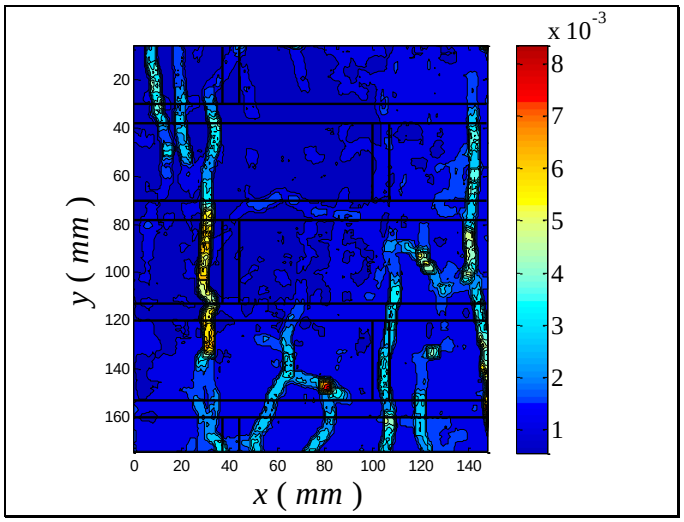

- H: 113.00 kips; 32,73 MPa

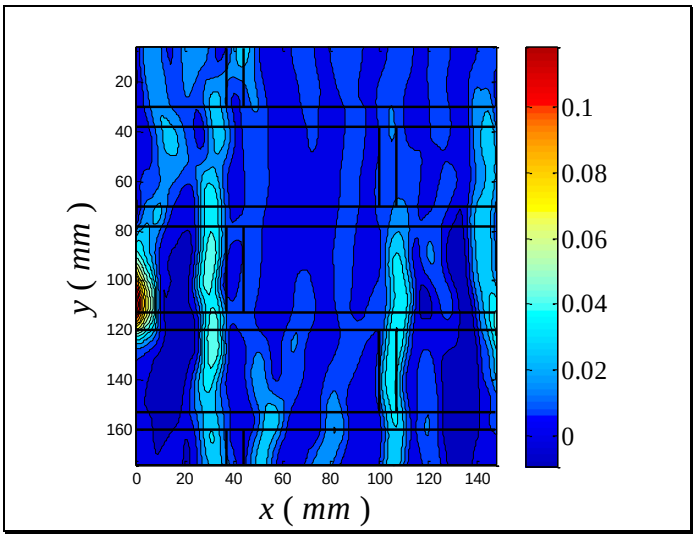

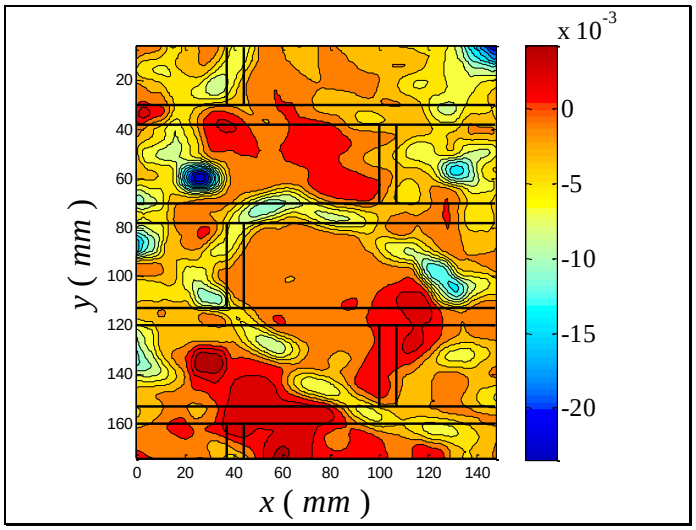

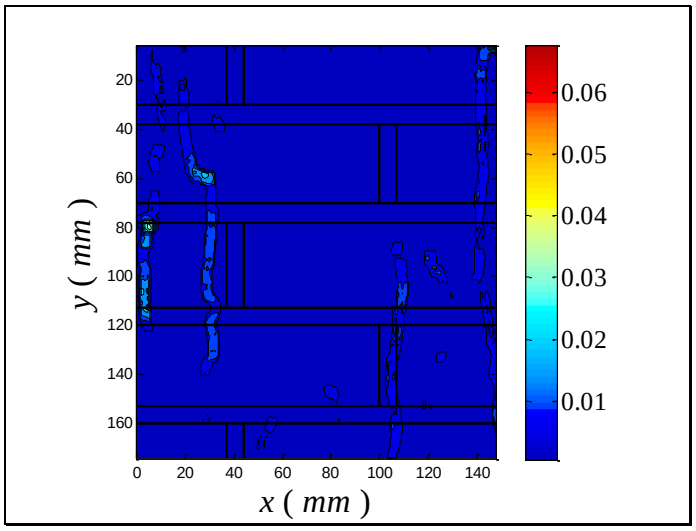

5.2.1.3. Rectangular1 wall wrapped 3

Fig.5.30 – Rectangular1 wall wrapped 3

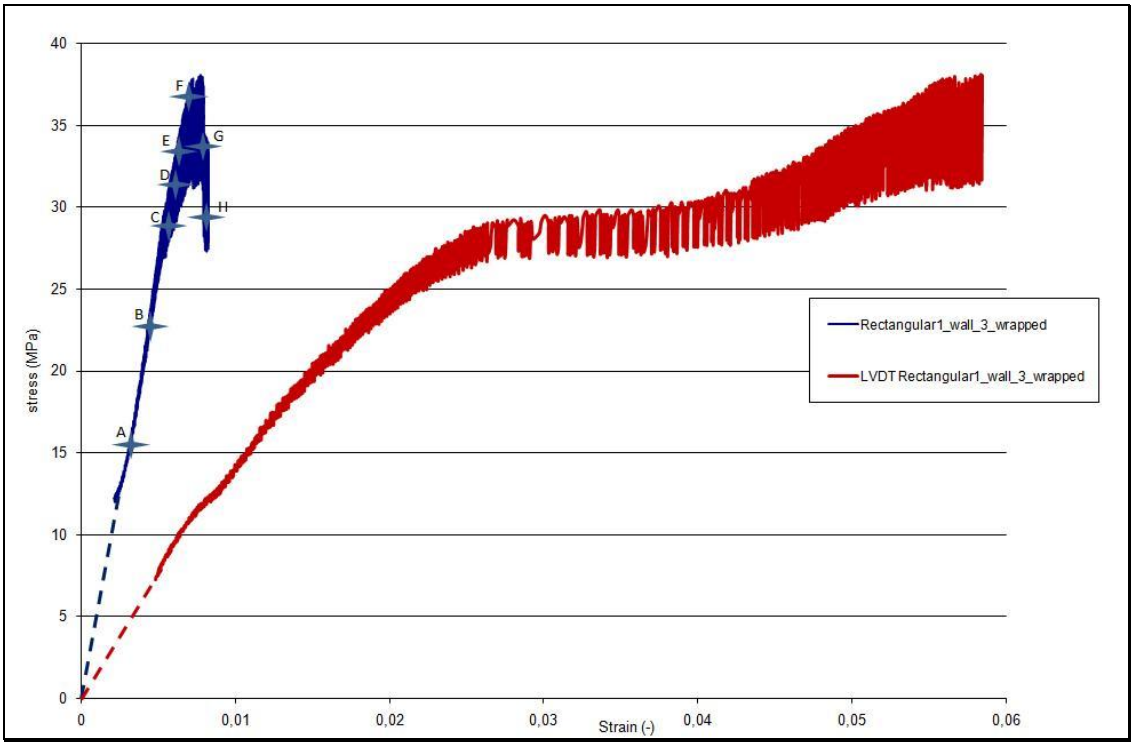

Fig.5.31 – Stress–strain diagram of rectangular1 wall wrapped 3

The contour plots of ε_{xx} , ε_{yy} and the correlation factor for all the points in figure are reported below.

- A: 53.50 kips; 15,50 MPa

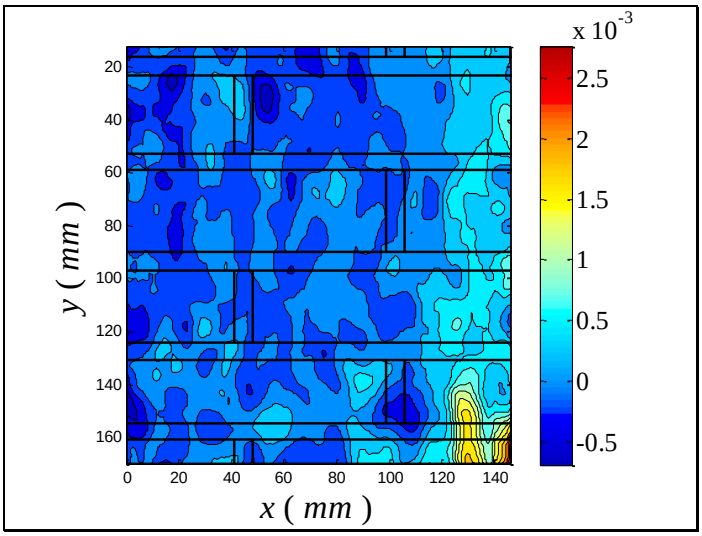

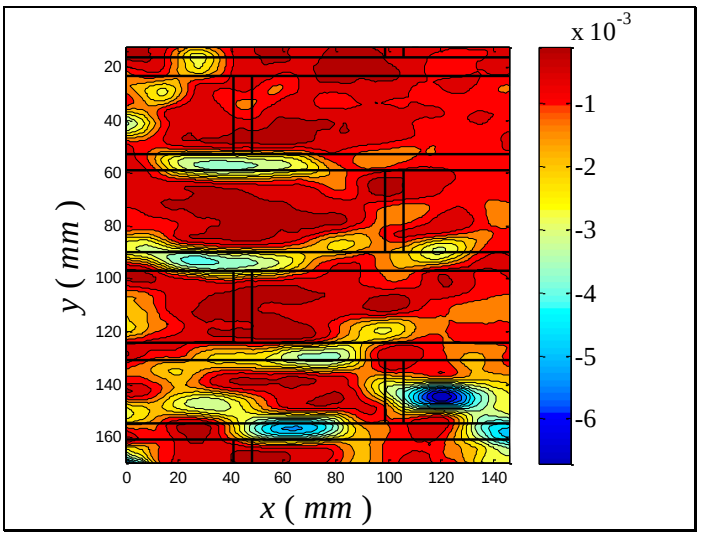

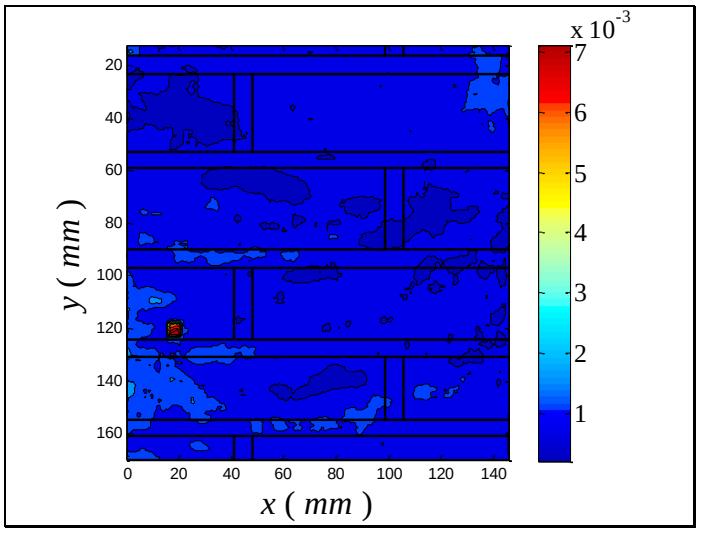

- B: 80.77 kips; 23,40 MPa

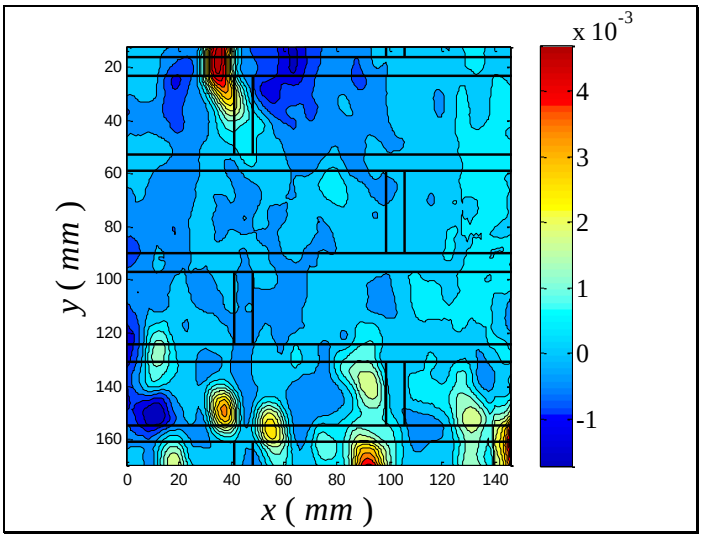

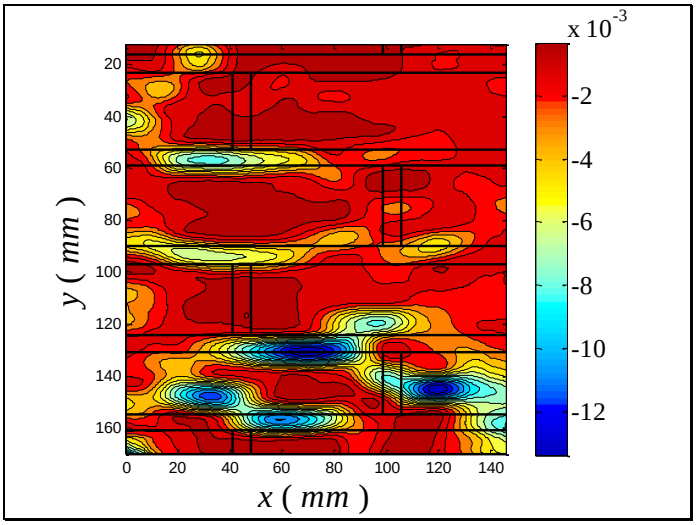

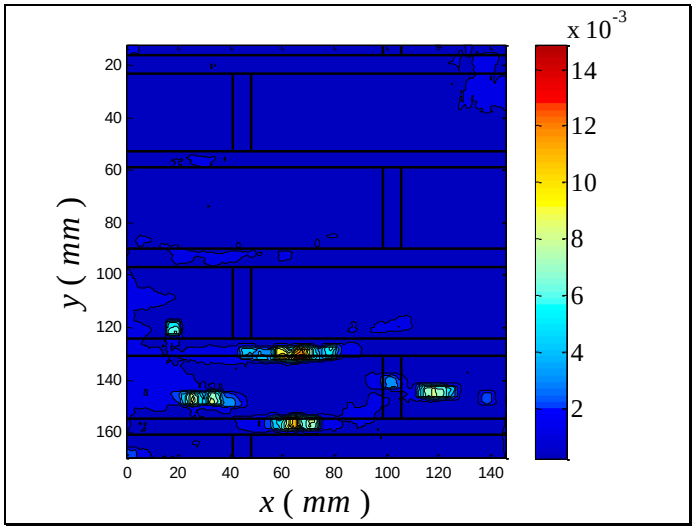

- C: 102.20 kips; 29,61 MPa

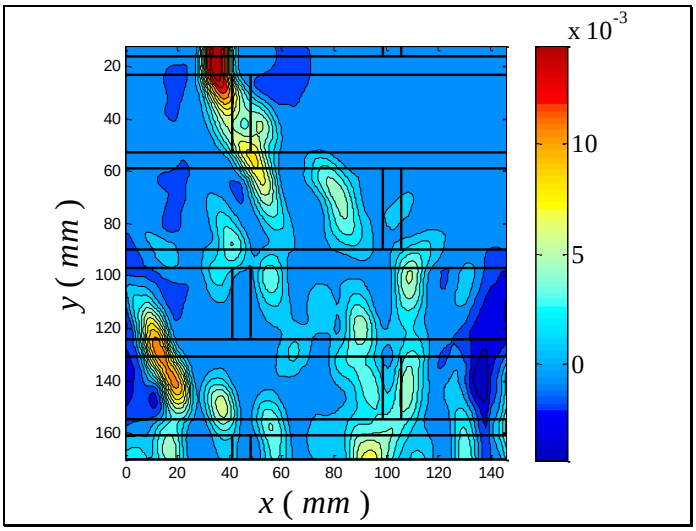

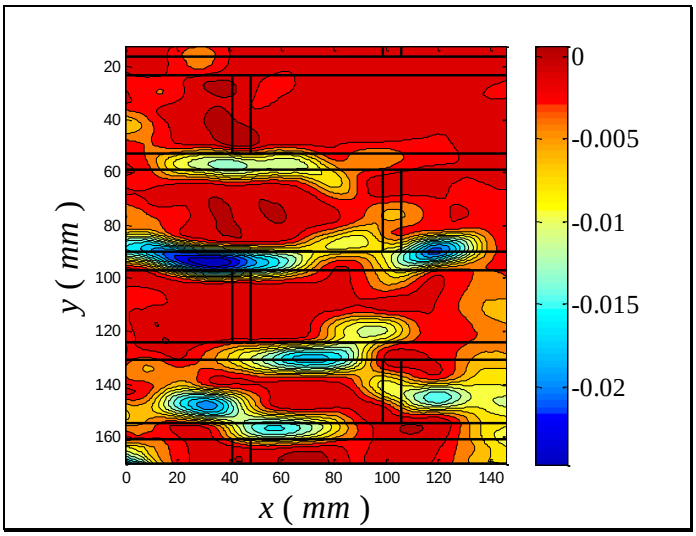

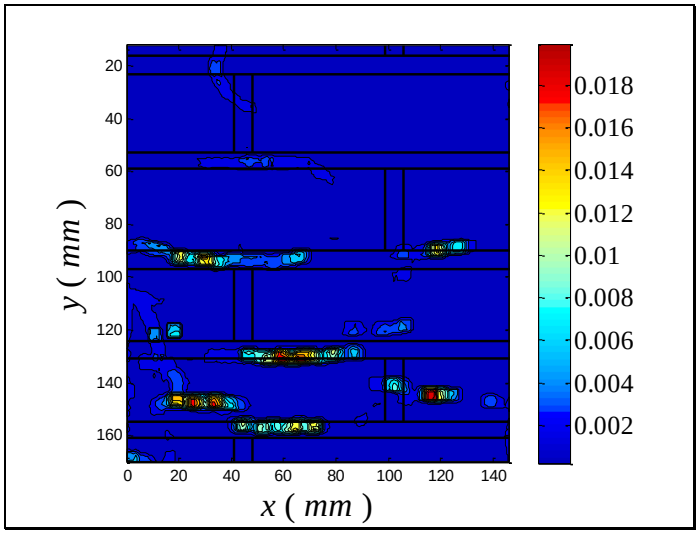

- D: 110.20 kips; 31,92 MPa

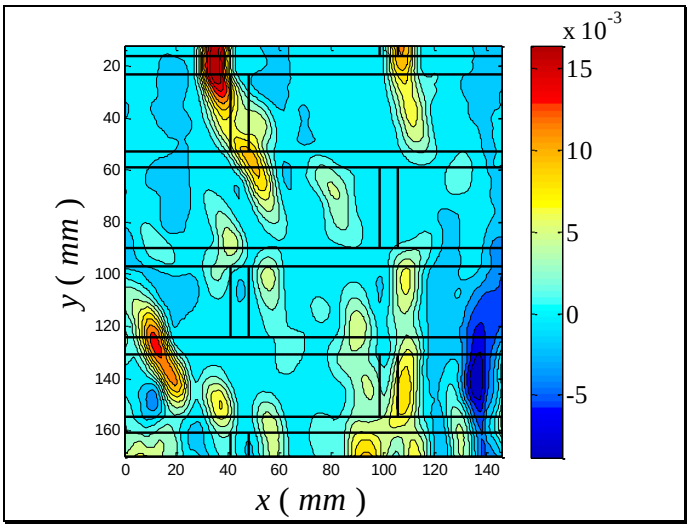

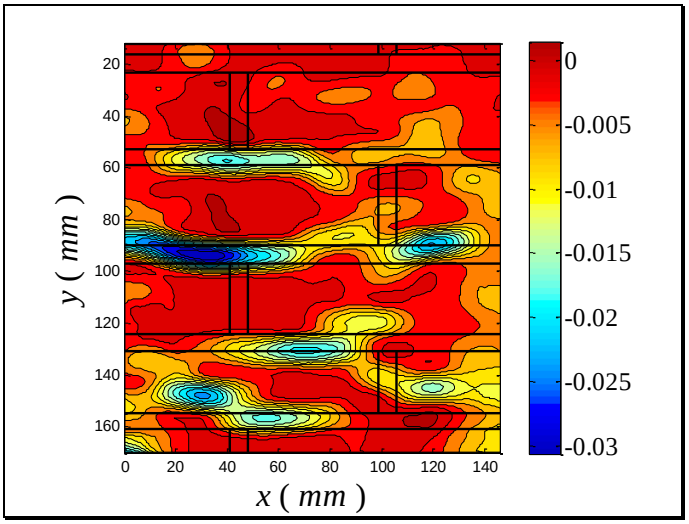

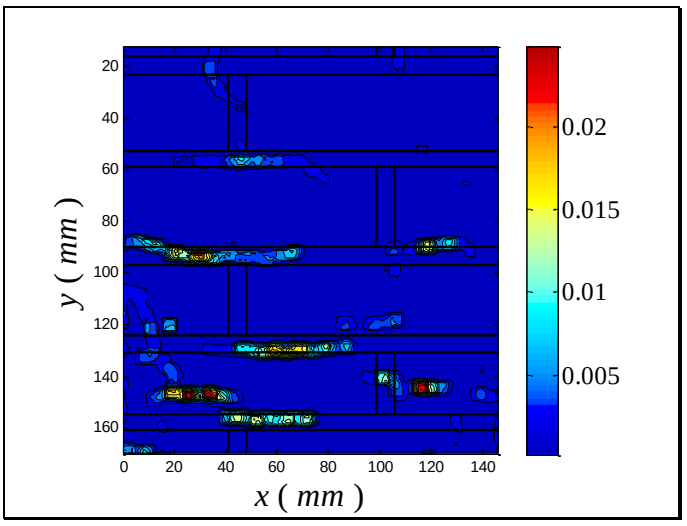

- E: 115.30 kips; 33,40 MPa

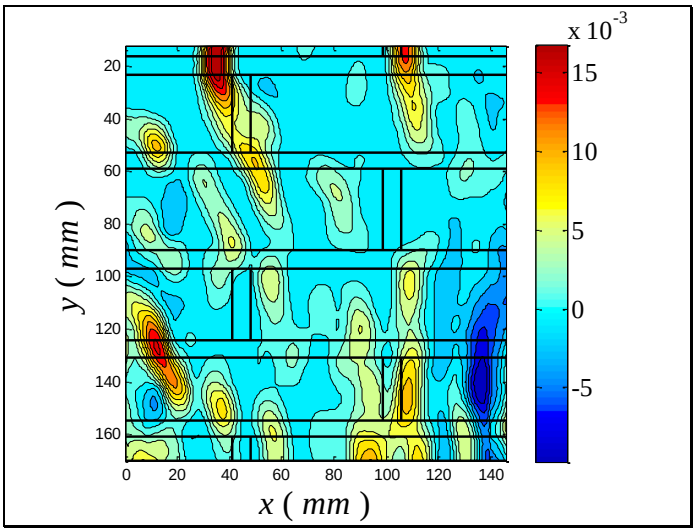

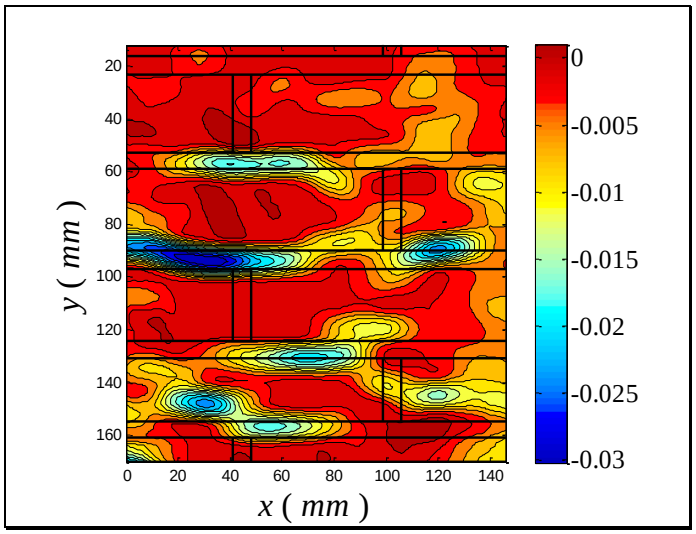

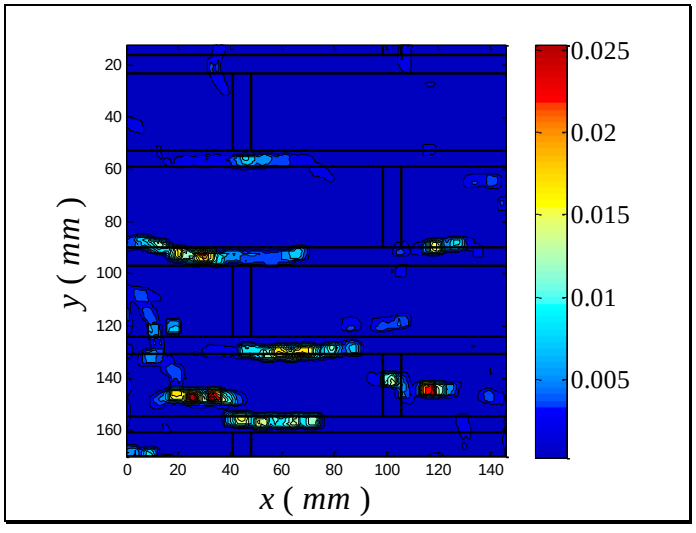

- F: 125.30 kips; 36,30 MPa

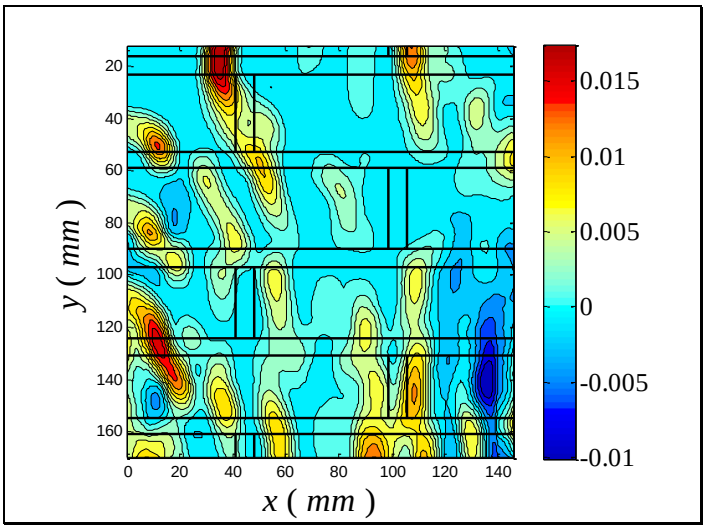

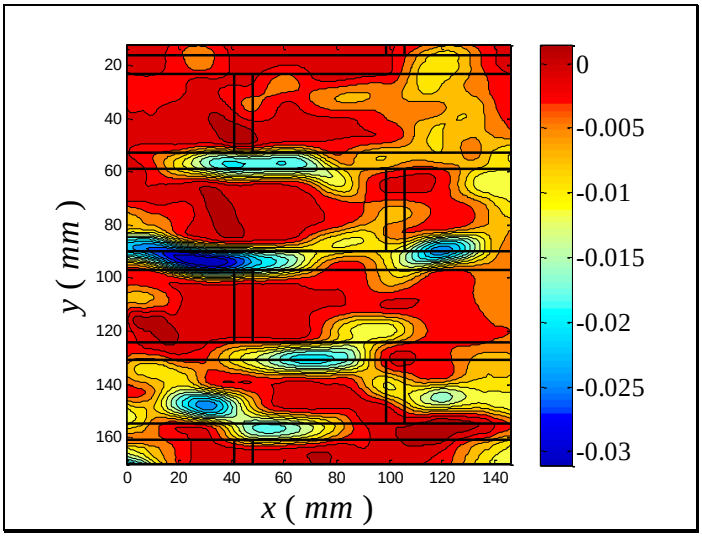

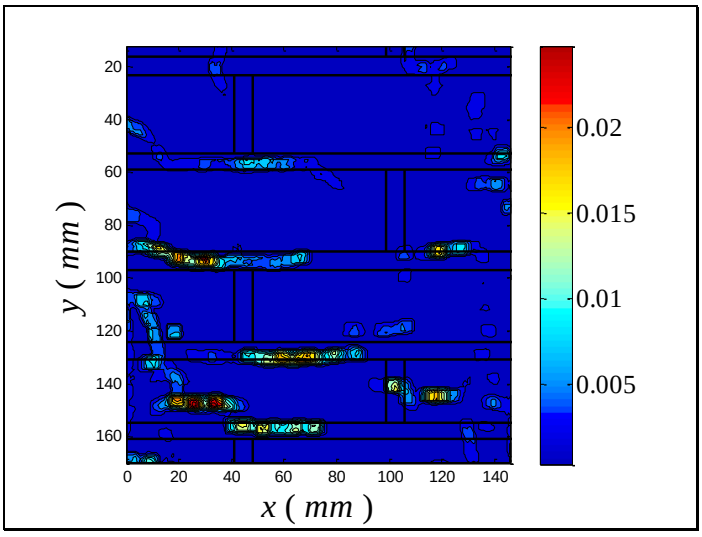

- G: 116.10 kips; 33,63 MPa

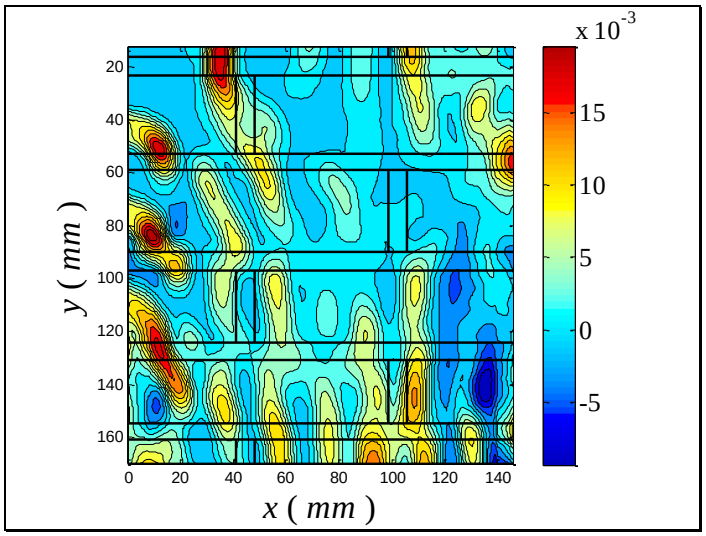

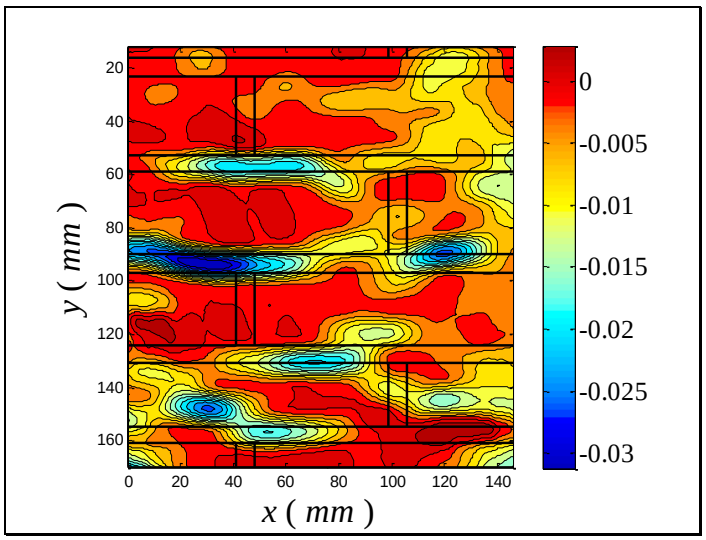

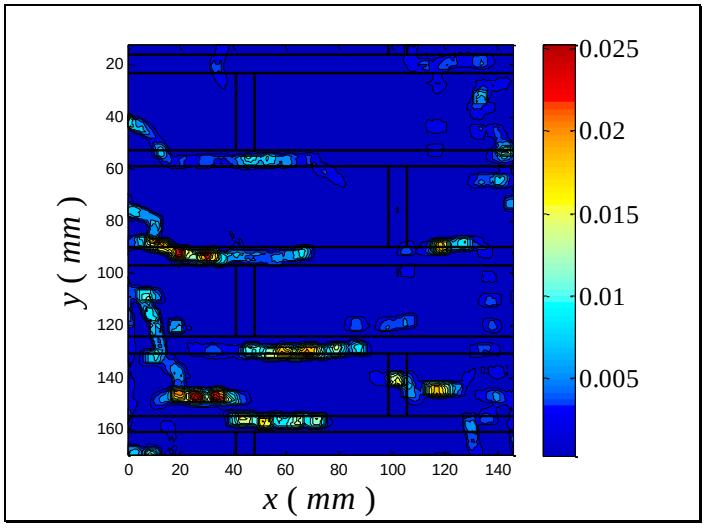

- H: 102.00 kips; 29,55 MPa

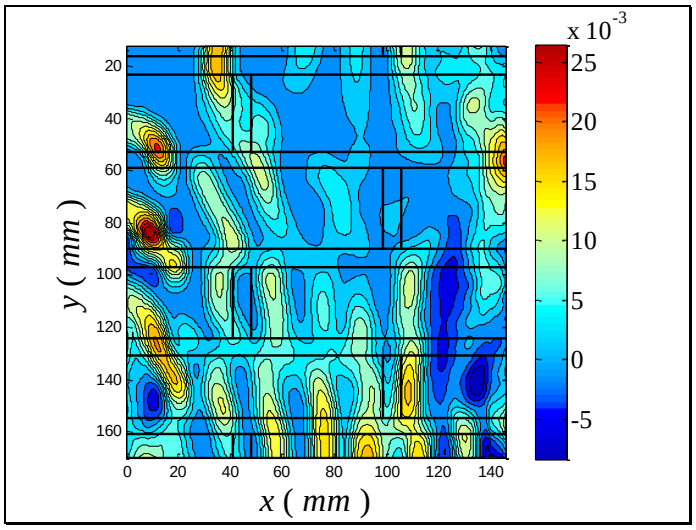

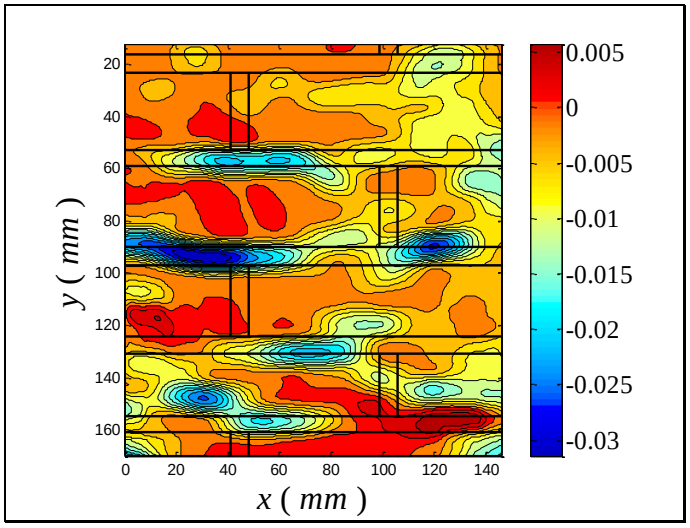

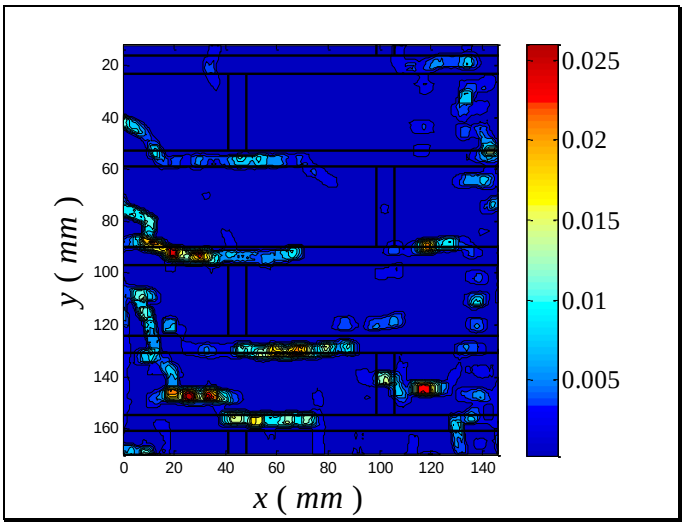

5.2.2. Discussion of result

In this configuration, as in the other, the crush appeared to be initiated by crushing and squeezing of the mortar from the mortar joints and immediately the reinforcement begins to work containing the expansion of the mortar and the bricks, increasing the load-carrying capacity of the masonry.

The next figure shown the developing of the arch effect on the section after cutting in the middle 2 specimens.

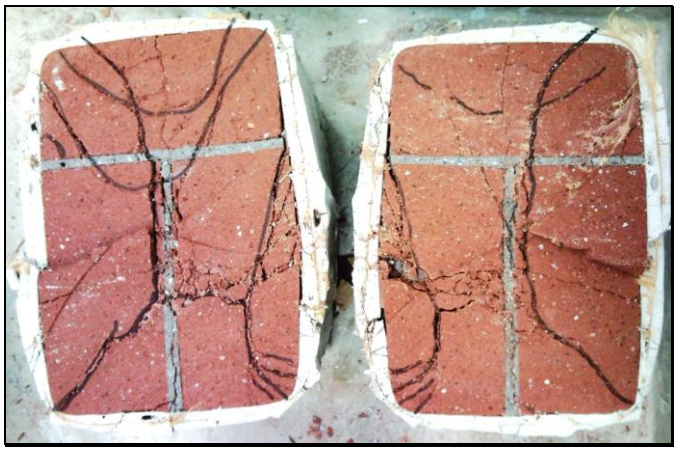

Fig. 5.32 – Section of rectangular1 wall wrapped 2

Fig. 5.33 – Section of rectangular1 wall wrapped 3

The main conclusions that can be drawn from the tests on laboratory specimens are as follows.

The arch effect is modified by the presence of vertical joints in this configuration. In particular after the cut in the middle of the specimens it's clear the presence of cracks diverted by the presence of horizontal joints forming different reacting area instead of a concrete specimen with the same dimension.

The effectively confined area is assumed as the region where the arching action has been fully developed as visible in figure 5.34.

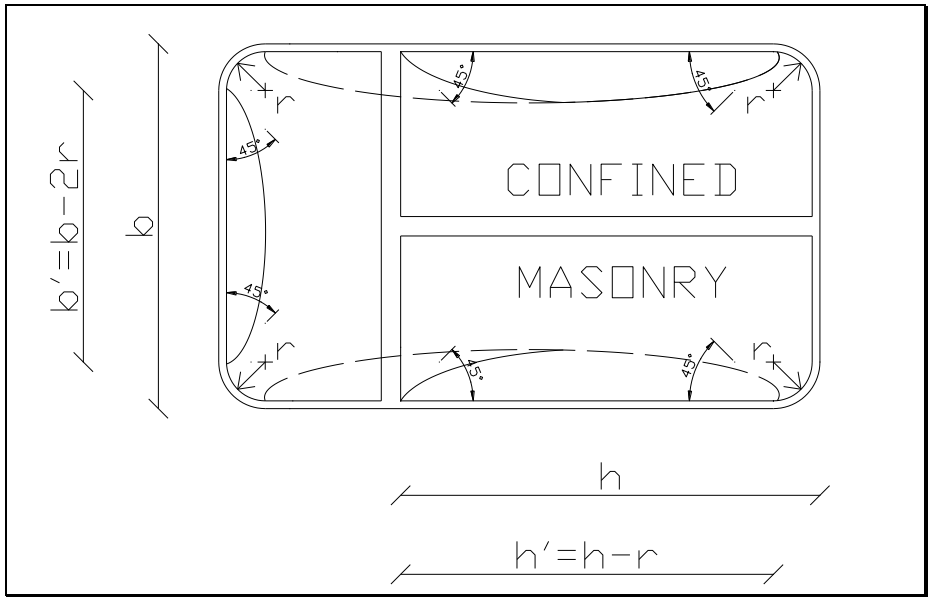

Fig. 5.34 – Effectively confined masonry in rectangular1 section walls

The critical point continued to be the mortar joints, horizontal and vertical as it is shown in the DIC picture.

The compressive strength of masonry is really increased with the use of the FRCM in this configuration because it contain the expansion of the component, in particular of the joints, vertical and horizontal.

The stress and the strain are almost doubled as it's clear in the diagram, figure 5.35 and 5.36.

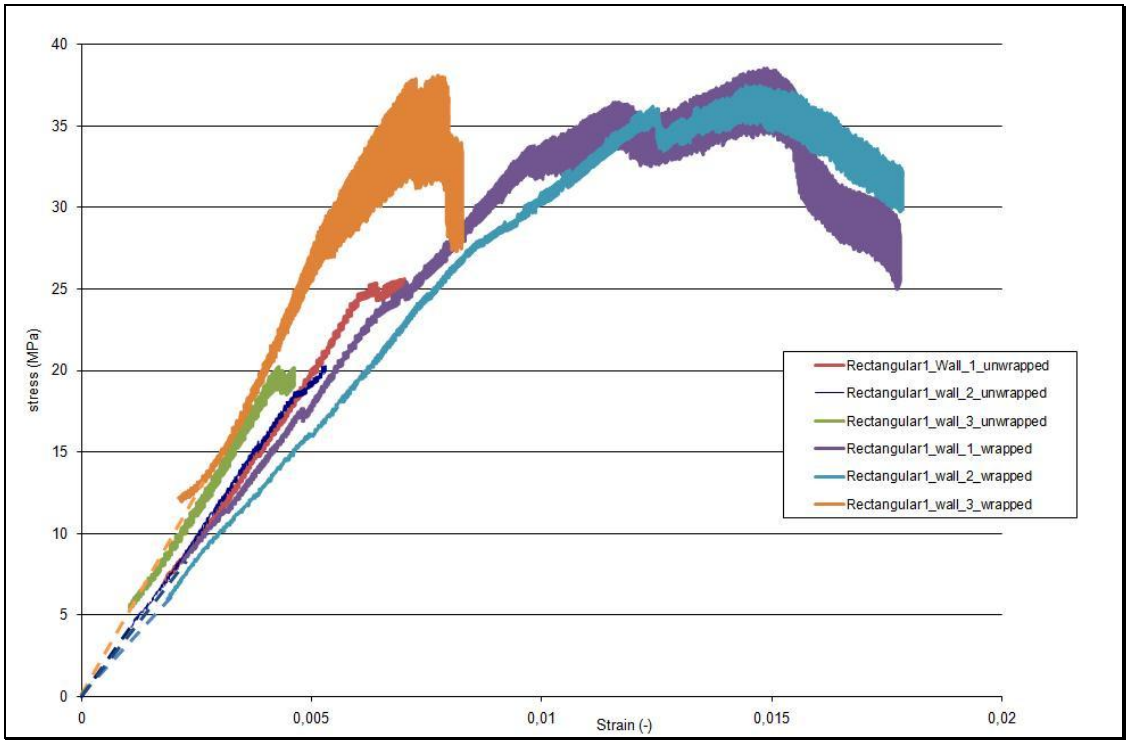

Fig. 5.35 – Stress–strain diagram of rectangular1 walls wrapped and unwrapped compared

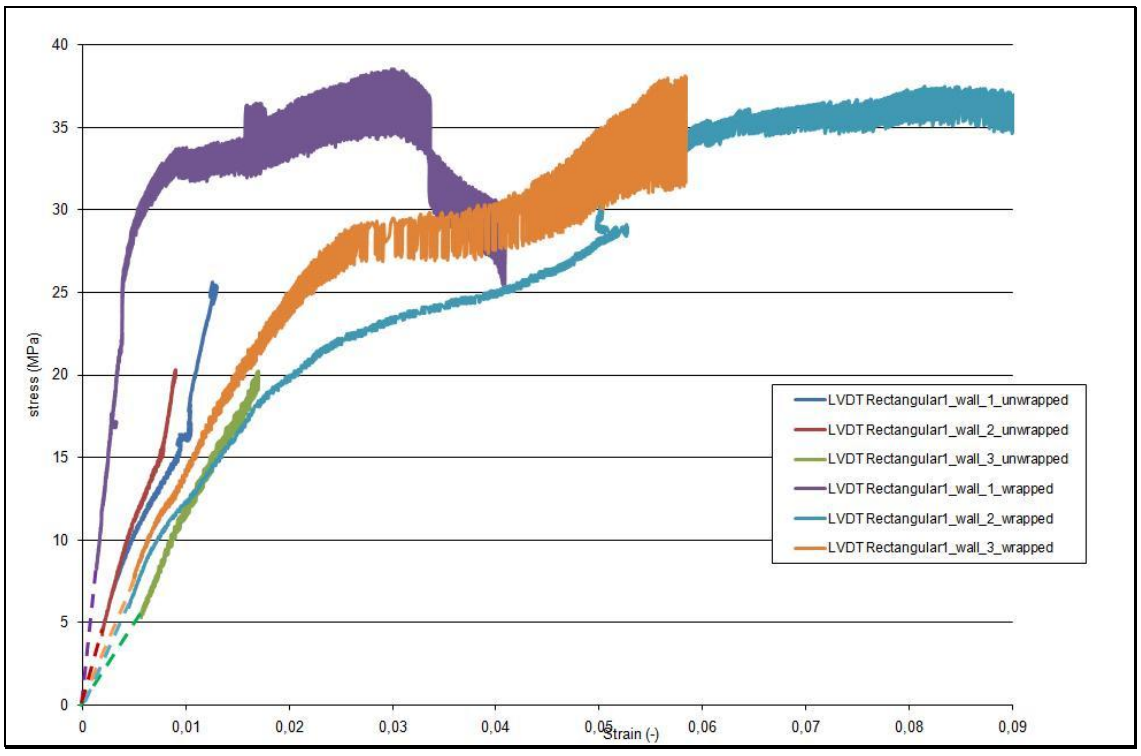

Fig. 5.36 – Stress–LVDTstrain diagram of rectangular1 walls wrapped and unwrapped compared

With the DIC pictures is possible to see an interaction between the vertical and the horizontal joints that can modify the attended failure mechanisms for this configuration.

5.3. Axial Compression Test Third Configuration

This is the last configuration tested, in the unwrapped specimens was clear how the presence of many vertical joints brought the masonries to sudden and premature failure. Presence of fibers improves notably the behavior.

Before wrapping all the corner were rounded using a grinding machine at a radius of 10 mm, figure 5.37.

Fig. 5.37 – Third configuration masonry wall with rounded corners

The specimens were wrapped with a layer of stabilized inorganic matrix and after the kevlar mesh, figure 5.38.

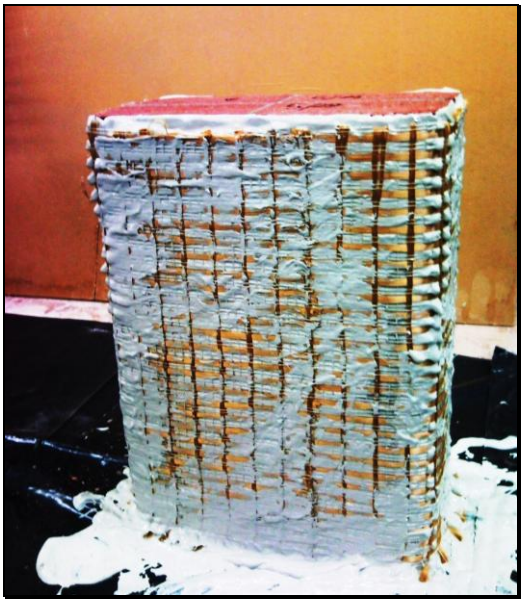

Fig. 5.38 – Wrapping of the masonry

Finally all the fibers were covered with the cementitious matrix with, also for this configuration, the finishing end of the mesh overlapping the starting end by approximately 100 mm.

Fig. 5.39 – Third configuration masonry wall after the complete wrapping

Only 2 specimens were tested wrapped and the DIC surface was painted with a layer of white and light drops black paint, figure 5.40

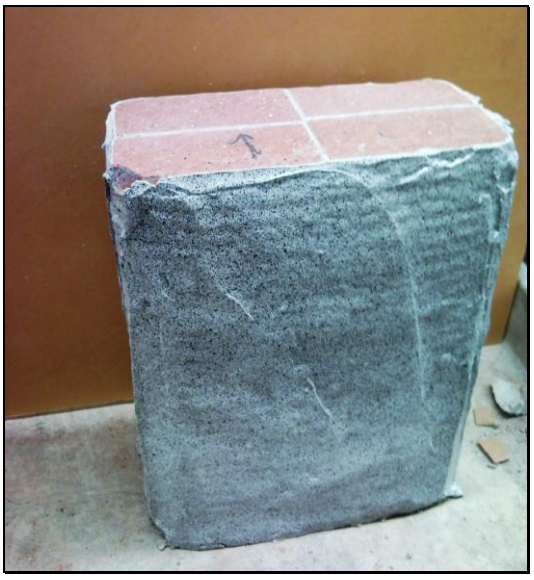

Fig. 5.40 – Third configuration masonry wall ready for the DIC

Displacements of the central section on each specimen were measured using also a Linear Variable Differential Transformer (LVDT) on the left side of the columns attached to the wrapping surface, as it's show in the pictures of the specimens.

5.3.1. Experimental result and failure mode

The main results of the tests are presented in the table 5.3.

Specimens notation	3 precycle (kN)	Maximum load (kN)	Area (cm^2)	Compressive strenght (MPa)	Ultimate machine strain ε
1	65-135	744,39	199,14	36,19	0,0042
2	135-200	705,20	199,14	34,29	0,0083
Displacement control mode of 0.008 inch/min, about 0.2 mm/min					

Tab. 5.3 – Summary of test results for rectangular2 walls wrapped

The stress-strain diagrams for the first configuration wrapped specimens are presented in figure 5.41.

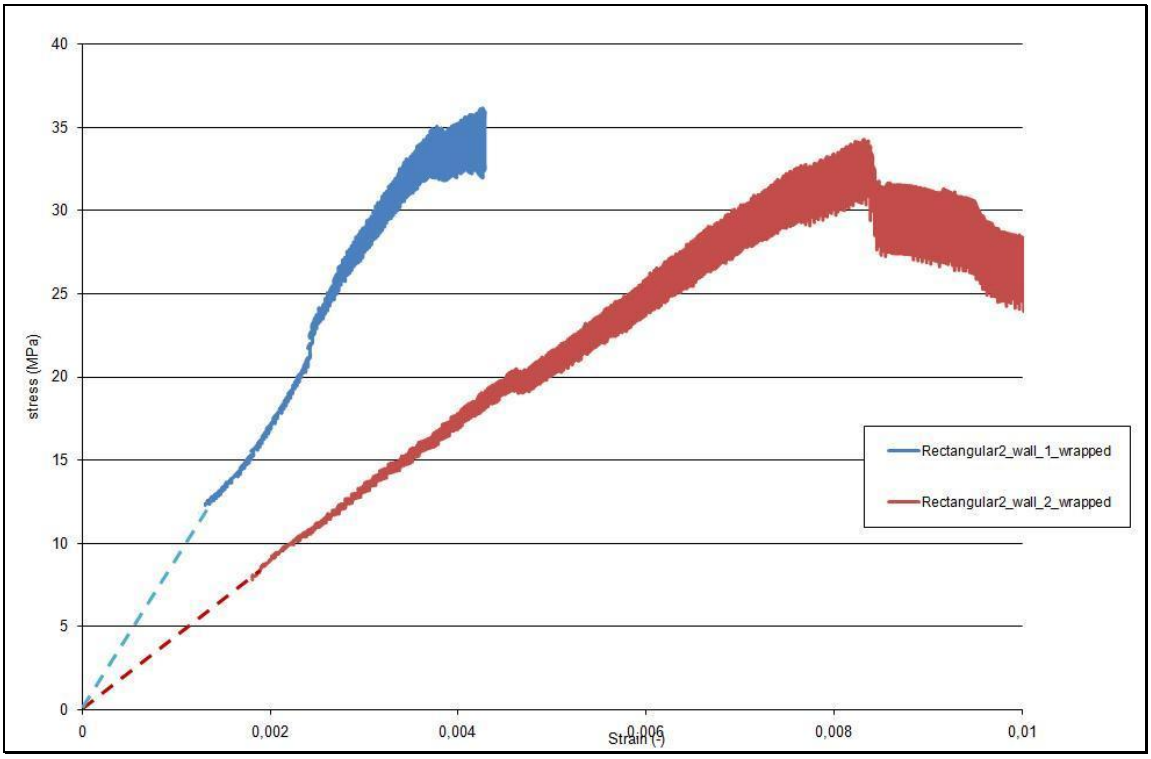

Fig. 5.41 – Stress–strain diagram of rectangular2 walls wrapped

It can be observed that in all cases the diagrams are linear up to about 80% of the maximum load.

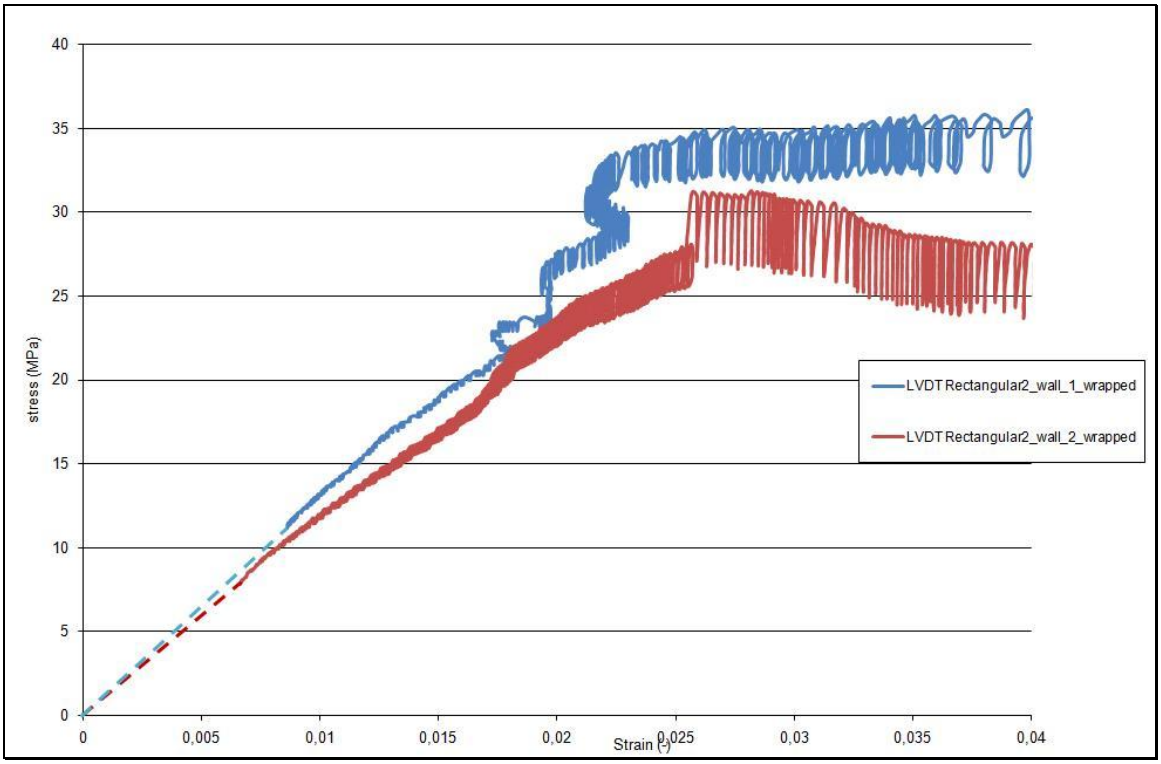

Fig. 5.42 – Stress–LVDTstrain diagram of rectangular2 walls wrapped

In this configuration the presence of reinforcement improves the behavior by almost doubling the ultimate stress and strain at failure. After the crack of the joints the reinforcement begins to work.

The formation of a lot of cracks, dued to the presence of many vertical joints, distributed in the whole masonry make the presence of the reinforcement fundamental for the behavior of the specimens.

The ε_{xx} DIC pictures show that both the tests failed by the formation of vertical cracks through the joints and the bricks under the wrapping layer.

The pressure of the bricks on the cover unthread the reinforcement on the overlap in the back of the specimens, as in the other configuration.

5.3.1.1. Rectangular2 wall wrapped 1

Fig.5.43 – Rectangular2 wall wrapped 1

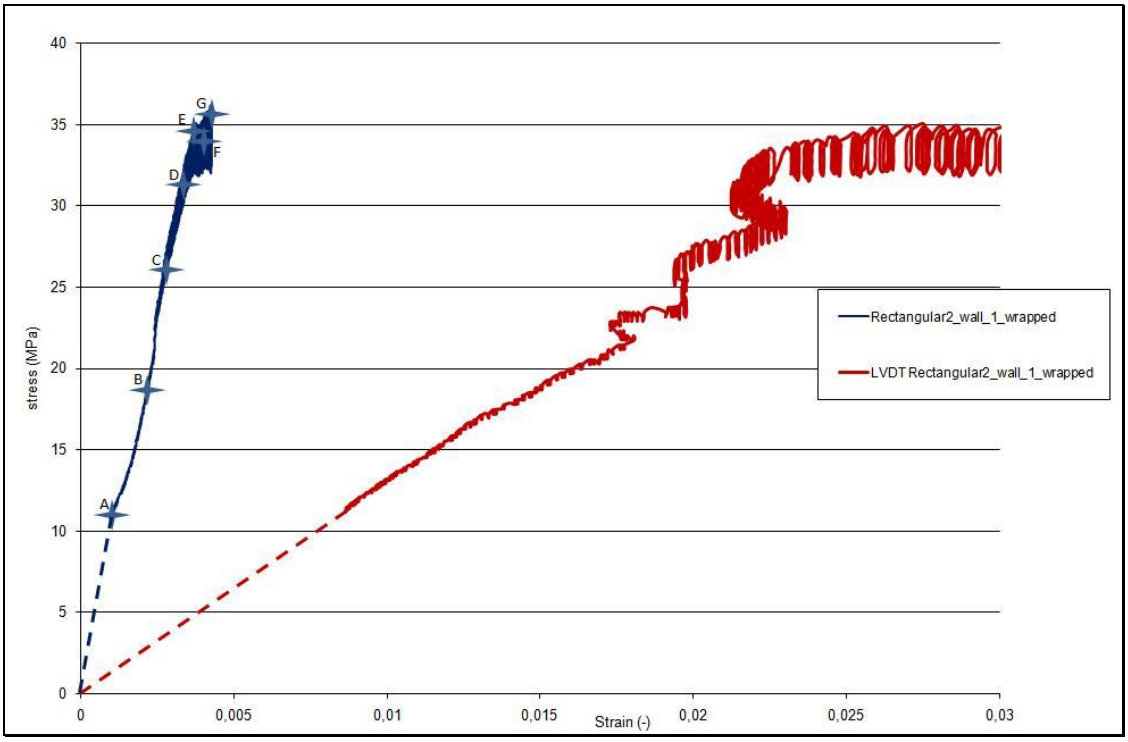

Fig.5.44 – Stress–strain diagram of rectangular2 wall wrapped 1

The contour plots of ε_{xx} , ε_{yy} and the correlation factor for all the points in figure are reported below.

- A: 50.08 kips; 10,83 MPa

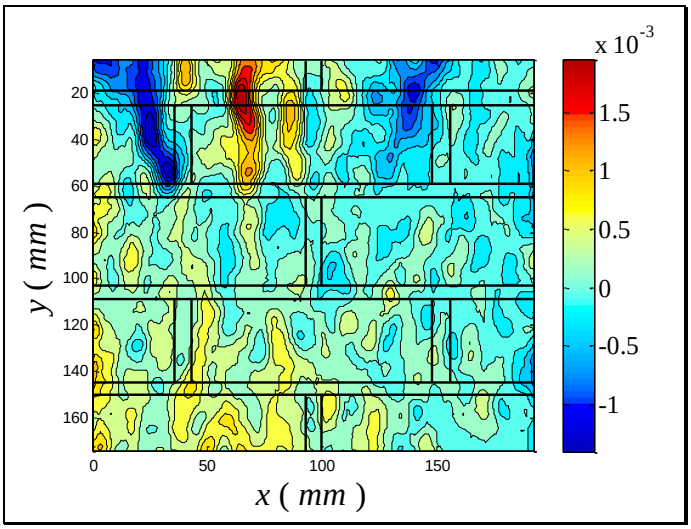

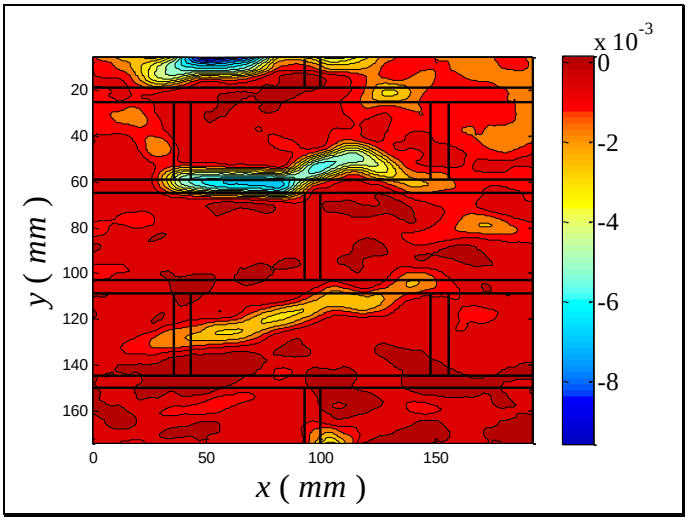

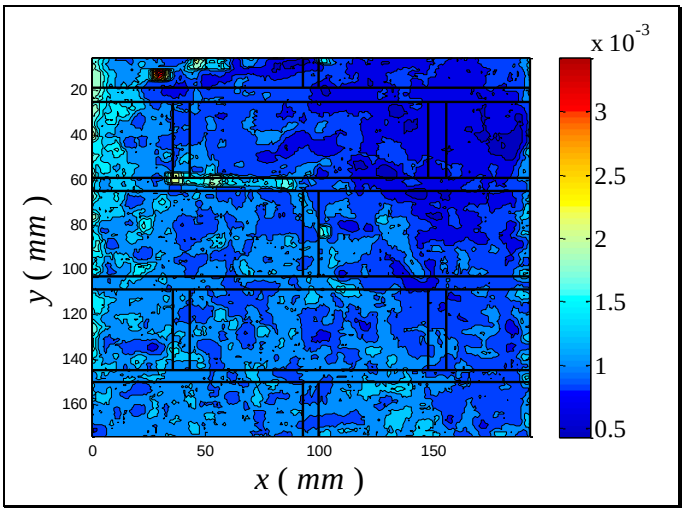

- B: 80.53 kips; 17,42 MPa

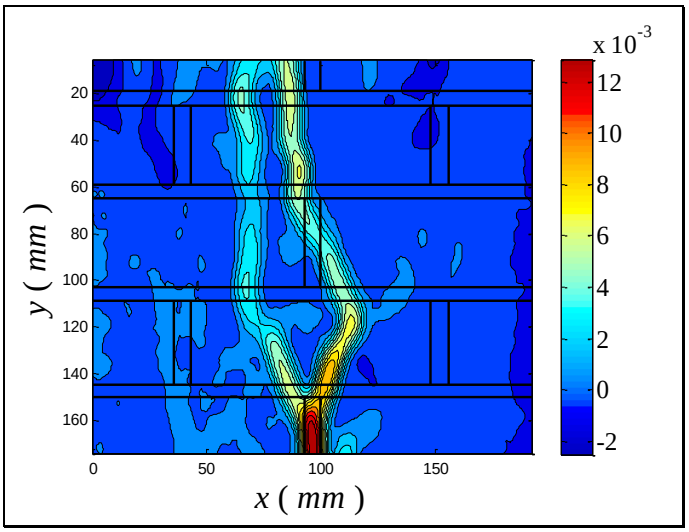

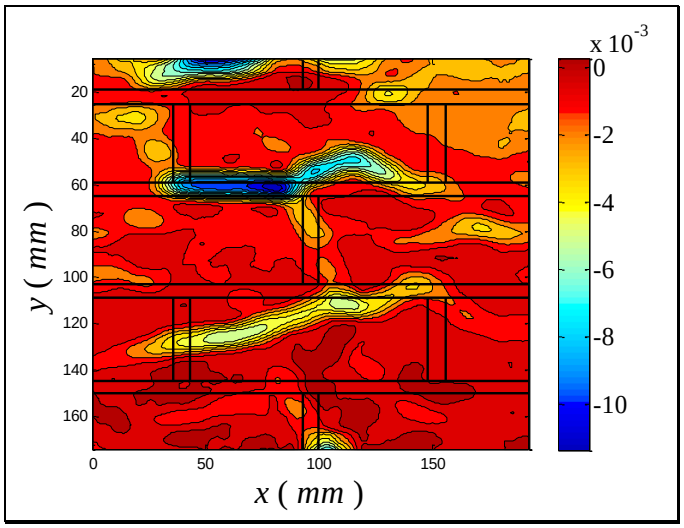

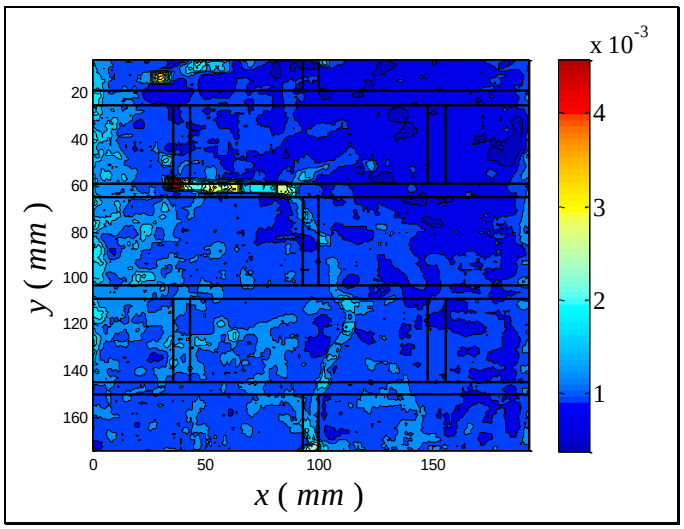

- C: 120.20 kips; 26,00 MPa

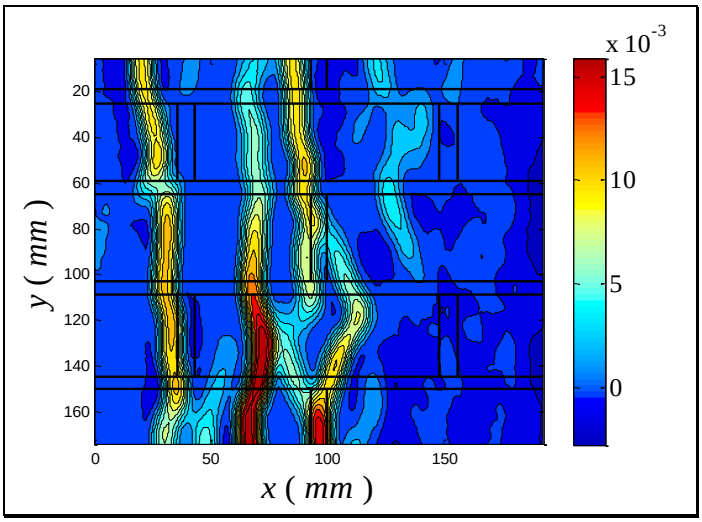

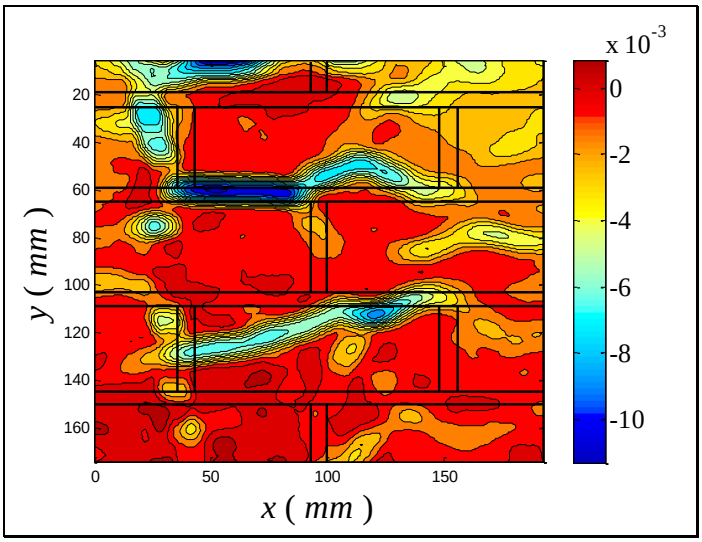

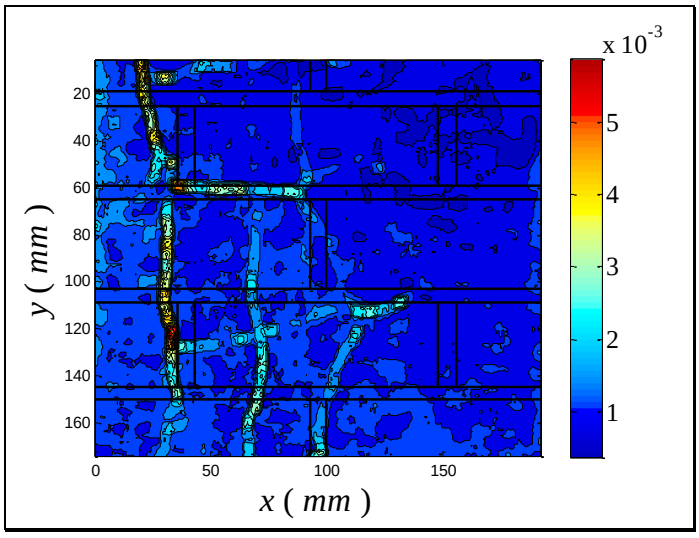

- D: 148.50 kips; 32,12 MPa

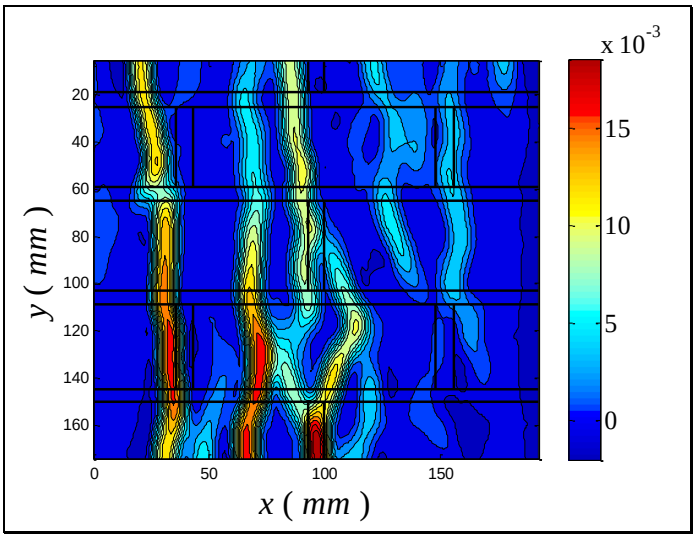

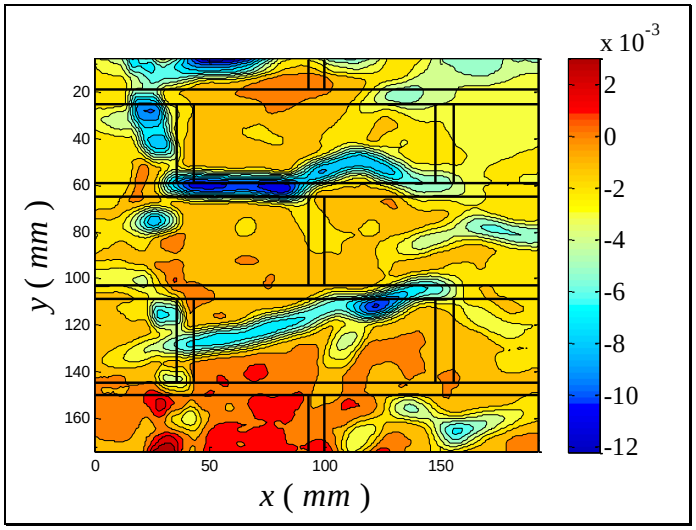

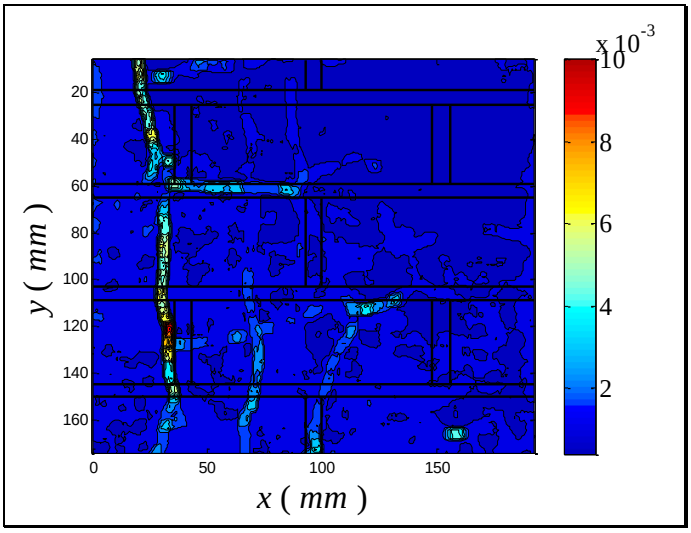

- E: 161.00 kips; 34,82 MPa

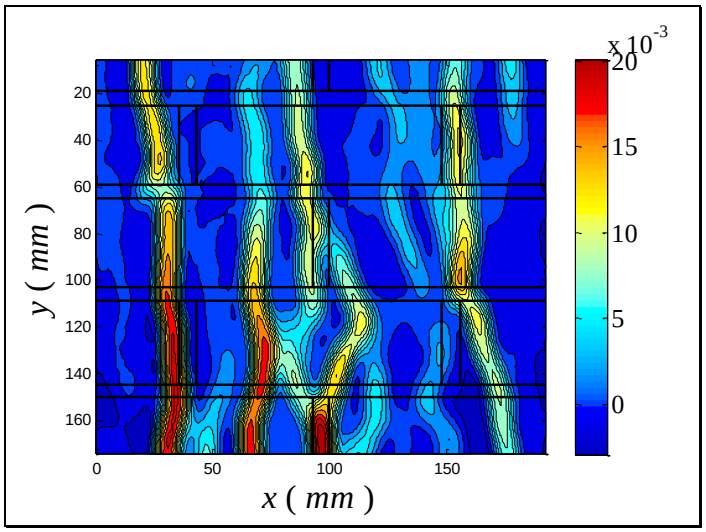

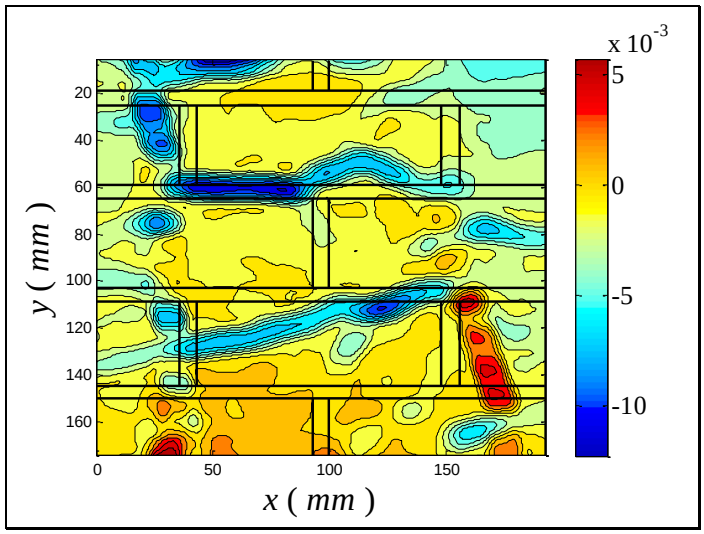

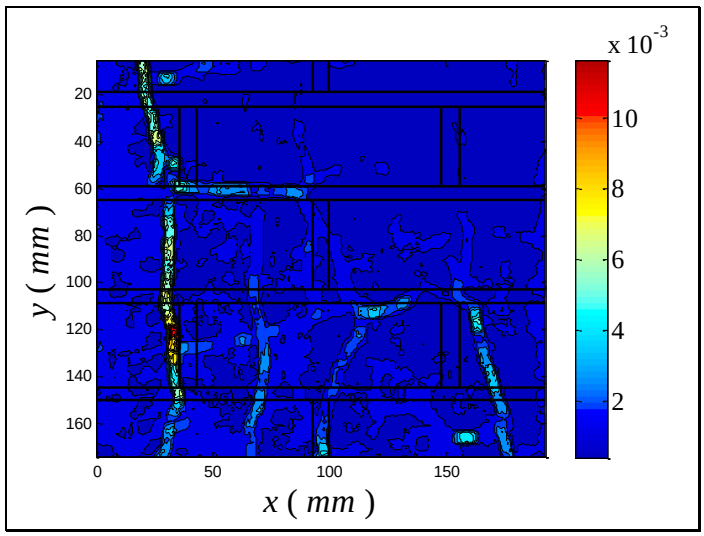

- F: 159.00 kips; 34,39 MPa

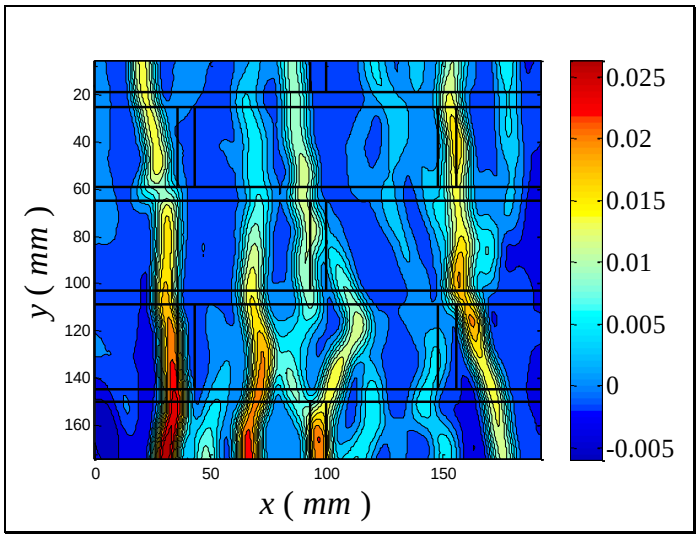

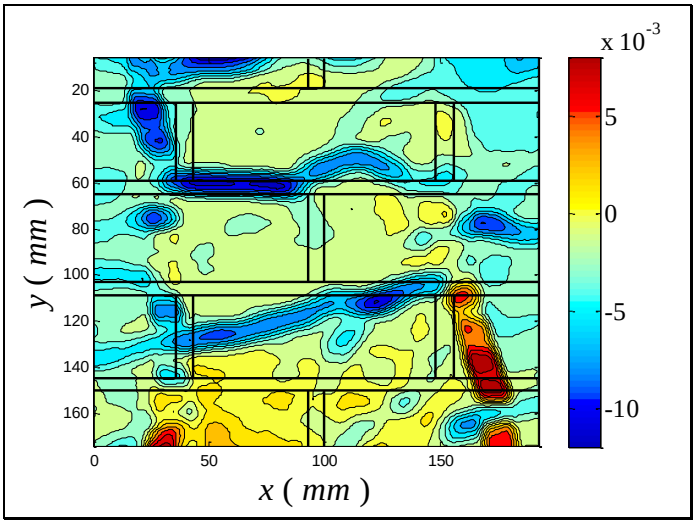

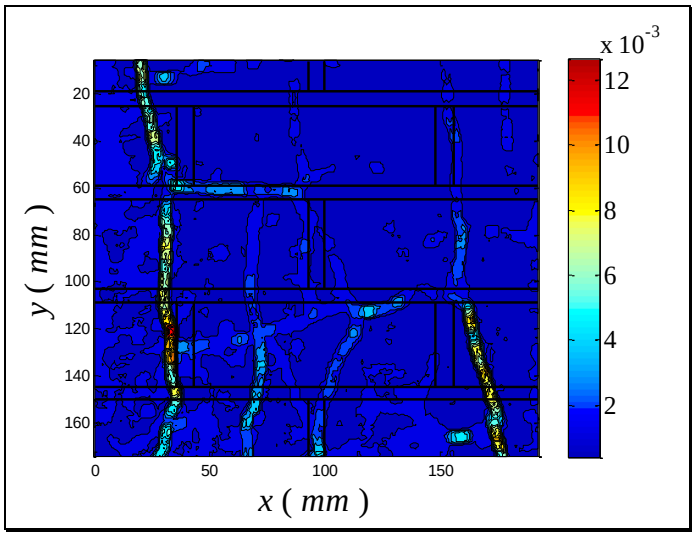

- G: 165.00 kips; 35,68 MPa

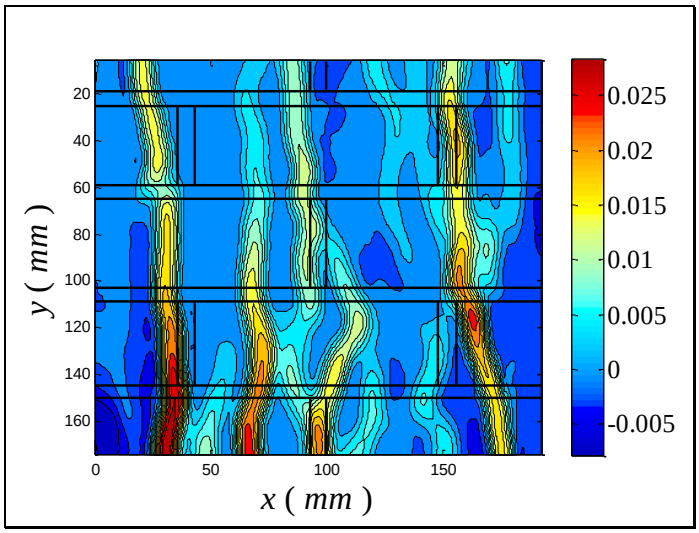

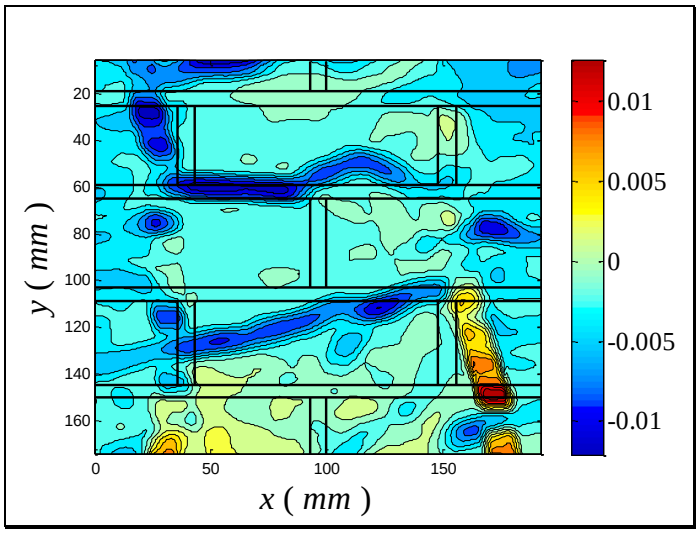

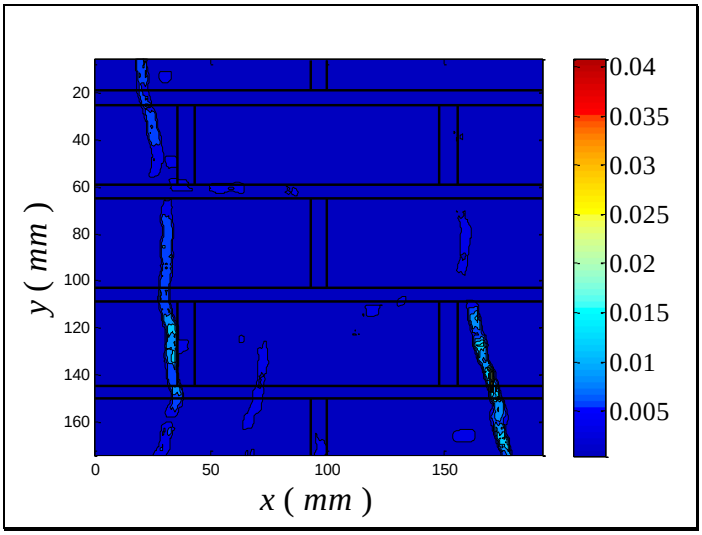

5.3.1.2. Rectangular2 wall wrapped 2

Fig.5.45 – Rectangular2 wall wrapped 2

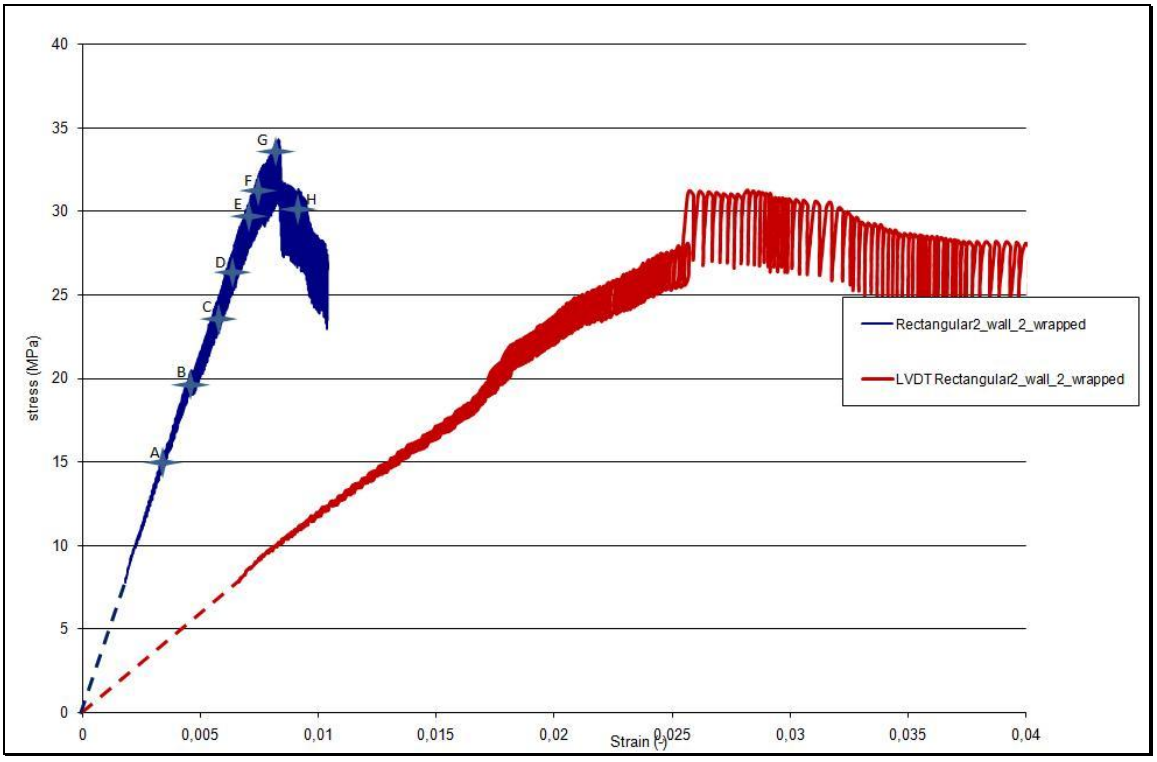

Fig.5.46 – Stress–strain diagram of rectangular2 wall wrapped 2

The contour plots of ε_{xx} , ε_{yy} and the correlation factor for all the points in figure are reported below.

- A: 70.67 kips; 15,28 MPa

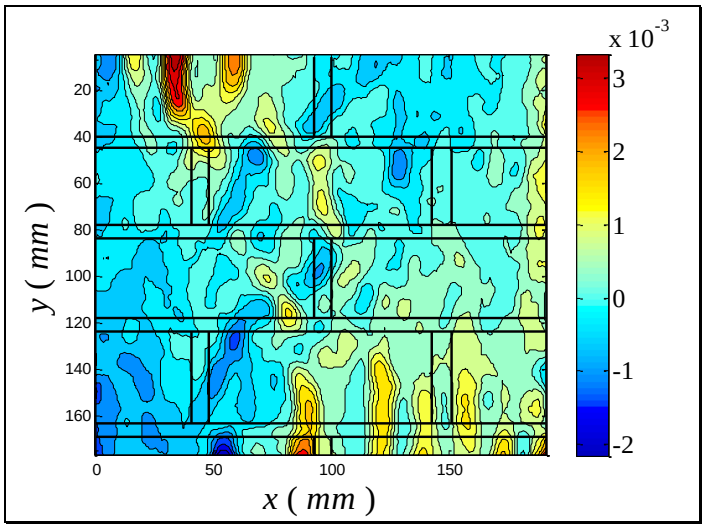

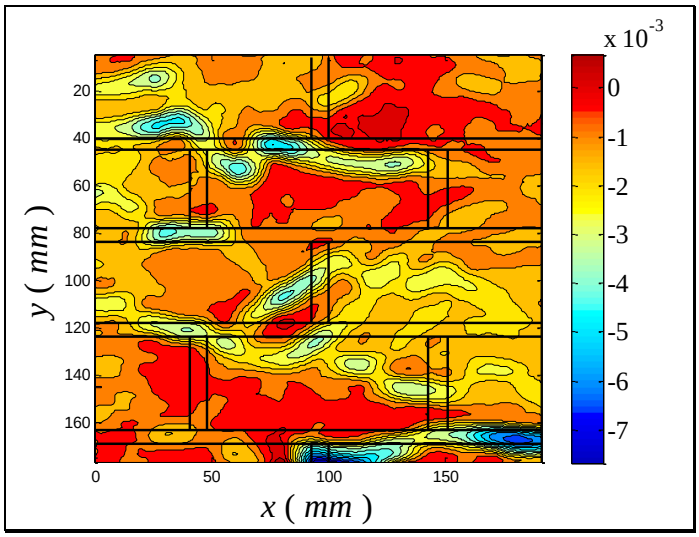

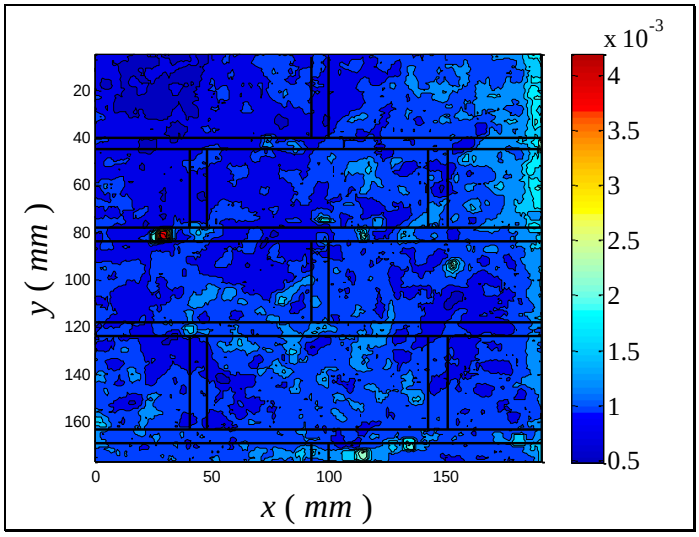

- B: 90.07 kips; 19,48 MPa

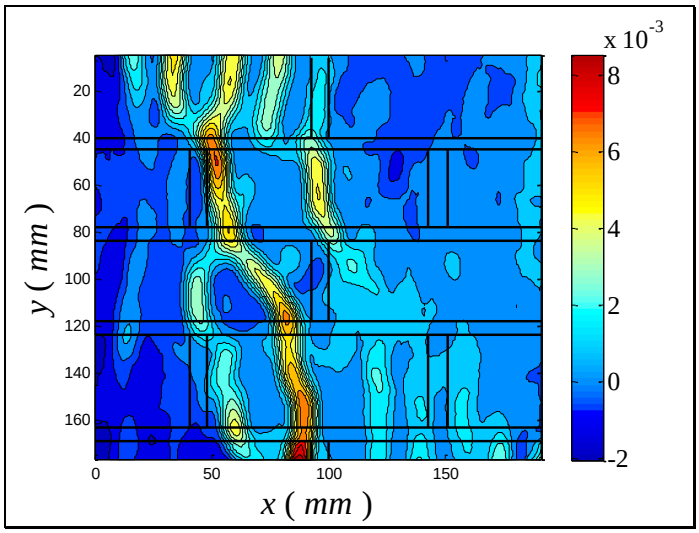

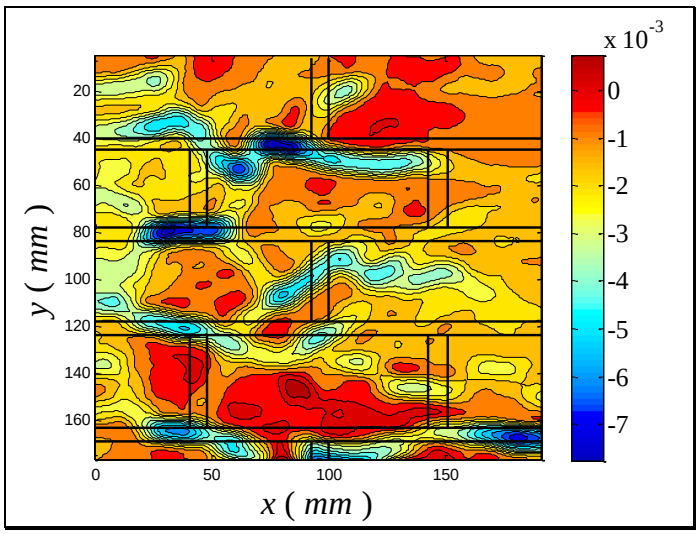

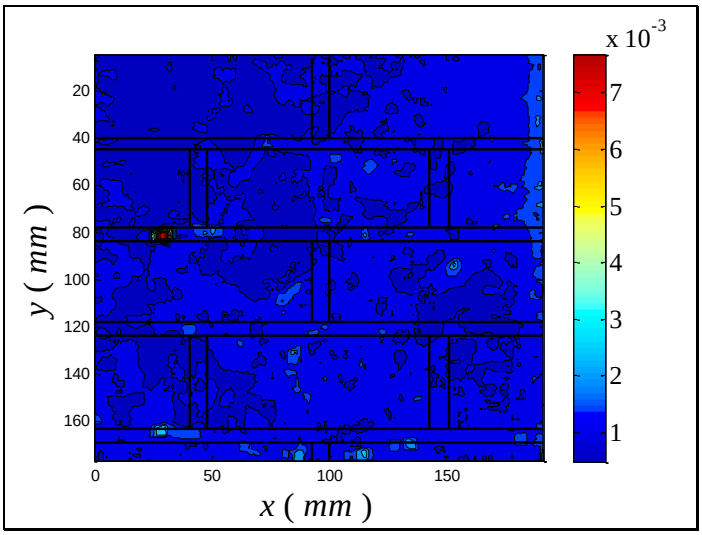

- C: 108.20 kips; 23,40 MPa

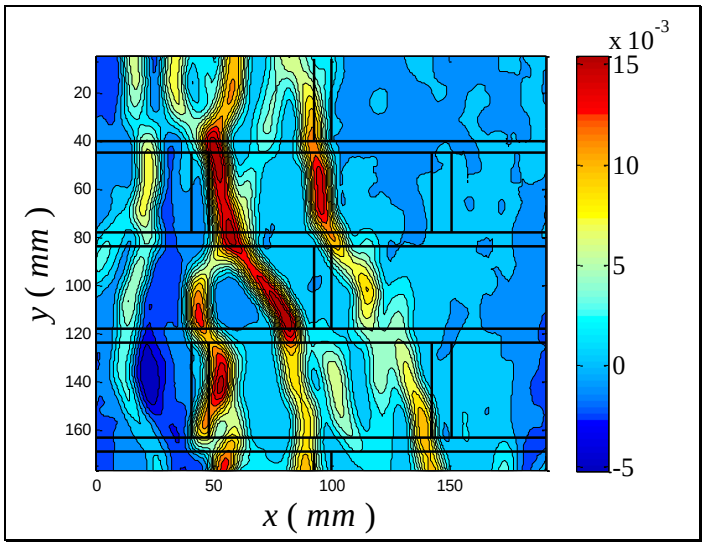

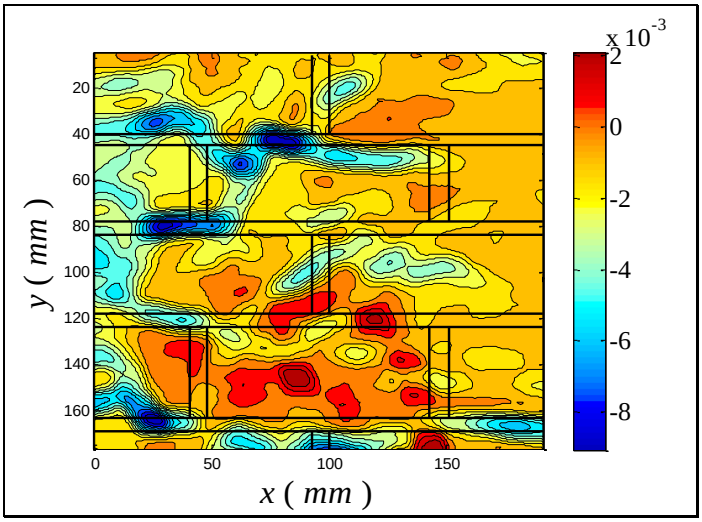

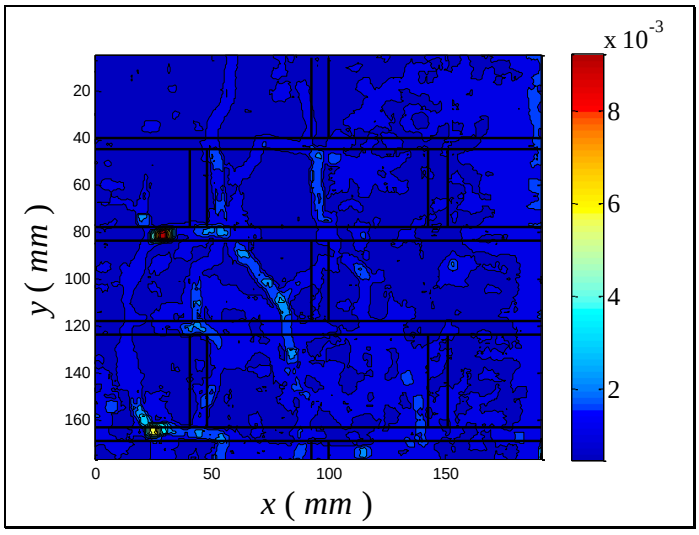

- D: 122.90 kips; 26,58 MPa

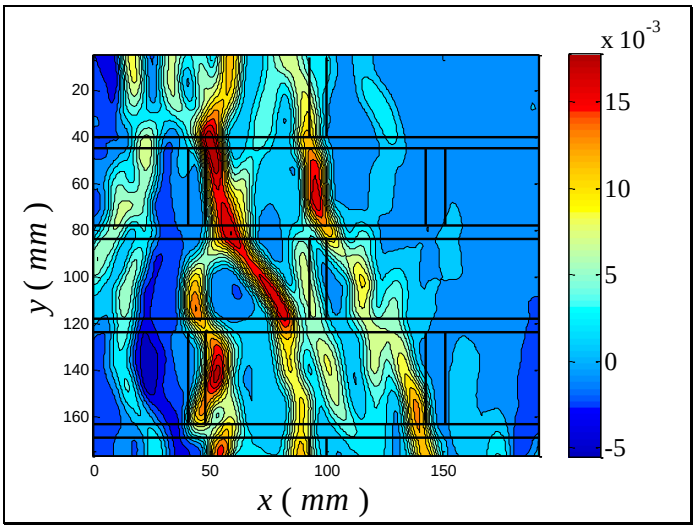

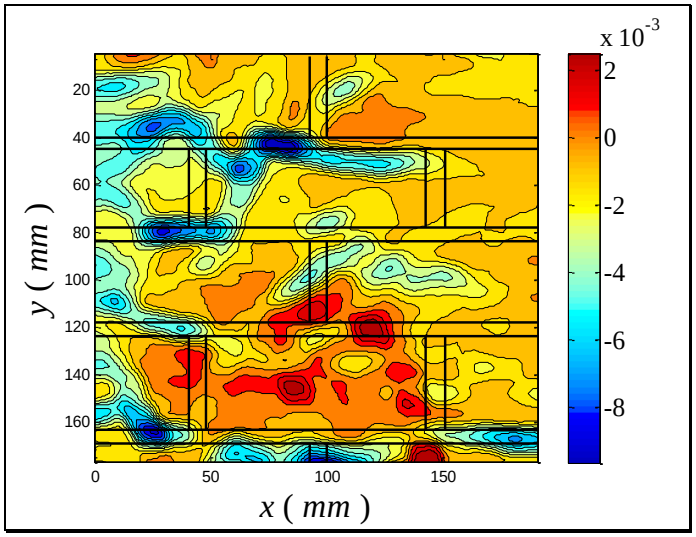

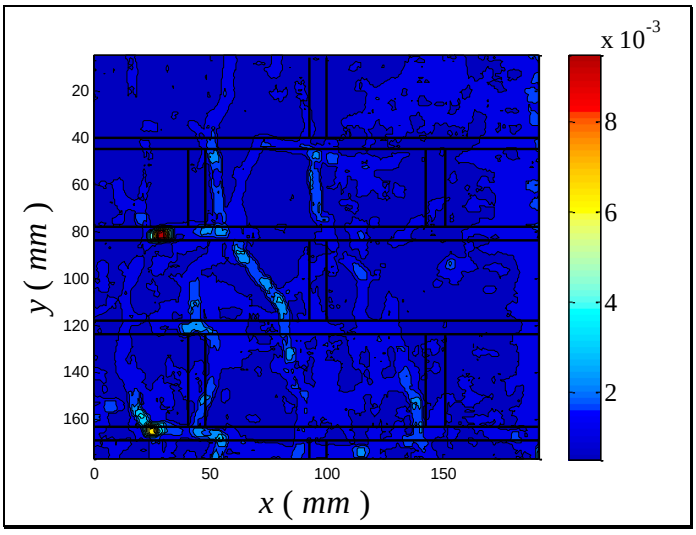

- E: 138.00 kips; 29,84 MPa

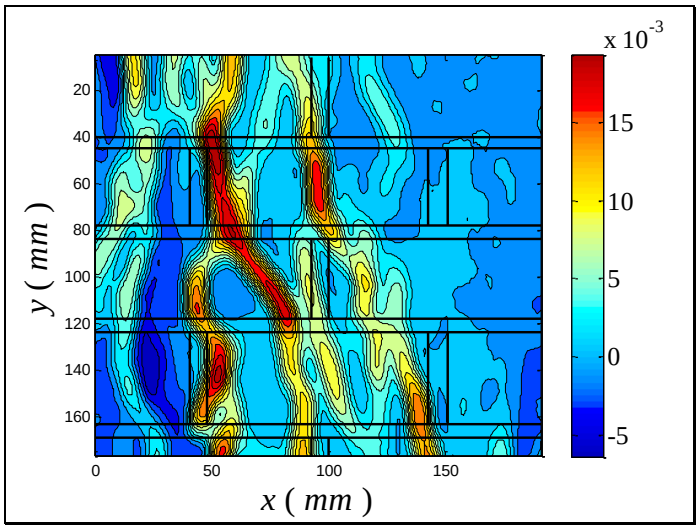

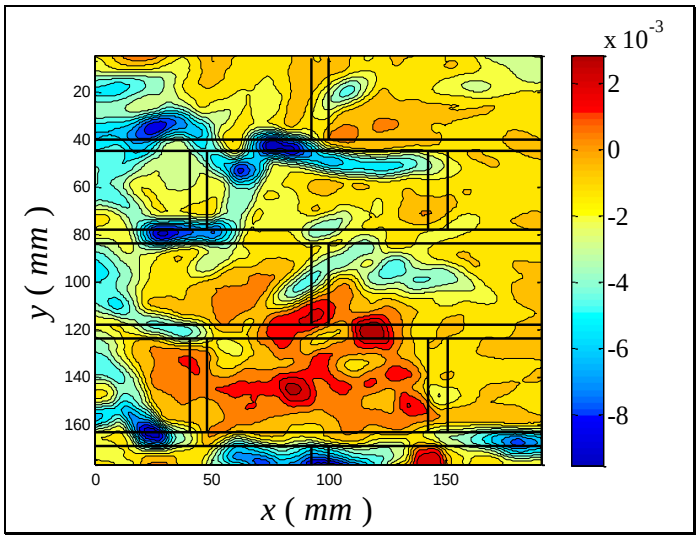

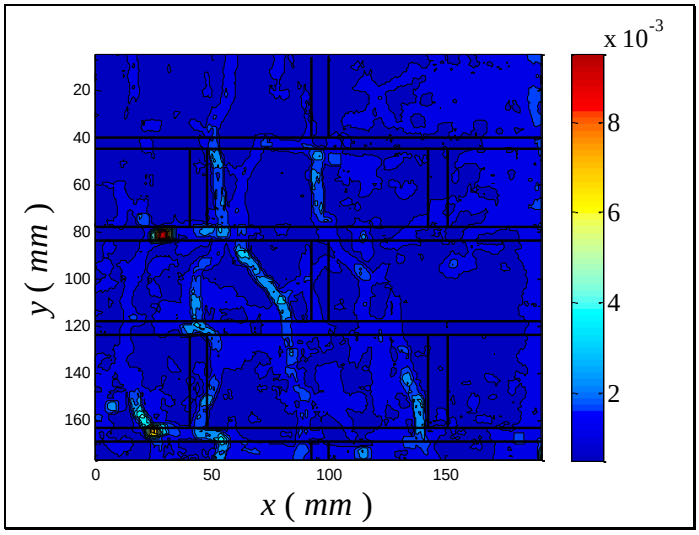

- F: 144.00 kips; 31,14 MPa

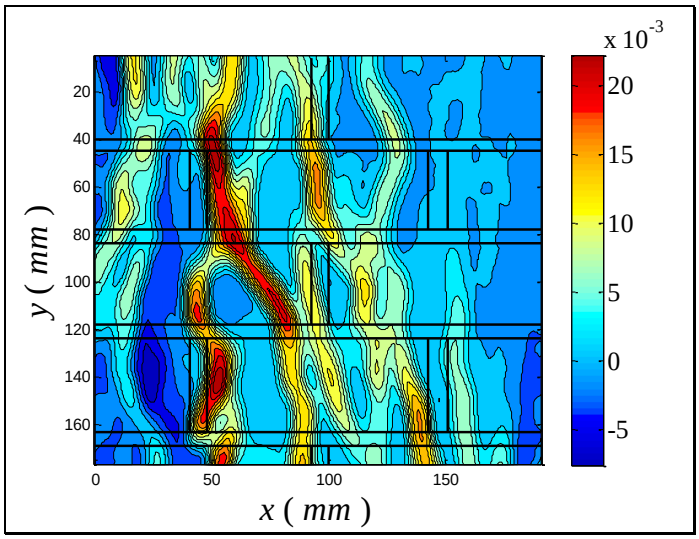

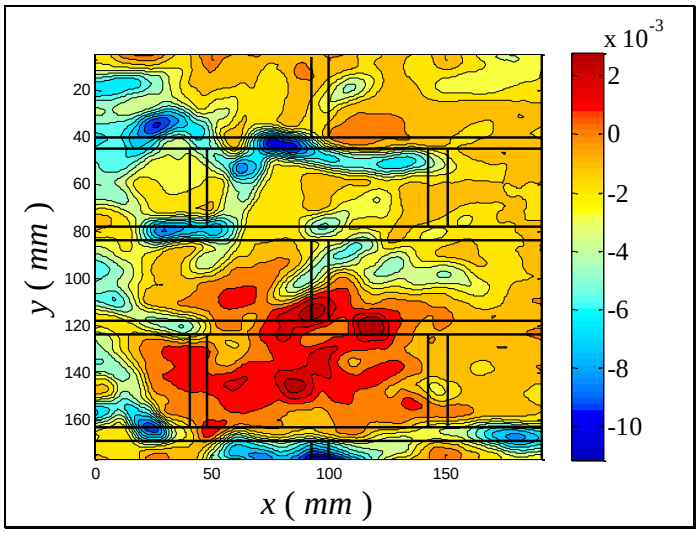

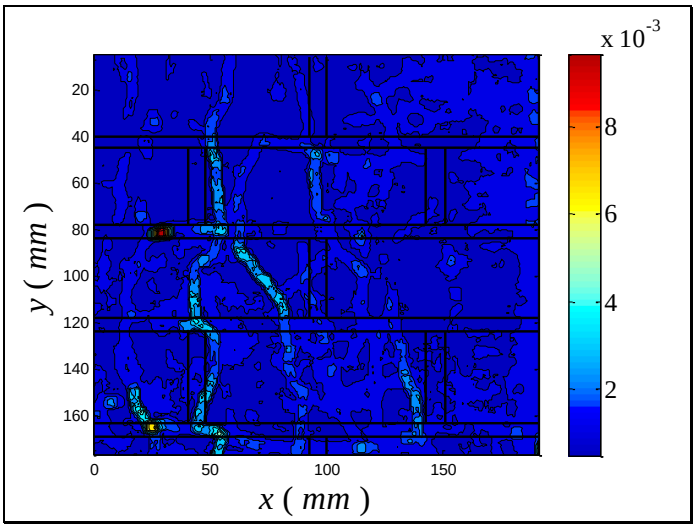

- G: 153.00 kips; 33,10 MPa

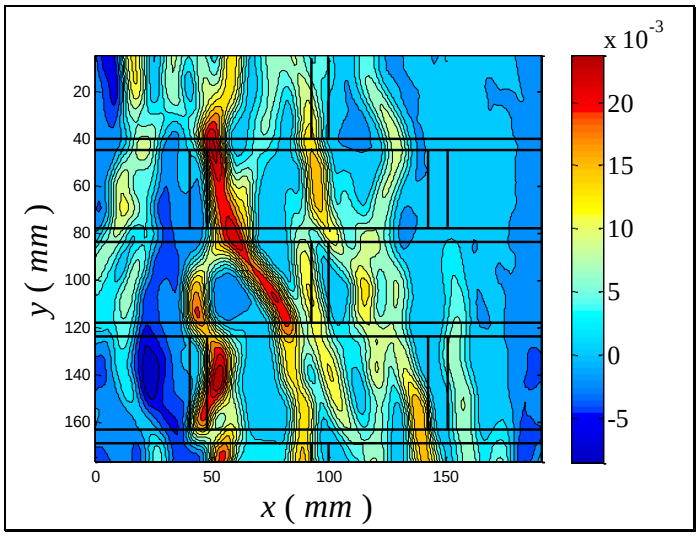

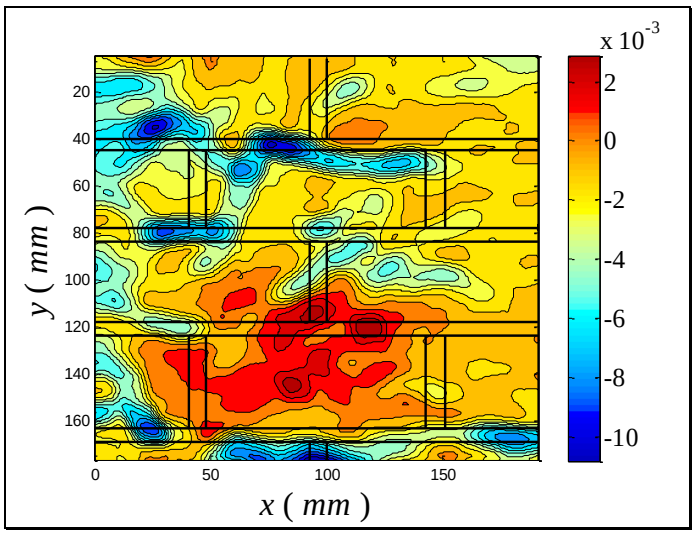

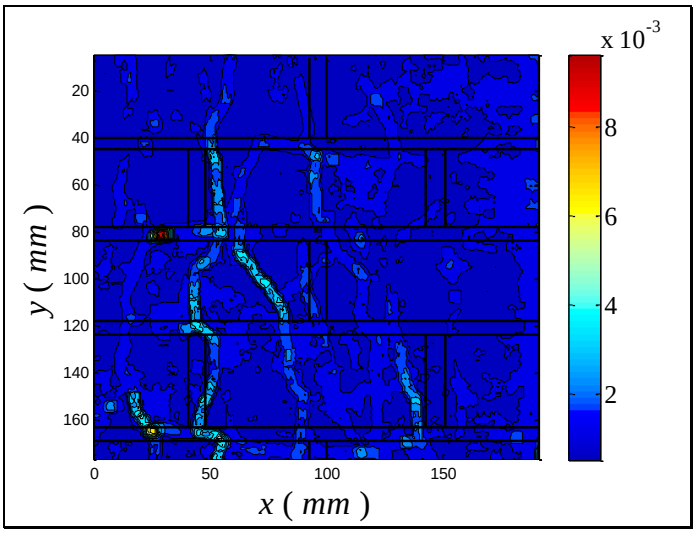

- H: 139.00 kips; 30,06 MPa

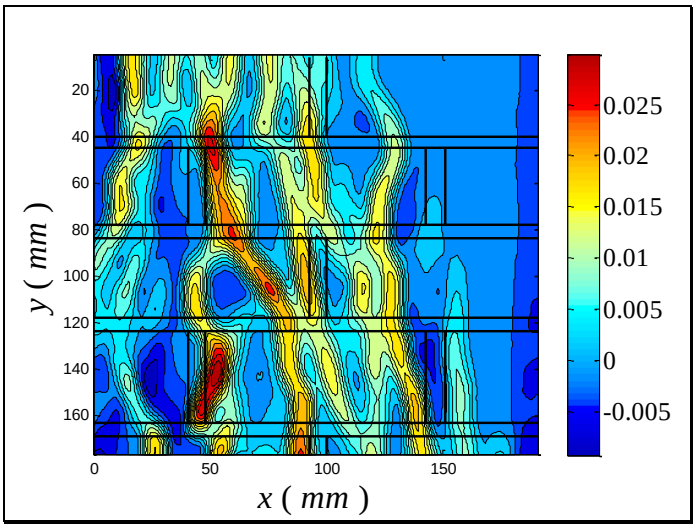

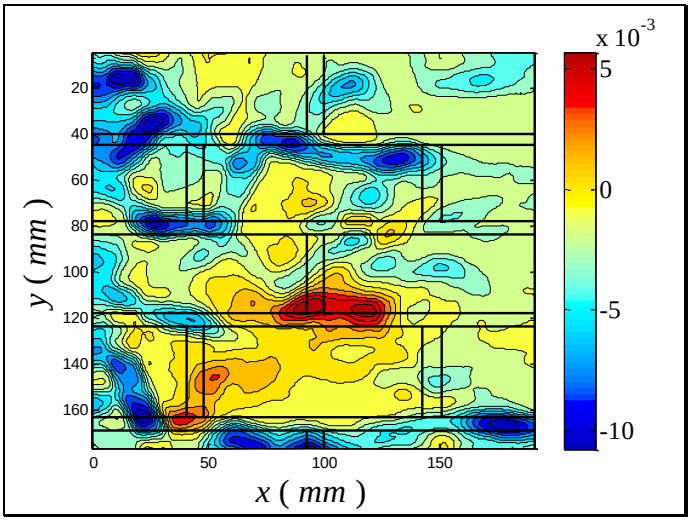

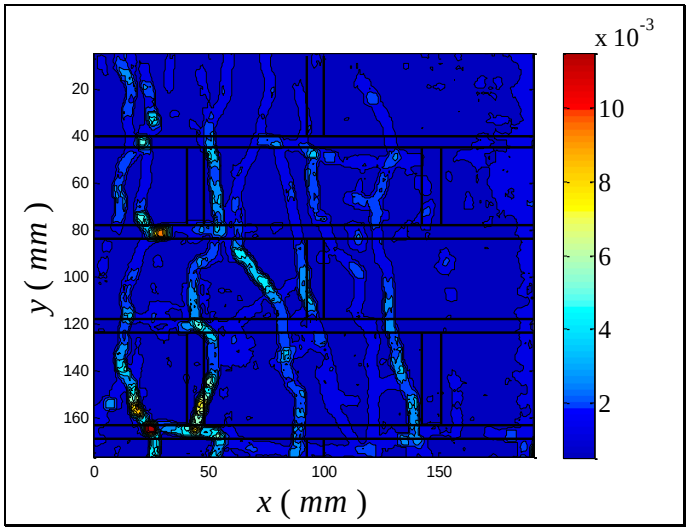

5.3.2. Discussion of result

The presence of a lot of vertical and horizontal joints in this configuration change completely the behavior of specimens with and without the reinforcement.

When the fiber begins to work containing the expansion of the mortar joints increasing the load-carrying capacity of the masonry, the stress and the strain are almost tripled.

The next figure shown the developing of the arch effect on the section after cutting in the middle a specimen.

Fig. 5.47 – Section of rectangular2 wall wrapped 1

The main conclusions that can be drawn from the tests on laboratory specimens are as follows.

The arch effect is modified by the presence of vertical joints in this configuration as in the other. In particular after the cut in the middle of the specimens it's clear the presence of cracks diverted by the presence of the 2 horizontal joints forming different reacting area instead of a concrete specimen with the same dimension.

The effectively confined area is assumed as the region where the arching action has been fully developed as visible in figure 5.48.

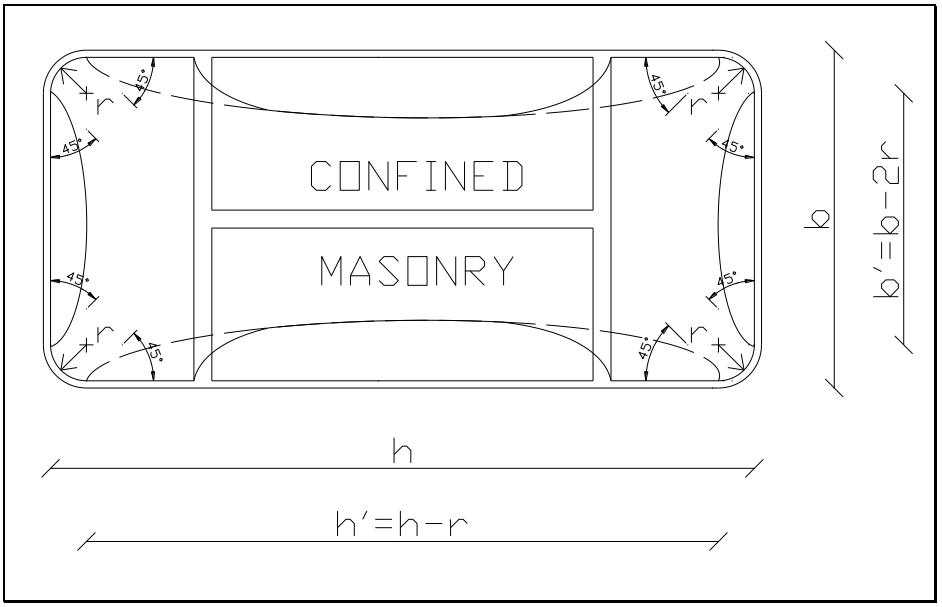

Fig. 5.48 – Effectively confined masonry in rectangular2 section walls

The critical point continued to be the mortar joints, horizontal and vertical as it is shown in the DIC picture.

The stress and the strain are directly improved by the fiber reinforcement proportional to the presence in the column tested of more horizontal joints, the diagram in figure 5.49 and 5.50 show this behavior.

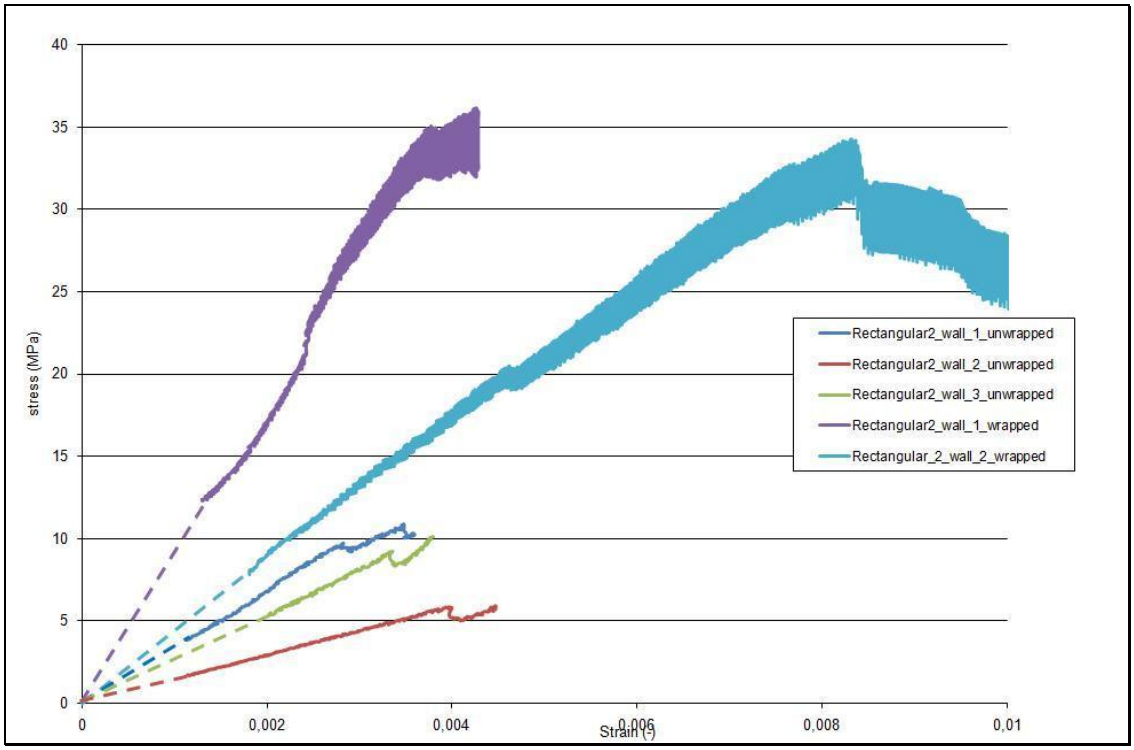

Fig. 5.49 – Stress–strain diagram of rectangular2 walls wrapped and unwrapped compared

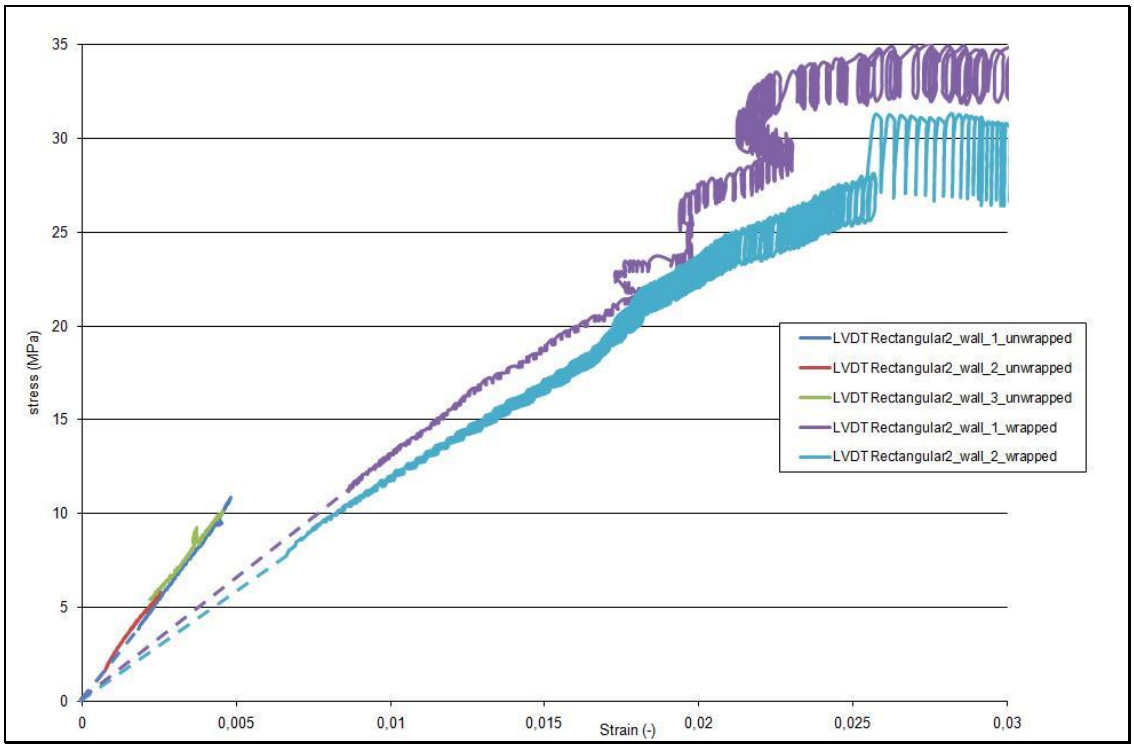

Fig. 5.50 – Stress–LVDT strain diagram of rectangular2 walls wrapped and unwrapped compared

With the DIC pictures is possible to see an interaction between the vertical and the horizontal joints that can modify the attended failure mechanisms for this configuration. But it's clear the parameter that increases the gap of the behavior between the walls wrapped and unwrapped is the presence of an increasing number of vertical joints.

CONCLUSIONS

CONCLUSIONS

Confinement of masonry with FRCM has not been investigated in the past. This dissertation presents an experimental investigation on the behavior of axially loaded masonries confined with FRCM-reinforcement. Axial compression tests were conducted on four configurations masonries, a total of 23 specimens: for each type were casted 3 unwrapped and 3 wrapped to compare the different behavior.

The results are summarized as follows:

- In general, FRCM-confined masonry behaves very much like FRP-confined concrete. The confinement provided by FRCM improves considerably both the load-carrying capacity and the deformability of masonry columns and walls.
- FRCM-reinforced columns did not show a consistent improvement in the load-carrying capacity, if compared with the unwrapped specimens. The behavior of this configuration is closer to wrapped concrete columns. The reinforcement helps the masonry be considered homogeneous in the direction of the load because prevents the expansion of the joints. Hence, the development of a confinement model for this configuration could be based on existing approached available for concrete columns.

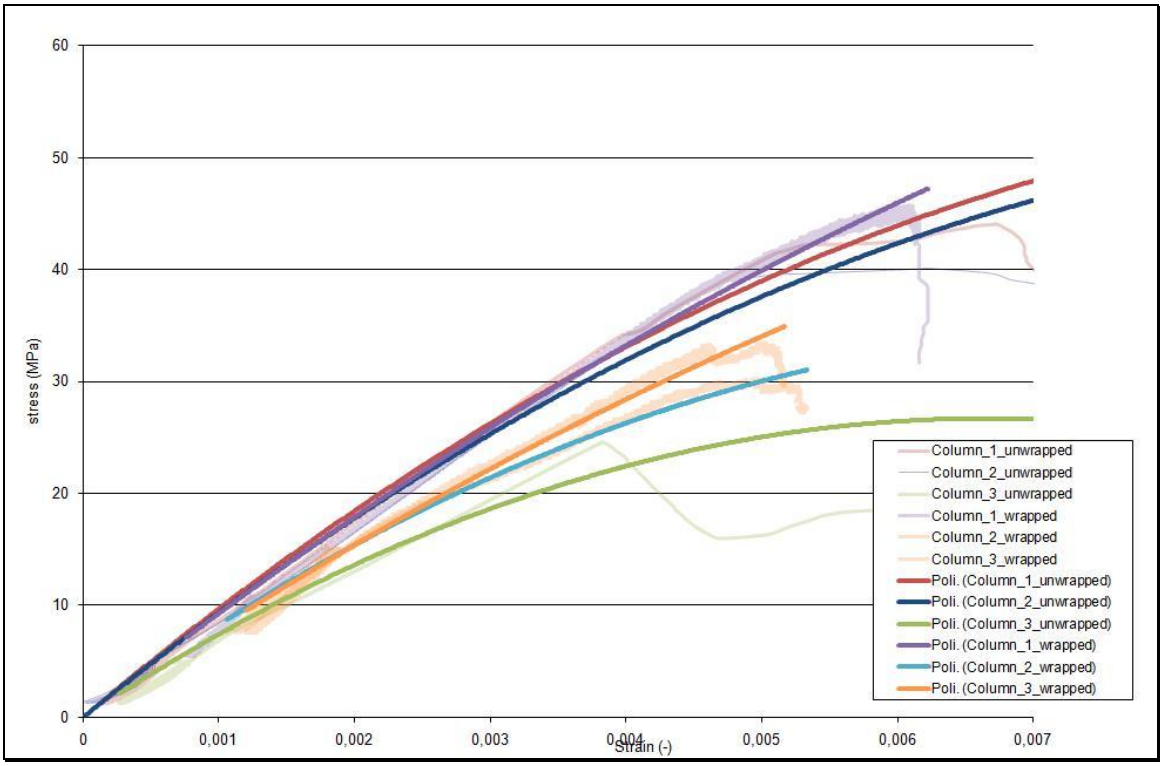

Fig. 6.1 – Stress–strain tendency diagram of wrapped and unwrapped columns compared

- FRCM-strengthened walls showed consistent improvement of the load-carrying capacity due for the presence of vertical joints in particular in the rectangular cross section.
- The square configuration test failed by crushing and squeezing of the horizontal mortar joints, followed by vertical splitting of the bricks. Immediately the reinforcement begins to work containing the expansion of the mortar and the bricks and increasing the load-carrying capacity of the masonry. The arch effect is not modified by the presence of vertical joints in this configuration. The cracks follow the development of the arch effect in both the side of the masonry. The compressive strength of masonry is not really increased with the use of the FRCM in this configuration. Approximately no more than 20% of the unwrapped strength.

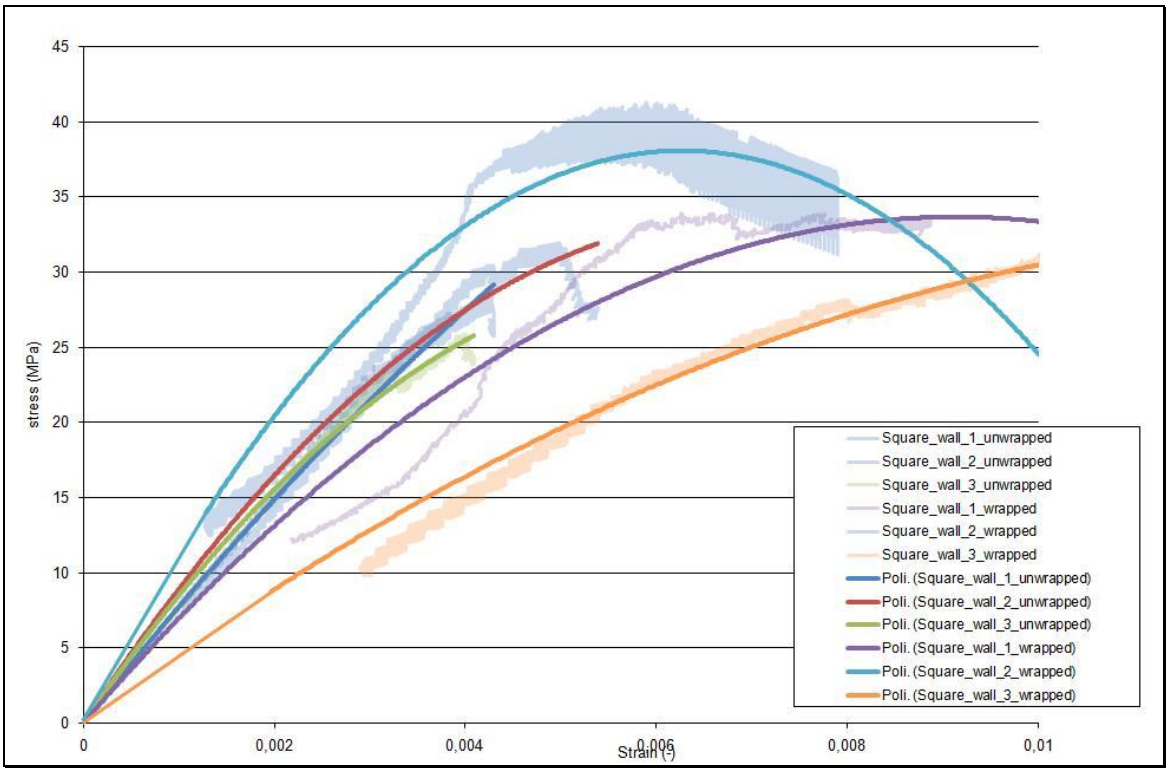

Fig. 6.2 – Stress–strain tendency diagram of square walls wrapped and unwrapped compared

- The rectangular1 configuration test failed by crushing and squeezing of the horizontal mortar joints, and immediately the FRCM reinforcement began to work containing the expansion of the mortar and the bricks, increasing the load-carrying capacity of the masonry. The arch effect is modified by the presence of vertical joints in this configuration. In particular the cut of the tests specimen in the center clearly shows how cracks diverted, as a result of the presence of horizontal joints, forming different reacting area instead of a concrete specimen with the same dimension. The compressive strength of masonry is significantly increased with the use of the FRCM because it prevents the expansion of the joints, both vertical and horizontal. With the DIC pictures is possible to see an interaction between the vertical and

the horizontal joints that can modify the failure mechanisms for this configuration.

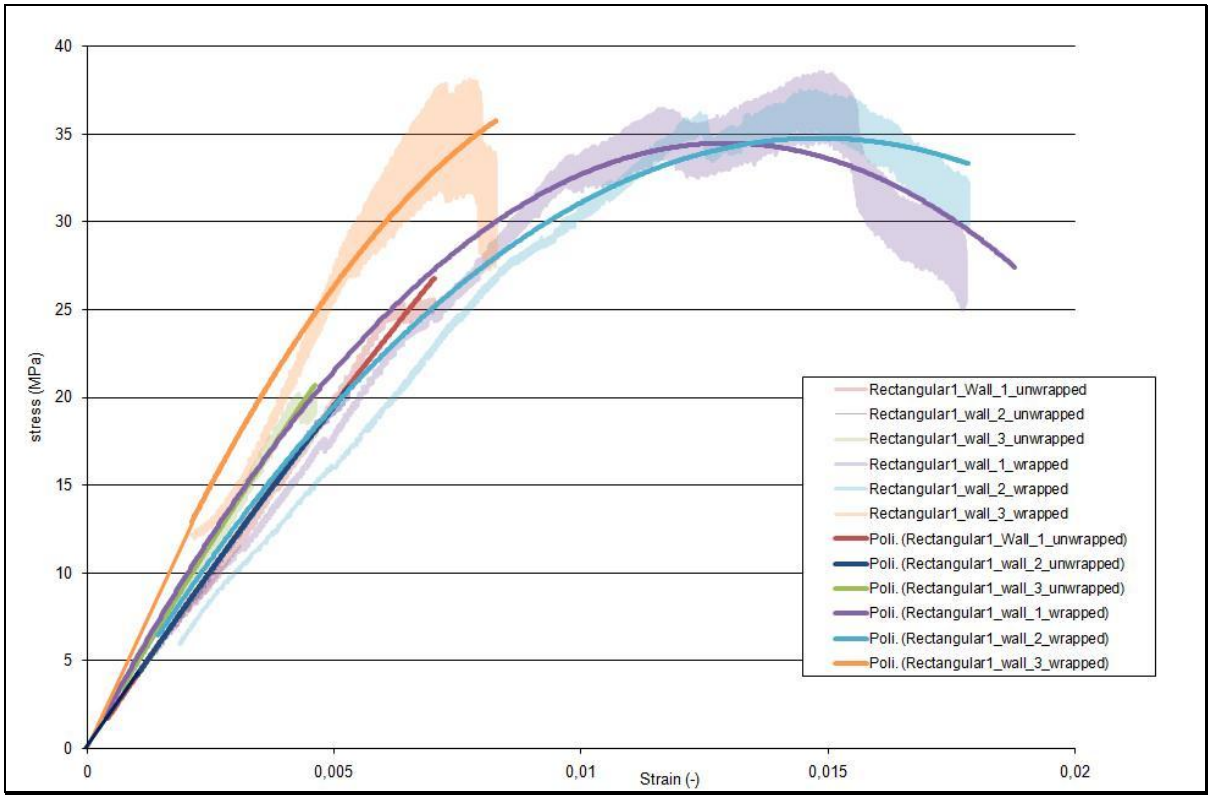

Fig. 6.3 – Stress–strain tendency diagram of rectangular1 walls wrapped and unwrapped compared

- The presence of several vertical and horizontal joints in the rectangular2 configuration completely changes the behavior of specimens with and without the reinforcement. When the fiber begins to work containing the expansion of the mortar joints increasing the load-carrying capacity of the masonry, the stress and the strain are almost tripled. The arch effect is modified by the presence of vertical joints as in the other configuration. In particular after the cut in the middle of the specimens, it's clear that the cracks, as the result of the presence of the two horizontal joints, deviated and formed different reacting area instead of a concrete

specimen with the same dimension. The critical point continued to be the mortar joints, horizontal and vertical as it is shown in the DIC picture.

The ultimate stress and the strain are improved by the presence of the FRCM and the extent of the increase is correlated to the number of more vertical joints. It's clear that the parameter that increases the gap of the behavior between the walls wrapped and unwrapped is the presence of an increasing number of vertical joints.

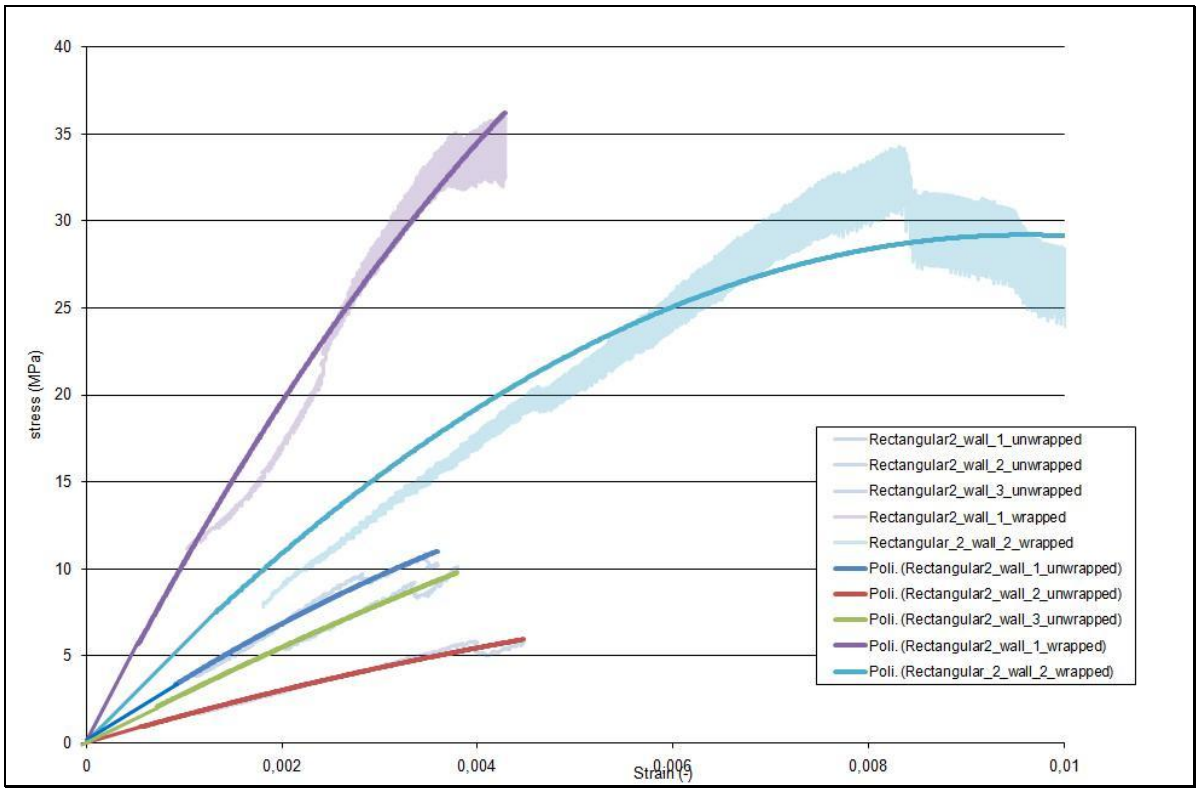

Fig. 6.4 – Stress–strain tendency diagram of rectangular2 walls wrapped and unwrapped compared

- The increase of the strength and deformability of the FRCM-strengthened masonry columns is related to the effectiveness of the confining action of the composite. Increasing the corner radius or decreasing the cross-section aspect ratio is beneficial to the strength and strain capacity of masonry. However, further experiments are

necessary to understand and quantify the influence of these parameter.

Emerging techniques that use Fiber-Reinforced Polymer composites for strengthening and conservation of historic masonry are becoming increasingly accepted. In the last decades steel plates or wood frames were used for external confinement in containing the lateral dilation of masonry columns subjected to axial loads. In the last years FRCM mesh or jackets were also employed to increase strength and ductility with encouraging results in terms of mechanical behavior and cost effectiveness.

Fig. 6.5 – Wood frames used for external confinement

There are a lot of challenges all equally interesting respect the research in understanding the debonding mechanism of failure in FRCM-reinforced masonry.

This study try to express, with the experimental analysis, the importance of research for answer to the demands of recovery and safeguard of the

existing buildings. This is effected with the use of new technologies that increase the mechanical properties, like Fiber Reinforced Cementitious Matrix.

The tests of new material and methodologies happens in laboratory with experimental tests like in this dissertation so it's very important to invest money for research and for purchase new equipments.

The natural prosecution of this research is certainly, after performing other experiments on similar masonries for more consistent data, the realization of a software that allows to all engineering company, after the insertion of the brick type and the masonry configuration properties which need to be restored, to calculate the number of layers and the disposition according to the characteristics of the fiber reinforcement that the engineer intends to use.

Fig. 6.6 – Software typologies

This should be obtained at first modeling the configuration where the tests are developed with a computational software and subsequently calibrating the response to get the behavior seen in the developed experimentations.

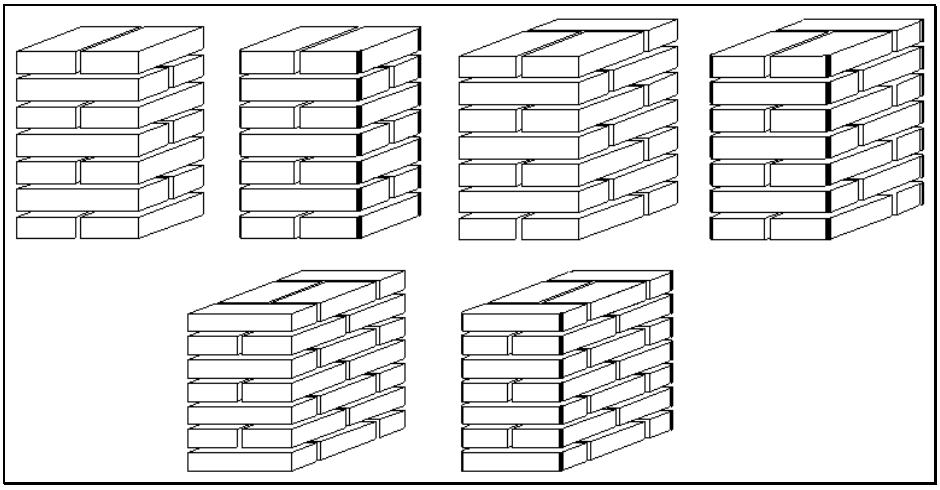

Fig. 6.7 – Masonry configuration tested

At the end, test results enabled the development of a simple confinement model for strength and ultimate strain of FRP-confined masonry. This model is consistent with test results obtained here, but should attract further experimental verification in the future to account for types of different masonry materials than those used in this study.

Remembering that a system of composite reinforcement is the result of the union of a fiber with mechanical performances and of a matrix with sticker function, that allows to transmit the solicitations from the structure strengthened to the fiber; we can affirm that, based on this research, beside FRP-reinforcements (Fiber Reinforced Polymer), also the FRCM (Fiber Reinforced Cementitious Matrix) can be used for restoration and structural consolidation.

This new system exploit the physical-mechanics properties of an inorganic cement based matrix without using an epoxy resins anymore, more difficult to manage.

The inorganic matrix combined with fibers like carbon and PBO showed their efficiency in the reinforcement to bending reinforced concrete beams increasing the load of collapse of values among 15% and 20%.

With FRP-reinforcement is possible obtain 30% of increase, but the FRCM-reinforcement upgrade is generally enough to guarantee a suitable increase of the performances for concrete structural elements.
In particular with this research is clear that presence of vertical joints decrease the axial load-carry capacity of masonry walls and how fiber reinforcement improves notably the behavior in proportional way to the presence of more joints.

In conclusion I would like to notice the vastness and the heterogeneity of the field of application of the composite reinforcements, that seem to be a good match among respect of the immense Italian cultural patrimony, represented by structures of rare architectural beauty and the necessity of safeguard and consolidation of the skeleton without upsetting the essence.

Fig. 6.8 – San Pietro square in Rome

Fig. 6.9 – The Rialto bridge in Venice

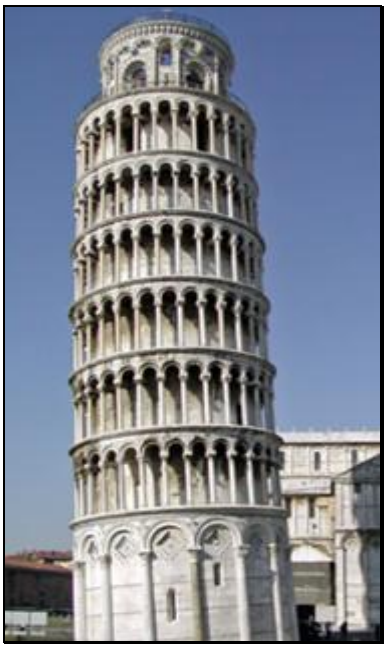

Fig. 6.10 – The Pisa tower

Fig. 6.11 – Segovia Roman aqueduct

REFERENCES

R E F E R E N C E S

1. **Sutton, M.A., et al.** *photomechanics.* 2000.
2. **D**antec dynamics. [Online] http://www.dantecdynamics.com/.
3. **Council National Research.** *Guide for the Design and Construction.* 2004.
4. **Tong, L., Mouritz, A.P. e Bannister, M.K.** *3D fiber reinforced polymer.* 2002.
5. *Masonry Confinement with Fiber-Reinforced Polymers.* **Krevaikas, Theofanis D. e Triantafillou, Thanasis C.** 2005.
6. *Investigation of the Interface Fracture during Debonding between FRP and Masonry.* **Carloni, Christian e Subramaniam, Kolluru.** 2009.
7. *Strenghtening of Unreinforced Masonry Walls Using FRPs.* **Albert, Michael L., Elwi, Alaa E. e Cheng, Roger J.** 2001.
8. *Structural Upgrading of Masonry Columns by Using Composite Reinforcements.* **Aiello, Maria Antonietta, Micelli, Francesco e Valente, Luca.** 2007.
9. *Confinement of brick masonry columns with CFRP materials.* **Corradi, M., Grazini, A. e Borri, A.** 2007.
10. *Experimental Investigation and Fracture.* **Ali-Ahmad, Mohamad, Ali-Ahmad, Kolluru e Ghosn, Michel.** 2006.
11. **Roberts, T.M., et al.** *Quasi-static and high cycle fatigue strength of brick masonry.* 2006.*FRP-confined concrete under axial cyclic compression.* **Lam, L., et al.** 2006.
12. *Modelling of rectangular RC columns strengthened with FRP.* **Maalej, M., Tanwongsval, S. e Paramasivam, P.** 2002.
13. *Review of Design Guidelines for FRP Confinement of Reinforced Concrete Columns of Noncircular Cross Sections.* **Rocca, Silvia, Galati, Nestore e Nanni, Antonio.** 2008.

14. *Width effect in the interface fracture during shear debonding.* **Subramaniam, Kolluru, Carloni, Christian e Nobile, Lucio.** 2006.

15. *FRP-confined concrete under axial cyclic compression.* **Lam, L., et al.** 2006.

16. **American Concrete Institute.** *Guide for the Design and Construction of Externally Bonded FRP Systems for Strengthening Concrete Structures.* 2008.

17. *Strength and strain capacities of concrete compression members reinforced with FRPg. Subramaniam, Kolluru, Carloni, Christian e Nobile, Lucio. 2006.* **Campione, G. e Miraglia, N.** 2003.

18. *Concrete confined by FRP material: a plasticity approach.* **Karabinis, A.I. e Rousakis, T.C.** 2002.

19. *Statistical analysis of compressive strength of clay brick masonry prisms.* **Saman Afqahi Aryana, The University of Texas at Arlington,** 2006.

20. *Web site: http://www.ruredil.it/*

ACKNOWLEDGMENTS

A C K N O W L E D G M E N T S

I would like to take this opportunity to thank Prof. Ing. Marco Savoia, Prof. Ing. Kolluru Subramaniam and Prof. Ing. Christian Carloni for the help and the opportunity they gave to me.

I would acknowledge Ruredil S.p.a. of San Donato Milanese for the materials supplied for this investigation.

Besides academics, this experience at the City College of New York has made me aware of my responsibilities as an engineer.

I have a natural curiosity about the world we live in and I'm greatly benefit from my study abroad experience. I'm eager to learn about other cultures and customs, and this experience make me respectful of various world views.

I have broaden my horizon as an engineer. I learned much from the exposure to a different culture and his values to the society.

I'm already grown as a person after this experience in the United States, and I think it will add a great deal to my personal development.

The thing always happens if you really believe in; and the belief in a thing makes it happen. If you work hard and serious there are many opportunities, my tuition will pay in full.